

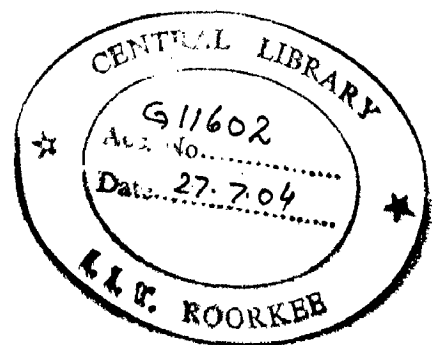
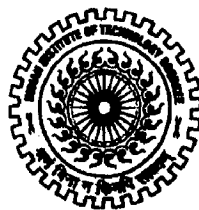
**CHARACTERIZATION AND SYNTHESIS OF
GRADED COPPER-ALUMINA COMPOSITES BY
POWDER METALLURGY & EXPLOSIVE
FORMING TECHNIQUE**

A DISSERTATION

*Submitted in partial fulfillment of the
Requirements for the award of the degree
of
MASTER OF TECHNOLOGY
in
METALLURGICAL & MATERIALS ENGINEERING
(With Specialization in Industrial Metallurgy)*

By

GAMA GUPTA



**DEPARTMENT OF METALLURGICAL & MATERIALS ENGINEERING
INDIAN INSTITUTE OF TECHNOLOGY, ROORKEE
ROORKEE – 247667 (INDIA)**

JUNE 2004

CANDIDATE'S DECLARATION

I here by declare that the work which is being presented in this Thesis entitled “**Characterization and Synthesis of Graded Copper-Alumina Composites by Powder Metallurgy & Explosive Forming Technique**”, in partial fulfillment of the requirement for the award of the degree of Master of Technology in Metallurgical & Materials Engineering with specialization in Industrial Metallurgy, submitted in the Metallurgical & Materials Engineering Department, Indian Institute of Technology Roorkee, Roorkee, is an authentic record of my own work carried out during the period from June 2003 to June 2004, under the supervision of **Dr. (Mrs.) Vijaya Agarwala**, Professor, **Dr. R.C Agarwala**, Associate Professor, Metallurgical & Materials Engineering Department, Indian Institute of Technology, Roorkee, and **Dr.K.Balasubramanian**, Director, NFTDC (Non Ferrous Materials Technology Development Centre), Hyderabad.

Date:

Place:

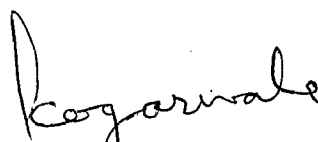

(Gama Gupta)

CERTIFICATE

This is to certify that the above statement made by the candidate is correct to the best of our knowledge.



(Dr. (Mrs.) Vijaya Agarwala)
Professor
Metallurgical & Materials Engg Dept,
Indian Institute of Technology,
Roorkee – 247667
India.



(Dr.R.C.Agarwala),
Associate Professor,
Metallurgical & Materials Engg Dept,
Indian Institute of Technology,
Roorkee – 247667
India



(Dr. K. Balasubramanian)
Director,
NFTDC
P.O Kanchanbagh
Hyderabad-500058.
India

ACKNOWLEDEMENT

Gratitude is the memory of the heart and in carrying out this academic project, persistent inspiration, unflinching support and encouragement of countless persons have served as the driving force.

I am deeply indebted to my guides **Dr.(Mrs.) Vijaya Agarwala**, Professor, **Dr. R.C Agarwala**, Associate Professor, Metallurgical & Materials Engineering Department, Indian Institute of Technology, Roorkee, and **Dr. K. Balasubramanian**, Director, NFTDC, for their unmatched guidance, encouragement and co-operation.

I wish to express my profound sense of gratitude to **Dr. K. Balasubramanian**, Director, NFTDC, and **Emeritus professor, Dr. T. R. Ramachandran**, for enduring me with their illuminating guidance and support while the completion of my dissertation. It was a great experience to part their knowledge and diffuse the same in my building personality.

I am highly thankful to **Dr. S. Prakash**, Professor and Head, Department of Metallurgical and Materials Engineering, Indian Institute of Technology Roorkee, for his sincere support to complete this dissertation.


I would like to thank all NFTDC staff for their support and co-operation. A special thanks to **Mr. Indranil Lahiri**, **Mr. M.Govindraju** and **Mr. Pawan kumar** for their invaluable support.

I would like to thank my friends **L.Venkat Raghavan**, **Chavan gurling krishna** and **Nitin Vardani** for their love and support to me during completion of this work.

Above all I would like to acknowledge that the greatest role has been of my parents, and other family members who have helped me to cultivate the system of values and instincts that shall always enlighten my path all these living years.

Place: Roorkee

Date: 30th june 2004


(Gama Gupta)

ABSTRACT

Specific and complex application of parts require materials that can fulfill the desired requirement. Gradient materials, well known functionally gradient materials (FGMs), are used for such applications where common materials can not yield satisfactory results.

In the present work, powder metallurgy and explosive forming techniques have been used to synthesize a Cu/Al₂O₃ gradient composite. In the powder metallurgy technique, powders were mixed in ball mill followed by hand mixing with addition of camphor as a binder. These mixed powders were compacted using 25kg load. Each pellet consisted of four layers differing in Alumina content from 1% to 10%. After preheating, sintering of pellets was done in vacuum. Sintering cycles were 1000⁰C for 2hr, 3hr and 4hr respectively and 800⁰C for 3hr, 6hr and 9hr respectively. 1000⁰C specimens show maximum electrical conductivity (54.1%IACS). 800⁰C specimens show lower conductivity but higher density than 1000⁰C specimens. Scattering in hardness was found during measurement. Characterization was done using optical microscopy and SEM.

In the explosive forming technique, two tubes of 40mm and 55mm inner diameter and 3mm thickness were used. Mixed powders were filled in 40mm inner diameter tube. Alumina content in successive layers varied from 0% to 100% in one specimen and 1% to 6% in another specimen. This filled tube was kept inside the 55mm inner diameter tube. This assembly was exploded and was characterized in a similar way as used in powder metallurgy specimens. Density of specimen obtained was 8.20 g/cm³. Due to presence of porosity it shows no electrical conductivity.

The objective of this work is to synthesis a graded material whose one end would be insulator and other end would be conductor.

CONTENTS

Page No.

CANDIDATES DECLARATIOPN	i
ACKNOWLEDGEMENT	ii
ABSTRACT	iii
CONTENTS	iv
LIST OF FIGURES	vi
LIST OF TABLES	xi

CHAPTER1

INTRODUCTION	1
---------------------	----------

CHAPTER 2

LITERATURE REVIEW	5
2.1 Powder Metallurgy Technique	5
2.1.1 Introduction of FGMs	5
2.1.1.1 Processing of FGMs	6
2.1.1.2 Methods of obtaining compositionally green bodies	15
2.1.2 Detail Analysis of FGMs	16
2.1.3 Introduction and basic properties of Copper	23
2.1.4 Introduction and basic properties of Alumina	30
2.2 Explosive Forming Technique	31
2.2.1 Introduction	31
2.2.2 Methods of explosive forming	32
2.2.3 Explosives	33
2.2.4 Die Materials	35
2.2.5 Transmission medium	35
2.2.6 Formability aspects	36
2.2.7 Analysis of explosive forming	36
2.3 Concluding Remarks	37

CHAPTER 3	39
FORMULATION OF PROBLEM	39
CHAPTER 4	41
EXPERIMENTATION	41
4.1 Powder Metallurgy Technique	41
4.2 Explosive Forming Technique	43
CHAPTER 5	45
RESULTS AND DISCUSSION	45
5.1 Powder Metallurgy Technique	45
5.2 Explosive Forming Technique	53
CHAPTER 6	55
CONCLUSIONS	55
CHAPTER 7	57
SCOPE OF FUTURE WORK	57
REFERENCES	59
APPENDIX A	
APPENDIX B	

LIST OF FIGURES

Fig. No.	Name	Page No
Microstructures of 1000⁰C Specimens		
1	First Boundary of C1	75
2	Second Boundary of C1	76
3	Third Boundary of C1	77
4	First Boundary of C2	78
5	Second Boundary of C2	79
6	Third Boundary of C2	80
7	First Boundary of C3	81
8	Second Boundary of C3	82
9	Third Boundary of C3	83
10	First Boundary of C4	84
11	Second Boundary of C4	85
12	Third Boundary of C4	86
13	First Boundary of C5	87
14	Second Boundary of C5	88
15	Third Boundary of C5	89
16	First Boundary of C6	90
17	Second Boundary of C6	91
18	Third Boundary of C6	92
Microstructures of 800⁰C Specimens		
19	First Boundary of C1	93
20	Second Boundary of C1	94
21	Third Boundary of C1	95
22	First Boundary of C2	96
23	Second Boundary of C2	97
24	Third Boundary of C2	98

25	First Boundary of C3	99
26	Second Boundary of C3	100
27	Third Boundary of C3	101
28	First Boundary of C4	102
29	Second Boundary of C4	103
30	Third Boundary of C4	104
31	First Boundary of C5	105
32	Second Boundary of C5	106
33	Third Boundary of C5	107
34	First Boundary of C6	108
35	Second Boundary of C6	109
36	Third Boundary of C6	110

Microstructures of after Rolling

Microstructures of 1000⁰C Specimens

37	Microstructures of C1	111
38	Microstructures of C2	112
39	Microstructures of C3	113
40	Microstructures of C4	114
41	Microstructures of C5	115
42	Microstructures of C6	116

Microstructures of 800⁰C Specimens

43	Microstructures of C1	117
44	Microstructures of C2	118
45	Microstructures of C3	119
46	Microstructures of C4	120
47	Microstructures of Explosive Forming Compact	121
48	Microstructures of Explosive Forming Compact	122
49	Microstructures of Explosive Forming Compact	123

SEM Micrographs

50	SEM micrographs of powders	124
51	SEM micrographs of sintered Specimens	125
52	SEM micrographs of sintered Specimens	126
53	SEM micrographs of sintered Specimens	127
54	SEM micrographs of Specimens after Rolling	128
55	SEM micrographs of Specimens after Rolling	129
56	SEM micrographs of Explosive Forming Specimens	130

Hardness Plots

57	Plot for C1 at 1000 ⁰ C for 2 hr	131
58	Plot for C3 at 1000 ⁰ C for 2 hr	131
59	Plot for C2 at 1000 ⁰ C for 2 hr	132
60	Plot for C2 at 1000 ⁰ C for 2 hr	132
61	Plot for C4 at 1000 ⁰ C for 2 hr	133
62	Plot for C5 at 1000 ⁰ C for 2 hr	133
63	Plot for C6 at 1000 ⁰ C for 2 hr	134
64	Plot for C6 at 1000 ⁰ C for 2 hr	134
65	Plot for C1 at 1000 ⁰ C for 3 hr	135
66	Plot for C1 at 1000 ⁰ C for 3 hr	135
67	Plot for C2 at 1000 ⁰ C for 3 hr	136
68	Plot for C3 at 1000 ⁰ C for 3 hr	137
69	Plot for C3 at 1000 ⁰ C for 3 hr	137
70	Plot for C4 at 1000 ⁰ C for 3 hr	138
71	Plot for C5 at 1000 ⁰ C for 3 hr	139
72	Plot for C5 at 1000 ⁰ C for 3 hr	139
73	Plot for C6 at 1000 ⁰ C for 3 hr	140
74	Plot for C1 at 1000 ⁰ C for 4 hr	141
75	Plot for C2 at 1000 ⁰ C for 4 hr	141
76	Plot for C3 at 1000 ⁰ C for 4 hr	142
77	Plot for C4 at 1000 ⁰ C for 4 hr	142
78	Plot for C5 at 1000 ⁰ C for 4 hr	143
79	Plot for C6 at 1000 ⁰ C for 4 hr	143
80	Plot for C1 at 800 ⁰ C for 3 hr	144

81	Plot for C1 at 800 ⁰ C for 3 hr	144
82	Plot for C2 at 800 ⁰ C for 3 hr	145
83	Plot for C3 at 800 ⁰ C for 3 hr	146
84	Plot for C4 at 800 ⁰ C for 3 hr	146
85	Plot for C5 at 800 ⁰ C for 3 hr	147
86	Plot for C5 at 800 ⁰ C for 3 hr	147
87	Plot for C6 at 800 ⁰ C for 3 hr	148
88	Plot for C6 at 800 ⁰ C for 3 hr	148
89	Plot for C1 at 800 ⁰ C for 6 hr	149
90	Plot for C1 at 800 ⁰ C for 6 hr	149
91	Plot for C2 at 800 ⁰ C for 6 hr	150
92	Plot for C3 at 800 ⁰ C for 6 hr	150
93	Plot for C4 at 800 ⁰ C for 6 hr	151
94	Plot for C5 at 800 ⁰ C for 6 hr	152
95	Plot for C5 at 800 ⁰ C for 6 hr	152
96	Plot for C6 at 800 ⁰ C for 6 hr	153
97	Plot for C6 at 800 ⁰ C for 6 hr	153
98	Plot for C1 at 800 ⁰ C for 9 hr	154
99	Plot for C1 at 800 ⁰ C for 9 hr	154
100	Plot for C2 at 800 ⁰ C for 9 hr	155
101	Plot for C3 at 800 ⁰ C for 9 hr	155
102	Plot for C4 at 800 ⁰ C for 9 hr	156
103	Plot for C5 at 800 ⁰ C for 9 hr	156
104	Plot for C6 at 800 ⁰ C for 9 hr	157
105	Plot for C6 at 800 ⁰ C for 9 hr	157
106	Plot for C1 at 1000 ⁰ C for 4 hr after Rolling	158
107	Plot for C2 at 1000 ⁰ C for 4hr after Rolling	159
108	Plot for C2 at 1000 ⁰ C for4 hr after Rolling	159
109	Plot for C3 at 1000 ⁰ C for 4 hr after Rolling	160
110	Plot for C3 at 1000 ⁰ C for 4 hr after Rolling	160
111	Plot for C4 at 1000 ⁰ C for 4 hr after Rolling	161
112	Plot for C4 at 1000 ⁰ C for 4 hr after Rolling	162
113	Plot for C5 at 1000 ⁰ C for 4 hr after Rolling	162
114	Plot for C6 at 1000 ⁰ C for 4 hr after Rolling	163

115	Plot for C1 at 800 ⁰ C for 9 hr after Rolling	164
116	Plot for C1 at 800 ⁰ C for 9 hr after Rolling	164
117	Plot for C2 at 800 ⁰ C for 9 hr after Rolling	165
118	Plot for C3 at 800 ⁰ C for 9 hr after Rolling	165
119	Plot for C4 at 800 ⁰ C for 9 hr after Rolling	166
120	Plot for Explosive Forming Compact	167

LIST OF TABLES

Table No.	Name	Page No
Table-1	Nominal Composition of Cu-Al ₂ O ₃ Powders in four Layers	63
Table-2	Density of 1000 ⁰ C Specimens	64
Table-3	Density of 1000 ⁰ C Specimens	64
Table-4	Density of 1000 ⁰ C Specimens after Rolling	64
Table- 5	Density of 1000 ⁰ C Specimens after Rolling	65
Table- 6	Percentage Change in Density of 1000 ⁰ C Specimens during sintering	65
Table- 7	Percentage Change in Density of 1000 ⁰ C Specimens during Sintering	65
Table- 8	Electrical Conductivity of 1000 ⁰ C Specimens	66
Table- 9	Electrical Conductivity of 800 ⁰ C Specimens	66
Table- 10	Electrical Conductivity of 1000 ⁰ C Specimens after Rolling	67
Table- 11	Electrical Conductivity of 800 ⁰ C Specimens after Rolling	67
Table- 12	Percentage Change in Electrical Conductivity of 1000 ⁰ C Specimens, at Layer with Lower Alumina Content, During Sintering	67
Table-13	Percentage Change in Electrical Conductivity of 1000 ⁰ C Specimens, at Layer with Higher Alumina Content, During Sintering	68
Table- 14	Percentage Change in Electrical Conductivity of 800 ⁰ C Specimens, at Layer with lower Alumina Content	68
Table- 15	Percentage Change in Electrical Conductivity of 800 ⁰ C Specimens, at Layer with Higher Alumina Content, During Sintering	68
Table- 16	Reduction in 1000 ⁰ C Specimens after Rolling	69
Table-17	Reduction in 800 ⁰ C Specimens after Rolling	69
Table- 18	Hardness of 1000 ⁰ C Specimens	70
Table- 19	Hardness of 800 ⁰ C Specimens	71
Table- 20	Hardness of 1000 ⁰ C Specimens after Rolling	72
Table- 21	Hardness of 800 ⁰ C Specimens after Rolling	73

Table- 22	Compositions and Thickness for First Tube powders of Explosive Forming	74
Table- 23	Compositions and Thickness for First Tube powders of Explosive Forming	74

INTRODUCTION

In general, semiconductor circuit is devised such that the semiconductor circuit is carried on a ceramic substrate to efficiently discharge the heat generated in the semiconductor circuit to the outside in order to stabilize semiconductor characteristics.

In such an arrangement, when the heat is generated from semiconductor circuit in a relatively large amount, the ceramic substrate can not efficiently deal with heat by itself. For this reason, a heat sink made of copper or aluminium is attached to ceramic substrate by means of brazing or soldering. In the case of MPU and large capacity electric power IGBT, for example, an artifice is made so that a radiating fin is provided to forcibly release the heat.

The ceramic substrate is required to have high thermal conductivity in order to maintain characteristics of semiconductor circuit at high levels. Further, the ceramic substrate is required to have insulation property, shielding property and low dielectric property. On the other hand, heat sink is also required to have high thermal conductivity. Usually, both of ceramic substrate and heat sink are designed to have thermal conductivity not less than 150 W/mK and have a coefficient of thermal expansion, which is approximate to the coefficient of thermal expansion of the semiconductor chip.

However, the brazing material or soldering material, which is used to join ceramic substrate and heat sink, has a coefficient of thermal expansion which is two fold or more as compare with those of ceramic substrate and heat sink, and a coefficient of thermal conductivity which is 1/2 to 1/7 as compare to those of ceramic substrate and heat sink. For this reason, the joining section, at which the brazing material or soldering material is applied, has a low coefficient of thermal expansion. Further, the joining section undergoes large thermal expansion as compare to other section. A problem is pointed out that a considerably large stress is generated at the joining section, and the reliability of joining is lowered.

Moreover, it is also feared that the heat tends to be accumulated in the joint section, and it is impossible to effectively exhibit the function of heat sink. Therefore, it is necessary to provide a considerably large heat sink and considerably large radiating surface so that a large thermal gradient is always maintained. As a result, a problem arises in that a conventional arrangement can not respond to the requirement of miniaturization.

Recently, a Functionally graded material has been known, which is interlayered and provided with characteristics of the ceramic which is excellent, for example, in corrosion resistance, insulation performance, and high temperature durability and the metal which is excellent in toughness. Such a Functionally graded material is usually produced by preparing a laminated compact (including 10 or more layers, if necessary) in which the composition gradient differs, and moulding the laminated compact into a predetermined shape, followed by application of sintering treatment.

However, for example, the sintering temperature, the coefficient of thermal expansion, and the coefficient of thermal conductivity greatly differ between metal and ceramic. Therefore, following problem is pointed out. That is, even though the laminated material is made in multiple layers, when the metal and ceramic are simultaneously sintered, peeling may occur at the interface between the different compositions, or crack and breakage may occur. For this reason, conventional functionally graded materials are not suitable for practical use.

Moreover in the case of conventional functionally graded material, the laminated material is made in multiple layers while gradually changing composition. For this reason, inconvenience arises in that the moldable thickness is large, it is impossible to obtain a functionally graded material which has a thin thickness, and hence conventional functionally graded material is inferior in performance of wide use. If a conventionally functionally graded material involves the following problem. That is, production steps are complicated, numbers of steps are large, and production cost becomes expensive.

An additional problem is pointed out. That is, when the laminated compact consists of more multiple layers, the peeling tends to occur during press molding at the interface at which composition changed, and it is impossible to obtain any stable shape. Further,

order to obtain a desired shape, it is necessary to use a large amount of organic additive. Therefore, inconvenience arises in that the densification during sintering is inhibited, and the metal layer is badly affected.

Further, there is a difference in sintering temperature of 300^o C to 1000^o C between metal and ceramic. The densification for ceramic part does not proceed at a densifying temperature for metal layer. For this reason, if it is intended to apply heat up to, sintering temperature for the metal layer, the melting point of almost all metals are exceeded. As a result, a problem arises in that softening takes place, and it is impossible to maintain the shape.

The densifying temperature region for the metal is greatly different from the densifying temperature region for the ceramic, coefficient of thermal conductivity and thermal expansion of former are greatly different from those of latter. Therefore, the following problem is pointed out. That is, a large thermal stress occurs to cause warpage and breakage during the sintering, and hence the conventional functional gradient material is not suitable for practical use.

In this present work, the problem of large difference in coefficient of thermal expansion is tried to be minimized by fabricating a graded composite material. In such graded material, alumina content (in copper) varies in different layers from very low (1%Alumina) to higher side (10%Alumina). It is tried by using two techniques, powder metallurgy and explosive forming technique. Since Cu has got a melting point of 1083^o C and Alumina has got a melting point of 2060^oC, sintering of two is done in vacuum. Vacuum is also required to avoid oxidation of copper. Thermal conductivity has to be measured for this component. Optical Microscopy, SEM analysis, density measurement and hardness test has to be done for better understanding of the component.

Objective of Work

The objective of this work is to develop a heat resisting gradient material, which can withstand temperature gradient within it. One end of such gradient material would be insulator and other end conductor.

LITERATURE REVIEW

This chapter has been divided into two parts. First part deals with powder metallurgy technique and second part deals with explosive forming technique.

2.1 Powder Metallurgy Technique

2.1.1. Introduction of FGMs

It is now well known that abrupt transition in materials composition and properties within the component often result in sharp local concentration of stress. It is also known that these stress concentrations are greatly reduced if the transition from one material to other is made gradual [1]. These two considerations form the logic underlying the concept of functionally gradient materials (FGM's). By definition, FGM's are used to produce components featuring engineered gradual transitions in microstructure and/ or composition, the presence of which is motivated by functional performance requirements that vary with location within the part. While in the case of Graded material transition is not gradual but layered [1].

As a formulated concept and coordinated research thrust in the engineering of structural components, the term 'functionally gradient materials' originated in mid-1980s in Japan. A series of government reports addressing the anticipated materials needs of a strongly growing Japanese involvement in aerospace research. Focused on a space plane project and came to conclusion that many of the stringent requirements for elevated temperature structural components called for structure in which compositional and microstructural gradients are deliberately induced to (i) make best overall use of available materials for the production of components and (ii) avoid stress- strain concentration that arise at sharp interfaces separating different materials, as a consequent of applied stress and / or temperature excursions. The results of these finding was launched in 1987 of a vast programme on FGMs. It was focussed on the specific requirements of a part which is actively cooled on one side while facing a very hot environment on the other. The overall organization of the programme comprises processing, design , and evaluation of various inorganic composite system amenable to functional grading of metals and ceramics. For the hot surface, target service temperature where of the order of 2000K in an oxidizing

environment; ceramic materials were chosen for these regions. Near the cold surface, of the order of 1000K lower in temperature, strong tough and thermally conductive materials were selected. Between the two surfaces, metals or carbon matrix composite structures, featuring engineered gradients in matrix/ ceramic ratio, were to be produced using a series of processes, Among which powder metallurgy, chemical or physical vapour deposition, plasma spraying, and self propagating high temperature combustion synthesis were emphasized.

2.1.1.1. Processing of FGMs

(a) Conventional Solid State powder consolidation

In order to produce a metal- ceramic FGM by conventional powder processing, a preform body of powder containing the desired gradient in phase volume fractions is first fabricated. Provided that the mutual diffusion of constituent phases is negligible, this initial distribution of phases will remain stable throughout the process. This will generally be the case unless the FGM is very thin. An important exception, however, is that of interstitial such as carbon in iron. The powder preform is then densified following conventional solid state procedures, by cold pressing and pressure less sintering, by hot isostatic pressing, or by hot pressing in a closed die. All of these routes have been used for FGMs, with demonstrated success [1].

Discrepancies in sintering rate are much more drastic when the inclusion volume fraction becomes sufficiently high for significant percolation of inclusions to obtain. Above this volume fraction, the second phase can carry load, and, if it does not also densify, it resists contraction of the composite powder mixture. For densification of the composite, both percolating phases must then densify. We consider these two cases in turn, and discuss the transition from one to other.

Single phase densification of composites

With a non-percolating and non-densifying refractory phase, the rate of densification of a powder matrix is generally reduced. Inclusions alter both the initial powder packing density and the evolution of interparticle neck geometries, so as to require greater deformation of the matrix particles to reach a given compact density.

The retarding influence of inclusions on matrix densification can be significant, although the spread in sintering rates with varying inclusion volume fraction in the non-percolating regime is not dramatic. Discrepancies in sintering rate are none the less undesirable, as they cause warping and, potentially, cracking in the FGM during densification. These effects may therefore have to be taken into account in FGM densification. In particular, this requires relatively uniform initial powder density within the green compact: if powder blends are packed initially to different volume fractions, subsequent full densification will cause uneven shrinkage in the component, resulting in warping of the dense FGM.

Two phase densification of FGMs

When a continuous refractory phase is desired, it must also densify during the FGM consolidation process. Furthermore, to avoid gross deformation, especially in unconstrained sintering, it becomes necessary that two phases present densify at the same rate. The deleterious effect of even slight differences in local sintering rates on sample morphology is clearly shown experimentally by Mizuno et al[2].

Achieving sintering rate uniformity across a wide span of volume fractions of two phases is a considerable challenge, because sintering rates vary significantly with the nature and properties of each phase; in particular, ceramics generally densify far slower than metals. Oxides, which have a higher level of ionic bonding and lower sintering temperatures, were retained as better candidates. For metallic-component, on the other hand, the higher end of possible sintering temperatures has to be considered. With commensurate sintering temperature ranges, fine-tuning of sintering kinetics must be accomplished such that the two powders densify at the same rate under identical temperature and pressure conditions.

(b) Coating Processes

Coating processes are constructive, in that full control can be exerted over the initial compositional gradation, often via a computer controlled gas or powder feeding devices.

(i) Plasma Spray Forming

When fed into a plasma flame, which can be created, using one of several possible plasma gun configurations, powder particle $\leq 100 \mu\text{m}$. dia. are very rapidly heated and accelerated. Considerable energy is conferred to the particles by the plasma flame, such that even very refractory materials are melted in this process; the chief cited limitation of this process is that material should not be allowed to decompose. The high velocity that is also characteristic of this process causes considerable flattening of the particles upon impact with a solid substrate. These features, especially when the process is carried out in low pressure or vacuum environments, enables the deposition of relatively low porosity coatings, reducing the need for subsequent processing.

(ii) Plasma Spraying Methods

In the plasma spraying method, the spraying source powder is transported to plasma jet by a torch nozzle. The molten source material is then sprayed on to the substrate to form a coating. There are mainly two types of plasma –sprayed FGM coatings; that is, the porosity-graded coating and Composition graded coating. Use of plasma spraying in the preparation of FGM coatings requires the clever design of an apparatus that provides a continuously changing the mixture ratio of the source powder transported to the torch nozzle.

Atmospheric Plasma Spraying Technique

Fukushima et al., (1990) developed a twin torch for use in FGM preparation. In this method two plasma torches are placed so that centerline of each torch is aligned to the point of spray deposition on the substrate. Two different source materials are sprayed from each nozzle simultaneously onto same spot on the substrate to obtain a coating of composite. Since each torch can be independently controlled for the required spray conditions for the required spray conditions, this method can easily use two source materials having widely differing melting points, such as metal and ceramic, to form an FGM coating.

Low Pressure Plasma Spraying Technique

Low Pressure plasma spraying is usually performed in an inert gas atmosphere such as Ar to restrain the oxidation of raw powder. To prepare an FGM, Shimoda et al. (1990)[4] developed a Low pressure plasma spraying gun with four ports. Ceramic and metal powders are simultaneously introduced into plasma jet using two ports each for each source material. On spraying under an atmospheric pressure of 26.7 kPa, they obtained a YSZ/NiCr FGM coating of thickness 1 mm on the Cu substrate using YSZ and Ni-20 wt% Cr powders.

(c) Physical Vapour Deposition

In the PVD method, a solid source material is energized using different kinds of energy source to obtain vaporized particles, which deposit on a substrate to form a film. There is also a technique to accomplish chemical reaction of the vaporized particles in a gas phase. The deposition speed of the PVD method is rather slow. Therefore only a thin FGM film can be produced using this method. However, since this technique does not require high temperature heating of the substrate, this method is preferred for the preparation of thin FGM films used in electronics.

PVD Methods

1. Electron Beam PVD Technique

Partially stabilized zirconia (PSZ) with a gradient density of 4.2-5 g/cm³ (70-84% theoretical) from the surface to the metal/ceramic interface has been prepared on a superalloy substrate by an electron-beam PVD technique.

2. Ion Plating Technique

HCD (hollow-cathode discharge) type PVD with Ar and C₂H₂ gases has been used to prepare a TiC/Ti FGM coating of a thickness between 10 and 15 μm on a Ti plate by changing the flow rate of C₂H₂ at 300^oC. High purity metallic Ti was used as the evaporation metal source. A TiN/Ti FGM prepared by a HCD technique showed a superior tone of golden color.

3. Activated Reactive Evaporation (ARE) Technique

Inoue et al., (1993)^[5] have successfully made an amorphous Al(Ti)N/hex Al(Ti)N FGM film. They used Al₈₀Ti₂₀ as the target for DC magnetron sputtering by changing the Ar and N₂ mixture ratios. The amorphous Al(Ti)N dispersoid is about 4 nm.

(d) Chemical Vapor Infiltration

The chemical vapour infiltration process, which evolved from the vapor deposition for surface coatings, uses porous materials such as ceramic bodies and ceramic cloths, which contain many residual pores. These materials are first placed inside a CVD furnace as a substrate. By decomposition or by chemical reaction of the source gases, a coating is deposited on the surface of the open-pore or the space inside of the porous substrate.

The construction of a combustor with a carbon fiber 2-D fabric can further improve its gas tightness by infiltrating its pores with SiC/C FGM. The SiC/C FGM is prepared by CVI using CH₄ and SiCl₄ gases at 1100-1500^oC and 1.3-13 kPa.

(e) Surface Chemical Reaction Methods

1. Chemical Gas Reaction Technique

In this technique the source gases are made to react on the surface or in the voids of a porous matrix, resulting in the chemical reaction products. The concentration of the end product continuously changes from the surface towards the inside by diffusion. This concentration gradient can be controlled by regulating the reaction temperature.

2. Surface Treatment Technique:

An FGM can also be obtained on the material surface by proper surface treatments such as Plasma treatment, nitridation, or carburization. Ion implantation of the material surface can result in the surface having FGM characteristics.

(f) Liquid Phase Methods

1. Solution Methods

Electrodeposition Technique

The electrodeposition technique is suitable for the production of thin-sheet, gradient metallic alloys. The composition or structure in the direction normal to the deposition surface can be continuously changed by either controlling the concentration of the metallic ions in the electrolytic solution or by controlling the electrical current.

Electroless plating Technique:

Osaka et al., (1990)^[6] obtained Co-Ni-Re-P film (composition ratio : 30-60-5-5) on a polyimide film substrate through the electroless plating technique. In the Co-Ni-Re-P film formed on the nonmagnetic NiMoP (thickness 30 nm) of an under layer, the initial deposit on the substrate exhibits a granular structure with a typical grain size of 10-20 nm. This initial deposit has an f.c.c structure and its orientation is random. The deposit formed at a later stage (i.e., the film surface layer), on the other hand, shows a columnar structure with a typical diameter of about 20-30 nm. Its structure is the h.c.p type and the <002> axis is oriented parallel to the deposition surface.

2. Sol-Gel method

A glass rod having a radially graded refractive index was prepared by using sol-gel method. This process employed the metal alkoxide of two binary systems $\text{Si}(\text{OCH}_3)\text{-Ge}(\text{OC}_2\text{H}_5)_4$ and $\text{Si}(\text{OCH}_3)_4\text{-Ti}(\text{O-n-C}_4\text{H}_9)$. Immersion of the rod-shaped wet gels in a neutral solution or acidic water solution results in leaching out of the dopant (Ge and Ti). The dopant left in the gels contributes to the formation of the concentration gradient. This concentration gradient remained in the densified glasses of $\text{SiO}_2\text{-TiO}_2$, as well as in the $\text{SiO}_2\text{-GeO}_2$ system. The FGM glass rods were obtained by drying and sintering of the leached gels.

3. Copolymerization Method

Koike et al. (1994)^[7] have prepared graded index-type polymer optical fiber using the Copolymerization method. The source materials for Copolymerization are methylmethacrylate (MMA) with a refractive index of 1.492, and benzyl methacrylate (BMA) with a refractive index of 1.562. First a polymer tube is prepared using poly-MMA. A monomer mixture of MMA and BMA is then added to this tube and circumferentially heated (60-80°C) to obtain polymerization. The inner wall of the polymer tubes swells, interacting with the monomer mixture, and interacting with the monomer mixture; and eventually a thin gel phase forms on the surface of the wall. Then the Copolymerization proceeds towards the center of tube. When the polymerization is completed a polymer solid is obtained that has a radially varied mixture ratio of two kinds of polymers from the center to the outer perimeter. The resulting solid has a radial distribution of refractive indices.

(g) Molten Metal Infiltration Methods

1. Sintered Porous body-Molten Metal Infiltration Technique:

This technique infiltrates molten metal into voids of a porous sintered body where the void fraction changes continuously from the surface of the body towards the inner body. During 1960s “graded turbine blades” were prepared by infiltrating a molten superalloy (Ni- or Co-based) into the TiC porous sintered body (density:60-80% theoretical) in a vacuum. These FGMs usually have high toughness at the outer superalloy portion and high creep resistance at the inner cermet portion.

2. Plasma Sprayed Porous Coating-Molten Metal Infiltration Technique

This method infiltrates molten metal into the pores by HIP. In this case the porous body with void fractions changing continuously from the surface to the inner body is prepared by plasma spraying. An SS/Cu FGM was produced using this method.

3. Centrifugal Casting Technique

The centrifugal force enables the ceramic powder mixed with a metal to create a gradient compositional distribution due to difference in the material density. A thick walled ring of SiC/Al FGM was fabricated by a centrifugal casting technique. In this technique, SiC powder (10 vol.%) is mixed with molten Al alloy at 900°C. This molten mixture is poured into the rotating mould and solidified to form an FGM.

(h) Solid Phase Methods

The powder metallurgical fabrication process accompanied by sintering is the most common solid phase process for the preparation of FGM. This process requires a proper compositional distribution of more than two kinds of solid source materials such as powder or fiber before sintering. The most common method involves the preparation of thin green sheets with different compositions, then laminating them according to the pre-designed compositional distribution profile to obtain a step-wise gradient the material's composition (thin green sheet lamination method). However, in recent times various compositional gradient mixing techniques for obtaining a continuous change in the composition have been suggested.

(i) Sintering Methods

1. Normal Sintering and High Pressure Sintering Techniques

On preparing FGM by sintering, cracks can often appear on the sintered body due to differences in the sintering characteristics and mixture ratio of the two source powders. Watanabe et al. (1994)^[8] controlled the shrinkage of the powder mixture by blending fine and coarse particle sizes.

Rabin and Heaps (1993)^[9] prepared six layered Al₂O₃/Ni FGM using the powder processing method. Graded compacts were produced by sequentially layering the powder mixture in the die followed by CIP at 140 MPa. The sintering was carried out at 1400°C for 3 h in Ar, or by HIP at about 1300°C for 1 h at a pressure less than 10 MPa. They concluded that for best quality FGM, careful selection and control of powder particle size ratio and preparation of a proper compositional distribution profile are necessary.

2. Temperature Gradient Sintering Technique

In preparing an FGM using source powders having a wide difference in their sintering temperatures (for example, ceramic/metal system), one sintering temperature cannot be used to obtain a good quality sintered body due to difference in shrinkage characteristics of each source powder. To overcome this problem, the portion containing more of the higher sintering temperature source is sintered at a higher temperature and the portion which contains more of the lowering sintering temperature. That is, the sintering

must be accomplished under a prescribed temperature gradient. One way to achieve this temperature gradient is to apply additional heat by use of a laser beam or infrared beam onto one side of the sample while it is in the sintering furnace.

It is possible to assign a gradient to the density by the use of temperature gradient sintering. Kawasaki and Watanabe (1990)^[16] sintered a cylindrical PZT powder compact in air for 1 h. They heated one side of the sample by an infrared lamp, and created a temperature gradient of 150°C within a depth of 5 mm from the sample surface. The resulting sintered body was of higher density in the upper portion, while the lower portion was of lower density. Such a density difference gives a continuous change in the piezoelectric characteristics within the material.

3. Plasma Activated Sintering Technique

In plasma activated sintering an instantaneous pulsed electric current is applied to the subject powder to initiate current discharges in the voids between the powder particles. Successful sintering can be accomplished by use of the heat generated by these discharges. Due to this current discharge, the powder surface is purified and activated. This method requires a relatively short time for sintering, and thus it is easier to control grain growth. This method is also suitable for sintering materials with lower melting points.

(j) Self-Propagating High Temperature Synthesis (SHS) Methods

This technique uses an exothermic reaction at temperatures exceeding 2000-3000°C to obtain reaction products at a relatively high speed. Because of its high-speed reaction the diffusion of atoms is prevented and thus it is possible to obtain a graded composition. When pressure (water pressure, gas pressure, etc.) is applied during the SHS process the synthesis of dense composites can be achieved.

1. Gas Reaction Sintering Technique

Ni powder and Al fine powder (0.42µm in diameter) are sintered in N₂ using the exothermic reaction of Al-N₂ to obtain AlN/Ni FGM. Using a similar technique, AlN/Al FGM can also be produced.

2. Hydrostatic Compression SHS Technique

TiB₂, Ti, B, and Cu powders are used as the source for preparation of TiB₂/Cu FGM by this technique. Using the automatic powder spraying and stacking device, these powders were sprayed onto a Cu substrate.

The stacked compact was then ignited at room temperature under a high hydrostatic pressure of 58 MPa. TiB₂/Cu FGM with diameter 30 mm and thickness 1 mm was obtained on the Cu substrate.

3. Gas-Pressure Combustion-Sintering Technique

First the source powders are formed into a compact by CIP at 250 MPa and sealed in a glass container under vacuum. This glass container is then embedded into the ignition agent consisting of Ti and C powders packed in a graphite crucible placed within the HIP apparatus. Next the container is heated to 700°C in Ar at 100 MPa and then the contents ignited. TiB₂/Ni, TiC/Ni, Cr₃C₂/Ni, and MoSi₂-SiC/TiAl FGMs are some examples of FGMs prepared using the gas-pressure combustion sintering technique.

(k) Martensitic Transformation Technique

Watanabe et al., 1993^[11] have attempted to prepare an FGM using crystallographic transformation. The paramagnetic phase in austenitic stainless steel (Fe-18Cr-8 Ni) transforms into the ferromagnetic α' martensitic phase by plastic deformation. The amount of martensite increases with increasing deformation (Strain). Thus the saturation magnetization of the deformed austenitic stainless steel increases with increasing strain. Using this phenomenon a magnetic gradient function can be assigned by inhomogeneously deforming the stainless steel.

(l) Diffusion and Reaction Techniques

A newly developed ceramic actuator was prepared by the diffusion bonding of two plates having different piezoelectric constants at 1200°C for 3-5 h. This attempt was made using the PZT-Pb (Ni_{1/3}Nb_{2/3})O₃ system. The compositionally graded material intermediate layer between the two plates tends to reduce the residual stress in the actuator, thus preventing crack formation. An FGM can be prepared by means of a chemical reaction on a material's surface. In an attempt to improve oxidation resistance of carbon material, a

carbon substrate was heated in silicon powder at 1450°C for 3 h to form a C/SiC FGM on the surface.

2.1.1.2. Methods of obtaining Compositionally Green Bodies

1. Powder Stacking Techniques

The pressing techniques are as follows: Using the proper materials (such as polymers, metals, and ceramics), two or more different powders or fibers are mixed at the desired compositional ratio. The mixture ratio is gradually changed in a die. Then pressure is applied to the mixture to obtain an FGM green body.

In the centrifugal technique a mixture of source powder is supplied to the centre of a rapidly rotating centrifuge. The mixture ratio of the powder is computer regulated. The mixture powder is deposited on the inner wall by the centrifugal source. For better stabilization of the concentration graded layer of the mixed powder, the deposited powder layer is preheated slightly and liquid, hot wax is injected before sintering. The FGM fabrication stages include: cold compaction, de waxing, and sintering.

In a spraying technique a powder suspension having a varied mixture ratio in ethanol solvent is sprayed using a roller pump or a compressed air nozzle on the preheated substrate. The resulting deposits are then dried to obtain FGM green body.

2. Powder Infiltration Technique

After the reduction of metallic chlorides by hydrogen, the metallic fine particles subsequently formed by chemical vapor reaction rate were infiltrated into ceramic powder packing. The control of gradients was accomplished easily by changing the purge gas flow rate and packing conditions.

3. Slurry Techniques:

During the slip casting technique source powders are mixed with water soluble binder or solvent binder to form a slurry. This slurry is then converted to a thin film by slip casting. An FGM green body is obtained by layering these films.

2.1.2 Detailed analysis of FGMs

An attempt has been made to produce Cu-Al₂O₃ composite powder with 20wt% Al₂O₃ and 35wt% Al₂O₃ by high energy ball milling. The nanocomposite powder was compacted and sintered in argon atmosphere at various temperatures. This work was focused on the densification and sintering aspects of the Cu-Al₂O₃ nano composite powder. From peak broadening of XRD patterns it was evident that with increase in milling time, the crystallite size reduces. Because of the ball-powder-ball collisions the ductile copper got flattened and the brittle oxide particles entrapped in it. On further milling the copper particle got work hardened and consequently the structure is refined. The decrease in crystallite size with increase in strain is quite evident. The microstructure observed in TEM, reveals fine Al₂O₃ particles of the order of 10nm dispersed in Cu matrix [12].

The influence of copper content upon the mechanical properties has been investigated based on observed microstructural characteristics. The composite fabricated by reducing and hot pressing of an Al₂O₃/ CuO powder mixture revealed that the nano-sized Cu particles were mostly intergranularly dispersed in Al₂O₃ matrix. The addition of Cu particles has resulted in the grain growth inhibition of the Al₂O₃ matrix. With increasing Cu content, the composite has shown increased fracture toughness and inhomogeneous microstructure due to the agglomeration of Cu particles. The Al₂O₃/ 2.5 and 5 vol% Cu composites have shown maximum fracture strength of 820MPa, which was 1.5 times larger than that of the monolithic Al₂O₃. The increase in fracture strength was explained by the decrease in matrix grain size and microstructural homogeneity [13].

Chemical interactions between Al₂O₃ and Cu have been investigated to be very weak. The surface oxidation of metallic coating leads to the formation of Cu₂O. The sintering study shows that the main parameters controlling the shrinkage are the sintering temperature and the heating rate in relation to oxygen partial pressures that are smaller than 1025 bar. For the higher temperatures investigated (above 1250^o C) a large shrinkage has been observed. The microstructure may lead to high mechanical properties due to the needle like shape of the CuAlO₂ grains [14].

Coating plays an important role in the compaction of powder during FGMs preparation. In the investigations it has been found that, coated powders containing

composites, shrink during sintering and reach an almost dimension stability. In the study of Ni-SiC/Al₂O₃ it was found that . Lack of both wettability and solubility of SiC and Al₂O₃ (uncoated powders) with copper prevent densification by grain shape accommodation and solution-reprecipitate. Uncoated powders of either SiC or Al₂O₃ had higher porosity content due to the lack of wettability [15].

Resistance sintering performances of copper powder mixed with alumina particles has been examined, including effect of post electrification pressing. Simultaneous joining of composites to a SUS 304 stainless steel disc and forming in the sinter process have been also attempted from the standpoint of effective use of heat and pressure. Results obtained were summarized as follow: (1) green compacts containing alumina particles up to 40wt% were able to be resistance sintered, and post electrification pressing increase the density of the sintered compacts (2) the simultaneous joining of composites to the stainless steel was successfully performed when heat input was sufficient, and post electrification pressing operated to increase the bond strength, and (3) the simultaneous forming of composite was possible when green compact was sufficiently under low pressure [16].

Al₂O₃/Cu nanocomposite has been fabricated by pulse electric current sintering (PECS) with a fast heating rate. Effects of Cu dispersion, on the microstructure and fracture toughness has been investigated. nanocomposite powders with crystallite size of about 25 nm were successfully synthesized by a high-energy ball milling process. This process resulted in the nano-sized Cu particles uniform distribution and they were situated on the grain boundaries of Al₂O₃ matrix [17].

Reduction sintering has been used for preparation of Cu/Al₂O₃ FGM. Two powder mixtures of Al₂O₃ and CuO or Cu-nitrate have been used to obtain Al₂O₃/5 vol% Cu composites. Microstructural investigations for the composite from Al₂O₃/Cu-nitrate have showed that fine Cu particles, about 150 nm in diameter, were homogeneously distributed within the Al₂O₃ matrix grains and at the grain boundaries. Fracture toughness of 4.8 MPam^{1/2} and strength of 953 MPa have been measured for the composite. The toughening and strengthening of the composites have been explained by the crack bridging/deflection and the refinement of the microstructure, respectively [18].

The influence of impurities the interfacial interactions has been investigated. Thin films of MO and W have been deposited on AlN and Al₂O₃ substrates by medium-energy, energy ion beam assisted deposition (IBAD) and e-beam evaporation. The interdiffusion of interfacial atoms at elevated temperatures have been investigated [19].

We use ceramic materials in fabrication of FGMs. Compaction behavior is an important powder property and it dictates the nature of the green compact ejected out of the die. A thorough understanding of powder behavior in a die during compaction enables the production of a defect free green compact of required density and is dependent on several factors such as the inherent hardness of the constituents of the powder, particle shape, internal porosity, particle size distribution and lubricants. For a basic understanding of powder compaction, an analytic equation of state would be desirable. However the information required for such purpose includes the flow properties of powders under stress, stress or pressure distribution within the compacts, the distribution of particle to particle stresses and the distribution strength of ceramic powder particles. Because of the unsolved analytical problems, several empirical equations using curve fitting methods have been proposed for understanding the densification behavior of powder compacts. Compaction study has been performed on magnesia, zirconia and titania ceramic powders [20].

Effects of sintering time, peak temperature, heating rate, and binder system on the sintered density of alumina compacts have been modeled using statistical methods. The traditional polyvinyl alcohol/polyethylene glycol (PVA/PEG) binder system produced more spherical spray dried granules and higher sintered densities than systems including hydroxylethylcellulose and 20,000 molecular weight PEG. The effects of sintering time, temperature, and ramp rate have been described with a partial quadratic model [21].

The effect of small levels of porosity on superplastic behaviour had been examined using specimens subjected to HIP. This provided an effective way of controlling the density of ceramic materials while avoiding appreciable grain growth. Results showed that low density specimens tended to have higher superplastic elongations to failure than higher density specimens. In the latter case, long cracks developed during deformation and grew perpendicular to the tensile axis; this led to premature failure. The uniformly distributed pores in the lower density specimens provided sites for both crack initiation and crack arrest, leading to a large number of short cracks, and to higher failure strains. TEM

observations gave evidence of significant dislocation activity in grain boundary regions of the deformed materials and this is tentatively interpreted in terms of the electronic contributions of the dopants to dislocation mobility [27].

Effect of particle size on the properties of FGMs has been investigated . In one study $\text{Al}_2\text{O}_3/\text{SiC}$ nanocomposites with a systematic variation in their SiC particle size together with monolithic alumina were produced using conventional powder processing, polymer pyrolysis and hot-pressing. All nanocomposites showed a clear increase in strength over similar grain size alumina but no clear dependence on the size of the SiC nano-reinforcement. However, the fracture toughness of the nanocomposites seemed to increase with the SiC particle size but with values little changed from the toughness of monolithic alumina as measured by the Vickers indentation technique. The surface and bulk flaw populations were characterized using a Hertzian indentation technique and a Griffith flaw size analysis of strength data. The investigations revealed a significant difference between the monolithic alumina and nanocomposites. The strength increase in the nanocomposites was explained by the observed decrease in both the surface and processing, flaw sizes, which further decreased with decreasing SiC particle size [23].

Role of residual stresses on the mechanical properties of FGMs have been investigated. It has shown that the stress relaxation can be responsible for the morphologies and spatial distribution of precipitates. Direct measurements of the residual stress were also emphasized and the influence of dislocations in the accommodation process and during interface crossing was exemplified. Residual stresses play a significant role on the mechanical properties of MMC [24].

Interfacial phenomenon has been investigated. Interfacial reactions have been found in Al–AlN composites. Alumina enriched surfaces of AlN particles reacted with the magnesium element of the Al alloys. This gave rise to the crystallization of numerous spinel crystals at the AlN interfaces. This can be detrimental for the mechanical behaviour if the Mg content is more than 3% as in the AlMg3-composite. A selective attack of AlN by the molten alloys was found. As a result, faceting of AlN interfaces was also observed. This was explained by surface energy consideration [25].

The influence of Ni coating on spreading kinetics and equilibrium contact angles of Al_2O_3 and SiC with liquid aluminum has been investigated. The effect of interfacial coatings on the wettability and reactivity of the liquid aluminum/ceramic couples has been revealed from sessile drop tests. The exothermic nature of the Ni–Al interaction together with the precipitation of new phases has been assumed to be an important factor on the wettability of coated ceramics. Nickel coatings applied to SiC and Al_2O_3 plates improved wettability with aluminum resulting from the dissolution of the coating in the liquid drop. Nickel coating led to the formation of intermetallics at the interface and the formation of aluminum–nickel eutectic zones in the drop. With the addition of nickel as a coating, there was no dissolution of SiC in the alloy, and interfacial carbon reaction products did not appear. The local reaction rates between the coating and liquid aluminum were actually so high that the spreading process was presumably controlled by local diffusion rather than chemical reaction kinetics [26].

The laser cladding technique has been used for preparation of FGMs. Laser cladding of Cu to alumina under different treatment conditions and gas medium has been investigated. The laser surface treatment of alumina substrates was conducted by injection of copper powder into the laser–substrate interaction region. Processing parameters included the laser power, the scan speed of the laser beam, the copper feed rate and heat treatments following the laser treatment. Laser treated alumina substrates and the alumina–copper system, which was treated in air and under argon, were studied. Possible reactions at the metal–ceramic interface were investigated. Sub-micron Cu particles were formed in the amorphous grain boundary glass, and CuAlO_2 phases were found in the alumina substrate after laser treatment [27].

New technique termed as gradient slurry disintegration and deposition has been used to fabricate FGMs. Gradient of SiC has been successfully made using this technique for starting weight percentage up to 20%. The results were confirmed using microstructural characterization techniques and microhardness measurements. Functionally gradient material synthesized using this method holds the promise where differential tribological characteristics and the strength/toughness combination may be required from the opposite surface [28].

In-situ powder metallurgy processing of functionally gradient material has been used. This technique uses a preceramic polymer binder system with the metal and / or ceramic powders have been used to produce the intermediate layers of the composite. The invention has also provided a method of controlling shrinkage of functionally gradient material during processing while still preserving the desired density of the intermediate layers by controlling the preceramic polymer binder content within the functionally gradient material.[29].

A functionally gradient material superior in Heat resistance, corrosion resistance and resistance to thermal fatigue has been prepared by distributing a third component having a lower young's modulus or formed of high strength material sufficiently durable to the fracture strength among ceramics as a first component to change the function [30].

A functionally gradient material having desired characteristics without having any joining section has been efficiently obtained by means of integration effected by a sintering treatment. Functionally gradient material was comprised with a metal part composition containing predetermined components based on a basic composition of tungsten and copper and a ceramic part composition containing predetermined components based on a basic composition of aluminium nitride and aluminium. The metal and the ceramic were integrated into one unit without providing any joining section to give a high joining reliability and high thermal conductivity [31].

A gradient material has been produced by molding and there after firing. A slurry which contained a plurality of groups of particles included at least a first group of particles and a second group of particles. The first group of particles comprised a group of nonmetal particles having a specific gravity ranging from about 3 to 7 and a maximum particle diameter equal to or smaller than a deflocculation limit. Said nonmetal particles were being made of an oxide, a carbide, a nitride and an oxynitride. The second group of particles comprised a group of metals particles having a specific gravity which was about 1.5 times the specific gravity of said first group of particles, and particle diameter distributed across the deflocculation limit. The gradient function material has been manufactured by preparing a slurry containing a plurality of groups of particles and / or a plurality of slurries and supplying the slurry or slurries into a porous mold, to form a deposited region in the porous mold, initially primarily influenced by way of attraction of porous mold and

subsequently primarily influenced by a deflocculating effect of the particles in the slurry or slurries or under the influence of gravity [32].

A method of manufacturing a dense and functionally gradient composite material has been provided. The method included steps of preparing a reactant compact made of composite materials, igniting the reactant compact so that a combustion wave was propagating on the reactant compact, and compressing the reactant compact while the temperature profile of the reactant compact was gradient to obtain the dense and functionally gradient composite material [33].

Colloidally processed submicron alumina powders have been used to investigate the effect of particle size distribution on their sintering characteristics. The results have shown that in the absence of agglomerates and macroscopic size segregation, a broader particle size distribution leads to two opposing phenomena during sintering—enhanced overall sintering characteristics and a higher degree of local differential densification. The former was a result of both the higher initial green density and smaller isolated pores in the final stage of sintering brought about by enhanced grain growth during the intermediate stage. The latter was promoted by a higher degree of variation in local particle packing and may negate the enhanced sintering effect at sufficiently broad particle size distribution. There therefore existed an optimum range of particle size distribution for best sinterability. Since the optimum particle size distribution may vary considerably even for a given powder system, depending on the compaction technique and conditions used, narrow size distribution powder was preferred to monosized or broad size distribution powders for high sinterability and microstructure control of powder compacts, provided that agglomerates in the starting powder were removed by appropriate means. For the agglomerate-free, submicron alumina powder system studied, the optimum particle size distribution was found to have a geometric standard deviation value lying in between 1.6 and 1.9 [34].

A gradient material has been produced by molding and there after firing. A slurry, which contained a plurality of groups of particles included at least a first group of particles and a second group of particles. The first group of particles comprised a group of nonmetal particles having a specific gravity ranging from about 3 to 7 and a maximum particle diameter equal to or smaller than a deflocculation limit. Said nonmetal particles were being made of an oxide, a carbide, a nitride and an oxynitride. The second group of particles

comprised a group of metals particles having a specific gravity which was about 1.5 times the specific gravity of said first group of particles, and particle diameter distributed across the deflocculation limit. The gradient function material has been manufactured by preparing a slurry containing a plurality of groups of particles and / or a plurality of slurries and supplying the slurry or slurries into a porous mold, to form a deposited region in the porous mold, initially primarily influenced by way of attraction of porous mold and subsequently primarily influenced by a deflocculating effect of the particles in the slurry or slurries or under the influence of gravity [32,34].

A method of manufacturing a dense and functionally gradient composite material has been provided. The method included steps of preparing a reactant compact made of composite materials, igniting the reactant compact so that a combustion wave was propagating on the reactant compact, and compressing the reactant compact while the temperature profile of the reactant compact was gradient to obtain the dense and functionally gradient composite material [33,34].

2.1.3. Introduction and Basic Properties of Copper [35]

Copper has been used by man for longer than any other metal for a continuous period of some 6,000 years, its application changing as the needs of the time changed and as more knowledge about its properties became available. The earliest metallurgical books provide much information about copper, and many mines in Europe have long histories of production going back to the 13th century and earlier. Throughout its history of some sixty centuries it has played an important part in the development of civilization. Its role has changed through the years and it has been a major industrial metal since the mid-nineteenth century, with an ever-increasing world production. The greatest impetus to copper production and to the determination of its properties was given by the development of electric power following Faraday's mid-nineteenth century researches. The high conductivity of copper, coupled with its availability in the form of strip and wire, made it the preferred material for power cables and electrical equipment of all kinds. Its applications will undoubtedly continue to change to meet new conditions and although it is not abundant element in the earth's crust, its future availability is not in doubt. Allied to its chemical and physical characteristics, its ability to form a wide range of copper base alloys

ensures its usage both in bulk and in a large number of small quantities. The atomic properties of copper are given in Appendix Table 1.

Some of the important properties of copper are discussed below.

Electrical properties [35]

The high electrical conductivity, exceeded only by that of silver, accounts for the major use of copper. Hence there is a great deal of information on this property and on the effect of impurities. In 1913, the standard conductivity of pure annealed copper was fixed by the International Electrotechnical Commission (IEC) as that of an annealed copper wire 1m long, weighing 1g and having a density of 8.89g/cm^3 . The wire exhibited a resistance of $0.15328\ \Omega$. This value was assigned a volume conductivity of 100 % of the International Annealed Copper Standard, written 100 % IACS (International annealed copper standard). It corresponds to a volume resistivity of $0.017241\ \Omega\text{-mm}^2 / \text{m}$.

Chemical properties [35]

Copper combines readily with many other elements and with acid radicles and therefore its chemical properties make it suitable for a wide variety of purposes. Its resistance to corrosion is high and this is reflected in the ability of the copper base alloys to resist attack, though there are, of course, many differences depending on exact composition and microstructure.

In dry air at normal temperatures copper becomes covered with a thin invisible film of cuprous oxide (Cu_2O) which enhances the resistance of the metal to further attack. The rate of oxide formation increases as the temperature rises and heating to 150°C gives a useful protective film. After exposure for longer periods the oxide is converted into complex basic salts, principally carbonates and sulphates, with color changing through reddish green, brown and blue to the well-known green patina of copper roofs after about 10 years. The patina is protective and means of forming it artificially have been developed.

It is not possible to prevent rapid oxidation above 200°C and heavy scaling occurs in processing unless protective atmospheres are used. In service, copper oxides rapidly at raised temperatures but some alloying additions reduce the oxidation rate by the

development of thin protective films: for example, additions of aluminium and silicon, but they reduce conductivity and the ease with which copper is cold worked.

Elasticity [35]

The elasticity modulus is an important property in design but it does not vary as widely as a result of working operations or alloying as do the mechanical properties. Appendix A Table 3 gives the values for soft copper and work hardened metal in the isotropic condition (that is, with grains oriented at random).

Mechanical properties [35]

The mechanical properties of the commercial grades of copper depend upon the composition and the degree of cold working, the range being shown in Appendix table 4. Copper is very malleable and a wide range of strength/ductility values can be obtained. The tensile strength of annealed copper is 215 to 245 N/mm², higher purity giving lower values. The strength of copper is increased by cold working which reduces its ductility. The properties of cast copper depend on the process used, sand castings having lower mechanical properties than chill cast metal. Hot- and cold-worked copper has a more dense and finer structure with correspondingly better properties. Annealing softens cold worked metal, the changes in strength and ductility.

Copper shows no definite yield point in a tensile test, being thus similar to other non-ferrous metals, and the 0.1 or 0.2 % proof stress is generally measured. The strength of the copper is the same in compression as in tension and the shear strength is taken as 60 % of the ultimate tensile stress. The high elongation and reduction in area values obtained in tensile tests on annealed copper indicate the ease with which it can be deformed. The hardness of soft copper is 45 on the Vickers scale and 40 Brinell, rising to 85/90 when cold worked.

Copper Alloy Systems [35]

Copper is the parent metal of a large family of alloys that have many properties closely allied to those of the metal itself and are important in wide-ranging applications in all the engineering industries. The principal alloy groups are:

Low alloyed coppers are basically the high purity metal with additions to improve certain properties without significant reduction in conductivity values. Examples are 1. Copper-

Oxygen 2. Copper-Sulphur 3. Copper - Selenium 4. Copper - Tellurium 5. Copper-Silver 6. Copper-Cadmium 7. Copper - Arsenic.

Brasses are copper plus zinc (upto some 45%), to which may be added other elements giving modified properties; in particular: iron, manganese and aluminium, which produce the high tensile brasses; and lead and magnesium which improve machinability.

Bronzes are copper plus tin (upto 12% in general), usually combined with other elements to form, for example, phosphor bronzes or the gunmetals which have zinc and, some nickel, additions.

Aluminium bronzes are copper plus aluminium (upto about 12 %), again with small additions of iron, manganese or nickel.

Cupro-nickels are copper plus nickel (upto 30%), sometimes with added iron.

Nickel silvers are copper plus zinc and nickel.

Cupro-silicon (silicon bronze) is copper plus silicon (about 3%, with iron or manganese).

Beryllium bronze is copper plus beryllium (about 2%).

Chromium copper is copper plus chromium (1% chromium).

Zirconium copper is copper plus zirconium (0.1%).

Copper - manganese is copper plus manganese (around 50%)

Precipitation hardening alloys [36]

The necessary condition for precipitation from solid solution is the existence of a sloping solvus line. Therefore precipitation occurs to some degree in almost all alloy systems and to a marked extent in hundreds of known cases. There is no doubt that virtually any metal can be made to precipitation harden by the addition of a properly chosen alloying element, and still further hardening should be possible in ternary or higher component alloys. Limited solid solubility is taken advantage of in several copper systems, most notably Cu- Be, Cu- Cr, and Cu-Zr. These systems contain alloys that can be precipitation hardened. The phenomenon, which is also called precipitation strengthening and age- hardening, is possible because the limit of solubility contracts with decreasing temperature, a condition known as retrograde solubility.

Few examples are illustrated with respective phase diagrams (equilibrium diagrams) in Appendix B.

by composition, cold working and heat treatment, all alloys showing the same general tendencies, namely:

- (a) Increasing amounts of alloying elements give increasing strength and hardness with decreasing ductility.
- (b) Increased cold working also results in increased strength and a decrease in ductility.
- (c) Annealing softens cold worked material and increases its ductility but may also cause unwanted increases in grain sizes.

Effects of temperature on mechanical properties [35]

Low temperatures have no ill-effects on the properties of copper and its alloys, virtually down to 0 K. As temperature is decreased the tensile strength and hardness tend to increase with no reduction, or even minor improvements, in ductility and toughness as measured by

the elongation and reduction in area or by the impact tests. Hence, they are used widely in cryogenic applications in the liquid air and liquid helium temperature ranges, design stresses based on normal temperature data providing an extra margin of safety.

Copper- base materials are not generally suitable for service at raised temperatures as they lose strength rapidly with increases in temperature, but again detailed information must be obtained from the literature. For some varieties of copper and some types of alloy short-term tensile tests show serious reductions in both strength and ductility at temperatures in the 400 to 500° C range. It is not always clear why such reductions in properties occur but reference to equilibrium diagrams may indicate whether structural changes are likely to occur as temperatures increase. Appendix B Fig. 4 shows the effect of test temperature on tensile strength of C15000 alloy.

Material was solution treated 15 min at 900°C, quenched, cold worked, and aged. The TH03 temper material was cold worked 54%, then aged 1 h at 400°C; the TH08 temper material was cold worked 84%, then aged 1 h at 375°C.

Long -term creep tests show that copper-base materials are not generally suitable for carrying sustained stresses for lengthy periods even at temperatures around 200°C. Copper is not used above 120°C and the brasses have an upper limit around 150°C. Usually creep tests have been based on the stress to produce 0.1 % plastic strain in 10⁴ hours. The

Oxygen 2. Copper-Sulphur 3. Copper - Selenium 4. Copper - Tellurium 5. Copper-Silver 6. Copper-Cadmium 7. Copper - Arsenic.

Brasses are copper plus zinc (upto some 45%), to which may be added other elements giving modified properties; in particular: iron, manganese and aluminium, which produce the high tensile brasses; and lead and magnesium which improve machinability.

Bronzes are copper plus tin (upto 12% in general), usually combined with other elements to form, for example, phosphor bronzes or the gunmetals which have zinc and, some nickel, additions.

Aluminium bronzes are copper plus aluminium (upto about 12 %), again with small additions of iron, manganese or nickel.

Cupro-nickels are copper plus nickel (upto 30%), sometimes with added iron.

Nickel silvers are copper plus zinc and nickel.

Cupro-silicon (silicon bronze) is copper plus silicon (about 3%, with iron or manganese).

Beryllium bronze is copper plus beryllium (about 2%).

Chromium copper is copper plus chromium (1% chromium).

Zirconium copper is copper plus zirconium (0.1%).

Copper - manganese is copper plus manganese (around 50%)

Precipitation hardening alloys [35]

The necessary condition for precipitation from solid solution is the existence of a sloping solvus line. Therefore precipitation occurs to some degree in almost all alloy systems and to a marked extent in hundreds of known cases. There is no doubt that virtually any metal can be made to precipitation harden by the addition of a properly chosen alloying element, and still further hardening should be possible in ternary or higher component alloys. Limited solid solubility is taken advantage of in several copper systems, most notably Cu- Be, Cu- Cr, and Cu-Zr. These systems contain alloys that can be precipitation hardened. The phenomenon, which is also called precipitation strengthening and age- hardening, is possible because the limit of solubility contracts with decreasing temperature, a condition known as retrograde solubility.

Few examples are illustrated with respective phase diagrams (equilibrium diagrams) in Appendix B.

Cu- Be system [35]

The Cu- Be equilibrium diagram is shown in Appendix B Fig. 1. Commercially important copper - beryllium alloys nominally contain less than about 2.5 wt % Be (0.15 at % Be). They are heat treated to remarkably high strengths in two steps. The first step involves solution annealing at temperatures above those defined by the retrograde solubility line, between 790 and 925° C (1450 and 1700° F) depending on composition, followed by quenching in water. The rapid drop in temperature inhibits formation of the beryllium- rich γ phase (body centred cubic, ordered phase) which, according to the phase diagram, is stable below the solubility line. Next, alloys are reheated to between roughly 300 and 500° C (575 and 930° F). This provides sufficient thermal energy to cause γ phase precipitation from microscopic regions known as Guiner- Preston zones, where local Be supersaturation is at its highest. The resulting fine precipitates are coherent with (bound to) the matrix copper. This coherence gives rise to strain fields surrounding each particle. The strain fields induce stresses that inhibit the movement of dislocations, thereby strengthening the alloy.

Cu-Cr system [35]

The copper - rich portion of the equilibrium diagram is given in Appendix B Fig.2 but the values given are not strictly definitive. The eutectic appears to be at 1070° C at about 1.5 % chromium. Solid solubility is low, falling from about 0.65 at 1070° C to 0.15 % at 800° C and less than 0.01 at normal temperature, thus providing the basis for solution and precipitation heat treatment operations.

The commercially available copper - chromium alloy contains 1 % chromium and is solution treated to give a conductivity of 45 % IACS followed by precipitation treatment to raise this to over 80 %. Tensile strength is increased by full heat treatment and the softening temperature to some 400° C, that is, twice that of cold worked copper. This alloy may be used in the as-cast and in wrought conditions.

Cu-Zr system [35]

Copper forms an eutectic system with the intermetallic compound $ZrCu_3$ which contains 32.87 % zirconium and melts at 1138° C. The relevant portion of the copper - zirconium equilibrium diagram is shown in the inset of Appendix Fig 3. It shows the eutectic point to be at about 12.9 % zirconium and 965° C. The solid solubility of $ZrCu_3$ is

low, falling from 0.15 %zirconium at 965° C to 0.08% at 900° C and less than 0.01 % at normal temperature.

Heat treatment involves quenching from temperatures between 850 and 900° C followed by precipitation in the range 375 to 450° C which may also involve cold working after solution treatment. The resulting alloy has a conductivity exceeding 90 % IACS with tensile strength at normal and raised temperatures superior to the usual copper- chromium alloys

Other commercially important alloy systems in which precipitation strengthening is exploited include copper-chromium-zirconium alloys. Alloys containing chromium, iron, or iron and phosphorus also benefit from the precipitation of second phases, but these materials are not normally heat treated in the same sense of the word.

Precipitation leaves the surrounding matrix nearly devoid of the precipitated element, thereby raising the matrix's electrical conductivity. Dilute precipitation - hardened alloys have, therefore, found extensive use in electrical and electronic applications ranging from resistance welding electrodes (Cu- Cr, Cu-Cr-Zr) to electrical/electronic connectors and lead frames (Cu-Zr, Cu-Be). The so-called "high conductivity" beryllium coppers were specifically designed for heavy-duty electrical/electronic connector applications.

American Society for Testing and Materials (ASTM) Standards

Copper and its alloys are divided according to two categories: UNS (Unified Numbering System) numbers C10 000- C79 999 for wrought copper alloys, and C80 000- C99 999 for cast copper alloys (ASTM, 1991). Within these two categories, the compositions are grouped into families of copper and copper alloys, as shown in Appendix table 5. Other national standards are also applied worldwide, e.g., BS (British Standard) in the United Kingdom or DIN (Deutsches Institut fur Normung) in Germany.

Properties Of Copper Alloys [35]

The mechanical and electrical properties of some of the relevant copper alloys are briefly described in this section. The average mechanical and electrical properties of low alloyed coppers are shown in Appendix A, table 6. Mechanical properties are determined

by composition, cold working and heat treatment, all alloys showing the same general tendencies, namely:

- (a) Increasing amounts of alloying elements give increasing strength and hardness with decreasing ductility.
- (b) Increased cold working also results in increased strength and a decrease in ductility.
- (c) Annealing softens cold worked material and increases its ductility but may also cause unwanted increases in grain sizes.

Effects of temperature on mechanical properties [35]

Low temperatures have no ill-effects on the properties of copper and its alloys, virtually down to 0 K. As temperature is decreased the tensile strength and hardness tend to increase with no reduction, or even minor improvements, in ductility and toughness as measured by

the elongation and reduction in area or by the impact tests. Hence, they are used widely in cryogenic applications in the liquid air and liquid helium temperature ranges, design stresses based on normal temperature data providing an extra margin of safety.

Copper- base materials are not generally suitable for service at raised temperatures as they lose strength rapidly with increases in temperature, but again detailed information must be obtained from the literature. For some varieties of copper and some types of alloy short-term tensile tests show serious reductions in both strength and ductility at temperatures in the 400 to 500° C range. It is not always clear why such reductions in properties occur but reference to equilibrium diagrams may indicate whether structural changes are likely to occur as temperatures increase. Appendix B Fig. 4 shows the effect of test temperature on tensile strength of C15000 alloy.

Material was solution treated 15 min at 900°C, quenched, cold worked, and aged. The TH03 temper material was cold worked 54%, then aged 1 h at 400°C; the TH08 temper material was cold worked 84%, then aged 1 h at 375°C.

Long -term creep tests show that copper-base materials are not generally suitable for carrying sustained stresses for lengthy periods even at temperatures around 200°C. Copper is not used above 120°C and the brasses have an upper limit around 150°C. Usually creep tests have been based on the stress to produce 0.1 % plastic strain in 10⁴ hours. The

copper-chromium and copper-zirconium alloys are the most creep-resistant high conductivity materials and the producers of copper alloys can generally supply detailed test data on their materials. Some typical creep data for these alloys are given in Appendix A table 7 and in Appendix B figures 5 and 6.

The influence of aging temperature and time on hardness and electrical conductivity of Cu-Cr has been studied. The properties are given in Appendix A table 8. Appendix B Figure 7 shows a plot of hardness variations after aging. It can be seen that for alloys with a chromium content below and above the limiting value alike it is possible to acquire an almost threefold increase in hardness compared with the solution treated condition.

Typical mechanical and electrical properties of C15710 (Cu- 0.2Al₂O₃) and C15720 (Cu-0.4 Al₂O₃) are given in Appendix A, tables 9 and 10 respectively.

2.1.4. Introduction And Basic Properties Of Alumina

Alumina is the most versatile engineered ceramic because of its high temperature service limit along with its chemical, electrical, and mechanical properties. It is also relatively low cost, is easily formed and finished using a number of fabrication methods. It is often compounded with silica or trace elements to enhance its properties pr fabrication and commonly will range from 92% to 99.8% Al₂O₃.

Alumina engineered ceramic parts can formed by single axis pressing, isostatic pressing, injection moulding, slip casting, or extrusion. Parts can “green machined” to near net size before firing and then “hard” ground using diamond tooling to tolerances less than 0.0002 (0.005 mm). Special grades of alumina can be metallized and/or brazed to metal parts. General property of Alumina has been given in Appendix A Table 11.

2.2 Explosive Forming Technique

2.2.1 Introduction [36]

Explosive forming has evolved as one of the most dramatic of the new metal working techniques. Explosive forming is employed in Aerospace and aircraft industries and has been successfully employed in the production of automotive-related components. Explosive Forming or HERF (High Energy Rate Forming) can be utilized to form a wide variety of metals, from Aluminium to high strength alloys. In this process the punch is replaced by an explosive charge. The process derives its name from the fact that the energy liberated due to the detonation of an explosive is used to form the desired configuration. The charge used is very small, but is capable of exerting tremendous forces on the work piece. In Explosive Forming chemical energy from the explosives is used to generate shock waves through a medium (mostly water), which are directed to deform the work piece at very high velocities.

Explosive forming was first documented in 1888. It was used in the engraving of iron plates. In this engraving, the explosive was placed in direct contact with metal, and the thickness of the explosive layer on the plate determined the depth of indentation made after detonation.

Over time, many other applications for explosives have been found. The research performed on the effects of explosives and shockwaves on metals has had its roots in military applications. During World War I and II, especially, many programs investigated such phenomena for the development of torpedoes and other weapons designed to attack armored vehicles.

The development of explosives, propellants, and other exothermic chemicals, has been intimately tied to military weapon development. The need for more powerful guns and projectiles drove research of propellants and mechanisms of explosives. The in-depth analysis of modern gun propellants has been crucial to explosive forming, and today's engineer will find these propellants both well characterized and readily obtainable.

As early as the 1950's, aerospace companies in the United States, such as Rocketdyne, Aerojet General Corporation, and Ryan Aeronautical were using explosive

forming for the manufacture of complex curved aerospace components. Explosive forming was especially important in the development of short-production-run missile components—particularly for the curved domes of missiles and rocket nose cones.

Other aerospace components were produced through explosive forming: complex corrugated panels for aircraft, and fuel filters and asymmetrical exhaust tubes for jet engines. During this time, the Soviet Union also began using explosive forming in their rocket industries for large curved panels.

2.2.2. Methods of Explosive Forming [36]

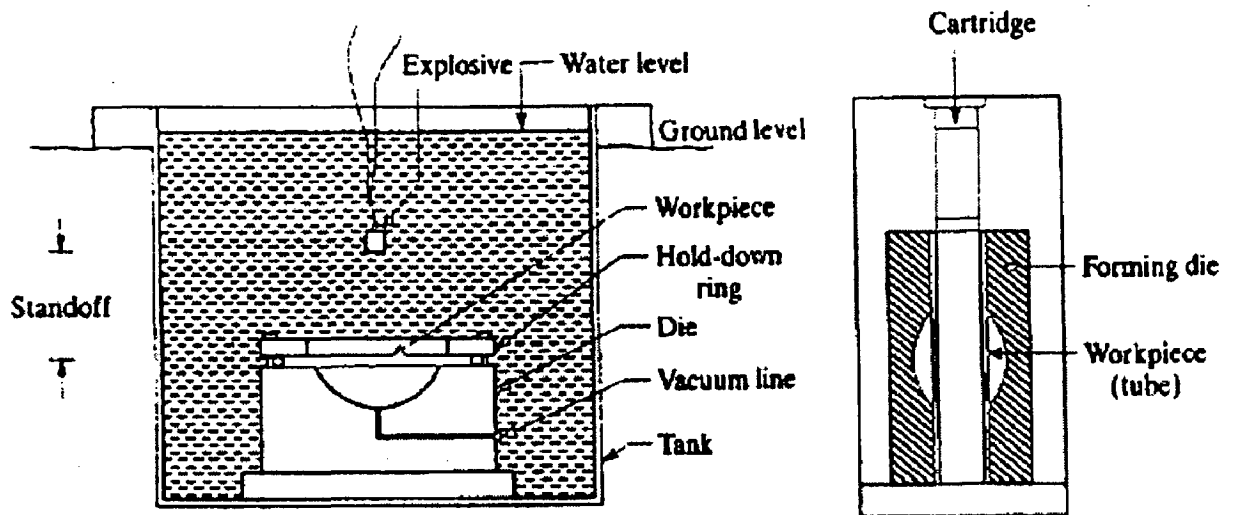
Explosive Forming Operations can be divided into two groups, depending on the position of the explosive charge relative to the work piece.

2.2.2.1 Standoff Method [36]

In this method, the explosive charge is located at some predetermined distance from the work piece and the energy is transmitted through an intervening medium like air, oil, or water. Peak pressure at the work piece may range from a few thousand psi (pounds/inch²) to several hundred thousand psi depending on the parameters of the operation.

2.2.2.2 Contact Method [36]

In this method, the explosive charge is held in direct contact with the work piece while the detonation is initiated. The detonation produces interface pressures on the surface of the metal up to several million psi (35000 MPa).



(a) Schematic representation of the explosive forming process (b) Illustration of confined method bulging of the tubes

Other forms of Explosive Metal Working

There are numerous types of metalworking done with explosives. This paper will focus only on explosive forming. However, some other metal working techniques are:

- Explosive welding
- Explosive cutting
- Explosive powder forming
- Explosive sheet lamination
- Explosive coating
- Explosive stress relieving
- Explosive compaction
- Explosive cleaning

2.2.3. Explosives

Explosives are substances that undergo rapid chemical reaction during which heat and large quantities of gaseous products are evolved. Explosives can be solid (TNT-trinitro toluene), liquid (Nitroglycerine), or Gaseous (oxygen and acetylene mixtures). Explosives are divided into two classes; Low Explosives in which the ammunition burns rapidly rather

than exploding, hence pressure build up is not large, and High Explosive which have a high rate of reaction with a large pressure build up. Low explosives are generally used as propellants in guns and in rockets for the propelling of missiles.

Features of Low and High Explosives [36]

Property	High Explosives	Low Explosives
Method of initiation	Primary HE-ignition, spark, flame, or impact	Ignition
	Secondary HE-detonator, or detonator booster combination	
Conversion time	Microseconds	Milliseconds
Pressure	up to about 4,000,000psi	up to about 40,000psi

+ Time required to convert, a working amount of high explosive into high-pressure gaseous products

Properties of Some Explosives [36]

<i>Explosive</i>	<i>Relative power %</i>	<i>Form charge</i>	<i>Detonation velocity, m/s</i>	<i>Energy, KJ/kg</i>	<i>Maximum pressure, C</i>
RDX (Cyclotrimethylene trinitramine, $C_3H_6N_6O_6$)	170	Pressed granules	8380	1270	23.4
TNT (Trinitrotoluene, $C_7H_5N_3O_6$)	100	Cast	7010	780	16.5
PETN (Pentaerythritol tetranitrate, $C_5H_8N_{12}O_{20}$)	170	Pressed granules	8290	1300	22.1
Tetryl (Trinitrophenylmethylnitramine, $C_7H_5O_8N_5$)	129	Pressed granules	7835	----	----
Blasting gelatin	99	Cartridge plastic	7985	1220	17.9

Advantages of Explosion Forming

- Maintains precise tolerances.
- Eliminates costly welds.
- Controls smoothness of contours.
- Reduces tooling costs.
- Less expensive alternative to super-plastic forming.

2.2.4. Die Materials [36]

Different materials are used for the manufacture of dies for explosive working, for instance high strength tool steels, plastics, concrete. Relatively low strength dies are used for short run items and for parts where close tolerances are not critical, while for longer runs higher strength die materials are required. Kirksite and plastic faced dies are employed for light forming operations; tool steels, cast steels, and ductile iron for medium requirements.

Material of Die	Application Area
Kirksite	Low pressure and few parts
Fiberglass and Kirksite	Low pressure and few parts
Fiberglass and Concrete	Low pressure and large parts
Epoxy and Concrete	Low pressure and large parts
Ductile Iron	High pressure and many parts
Concrete	Medium pressure and large parts

Characteristics

- Very large sheets with relatively complex shapes, although usually axisymmetric.
- Low tooling costs, but high labor cost.
- Suitable for low-quantity production.
- Long cycle times.

2.2.5. Transmission Medium [36]

Energy released by the explosive is transmitted through medium like air, water, oil, gelatin, liquid salts. Water is one of the best media for explosive forming since it is available readily, inexpensive and produces excellent results. The transmission medium is important regarding pressure magnitude at the work piece. Water is more desirable medium than air for producing high peak pressures to the work piece.

2.2.6. Formability Aspects [36]

Formability has been defined as the ability of a sheet metal to be deformed by a specific sheet metal forming process from its original shape to a defined shape without failure. In normal explosive forming operations, the major characteristics of the work metal that determine formability are ductility and toughness. It is general practice not to exceed the elongation, as determined by the tension testing, in forming a part from the same metal. Following table shows the comparison of the formability of some metals, using annealed aluminium alloy 1100 as a basis.

2.2.7. Analysis of Explosive Forming [

The effect of explosive pad thickness and related parameters such as impact energy imparted to the powder and ratio of explosive mass to powder mass on the density of compact have been investigated. Microstructural variations, with respect to processing parameters have been also investigated. After detailed investigation it has been found that metal matrix composite can be compacted using explosive compaction without any need of expensive machinery. The densification in metal matrix composite can be described in term of explosive pad thickness, the ratio of explosive mass to powder mass or impact energy. Any increase in pad thickness from optimum resulted in decrease from highest density. Peak hardness was increased and peak ageing time was decreased by the presence of SiC reinforcement. Explosively compacted and then rolled composite compacts had equivalent mechanical properties to those produced by vacuum hot pressing and rolling [37].

Ball-milled and fully disordered intermetallic powders of iron aluminide and titanium trialuminide (Al_3Ti) have been stabilized to cubic structure by alloying with Mn. Properties of compacts of hot pressing and explosive shock wave compaction [38].

A new process, impeller-dry-blending, which offers the possibility of producing large bulk-FGMs of a wide range of controllable continuous gradients and compositions, has also been used. This study has demonstrated the viability of the impeller-dry-blending process for producing linear- gradient continuous bulk FGMs. Impeller-dry-blending processing times were in the order of 1 cm/min, i.e. very rapid. Hydrostatic-shock-forming trials are in the early stages, but the process shows promise. The stainless steel–silicon carbide and copper–silicon carbide FGM systems of this study were merely representative of the potential of this impeller-dry-blending/ hydrostatic-shock-forming approach. There are many electrical/thermal ceramic FGM systems with commercial applicability that can be investigated in future studies [39].

Investigations have shown that nano-ceramics, grain sizes below 100nm, have special properties: high hardness, low friction and very small pores. This is difficult to retain during conventional processing. It was suggested that this problem could be solved by explosive compaction. Explosive compaction of nano- Al_2O_3 has shown that near-full density could be attained. Electron microscopy showed that phase transitions occurred and sub-grain size diminished [40].

2.3. Concluding Remarks

Detail analysis of literature survey encourages us to proceed toward our objective of synthesis of copper- alumina graded material. It shows that feasibility of synthesis of copper – alumina graded material is very good. Powder metallurgy technique and explosive forming technique both have got good potential for synthesis of such graded material.

Problems in synthesis of this material is found to be large difference in melting point, coefficient of thermal expansion, oxidation problem of copper powder, clustering of alumina particles etc.

FORMULATION OF PROBLEM

By definition, FGM's are used to produce components featuring engineered gradual transitions in microstructure and/ or composition, the presence of which is motivated by functional performance requirements that vary with location within the part. While in the case of Graded material transition is not gradual but layered. The variation in composition/ microstructural parameters leads to the variation in the property/ properties or functions of interest allowing the material to withstand different service conditions, at the same time across the cross-section.

In recent times, various fabrication methods have been employed for the fabrication of FGMs and these methods include solidification processing, spray atomization, codeposition, chemical vapour deposition and powder metallurgy techniques. These techniques besides having their suitability for certain specific application suffer from one or more of the following limitations.

1. low thickness of functionally gradient bulk material.
2. low deposition rate
3. complex process requirement
4. high cost of the manufacturing process

The principle object of present study is provide a method for producing FGM in which a metal composition gradient ceramic composition gradients are reliably integrated into one unit by means of simple production steps. In the present study it is proposed to go through powder metallurgy and explosive forming methods, where one is able to overcome the limitations out lined above and at the same time offer an attractive, reliable and inexpensive way of fabricating FGMs that allows bulk production of large parts. The processes involve mixing of reinforcing particles and matrix particles followed by compaction and sintering. To get a gradient, layers with different reinforcement particles content were stacked one above other.

It is proposed to combine copper as matrix and alumina as ceramic reinforcement phase. Alumina as a insulator, hard wear resistance ceramic and copper as a conductive,

tough metal, are graded along the thickness of compact. Two sintering parameters time and temperature is to be varied.

Same kind of stacked powder layers are to be compacted by explosive forming technique. Two processes are to be compared in term of economy and potential for application.

EXPERIMENTATION

This chapter has been divided in two parts. First part deals with powder metallurgy technique and second part deals with explosive forming technique.

3.1. Powder Metallurgy Technique

3.1.1. Mixing of Powders

The materials used in the experiments are 99.6% pure copper powder of 45-75 μm (sieve Analysis) and 99.8% pure alumina of 10 μm (ACC grade).

Cu-Al₂O₃ powders were mixed in ball mill at a speed of 100rpm for 1.5hr. Mixing was performed with cylindrical alumina balls in toluene medium at a ball to powder weight ratio of 10:1. Wet mixing was chosen to avoid oxidation of copper powder. Ball mill mixing was followed by hand mixing in toluene medium to ensure proper mixing. During hand mixing 2-2.5% Camphor was used as binder. Benzene was used as solvent to dissolved camphor.

The nominal compositions of specimens investigated in this study are listed in Table 1. Each specimen contains four layers of different composition with varying Alumina content in copper. Layer thickness for each specimen has been taken 1mm each for three lower Alumina content and 2mm for higher Alumina content (ie 1mm,1mm,1mm,2mm).

3.1.2. Compaction of Powders

The powder mixtures were compacted into cylindrical pellets of 40mm diameter in a manually operated single acting hydraulic press at a pressure of 25kg (198MPa). Layers were stacked one above other in die before compacting, having layer with higher Alumina content at bottom.

3.1.3. Sintering of Compacts

Green pellets were preheated in vacuum of 10^{-4} - 10^{-5} MPa at a temperature of 300°C for 1hr. It is done to remove binder. After preheating pellets were sintered. Sintering

was done in vacuum of 10^{-4} - 10^{-5} MPa. Sintering was done at 1000°C for 2hr, 3hr and 4hr respectively also at 800°C for 3hr, 6hr and 9hr respectively. Sintering of pellets was followed by quenching with argon gas. Characterization, electrical conductivity and density measurement was done after each sintering cycle. The density of pellets was determined by Archimedes principle. Characterization was done by optical microscope and SEM analysis. Specimens of 1000°C for 4hr and 800°C for 9hr sintering cycle were rolled. Characterization, electrical conductivity and density measurement was done for each rolled specimens.

3.1.4. Measurement of Electrical Conductivity

Conductivity meter type 979 was used for electrical conductivity measurements. After each sintering cycle specimens were cleaned with acetone and electrical conductivity was measured. Electrical conductivity was measured along diameters of the specimen point by point. Electrical conductivity was measured at the surface with layer of lower alumina content as well as at the surface with layer of higher alumina content. Before measurement of electrical conductivity, electrical conductivity meter was calibrated for 100%IACS electrical conductivity and 21.6%IACS electrical conductivity. It was done with help of pure annealed copper plate (100%IACS electrical conductivity) and brass plate (21.6%IACS electrical conductivity).

3.1.5. Optical Microscopy

Olympus Bx60m microscope was used for optical microscopy. A small portion of pellets was cut along thickness, from the periphery of circular pellets. These portions of pellets were used for optical microscopy and density measurement. The remaining pellets were used for further sintering. Cut portions were again cut into three parts. Middle parts were used for optical microscopy. Remaining two parts were used for density measurement.

The part for optical microscopy was grinded on the wheel grinder to make the surface flat and for rough grinding. In order not to alter superficially the structure specimens were kept cool by frequently dipping into water. After grinding, these parts were mounted on the mounting machine. For fine grinding, emery papers were used. After grinding on subsequent emery papers, fine polishing was done with help of polishing cloth. For fine polishing diamond paste was used as abrasive medium. After polishing on cloth,

specimens were directly characterized by optical microscope. Here we did not use any etchant as we were able to see a good microstructure. Micrographs were taken at 50x, 100x, 200x and 500x. Micrographs were taken both in bright field as well as in dark field.

3.1.6. Density Measurement

The density of pellets was determined by Archimedes principle. Remaining two parts were used for density measurement. Parts were cleaned with acetone before measurements. Care was taken to change water from earlier measurements. We used distilled water (milipore water) for our measurements. Balance was set to zero before taking weight in air and weight in water. Care was taken to remove bubble during measurements.

3.1.7. Hardness Measurement

Mounted samples after microscopy were used for hardness measurement. Vickers hardness tester with 2.5kg load was used for hardness measurement. Time given for indentation was 10 seconds. Measurements were taken at four points in each of four layers as well as three boundaries. Average of four points in each layers and boundaries was used for drawing the plots.

3.1.8. Rolling of Specimens

Specimens of 1000⁰C for 4hr and 800⁰C for 9hr sintering cycle were rolled. Specimens were cleaned with acetone before rolling. Specimens were passed through rolls until cracks were generated.

3.1.9. Scanning Electron Microscopy (SEM)

Mounted samples after microscopy were used for SEM analysis. SEM analysis was done using LEO 435-25-20 scanning electron microscope (SEM). SEM analysis was done along each layer as well as along the thickness of specimen. SEM analysis of powders of copper and alumina and rolled specimens was also done. Rolled specimens were examined for crack initiation and their size.

3.2. Explosive Forming Technique

In this technique Cu-Al₂O₃ powders were mixed as in Powder metallurgy technique. Here we have taken two hollow cylindrical MS tubes of 55mm and 40mm inner diameter respectively and 3mm wall thickness. Length of each tube was 100mm. Tubes

were open on both sides. We have taken two such set of tubes. Mixed powders were filled in 40mm inner diameter tube layer by layer. One side of tube was closed by exact fitting MS plug before filling powder into it. The composition of each layer and layer thickness has been given in Table. After filling powder other side of tube was closed by other exact fitting plug. This 40mm inner diameter tube was kept inside the 55mm inner diameter tube. 55 mm diameter tube was also closed by exact fitting plugs from both sides.

These sets of tubes were sent to Explofab Metals (India) Pvt.Ltd, Metal Cladding Division, Hyderabad. There they exploded these sets of tube in their own set up. After explosion MS tubes were removed by milling. Compacted materials were characterized by optical microscope and SEM analysis. Electrical Conductivity and density ^{or} was also measured.

RESULTS AND DISCUSSION

This chapter has been divided in two parts. First part deals with powder metallurgy technique and second part deals with explosive forming technique.

4.1. Powder Metallurgy Technique

4.1.1. Density of Graded Materials

From Table 2 and Table 3, density of graded material increases as sintering time increases. But from Table 6 and Table 7, Sintering rate decreases with sintering time. This increase in density and decrease in sintering rate with sintering time is as expected. This result is consistent for all graded specimens from C1 to C6 and for two sintering temperature, 1000⁰C and 800⁰C. Maximum sintering is achieved during first sintering cycle (Table 6 and Table 7). Specimens subjected to 800⁰C sintering temperature have achieved more sintering during first cycle than 1000⁰C sintering temperature specimens. Reason is effective sintering time. It is more for 800⁰C sintering temperature specimens than 1000⁰C sintering temperature specimens for first cycle. Rate of decrease in sintering is more in 1000⁰C sintering temperature specimens than 800⁰C sintering temperature specimens during second and third cycles.

Figure 37 to Figure 42 shows hardness plots of specimens. From plot 1 to 6, linearity of composition C1 and C4 is 100% ($R^2=1$), linearity of composition C3 ($R^2=0.9797$) is more than C2 ($R^2=0.9657$), linearity of composition C5 and C6 is equal ($R^2=0.9888$) but more than C2 and C3. Comparison of densities in table 2 and table 3 shows that it follows same trend as linearity. C4 ($R^2=1$) is achieving maximum density in all three cycle for both sintering temperature. Density from C1 to C2 decreases, from C2 to C4 increases, from C4 to C5 decreases. Though R^2 values for C5 and C6 are same, density of C6 is more than C5. Reason could be higher Alumina content in C6.

Dependence of density on linearity of composition is as expected. Densification of material during sintering takes place by elimination of pores and vacancy. For this atoms

have to move from one position to other position. At 1000⁰C and 800⁰C movement of copper atoms is very vigorous but movement of alumina atoms is very less. It is due to melting point difference of copper (1083⁰C) and alumina (2060⁰C). As Alumina content increases, hindrance to copper atoms movement increases. Hindrance in motion of atoms can be marked by change in shape of pellets.

During sintering shape of pellets is changing from flat to concave. Surface of Layer with lower alumina content is taking a concave shape and surface of layer with higher alumina content is taking a convex shape. This shows that there is more shrinkage in layer with lower alumina content. If composition gradient is maintained in linear fashion, transition of atoms from one layer to next layer will be easy. But if there is abrupt change in composition, this will produce hindrance to motion of atoms and atoms can not move one layer to next layer easily. This will affect final density of materials. This effect is clearly visible in our results. As C1 and C4 follow linear curve its density is maximum among all. Although C1 and C4 both have same R² value (i.e 1) density of C4 is more than C1. Reason for this is given below.

Comparison of Table 2 and Table 3 shows that density of specimens at 800⁰C is more than density of specimens at 1000⁰C. Reason is more effective sintering time given to these specimens.

From Table 4 and Table 5, there is no significance increase in density. Generally after rolling density should increase, but here it is not increasing. Even for some of specimen it is decreasing. During rolling of specimens it is getting cracked. Due to presence of cracks in specimens we are not able measure actual density of specimens.

4.1.2. Electrical Conductivity of Graded Materials

From Table 8, Electrical conductivity of materials increases with sintering time. This increase in electrical conductivity is as expected. As sintering time increases vacancies get eliminated. Hence hindrance to motion of electrons decreases. But as sintering time increases rate of increase of electrical conductivity decreases (Table 12). It is also as expected, as densification rate decreases with sintering time.

In Table 8 we are getting a contradictory result. Although C4 have maximum density (Table 2) it shows lowest electrical conductivity among C1 to C5. C3 shows maximum electrical conductivity.

Particle size of copper and alumina is 45-75 μ m and 10 μ m respectively. Layer with lower alumina content will have maximum porosity. Hence there is porosity gradient in material with higher porosity at layer with lower alumina content and lower porosity at layer with higher alumina content. Also specimens are taking concave shape during sintering. Layer with lower alumina content is taking concave shape. From thermodynamics, Flow of vacancies during sintering will be from layer with lower alumina content to layer with higher alumina content. Due to change in shape of specimens there is creation of vacancies. Specimens with more curviness will have more vacancies. Curviness of material depends upon the composition gradient in different layers. Specimens with more curviness will have more vacancies at layer with lower alumina content.

From Table 8, C1 and C4, C2 and C5 have got almost same electrical conductivity. C3 has got maximum electrical conductivity. These results show that shape factor has got more dominating effect than others. Reason for lowest electrical conductivity of C4 among C1 to C5 is linear composition variation. It is taking much more curve shape than others.

Electrical conductivity of specimens at layer with higher alumina content decreases as alumina content of layer increases (Table 8). It is as expected. Alumina particles produce hindrance to the motion of electron which in term decrease electrical conductivity. This fact also provides a proof that layers with higher alumina content have lower porosity. C6 has got lowest electrical conductivity among C1 to C6. It is due to higher alumina content of layers.

Reason for highest density of C4 is linearity in composition gradient and higher alumina content in second, third and fourth layer. Due to higher alumina content porosity is less in such layer and due to linearity elimination of vacancies is easy. Due to linearity C1 has got similar density as C4 and due higher alumina content in all four layers C6 has also got similar density.

From Table 9, Electrical conductivity of materials increases with sintering time. This increase in electrical conductivity is as expected. Here also C3 has got highest electrical conductivity. But instead of C4, C1 has got lowest electrical conductivity. It is contradictory to results for 1000⁰C specimens.

During sintering of pellets at 1000⁰C, pellets were kept as surface with layer of higher alumina content at the bottom and surface with layer of lower alumina content at the top. While, during sintering of pellets at 800⁰C, pellets were kept as surface with layer of lower alumina content at the bottom and surface with layer of higher alumina content at top. After sintering of pellets at 1000⁰C, pellets have taken concave shape. While after sintering of pellets at 800⁰C, pellets are almost flat. While motion of vacancies is from layer with lower alumina content to layer with higher alumina content (i.e from bottom to top), motion of atoms is reverse (i.e from top to bottom). But due to gravity force motion of atoms is hindered.

Electrical conductivity from C1 to C3 increases then from C4 to C6 decreases. Lowest electrical conductivity of C6 is due to higher alumina content of layers. There is no general trend for electrical conductivity at with layer of higher alumina content.

Comparison of Table 8 and Table 9 shows that electrical conductivity of 1000⁰C specimens is more than 800⁰C specimens at surface with layer of lower alumina content. But there is no such trend for electrical conductivity at surface with layer of higher alumina content. Reason for lower electrical conductivity of 800⁰C specimens at surface with layer of lower alumina content is less densification of layer with lower alumina content. Second reason for lower electrical conductivity is recrystallization of materials at 800⁰C. From micrograph we can conclude that there is significant recrystallization in material. It is due to more time given to specimens at 800⁰C.

After rolling there is significance increase in electrical conductivity of specimens. It is a contradictory result. Generally electrical conductivity of material decreases after rolling. This decrease in electrical conductivity is due to increase in strain hardening of materials.

We are getting maximum theoretical density of 95.17%. Means we are still left with 5 to 6 % of vacancies. Presence of 5-6% of vacancies decreases electrical conductivity. But during rolling along with increase in strain hardening there is significance decrease in vacancies. Here increase in electrical conductivity due vacancies reduction is more dominant than decrease in electrical conductivity due to strain hardening.

4.1.3. Hardness of Graded Materials

From Table 18 and 19, Hardness of graded material is decreasing along layer with lower alumina content to layer with higher alumina content. There are two reasons for decrease in hardness. First reason is presence of porosity gradient at different layer, second particle size of alumina.

Presence of porosity gradient is due to flow of vacancies from layer with lower alumina content to layer with higher alumina content. It is also due to shape factor. As material takes curve shape there is formation of vacancies. We are getting maximum hardness at surface with lower alumina content. Although this layer has maximum porosity during compaction it is open to atmosphere. Rate of elimination of vacancies is more at this layer. Layer with highest alumina content is also open to atmosphere but due to higher alumina content rate of elimination of vacancies is slow. Even after third cycle hardness of layer with highest alumina content is almost same.

Hardness of materials is directly related to ability of second phase particle (i.e alumina) to resist the motion of dislocation. Alumina may form bohemite which has a very high sticking tendency. Due to clustering of alumina particles to each other particle size of alumina can increase above critical size.

There is large scattering in hardness value during first cycle. Scattering of hardness value decreases during second and third cycle. It is due to removal of porosity during subsequent cycle. Scattering in hardness value is due to uneven distribution of porosity.

From Table 20 and Table 21, Hardness of specimens increases after rolling. This is clear from hardness plot for C1 at 1000⁰C, C2 and C3 at 800⁰C. Reduction in hardness for other specimens is due to presence of cracks.

4.1.4. Reduction in Graded materials after Rolling

From Table 16 and Table 17, specimen C1 has got maximum reduction. C3 has got next maximum reduction among specimens at 1000⁰C. Maximum reduction in C1 is due to lower alumina content in four layers as well as linear composition gradient across thickness. C2 has got next maximum reduction after C1 among specimens at 800⁰C. C5 and C6 among specimens at 1000⁰C and C4, C5 and C6 among 800⁰C are tiered. Tearing of such specimens is due to higher alumina content in Layers.

4.1.5. Microstructure of Graded Materials

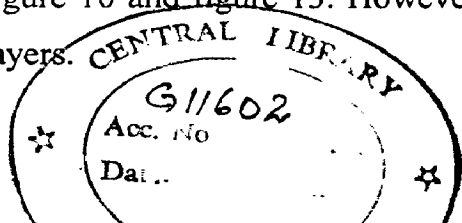
4.1.5.1. Microstructures of Sintered specimens

Figure 1 to figure 36 show microstructures of sintered specimens. In these microstructures white phase is copper and black phase is alumina and porosity present.

4.1.5.1.1. Microstructures of 1000⁰C Specimens

From figure 1 to figure 18, microstructures show that in the first cycle of sintering, boundaries are not present. It indicates present of porosity and poor joining of particles during sintering. Microstructures also show that distribution of alumina particles is not uniform in layers. Clustering of alumina particles is also visible in the first cycle of sintering. As alumina content, from C1 to C6 increases in successive layers clustering of alumina increases. Clustering of alumina is reason for decrease in hardness from layer with lower alumina content to layer with higher alumina content. Even scattering of hardness data during first cycle is also due clustering. Boundary between two layers is clear in First sintering cycle.

From figure 1 and figure 4, Comparison of first layer of C1 to first layer of C2 shows that it is denser than first layer of C2. This result is clearly visible in our results. Density of C1 is more than C2. Similar results can be derived by comparison of figure 7, figure 10 and figure 13. However, higher density of C4 is, due to densification of all four layers.



From figure 1 to figure 18, it is clear that during second cycle of sintering densification of material has taken place. Two or more copper particles have joined to form a single particle. Due to thermal agitation there is distribution of alumina particles. There is formation of grain boundaries also.

From figures, it can be seen that during third sintering cycle recrystallisation has taken place. Microstructures are very fine after third sintering cycle. Drastic decrease in rate of increase (Table 6), in electrical conductivity is attributed to fine microstructure. Recrystallisation in material was confirmed by observation of material at higher magnification.

From figure 7 and figure 10, comparison of third layer of C3 to third layer of C4 shows that C4 has more pores (more black area) than C3. As a result C3 showed higher electrical conductivity than C4. In the layers with higher alumina content, change in microstructure is marginal. It can be clearly observed in figure 18.

Profiles of boundaries between two layers show that movement of atoms is from layer with higher alumina content to layer with lower alumina content. It is in confirmation with our theory.

4.1.5.1.2. Microstructures of 800⁰C Specimens

From figure 19 to figure 36, observation shows that boundaries between two layers are not clear unlike 1000⁰C specimens. Presence of more black area in first layer after third cycle, indicate that porosities are present there. This is the reason that 800⁰C specimens show lower conductivity than 1000⁰C specimens.

Microstructures also reveal that densification of layer with higher alumina content is more than densification of layer with lower alumina content. This result is evident from figure 20 to figure 36 for C2 to C6. This is reason that electrical conductivity at the surface with higher alumina content is more for 800⁰C specimens than 1000⁰C specimens. In the 800⁰C specimens recrystallisation takes place at the layer with higher alumina content. While in case of 1000⁰C specimens it takes place at layer with lower alumina content.

There is very little change in the microstructure of layers with higher alumina content for 1000⁰C specimens.

4.1.5.2. Microstructures of Rolled Specimens

Figure 37 to figure 46 shows microstructures after rolling. From figure 1 and figure 37, first layer in figure in 37 has got more black area, it shows creation of crack in the material after rolling. There are more cracks in fourth layer (Higher Alumina content) than first layer (Lower Alumina content). From figure 37 and figure 42, we can see that there is elongation of microstructures after rolling direction. From figure 37 and figure 44, microstructures are similar. But C1 of 1000⁰C specimens has got higher reduction than C1 of 800⁰C specimens. This result shows that first layer of C1 in 800⁰C specimens have more cracks. Even C1 of 800⁰C specimens has gone less number of rolling pass. Creation of more cracks in fourth layer is attributed to higher content of brittle alumina.

4.1.6. SEM Analysis

Figure 47 to figure 52, show SEM micrographs of specimens. Figure 47, shows SEM micrographs of copper and alumina powders. Figures, 47(a) & 47(b) show micrographs of copper powder and Figures, 47(c) & 47(d) show micrographs of alumina powder. From these figures show that copper particle are spherical in shape while alumina particles are irregular in shape.

Figure 48 to figure 50, show micrographs of sintered specimens. Figure 48(a) shows very poor densification of fourth layer. Figure 48(c) shows network of alumina along grain boundaries. This network has been seen during optical microscopy under dark field examination. Figures 48(f), 49(d) & (e), show presence of porosity in material. Figure 49(c) shows distribution of alumina particles in the copper matrix. Figure 50(c) shows adjustment of, smaller copper particles and alumina particles, in between larger copper particles. Figure 50(e) shows that shape of copper particle is no more spherical.

Figure 51 and Figure 52, show micrograph of rolled specimens. Figure 52(a) presence of cracks in first layer (lower alumina content) and in fourth layer (higher alumina content). Figure 50(a) shows crack in first layer and figure 50(e) shows crack in fourth layer. Figure 50 (b), (c) and (d) show presence of cracks in second and third layer.

4.1.7. Concluding Remarks

In this technique two parameters (time and temperature) of sintering were varied. Firstly, temperature was kept constant (800°C) and time was varied (3hr, 6hr, 9hr). Secondly, temperature was increased (1000°C) and time was decreased (2hr, 3hr, 4hr).

Detailed analysis of optical microscopy and SEM show that maximum density of C4 among 1000°C & 800°C specimens is due linear variation of alumina content in four successive layers. First layer is getting more densification in 1000°C specimens. Maximum density of C4 of 800°C among 800°C & 1000°C specimens is due to effective densification in all four layers. Maximum electrical conductivity of C3 among 800°C & 1000°C specimens is due to more densification of first layer. Presence of porosity and distribution of alumina in different layers results in lower electrical conductivity. Rolling shows marked increase in electrical conductivity. But there crack formation in the material during rolling which create problems during density measurements.

4.2. Explosive Forming Technique

In this technique, two sets of tubes were taken. First tube contains six layers of powders (Table 22). Second tube contains ten layers of powders (Table 23). After explosion first tube results in no compaction of powders. It was due to faulty design of set up for explosion. Second tube gives a compact which shows a density of 8.2 gm/cm^3 . It does not show electrical conductivity. Reason for no electrical conductivity is porosity and higher alumina content.

Figure 126, shows hardness plot of explosive specimen. Hardness plot for explosive compact is in accordance with sintered compacts. Density is decreasing from layer with lower alumina content to layer with higher alumina content. But here hardness is more than hardness of sintered compacts. We are getting maximum hardness of 150 (VHN) at second layer and minimum hardness of 91.4 (VHN) at sixth layer, considering layer with lowest alumina (pure copper) content as first layer. Higher hardness value of explosive compacts compare to sintered compact is due to no clustering of alumina during explosive forming. First layer (pure copper) shows hardness of 148.25 (VHN). But hardness of annealed

copper is around 45 (VHN). This drastic increase in hardness indicates presence of internal stresses in the material.

Figure 47 to figure 49, show microstructures of explosive compact. From figure, boundaries between two layers are clearly visible. Uniform composition of powders can also be seen. Microstructures also show uniform distribution of alumina. Increase in alumina content in different layers is clearly visible from micrographs.

Micrographs of SEM analysis (Figure 56), confirm uniform compaction and layer wise increase in alumina content (figure 56(a) & (b)). Distribution of alumina is also good (figure 56(d)). Figure 56(c) shows that after compaction, copper particles are of almost same shape. It gives good density of 8.20 gm/cm^3 .

4.2.1. Concluding Remarks

Detailed analysis of explosive compacts shows that, this technique has got very good potential for synthesis of such graded materials. But design of the set up should be properly studied.

4.3. Comparison of Powder Metallurgy and Explosive Forming Technique

Powder metallurgy technique gives maximum hardness of 8.41 gm/cm^3 for 800°C specimens. Explosive forming gives compact hardness of 8.20 gm/cm^3 . Maximum electrical conductivity of powder metallurgy technique is 54.1%IACS while explosive forming technique shows no electrical conductivity. Reason for no electrical conductivity of explosive forming compact is higher alumina content present in successive layers (Table 23).

Explosive forming compacts were made in a single setup. Explosion of first tube results in no compaction of powder. Second tube, with powders of higher alumina content, results in a compact of density 8.20 gm/cm^3 . No compaction of first tube was due to uncontrolled force of explosion.

Hence, design of setup for explosion play an important role in the determination of properties of compacts. Characterization and properties measurements of second tube compact shows that explosive forming technique has got good potential for synthesis of graded material.

Copper alloy C15710, 99.8Cu-0.2Al₂O₃, shows electrical conductivity of 90%IACS(at 20⁰C) and density of 8.82 gm/cm³ [41]. Copper alloy C15720, 99.6Cu-0.4Al₂O₃ , shows electrical conductivity of 89%IACS (at 20⁰C) and density of 8.80 gm/cm³ [41]. These two data show that there is provision for improvement of electrical conductivity for these two techniques.

CONCLUSIONS

The following are the conclusions which are drawn based on the results obtained in the present study:-

1. Powder metallurgy and explosive forming techniques have been used for synthesis of Cu / Al₂O₃ graded composite.
2. Two parameters (i.e time and temperature) of sintering were varied. In First set of experiments temperature was kept constant (800⁰C) and time was varied (3hr, 6hr, 9hr).In the second set of experiments temperature was increased (1000⁰C) and time was decreased (2hr, 3hr, 4hr).
3. Specimens of 800⁰C set result in higher density (maximum density 96.19% of theoretical) than specimens of 1000⁰C set (maximum density 95.17% of theoretical). This is due to more time given to 800⁰C specimens for sintering.
4. Specimens of 800⁰C set result in lower electrical conductivity (maximum electrical conductivity of 48.9%IACS) than specimens of 1000⁰C set (maximum electrical conductivity of 54.1%IACS). Reason for lower electrical conductivity of 800⁰C set of specimens is placement of specimens in furnace during sintering. Layer with higher alumina content should at bottom for better electrical conductivity.
5. Variation in the properties of compacts is found to be related with variation of alumina content in four layers.
6. There is scattering in the hardness values due to presence of porosities. It reduces with increase in sintering time.

7. Hardness decreases from layer with lower alumina content to layer with higher alumina content. It is due to presence of porosities and clustering of alumina particles.
8. Explosive forming technique results in a compact with density lower than powder metallurgy compacts. It shows no electrical conductivity.
9. Explosive forming compact show higher hardness value than powder metallurgy compacts. It is due to presence of internal stresses after explosion. Hardness decreases from layer with lower alumina content to layer with higher alumina content.
10. SEM analysis and Optical microscopy reveals that explosive forming technique has got good potential for synthesis of graded materials.

SCOPE OF FUTURE WORK

Based on current study, it is suggested that work may be extended in following:

1. Powder metallurgy technique may be tried by varying layer thickness.
2. Powder metallurgy technique may be tried for higher alumina contents.
3. Powder metallurgy technique may be tried for different compaction load.
4. Reason for lower electrical conductivity may be due to use of binder and toluene as mixing media. Studies can be done on the effect of these materials on electrical conductivity of compacts.
5. Explosive forming technique has got good potential for synthesis of graded materials. Studies may be carried out for accurate setup design.
6. Explosive forming technique may be tried by varying layer thickness and alumina content from lower to higher.
7. Other techniques like infiltration technique, Electroless deposition technique etc, may be tried for comparison of techniques for synthesis of Cu / Al₂O₃ graded composite.

REFERENCES

1. Functionally graded metals and metal-ceramic composites: Part 1 Processing, A. Mortensen, S. Suresh, International Materials Reviews 1995, vol. 40, No. 6.
2. Functionally Gradient Materials, Y. Mizuno, A. Kawasaki, R. Watanabe, Metall. Trans., 1995, 26B, 75-79.
3. T. Fukushima, S. Kuroda, S. Kitahara: In proc. of 1st Int. Symp. on 'Functionally Gradient Materials', Sendai, Japan, 1990, Functionally Gradient Materials Forum, 145-150.
4. N. Shimoda, S. Kitagushi, T. Saito, H. Takigawa, M. Koga: In proc. of 1st Int. Symp. on 'Functionally Gradient Materials', Sendai, Japan, 1990, Functionally Gradient Materials Forum, 151-156.
5. Functionally Gradient Materials, S. Inoue, H. Uchida, Y. Tokunga, K. Takeshita, K. Koterazawa, J. Jpn Inst. Met., 1994, 58, 194-200.
6. D. Osaka, G. Barbezat: in 3rd Int. Symp. on 'Structural and Functional gradient materials', Lausanne, Switzerland, 1994, 123-128, Lausanne Presses Polytechniques et Universitaires Romandes.
7. H. T. Koike, T. Okumura, M. A. Okamoto, I. A. Nishida: in 3rd Int. Symp. on 'Structural and Functional gradient materials' Lausanne, Switzerland, 1994, 639-643, Lausanne Presses Polytechniques et Universitaires Romandes.
8. R. Watanabe, J. Takahashi, A. Kawasaki: in 3rd Int. Symp. on 'Structural and Functional gradient materials' Lausanne, Switzerland, 1994, 3-8, Lausanne Presses Polytechniques et Universitaires Romandes.
9. B. H. Rabin, R. J. Heaps: in 'Functionally graded materials', San Francisco, CA, Nov. 1992, Ceramic Transactions, vol. 34, 173-180; 1993.
10. A. Kawasaki, R. Watanabe: in proc. of 1st Int. Symp. on 'Functionally Gradient materials', Sendai, Japan, 1990, Functionally Gradient Materials Forum, 197-202.
11. Y. Watanabe, Y. Nakamura, Y. Fukui, K. Nakanishi: J. Mater. Sci. Lett., 1993, 12, 326-328.
12. Sintering of Cu-Al₂O₃ Nano - Composite Fabricated by Ball Milling T. Venugopal, B. S. Murty, K. Prasad Rao: in proc. of Symp. on 'Advanced materials and Technology', Bombay, 2003, A24, 1-5.
13. Processing And Properties Of Copper Dispersed Alumina Matrix Nanocomposite, Sung-Tag Oh, Mutsuo Sando, Tohru Sekino and Koichi Niihara

- Nano-Structured Materials, vol 10, no 2, pp-257-72, 1998.
14. Fabrication and Mechanical properties of 5vol% Copper Dispersed alumina nanocomposite, Sung-Tag Oh, Tohru Sekino and Koichi Niihara
J. Eur. Cera. Soc. 18(1998) 31-37.
 15. Copper Matrix Sic And Al₂O₃ Particulate Composites By Powder Metallurgy Technique, S.F. Moustafa, Z. Abdel-Hamid, A.M. Abd-Elhay
Materials lett. 53 (2002) 244-249.
 16. Application of Resistance Sintering Technique To Fabrication Of Metal Matrix Composite, S. Maki, Y. Harada, K. Mori, Journal of materials processing technology, 119 (2001) 210-215.
 17. Synthesis of Cu Dispersed Al₂O₃ Nanocomposites By High Energy Ball Milling And Pulse Electric Current Sintering, Young Do Kim, Sung-Tag Oh, Kyung Ho Min, Hyeongtag Jeon and In-Hyung Moon, Scripta mater. 44 (2001) 293–297.
 18. Fabrication of Cu Dispersed Al₂O₃ Nanocomposites Using Al₂O₃/CuO And Al₂O₃/Cu-Nitrate Mixtures, Sung-Tag Oha, Jai-Sung Leea, Tohru Sekinob and Koichi Niiharab, Scripta mater. 44 (2001) 2117–2120.
 19. Investigation of Diffusion Across the Interface Between Metal Films And AlN or Al₂O₃ Substrates, Xiangjun He, Si-Ze Yang, Kun Tao, Yudian Fan, Materials Lett. 1997) 175-179.
 20. A Compaction Study On Ceramic Powders, K.N. Ramakrishnan, R. Nagarajan, G.V. RamaRao, S. Venkadesan, Materials Lett. 33 (1997) 191-194.
 21. Optimization of the Sintered Density of Aluminum Oxide Compacts, C.A. Say, D.A. Earl, M.J. Thompson, Materials Lett. 53 (2002) 262–267.
 22. Superplasticity Of Ceramic Materials and their Effect of Initial Porosity and Doping On The Superplastic Behaviour Of Alumina, Z. C. Wang, T. J. Davies, N. Rridley and A. A.Ogwu, Acta mater. Vol. 44, No. 1 I. pp. 4301-4309. 1996.
 23. Silicon Carbide Particle Size Effects In Alumina-Based Nanocomposites, L. Carroll, M. Sternitzket and B. Derby, Acta mater. Vol. 44, No. 11, pp. 4543-4552, 1996.
 24. Influence Of The Elastic Stress Relaxation On The Microstructures And Mechanical Properties Of Metal–Matrix Composites, J. Douina, P. Donnadieub, A. Finela, G.F. Dirrasc, J.F. Silvaind, Composites: Part A 33 (2002) 1397–1401.
 25. New Al–AlN Composites Fabricated By Squeeze Casting: Interfacial Phenomena, J. Vicens, M. Chedru, J.L. Chermant, Composites: Part A 33 (2002) 1421–1423.

26. The Influence Of Nickel Coating On The Wettability Of Aluminum On Ceramics, C.A. Leona, R.A.L. Drewb, Composites: Part A 33 (2002) 1429–1432.
27. Laser Induced Cu/Alumina Bonding: Microstructure And Bond Mechanism, L. Shepeleva, B. Medres, W.D. Kaplan, M. Bamberger, M.H. McCay, T.D. McCay, M. Sharp, Surface and Coatings Technology 125 (2000) 40–44.
28. Functionally Gradient Materials And The Manufacture Thereof, Manoj Gupta US Patent 6,495,212 B1.
29. Method For Preparation Of A Functionally Gradient Material, Dietmar Seyferth, Powel Czubarow, US Patent 5,455,000.
30. Method Of Producing A Functionally Gradient Material, Masayuki Niino, Akie Suzuki, Toshio Hirai, Ryuzo Watanabe, Tohru Hirano, Nobuhito Kuroishi , US Patent 4,751,099.
31. Functionally Gradient Material And Method Of Producing The Same Mitsuo Kuwabara, US Patent 6,037,066.
32. Method Of Manufacturing Gradient Function Material, Hirotaka Ishibashi, Koichi Hayashi, Hiroyuki Nagayama, US Patent 5,653,924.
33. Method For Manufacturing Functionally Gradient Composite Materials Shyan-Lung Chung, Jiang-Ming Soon, US Patent 6,019,936.
34. Effect Of Particle Size Distribution On Sintering Of Agglomerate-Free Submicron Alumina Powder Compacts, J. Maa, L.C. Limb, Journal of the European Ceramic Society 22 (2002) 2197–2208.
35. Copper and its alloys" E.G. West, John Wily & Sons, p-21, 30, 126, 139,146, 148.
36. http://www.pml.tno.nl/en/products_services/emb/explosive_forming_technology_aero_space.html
37. Effect Of Process Parameters On The Densification Of 2124 Al-20 Vol% Sicp Composite Fabricated By Explosive Compaction, K.Shivakumar. T. Balakrishna Bhat, T. Ramakrishnan, Journal Of Materials Processing Technology 73 (1998) 268-275.
38. Fracture Toughness Of Intermetallic Compacts Consolidated From Nanocrystalline Powders, R.A. Varin, L. Zbroniec, T. Czujko c, Y.-K. Song
39. Functionally graded electrical/thermal ceramic systems A.J. Ruys, E.B. Popov, D. Sun, J.J. Russell, C.C.J. Murray

40. Explosive compaction of nano-crystalline alumina powder,

P.Weimar, R.Pruemmer. (Karlsruhe University, Karlsruhe, Germany.)

41. ASM Handbook, Properties and selection: Non ferrous alloys and special purpose materials. Volume 2, Page 282-283

Usually
Table No. &
Caption
should be
above the table ?

Name	Composition (%Al ₂ O ₃ in Cu)
C1	1%, 2%, 3%, 4%
C2	1%, 2%, 4%, 5%
C3	1%, 3%, 5%, 6%
C4	1%, 3%, 5%, 7%
C5	1%, 3%, 5%, 8%
C6	3%, 5%, 7%, 10%

Table 1
Nominal Compositions of Cu-Al₂O₃ Powders in Four Layers

Density Measurements

Name	Green Density	Density after First Cycle (1000 ⁰ C, 2hr)	Density after Second Cycle (1000 ⁰ C, 3hr)	Density after Third Cycle (1000 ⁰ C, 4hr)	% Density (Theoretical Density)
C1	6.86	7.65	8.11	8.34	94.59
C2	6.71	7.21	7.91	8.20	93.27
C3	6.81	7.20	7.83	8.21	93.78
C4	6.83	7.55	8.07	8.32	95.17
C5	6.91	7.14	7.52	7.75	88.77
C6	6.86	7.31	7.83	8.18	94.71

Table 2
Density of 1000⁰C Specimens

Name	Green Density	Density after First Cycle (800 ⁰ C, 3hr)	Density after Second Cycle (800 ⁰ C, 6hr)	Density after Third Cycle (800 ⁰ C, 9hr)	% Density (Theoretical Density)
C1	9.7	8.15	8.28	8.41	95.38
C2		7.67	8.14	8.31	94.52
C3		7.84	8.21	8.37	95.74
C4		7.88	8.25	8.41	96.19
C5		7.93	8.25	8.29	94.95
C6		7.90	8.24	8.26	95.63

Table 3
Density of 800⁰C Specimens

Name	Density
C1	8.35
C2	8.20
C3	8.19
C4	8.22
C5	8.14
C6	8.78

Table 4
Density of 1000⁰C Specimens after Rolling

Name	Density
C1	8.01
C2	8.05
C3	7.59
C4	7.90
C5	7.57
C6	7.51

Table 5
Density of 800⁰C Specimens after Rolling

Name	Green compact to first cycle	First cycle to Second cycle	Second cycle to third cycle
C1	11.51	6.01	2.83
C2	7.45	9.7	3.66
C3	5.72	8.75	4.85
C4	10.54	6.88	3.09
C5	3.32	9.66	3.05
C6	6.55	7.11	4.46

Table 6
Percentage change in Density of 1000⁰C Specimens during Sintering

Name	First cycle to Second cycle	Second cycle to third cycle
C1	1.59	1.57
C2	6.12	2.08
C3	4.71	4.38
C4	4.69	1.93
C5	4.03	0.48
C6	4.30	0.24

Table 7
Percentage change in Density of 800⁰C Specimens during Sintering

Electrical Conductivity Measurements

Name	First Cycle		Second Cycle		Third Cycle	
	Lower Conc	Higher Conc	Lower Conc	Higher Conc	Lower Conc	Higher Conc
C1	46.4	29.8	49.7	31.8	50.5	33.7
C2	46.4	22.7	49.5	24.7	51.1	25.1
C3	49.1	20.8	51.7	23.3	54.1	24.3
C4	44.5	14.5	47.0	15.4	49.3	16.3
C5	47.4	12.7	50.2	13.3	51.9	14.1
C6	41.4	10.6	43.5	10.6	45.0	11.2

Table 8
Electrical Conductivity of 1000°C Specimens

Name	First Cycle		Second Cycle		Third Cycle	
	Lower Conc	Higher Conc	Lower Conc	Higher Conc	Lower Conc	Higher Conc
C1	34.19	26.83	37.16	27.68	37.8	27.8
C2	41.57	26.35	42.59	27.37	43.4	28.9
C3	45.05	25.00	48.95	26.16	48.9	26.4
C4	41.79	20.47	43.43	20.8	46.0	27.4
C5	39.14	10.93	43.1	11.22	44.1	11.5
C6	31.57	10.6	32.96	10.9	30.3	11.0

Table 9
Electrical Conductivity of 800°C Specimens

Name	Layer with Lower Al ₂ O ₃ Content	Layer with Higher Al ₂ O ₃ Content
C1	53.6	39.7
C2	56.8	19.6
C3	60.2	19.3
C4	51.4	13.8
C5	53.0	Cracked
C6	48.8	Cracked

Table 10
Electrical Conductivity of 1000⁰C Specimens after Rolling

Name	Layer with Lower Al ₂ O ₃ Content	Layer with Higher Al ₂ O ₃ Content
C1	46.4	18.8
C2	52.3	14.4
C3	52.7	15.1
C4	49.9	Cracked
C5	Cracked	Cracked
C6	35.9	Low

Table 11
Electrical Conductivity of 800⁰C Specimens after Rolling

Name	First cycle to Second cycle	Second cycle to third cycle
C1	7.11	1.61
C2	6.68	3.23
C3	5.29	4.64
C4	5.61	4.89
C5	5.91	3.38
C6	5.07	3.44

Table 12
Percentage change in Electrical Conductivity of 1000⁰C Specimens at Layer with Lower Alumina content during Sintering

Name	First cycle to Second cycle	Second cycle to third cycle
C1	6.71	5.97
C2	8.81	1.61
C3	12.01	4.29
C4	6.2	5.84
C5	4.72	6.01
C6	1.88	5.66

Table 13
Percentage change in Electrical Conductivity of 1000⁰C Specimens at Layer with Higher Alumina Content during Sintering

Name	First cycle to Second cycle	Second cycle to third cycle
C1	8.68	1.72
C2	2.45	1.9
C3	8.65	0.1
C4	3.92	5.91
C5	10.11	2.32
C6	4.41	1.03

Table 14
Percentage change in Electrical Conductivity of 800⁰C Specimens at Layer with lower Alumina content during Sintering

Name	First cycle to Second cycle	Second cycle to third cycle
C1	3.16	0.43
C2	3.60	5.86
C3	4.64	0.91
C4	1.61	31.7
C5	2.65	2.49
C6	2.83	1.83

Table 15
Percentage change in Electrical Conductivity of 800⁰C Specimens at Layer with Higher Alumina Content during Sintering

Reduction in Specimens after Rolling

Name	Initial Thickness(mm)	Final Thickness(mm)	%Reduction
C1	6.134	3.152	48.61
C2	6.057	3.958	34.65
C3	6.147	3.876	36.94
C4	6.081	4.023	33.84
C5	6.177	Tiered	
C6	6.08	Tiered	

Table 16
Reduction in 1000⁰C Specimens after Rolling

Name	Initial Thickness(mm)	Final Thickness(mm)	%Reduction
C1	6.11	3.929	35.69
C2	5.883	3.923	33.31
C3	5.715	4.506	21.15
C4	6.08	Tiered	
C5	6.166	Tiered	
C6	6.028	Tiered	

Table 17
Reduction in 800⁰C Specimens after Rolling

Hardness Measurements

Name	First Cycle	Second Cycle	Third Cycle
C1	<p>Composition(1%Zn3%Sn1%1000C2hr</p> <p>Hardness (HV2.5)</p> <p>Distance (cm)</p> <p>$y = -1.924x + 41.431$ $R^2 = 0.2089$</p>	<p>Composition(1%Zn3%Sn1%1000C3hr</p> <p>Hardness (HV2.5)</p> <p>Distance (cm)</p> <p>$y = -1.5724x + 41.431$ $R^2 = 0.2089$</p>	<p>Composition(1%Zn3%Sn1%1000C4hr</p> <p>Hardness (HV2.5)</p> <p>Distance (cm)</p> <p>$y = -1.6515x + 36.794$ $R^2 = 0.6923$</p>
C2	<p>Composition(1%Zn4%Sn1%1000C2hr</p> <p>Hardness (HV2.5)</p> <p>Distance (cm)</p> <p>$y = -1.5107x + 39.891$ $R^2 = 0.81$</p>	<p>Composition(1%Zn4%Sn1%1000C3hr</p> <p>Hardness (HV2.5)</p> <p>Distance (cm)</p> <p>$y = -2.8014x + 41.168$ $R^2 = 0.3518$</p>	<p>Composition(1%Zn4%Sn1%1000C4hr</p> <p>Hardness (HV2.5)</p> <p>Distance (cm)</p> <p>$y = -1.7762x + 39.891$ $R^2 = 0.81$</p>
C3	<p>Composition(1%Zn5%Sn1%1000C2hr</p> <p>Hardness (HV2.5)</p> <p>Distance (cm)</p> <p>$y = -2.6701x + 39.891$ $R^2 = 0$</p>	<p>Composition(1%Zn5%Sn1%1000C3hr</p> <p>Hardness (HV2.5)</p> <p>Distance (cm)</p> <p>$y = -4.6701x + 54.153$ $R^2 = 0.6536$</p>	<p>Composition(1%Zn5%Sn1%1000C4hr</p> <p>Hardness (HV2.5)</p> <p>Distance (cm)</p> <p>$y = -3.1083x + 36.846$ $R^2 = 0.707$</p>
C4	<p>Composition(1%Zn6%Sn1%1000C2hr</p> <p>Hardness (HV2.5)</p> <p>Distance (cm)</p> <p>$y = -3.039x + 36.846$ $R^2 = 0.8446$</p>	<p>Composition(1%Zn6%Sn1%1000C3hr</p> <p>Hardness (HV2.5)</p> <p>Distance (cm)</p> <p>$y = -4.5459x + 41.17$ $R^2 = 0.8936$</p>	<p>Composition(1%Zn6%Sn1%1000C4hr</p> <p>Hardness (HV2.5)</p> <p>Distance (cm)</p> <p>$y = -2.5471x + 35.338$ $R^2 = 0.8446$</p>
C5	<p>Composition(1%Zn8%Sn1%1000C2hr</p> <p>Hardness (HV2.5)</p> <p>Distance (cm)</p> <p>$y = -2.4814x + 32.208$ $R^2 = 0.4563$</p>	<p>Composition(1%Zn8%Sn1%1000C3hr</p> <p>Hardness (HV2.5)</p> <p>Distance (cm)</p> <p>$y = -1.7902x + 32.208$ $R^2 = 0.4563$</p>	<p>Composition(1%Zn8%Sn1%1000C4hr</p> <p>Hardness (HV2.5)</p> <p>Distance (cm)</p> <p>$y = -4.6348x + 39.871$ $R^2 = 0.9813$</p>
C6	<p>Composition(1%Sn7%10%1000C2hr</p> <p>Hardness (HV2.5)</p> <p>Distance (cm)</p> <p>$y = 0.821x + 24.813$ $R^2 = 0.9113$</p>	<p>Composition(1%Sn7%10%1000C3hr</p> <p>Hardness (HV2.5)</p> <p>Distance (cm)</p> <p>$y = -8.3147x + 48.739$ $R^2 = 0.9113$</p>	<p>Composition(1%Sn7%10%1000C4hr</p> <p>Hardness (HV2.5)</p> <p>Distance (cm)</p> <p>$y = -3.5444x + 35.762$ $R^2 = 0.9113$</p>

Table 18
Hardness of 1000°C Specimens

Name	First Cycle	Second Cycle	Third Cycle
C1	<p>Composition(1%1%3%4%) 800C,2hr</p> <p>Hardness (HV0.05)</p> <p>Distance (cm)</p> <p>$y = -0.2817x + 24.187$ $R^2 = 0.2281$</p>	<p>Composition(1%2%3%4%) 800C,6hr</p> <p>Hardness (HV0.05)</p> <p>Distance (cm)</p> <p>$y = -0.1093x + 33.378$ $R^2 = 0.0067$</p>	<p>Composition(1%2%3%4%) 800C,9hr</p> <p>Hardness (HV0.05)</p> <p>Distance (cm)</p> <p>$y = -0.3789x + 32.46$ $R^2 = 0.3419$</p>
C2	<p>Composition(1%2%4%5%) 800C,2hr</p> <p>Hardness (HV0.05)</p> <p>Distance (cm)</p> <p>$y = -1.8228x + 32.874$ $R^2 = 0.8688$</p>	<p>Composition(1%2%4%5%) 800C,6hr</p> <p>Hardness (HV0.05)</p> <p>Distance (cm)</p> <p>$y = -0.9645x + 28.942$ $R^2 = 0.7119$</p>	<p>Composition(1%2%4%5%) 800C,9hr</p> <p>Hardness (HV0.05)</p> <p>Distance (cm)</p> <p>$y = -1.7152x + 36.894$ $R^2 = 0.5801$</p>
C3	<p>Composition(1%3%5%6%) 800C,2hr</p> <p>Hardness (HV0.05)</p> <p>Distance (cm)</p> <p>$y = -1.7126x + 28.352$ $R^2 = 0.8423$</p>	<p>Composition(1%3%5%6%) 800C,6hr</p> <p>Hardness (HV0.05)</p> <p>Distance (cm)</p> <p>$y = -0.8566x + 32.662$ $R^2 = 0.3378$</p>	<p>Composition(1%3%5%6%) 800C,9hr</p> <p>Hardness (HV0.05)</p> <p>Distance (cm)</p> <p>$y = -3.3648x + 40.185$ $R^2 = 0.8103$</p>
C4	<p>Composition(1%3%5%7%) 800C,2hr</p> <p>Hardness (HV0.05)</p> <p>Distance (cm)</p> <p>$y = -1.5521x + 28.814$ $R^2 = 0.5426$</p>	<p>Composition(1%3%5%7%) 800C,6hr</p> <p>Hardness (HV0.05)</p> <p>Distance (cm)</p> <p>$y = -1.9988x + 27.564$ $R^2 = 0.7761$</p>	<p>Composition(1%3%5%7%) 800C,9hr</p> <p>Hardness (HV0.05)</p> <p>Distance (cm)</p> <p>$y = -2.0707x + 32.164$ $R^2 = 0.8764$</p>
C5	<p>Composition(1%3%5%8%) 800C,2hr</p> <p>Hardness (HV0.05)</p> <p>Distance (cm)</p> <p>$y = -0.7907x + 24.555$ $R^2 = 0.3368$</p>	<p>Composition(1%3%5%8%) 800C,6hr</p> <p>Hardness (HV0.05)</p> <p>Distance (cm)</p> <p>$y = -2.0914x + 33.632$ $R^2 = 0.5261$</p>	<p>Composition(1%3%5%8%) 800C,9hr</p> <p>Hardness (HV0.05)</p> <p>Distance (cm)</p> <p>$y = -4.1841x + 41.59$ $R^2 = 0.963$</p>
C6	<p>Composition(1%4%5%10%) 800C,2hr</p> <p>Hardness (HV0.05)</p> <p>Distance (cm)</p> <p>$y = 0.3085x + 22.574$ $R^2 = 0.0015$</p>	<p>Composition(1%4%5%10%) 800C,6hr</p> <p>Hardness (HV0.05)</p> <p>Distance (cm)</p> <p>$y = -2.0911x + 33.632$ $R^2 = 0.5261$</p>	<p>Composition(1%4%5%10%) 800C,9hr</p> <p>Hardness (HV0.05)</p> <p>Distance (cm)</p> <p>$y = -0.3146x + 27.643$ $R^2 = 0.1034$</p>

Table 19
Hardness of 800°C Specimens

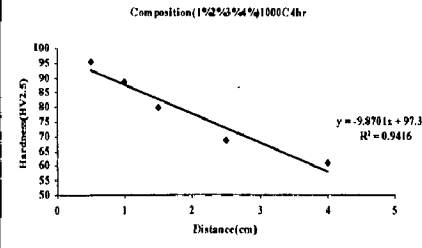
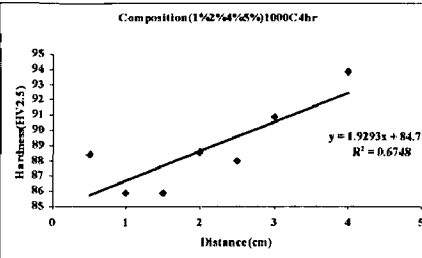
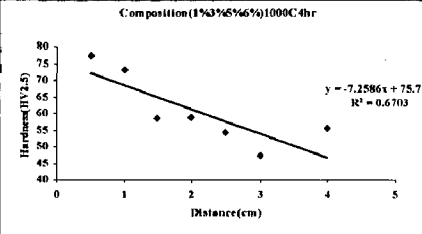
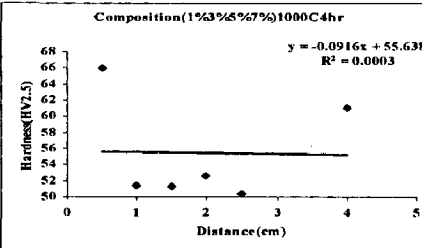
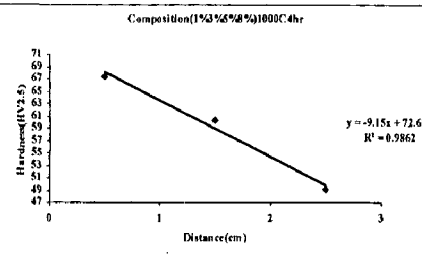
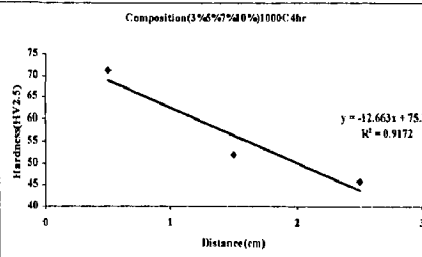
Name	Hardness
C1	<p>Composition (1%2%3%4%1000C4hr)</p>  <p>Hardness (HV2.5)</p> <p>Distance (cm)</p> <p>$y = -9.8701x + 97.303$ $R^2 = 0.9416$</p>
C2	<p>Composition (1%2%4%5%1000C4hr)</p>  <p>Hardness (HV2.5)</p> <p>Distance (cm)</p> <p>$y = 1.9293x + 84.754$ $R^2 = 0.6748$</p>
C3	<p>Composition (1%3%5%6%1000C4hr)</p>  <p>Hardness (HV2.5)</p> <p>Distance (cm)</p> <p>$y = -7.2586x + 75.718$ $R^2 = 0.6703$</p>
C4	<p>Composition (1%3%5%7%1000C4hr)</p>  <p>Hardness (HV2.5)</p> <p>Distance (cm)</p> <p>$y = -0.0916x + 55.638$ $R^2 = 0.0003$</p>
C5	<p>Composition (1%3%5%8%1000C4hr)</p>  <p>Hardness (HV2.5)</p> <p>Distance (cm)</p> <p>$y = -9.15x + 72.625$ $R^2 = 0.9862$</p>
C6	<p>Composition (3%4%7%10%1000C4hr)</p>  <p>Hardness (HV2.5)</p> <p>Distance (cm)</p> <p>$y = -12.663x + 75.36$ $R^2 = 0.9172$</p>

Table 20
Hardness of 1000⁰C Specimens after Rolling

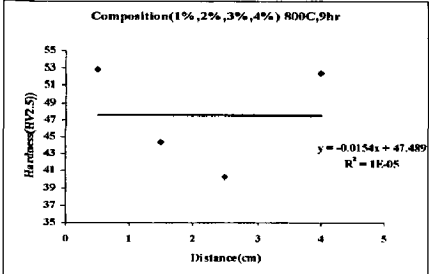
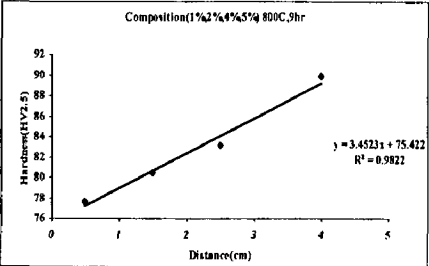
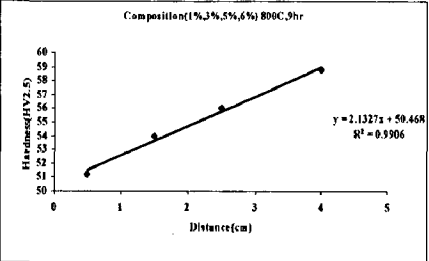
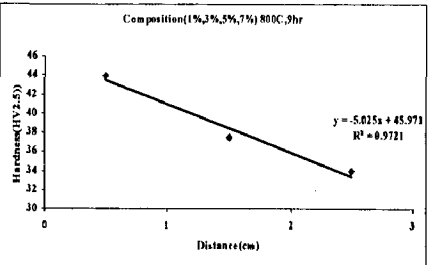
Name	Hardness
C1	<p>Composition(1%,2%,3%,4%) 800C,9hr</p>  <p>Hardness(HV2.5)</p> <p>Distance(cm)</p> <p>$y = -0.0154x + 47.489$ $R^2 = 1E-05$</p>
C2	<p>Composition(1%,2%,4%,5%) 800C,9hr</p>  <p>Hardness(HV2.5)</p> <p>Distance(cm)</p> <p>$y = 3.4523x + 75.412$ $R^2 = 0.9821$</p>
C3	<p>Composition(1%,3%,5%,6%) 800C,9hr</p>  <p>Hardness(HV2.5)</p> <p>Distance(cm)</p> <p>$y = 2.1327x + 59.468$ $R^2 = 0.9906$</p>
C4	<p>Composition(1%,2%,5%,7%) 800C,9hr</p>  <p>Hardness(HV2.5)</p> <p>Distance(cm)</p> <p>$y = -5.015x + 45.971$ $R^2 = 0.9711$</p>
C5	Tiered
C6	Tiered

Table 21
Hardness of 800^oC Specimens after Rolling

Composition	Layer Thickness (mm)
1%Al ₂ O ₃	5
3%Al ₂ O ₃	3
5%Al ₂ O ₃	3
6%Al ₂ O ₃	5
0% Al ₂ O ₃	Remaining length

Table 22
Composition and Thickness for First Tube

Composition	Layer Thickness (mm)
Pure Alumina	10
80%Al ₂ O ₃	1
60%Al ₂ O ₃	1
40%Al ₂ O ₃	1
30%Al ₂ O ₃	1
20%Al ₂ O ₃	1
15%Al ₂ O ₃	1
10%Al ₂ O ₃	1
5%Al ₂ O ₃	1
Pure copper	Remaining length

Table 23
Composition and Thickness for Second Tube

Microstructures:

Microstructures of 1000⁰C:

First Boundary of C1:

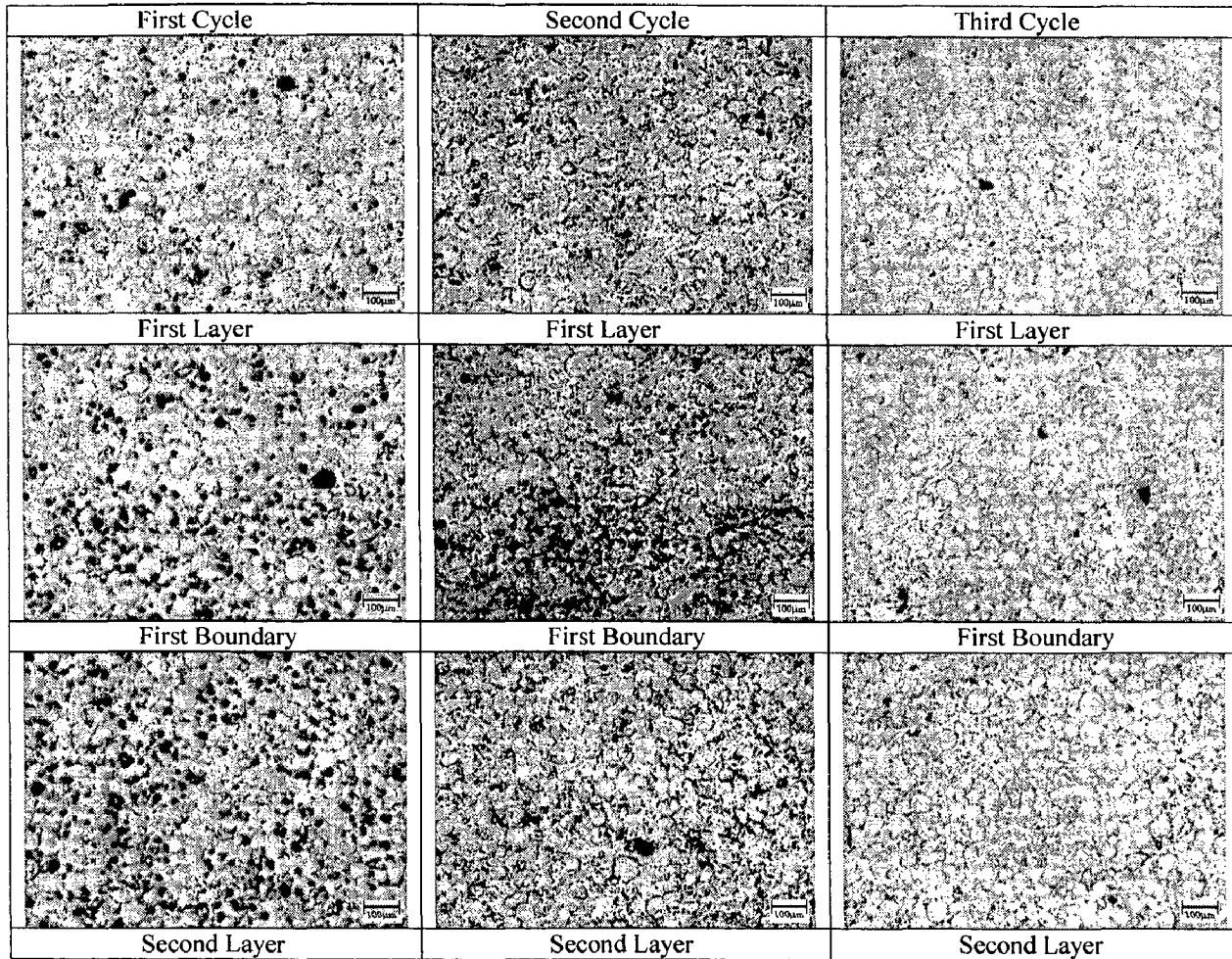


Figure 1

Second Boundary of C1:

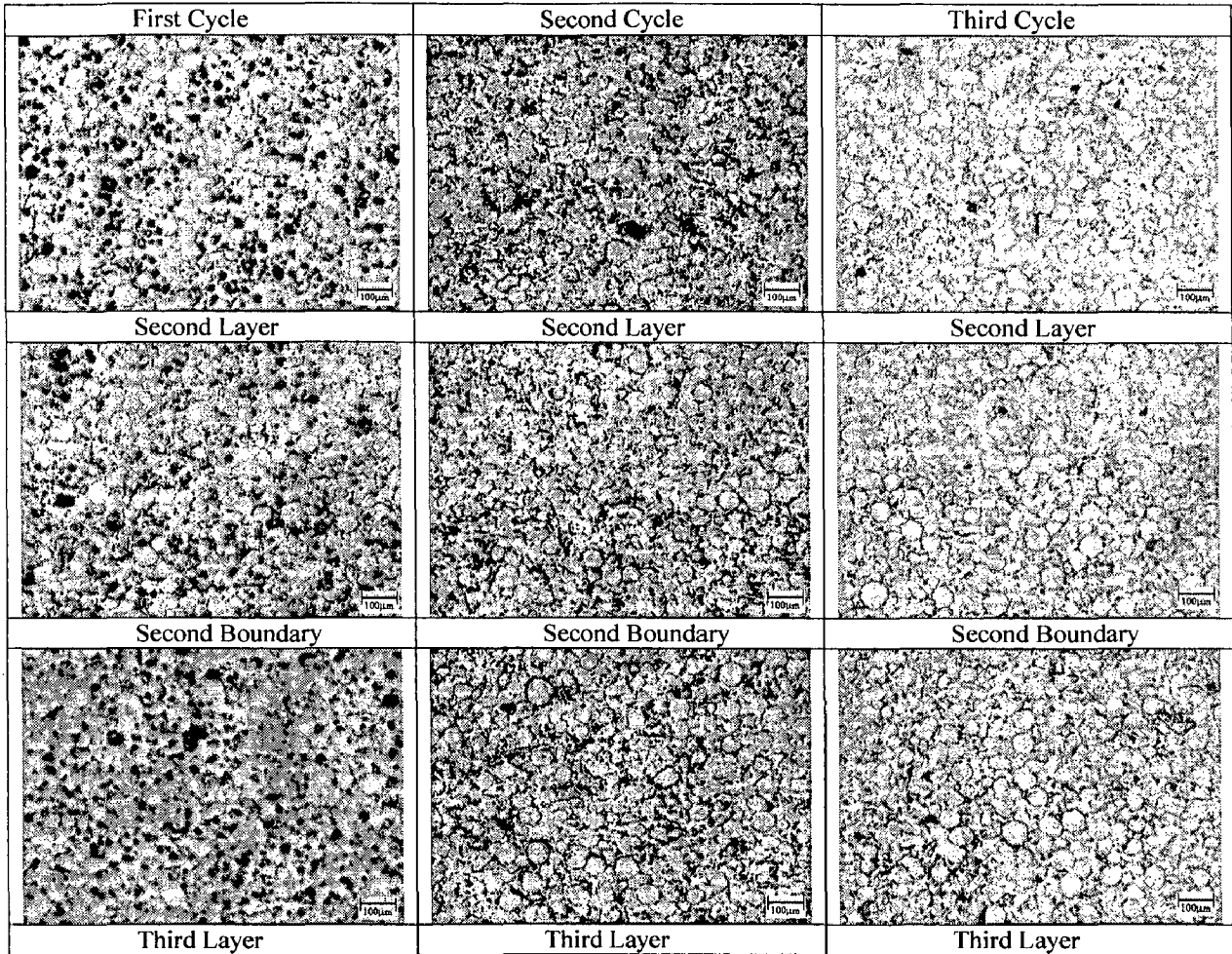


Figure 2

Third Boundary of C1:

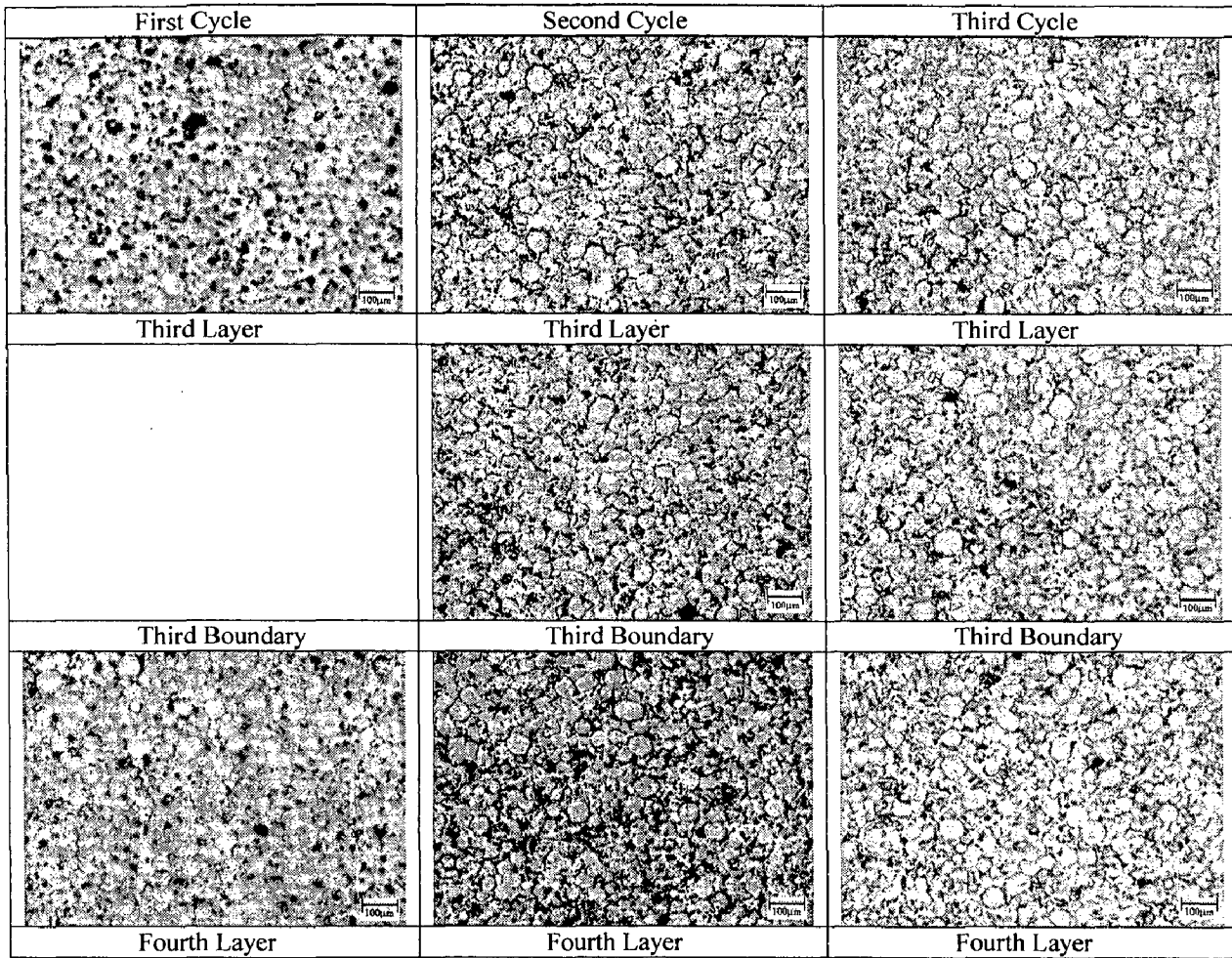


Figure 3

First Boundary of C2:

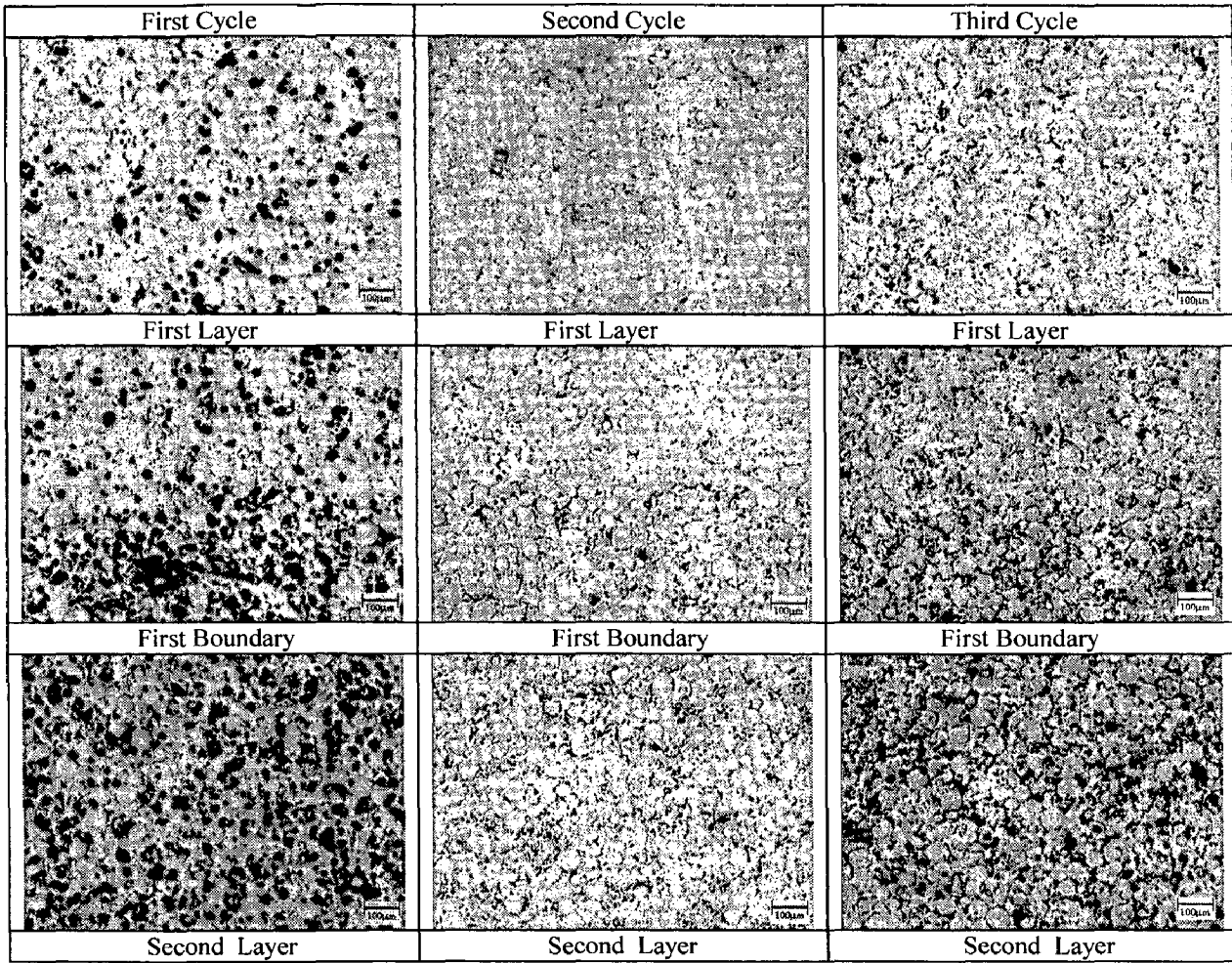


Figure 4

Second Boundary of C2:

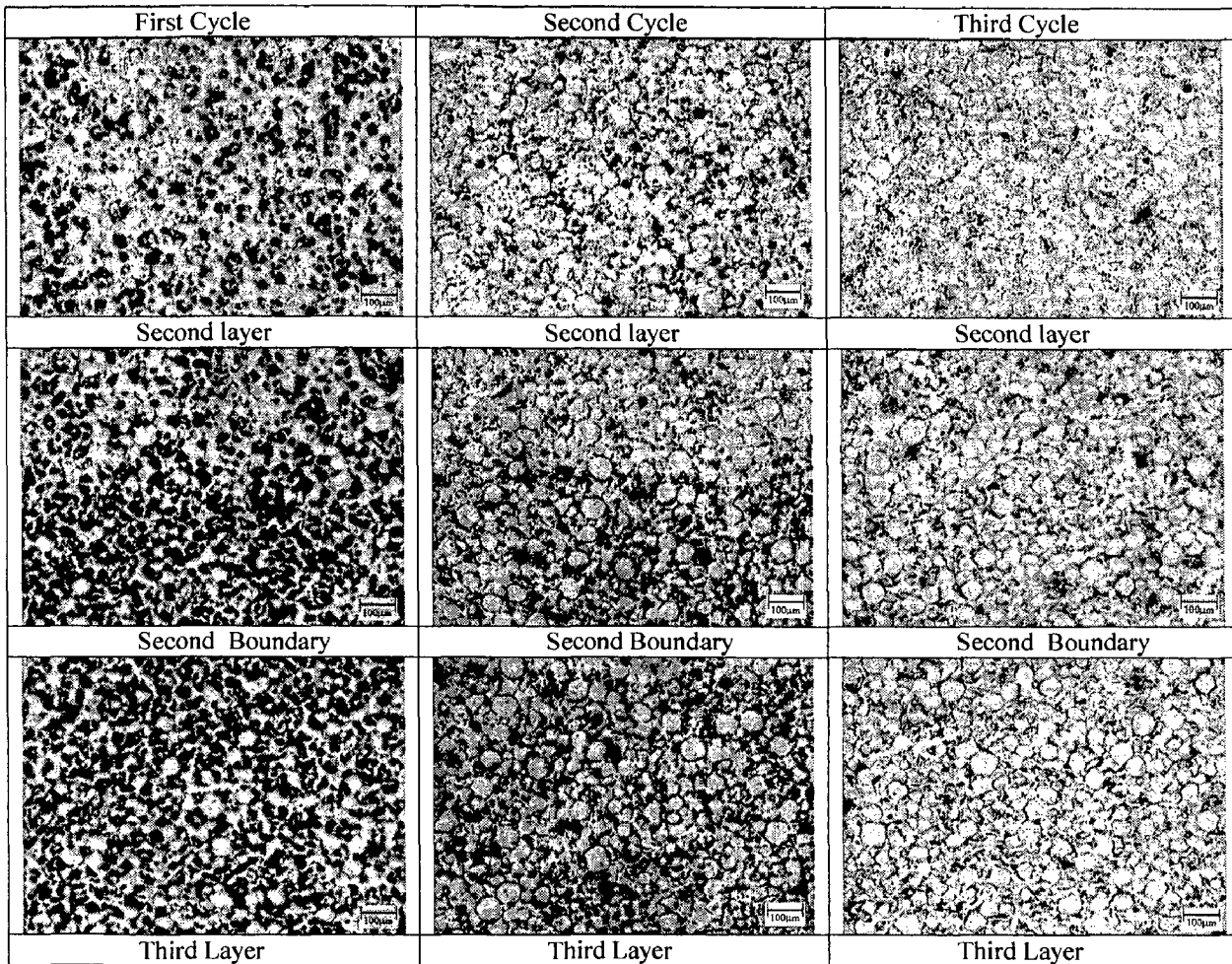


Figure 5

Third Boundary of C2:

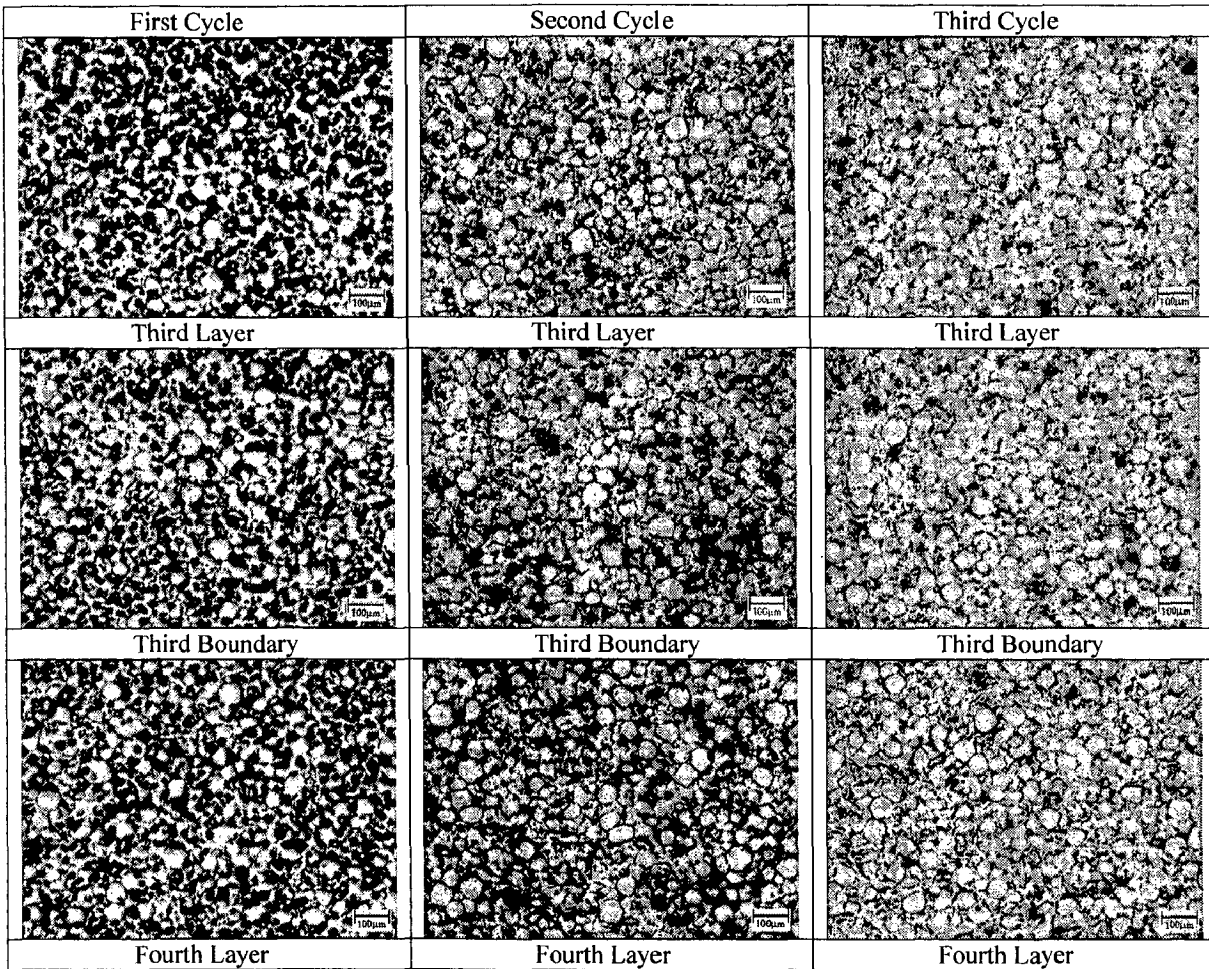


Figure 6

Third Boundary of C2:

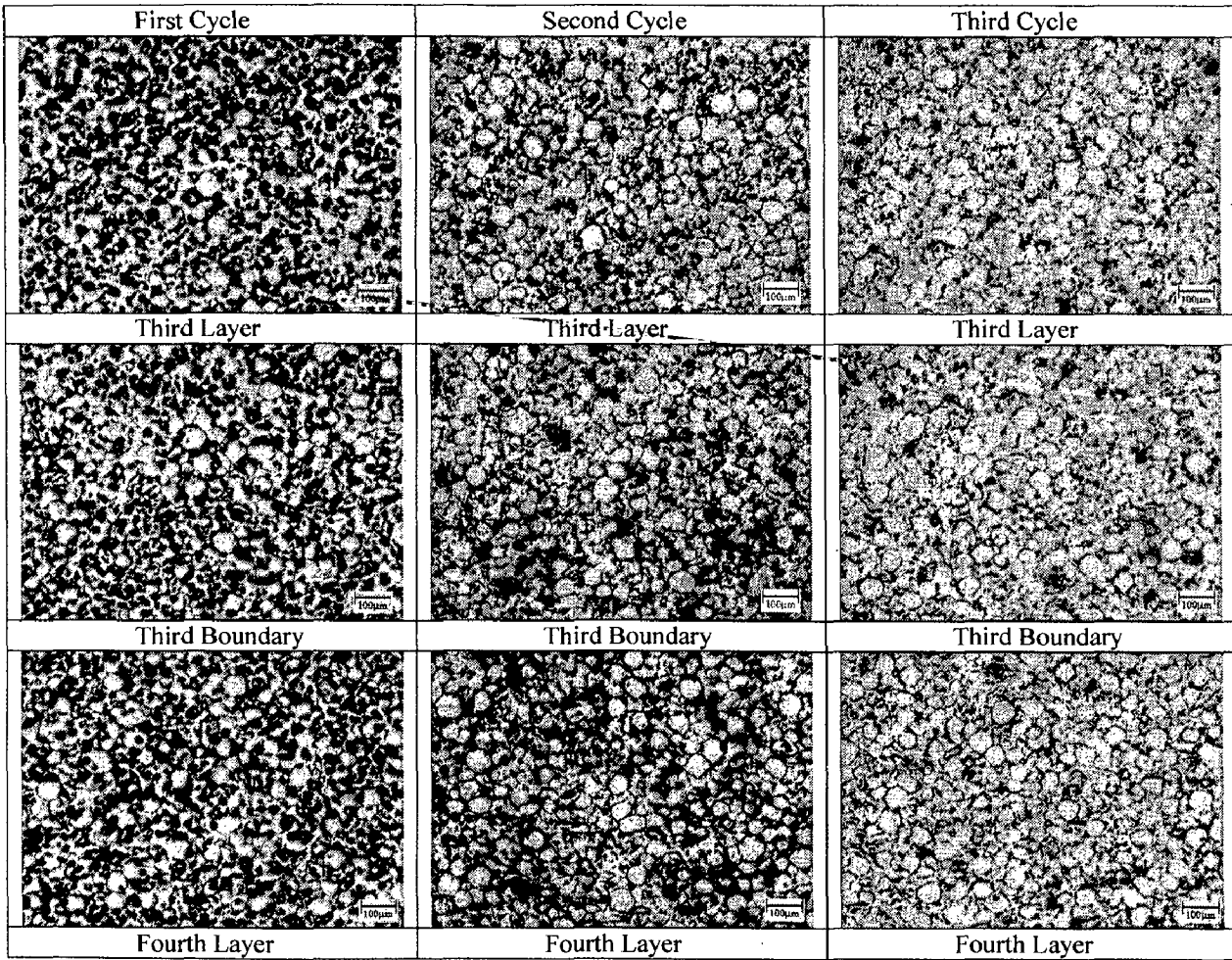


Figure 6

First Boundary of C3:

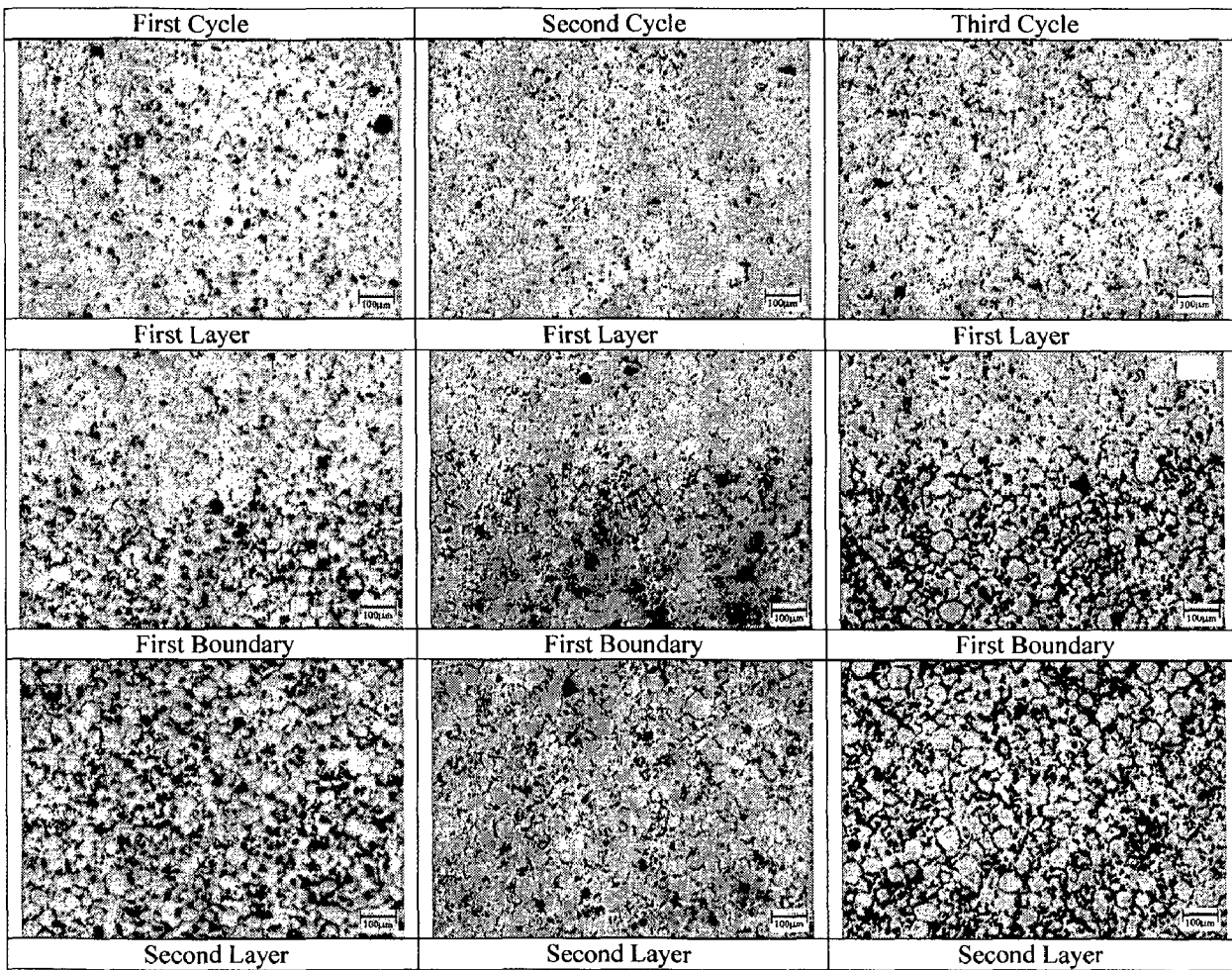


Figure 7

and Boundary of C3:

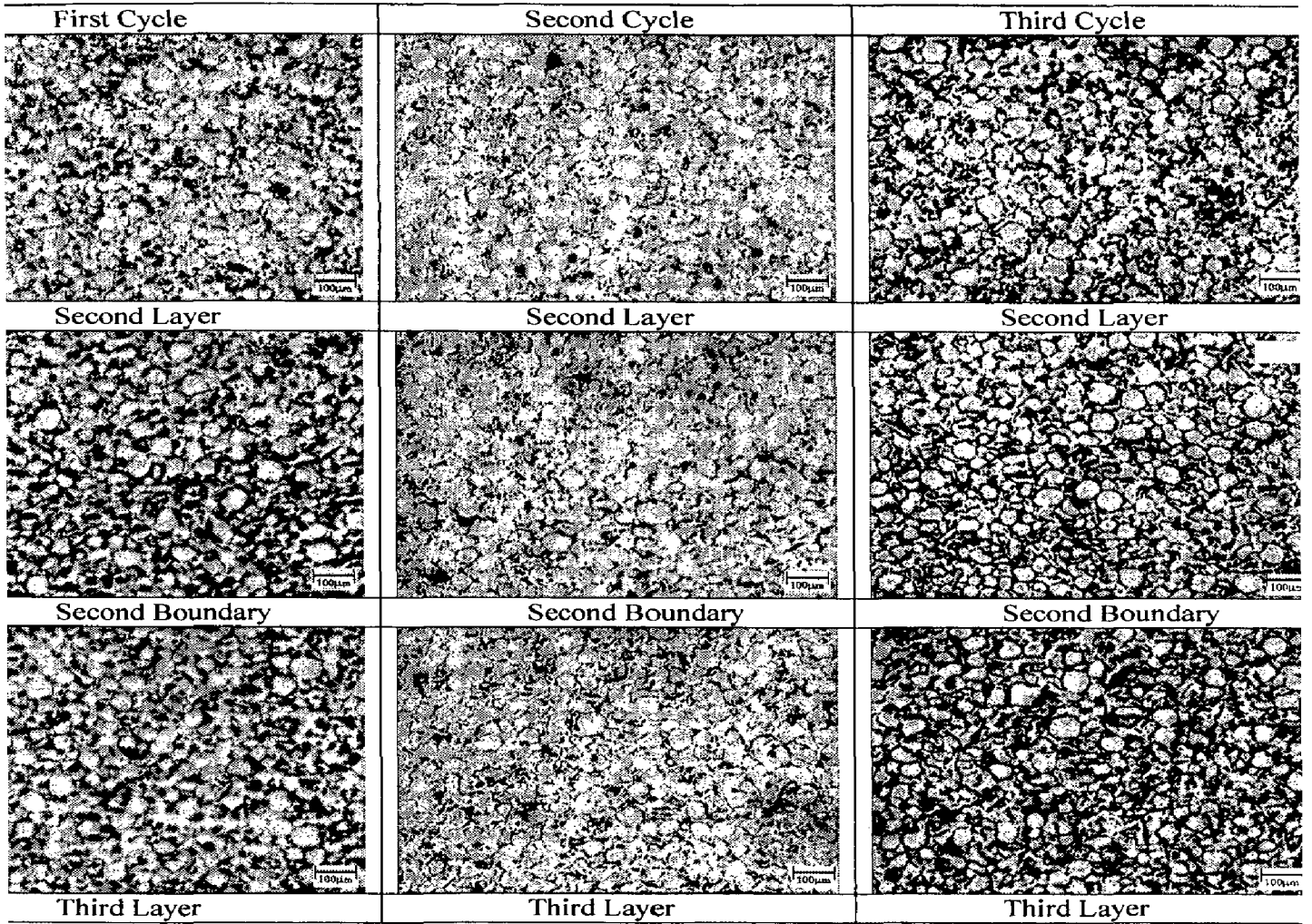


Figure 8

Third Boundary of C3:

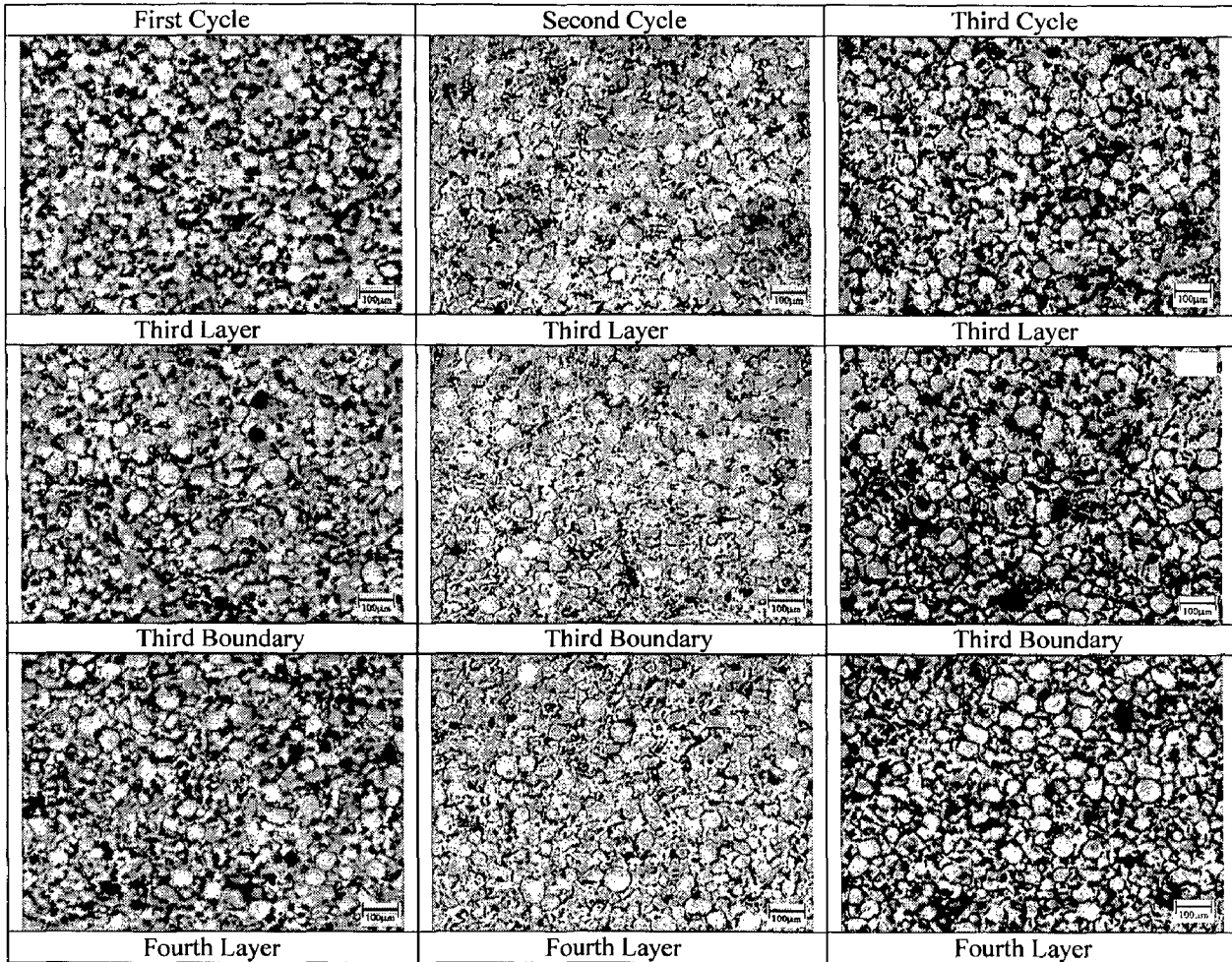


Figure 9

First Boundary of C4:

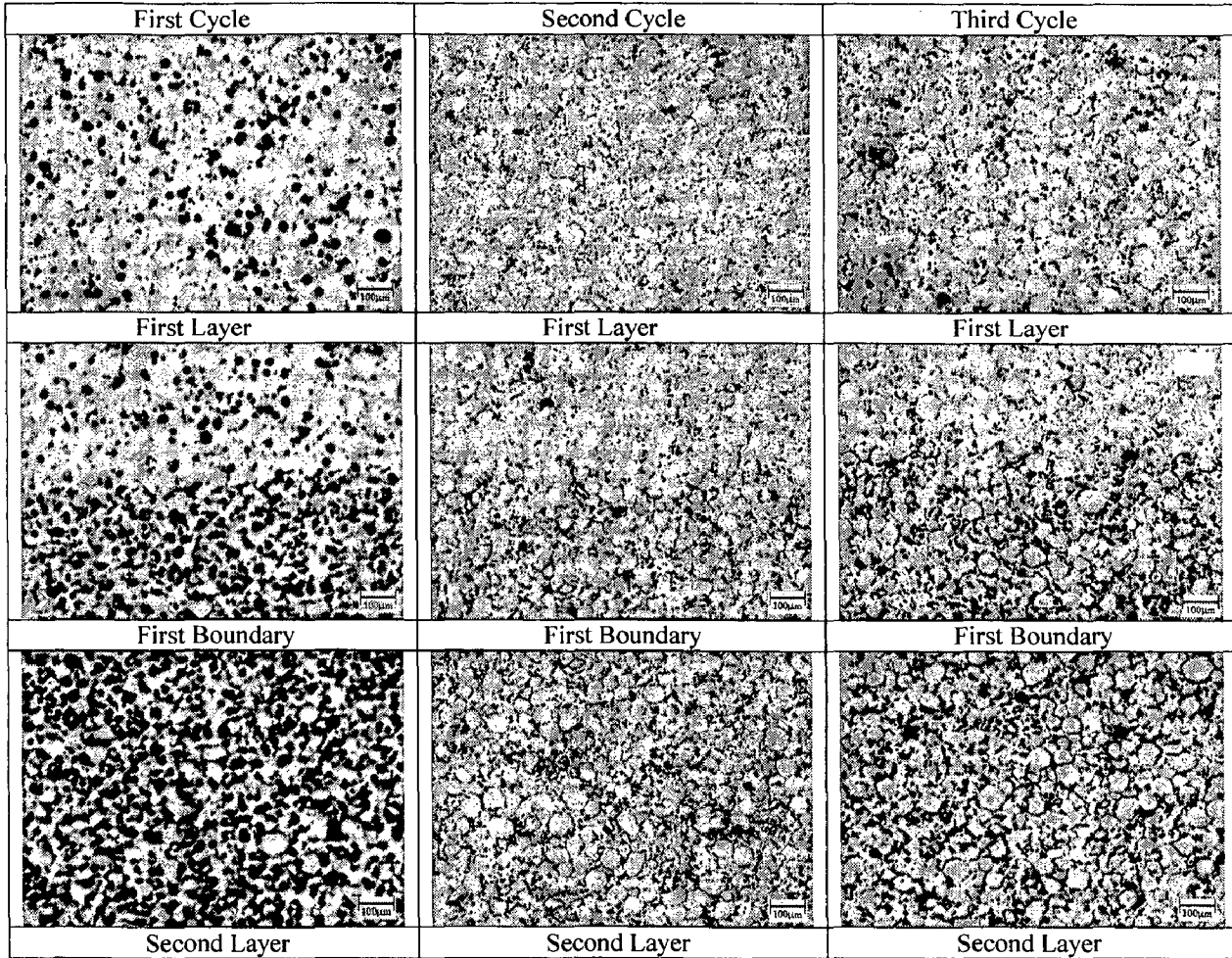


Figure 10

Second Boundary of C4:

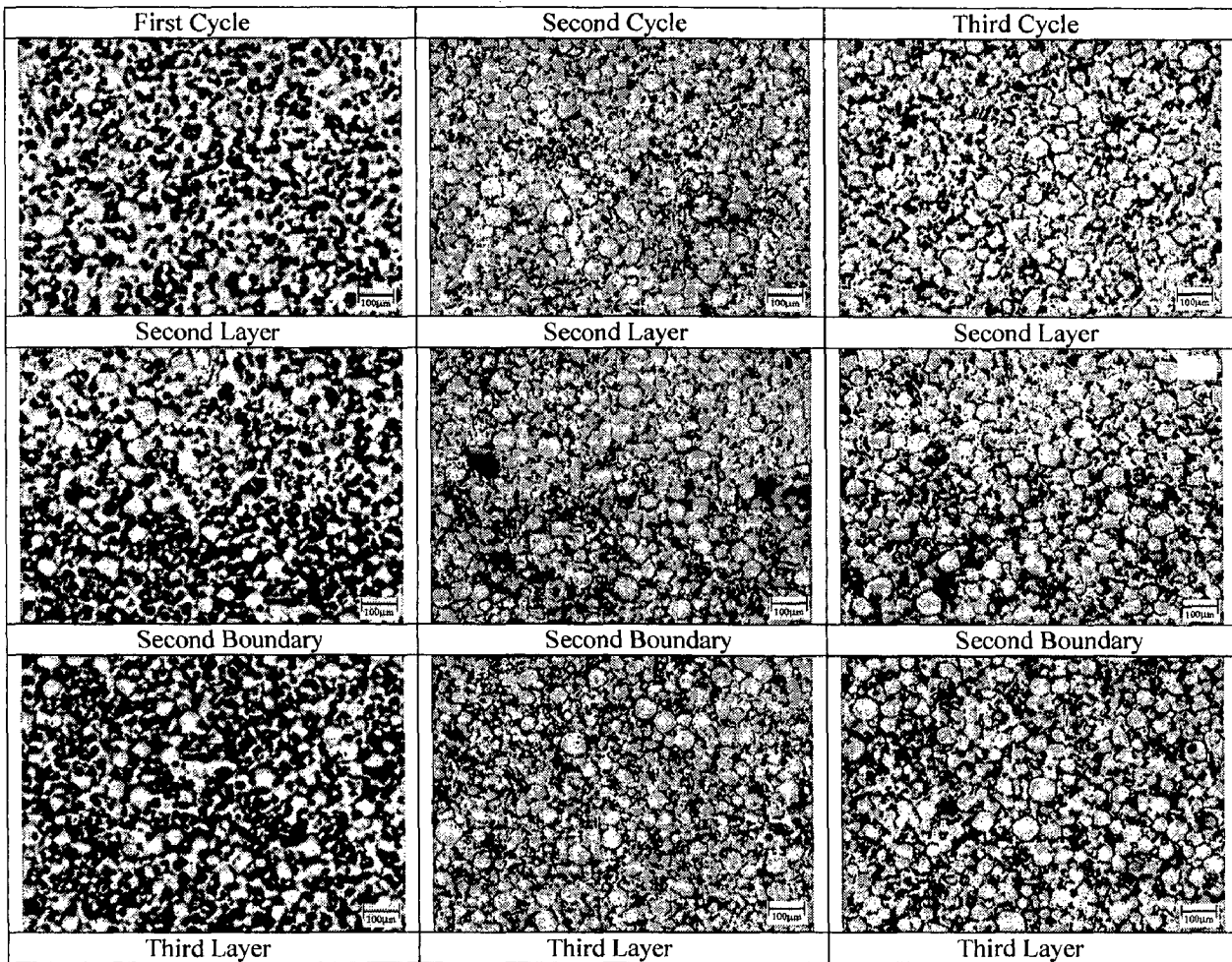


Figure 11

Third Boundary of C4:

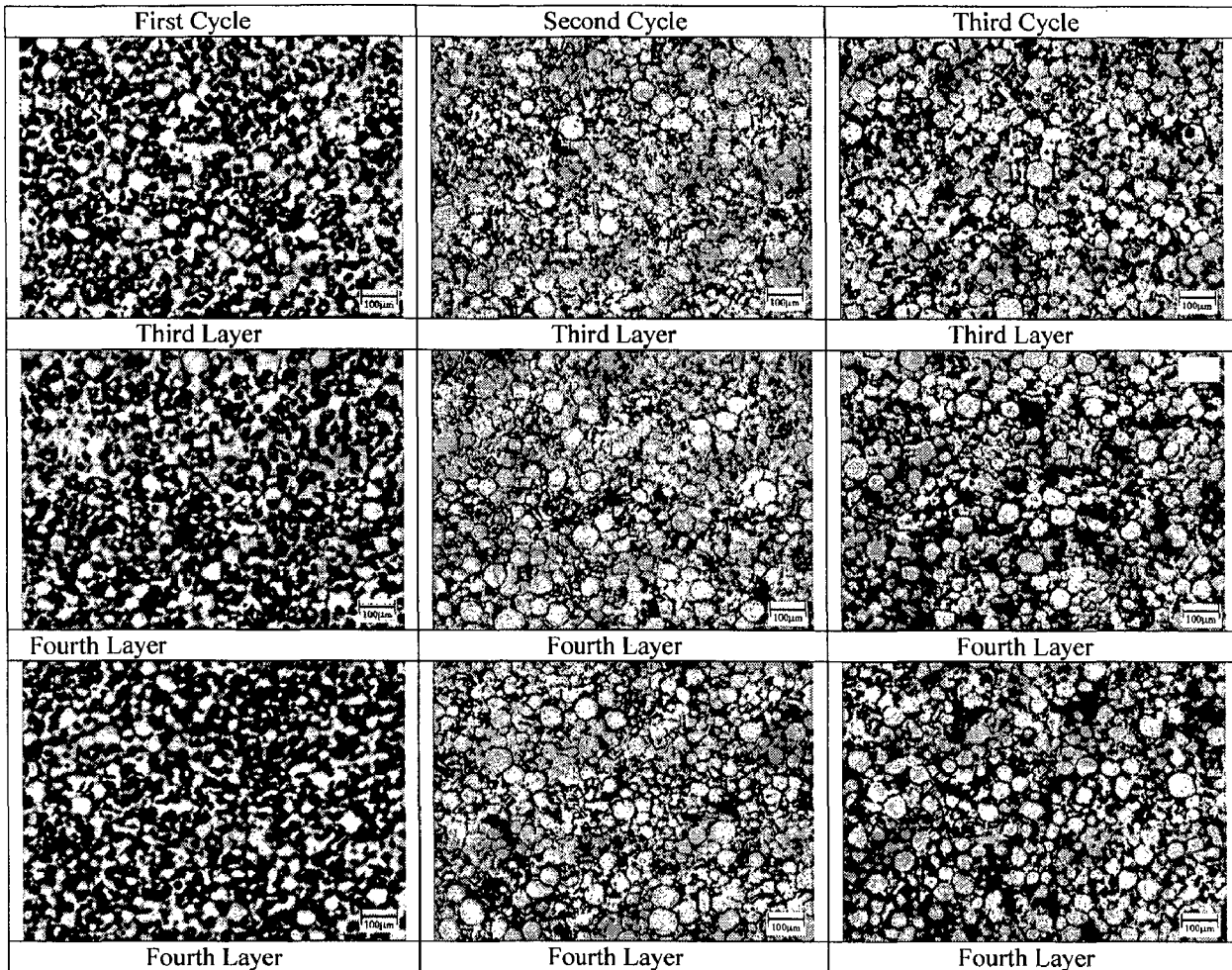


Figure 12

First Boundary of C5:

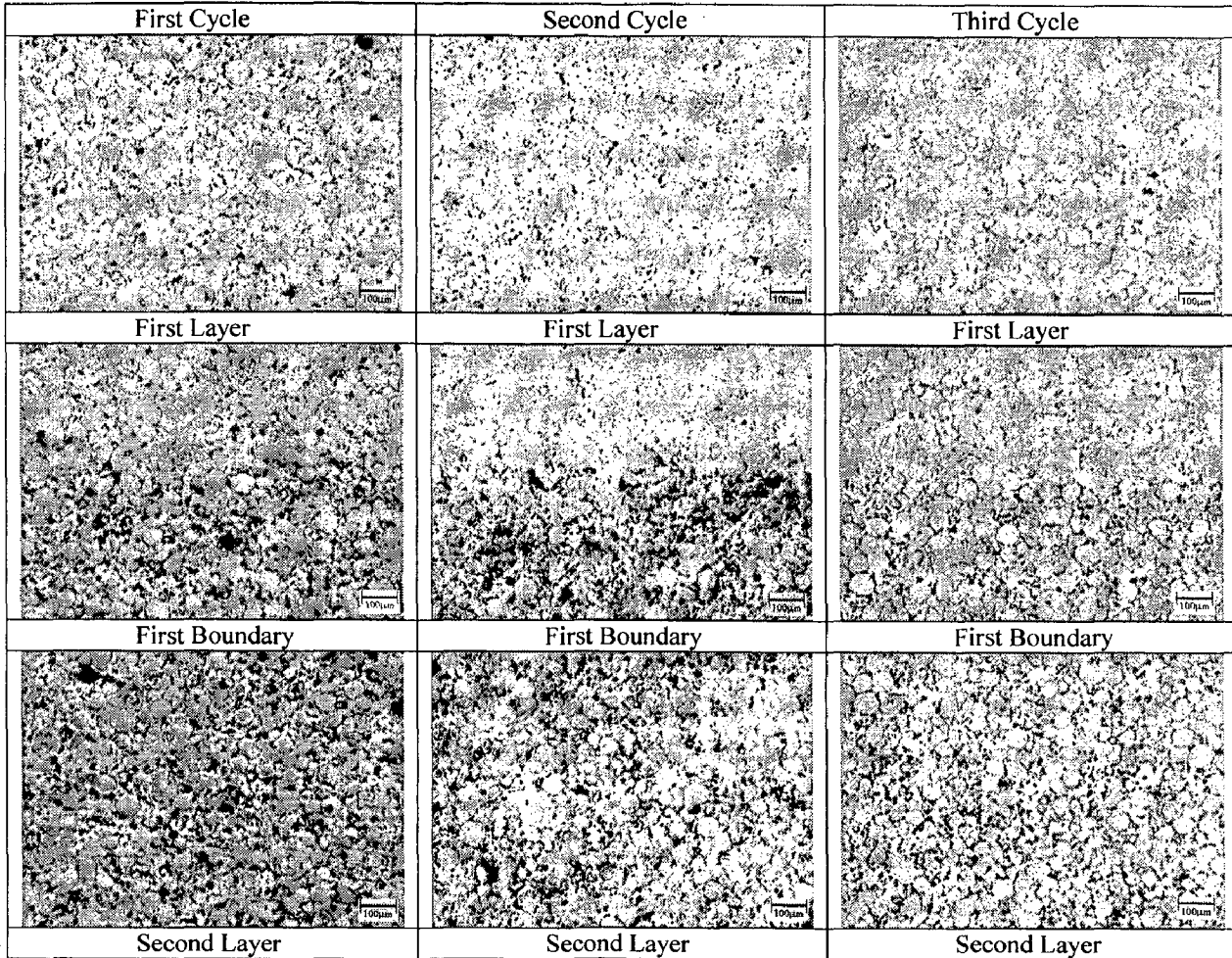


Figure 13

Second Boundary of C5:

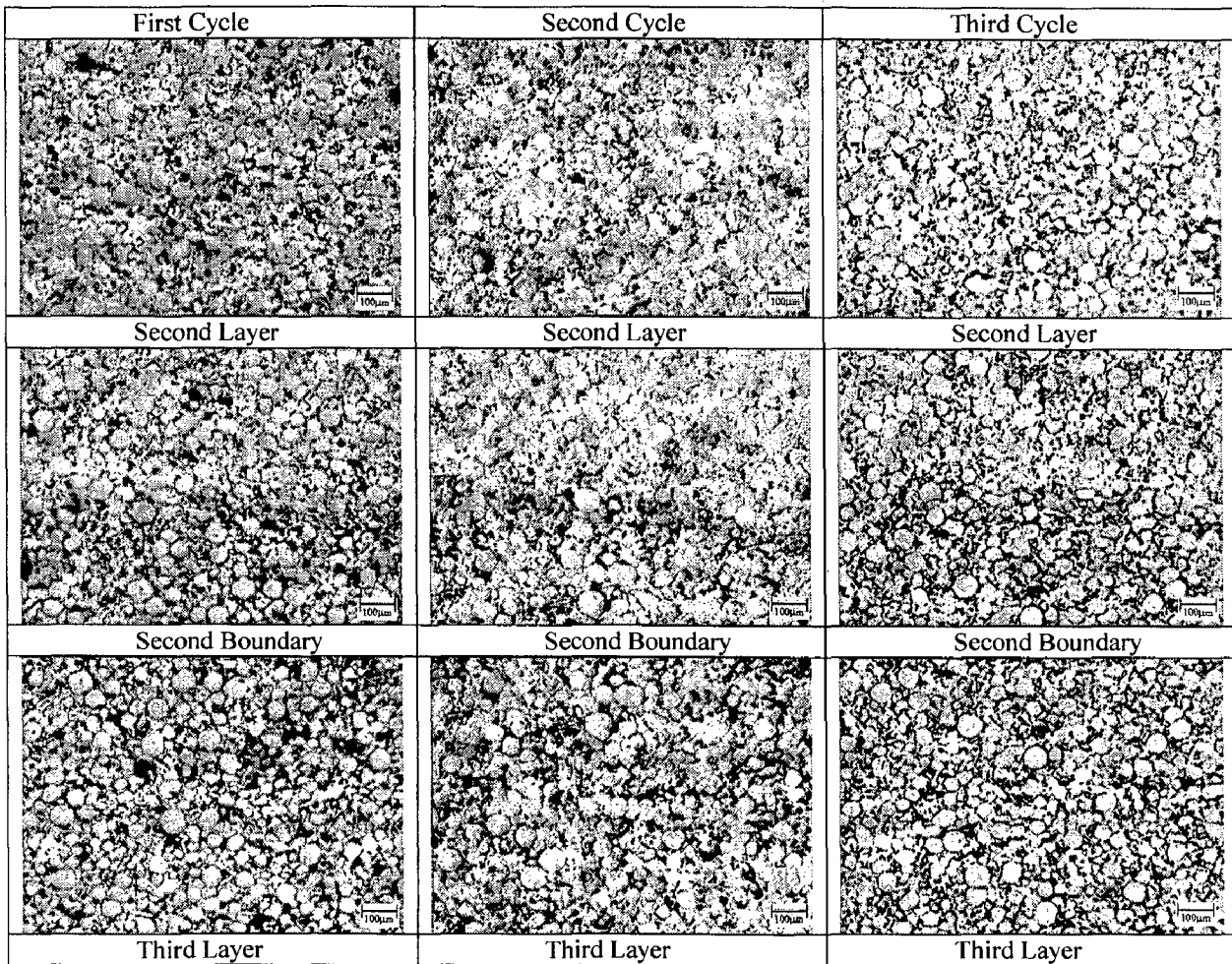


Figure 14

Third Boundary of C5:

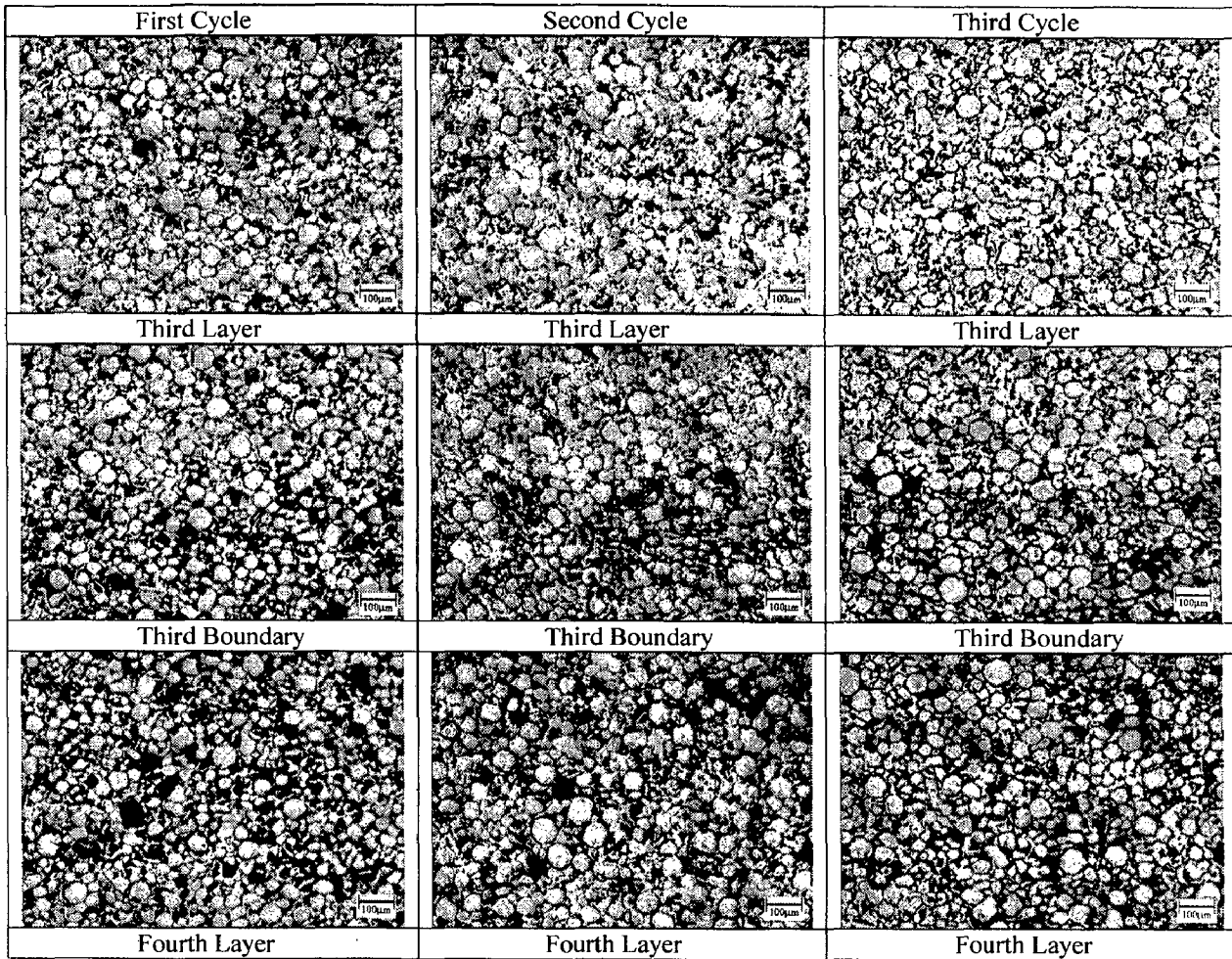


Figure 15

First Boundary of C6:

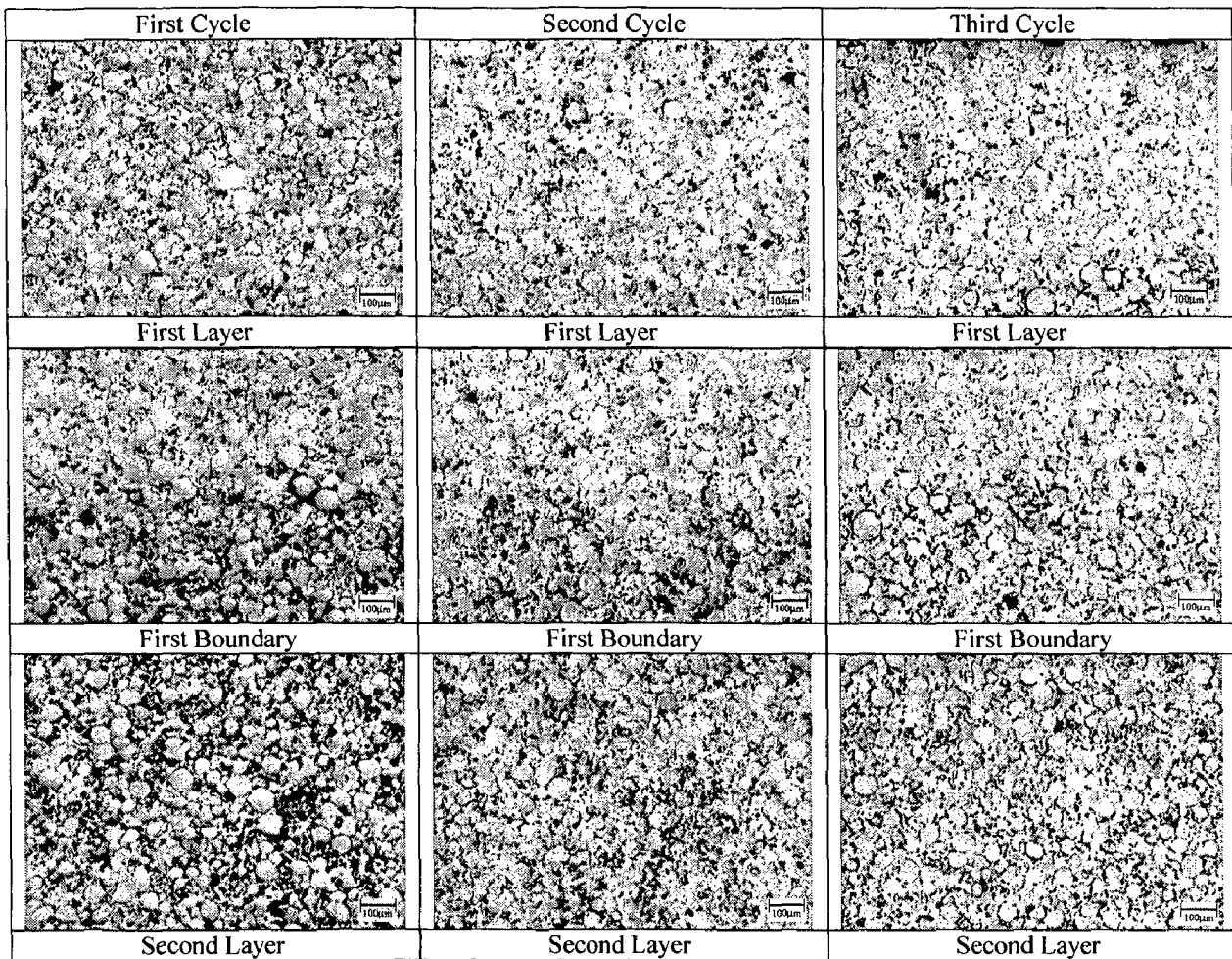


Figure 16

Second Boundary of C6:

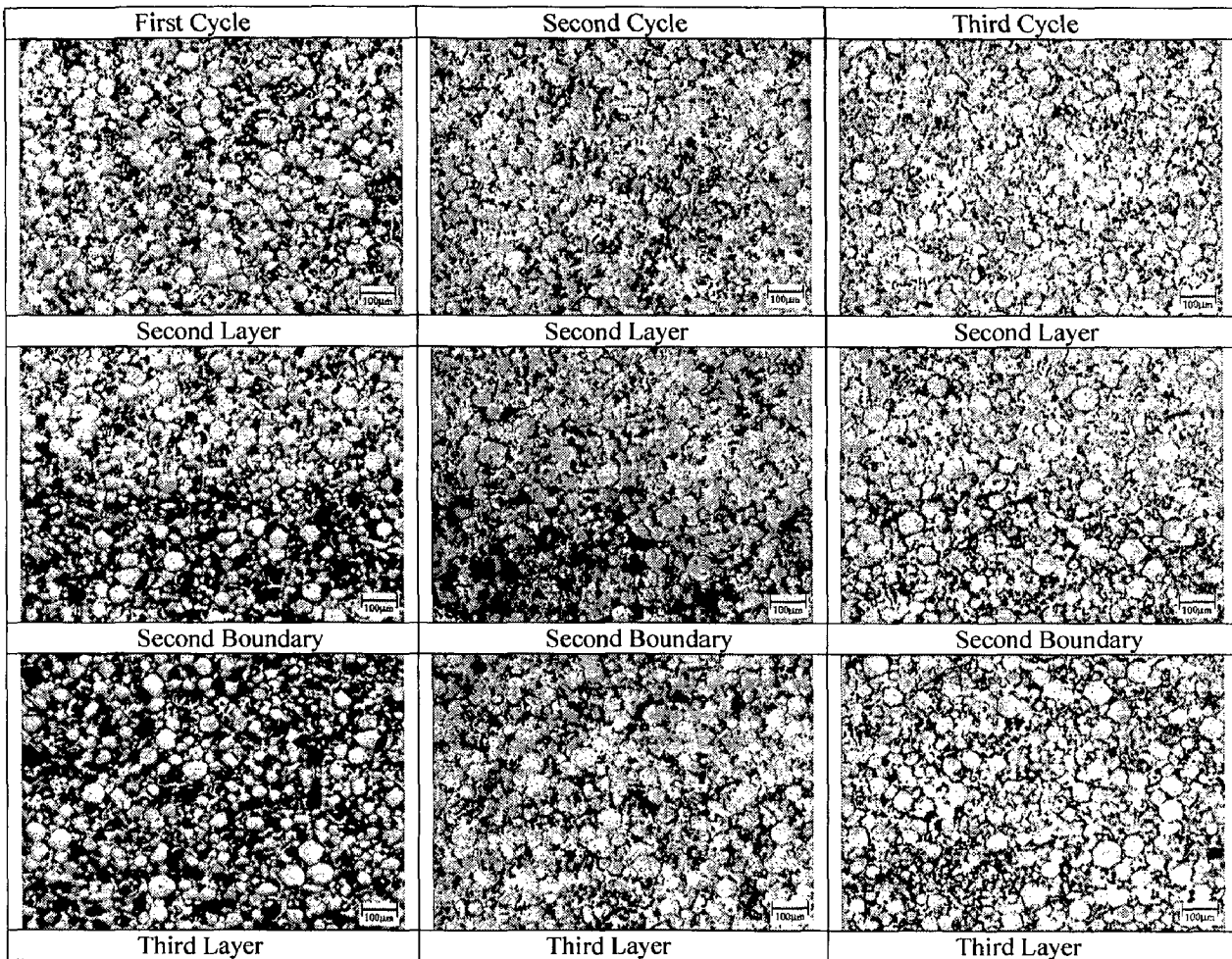


Figure 17

Third Boundary of C6:

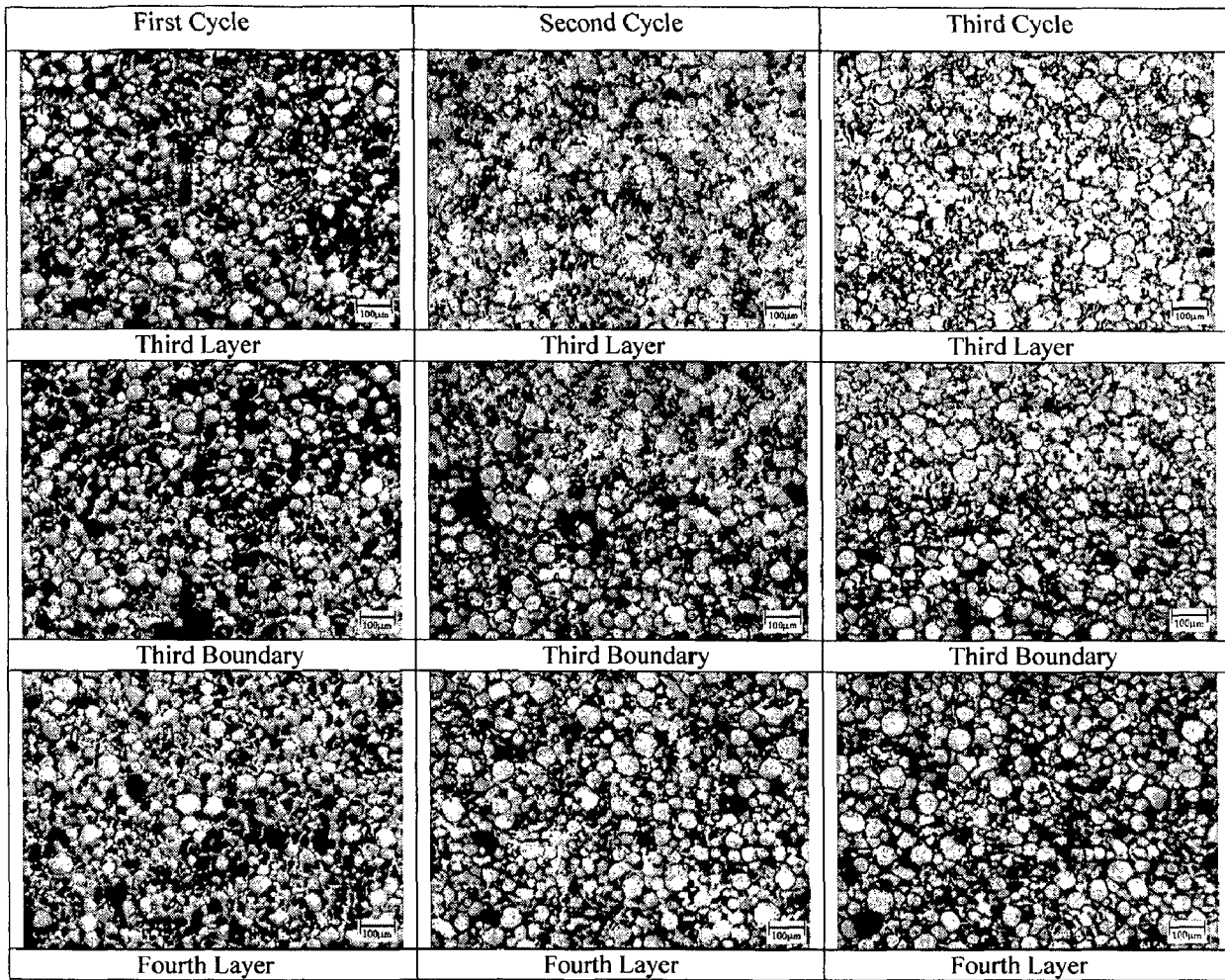


Figure 18

Microstructure of 800°C Specimens:

First Boundary of C1:

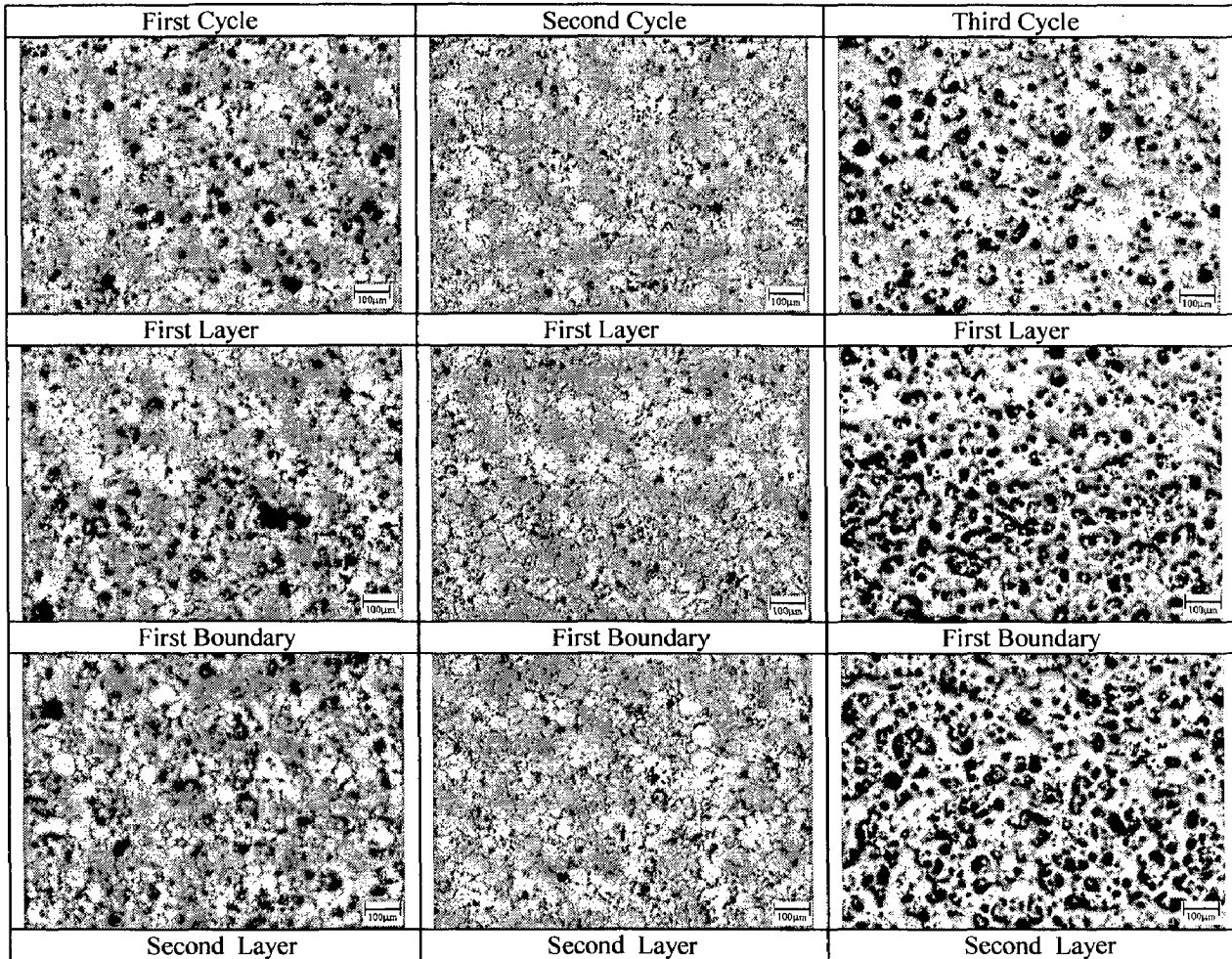


Figure 19

Second Boundary of C1:

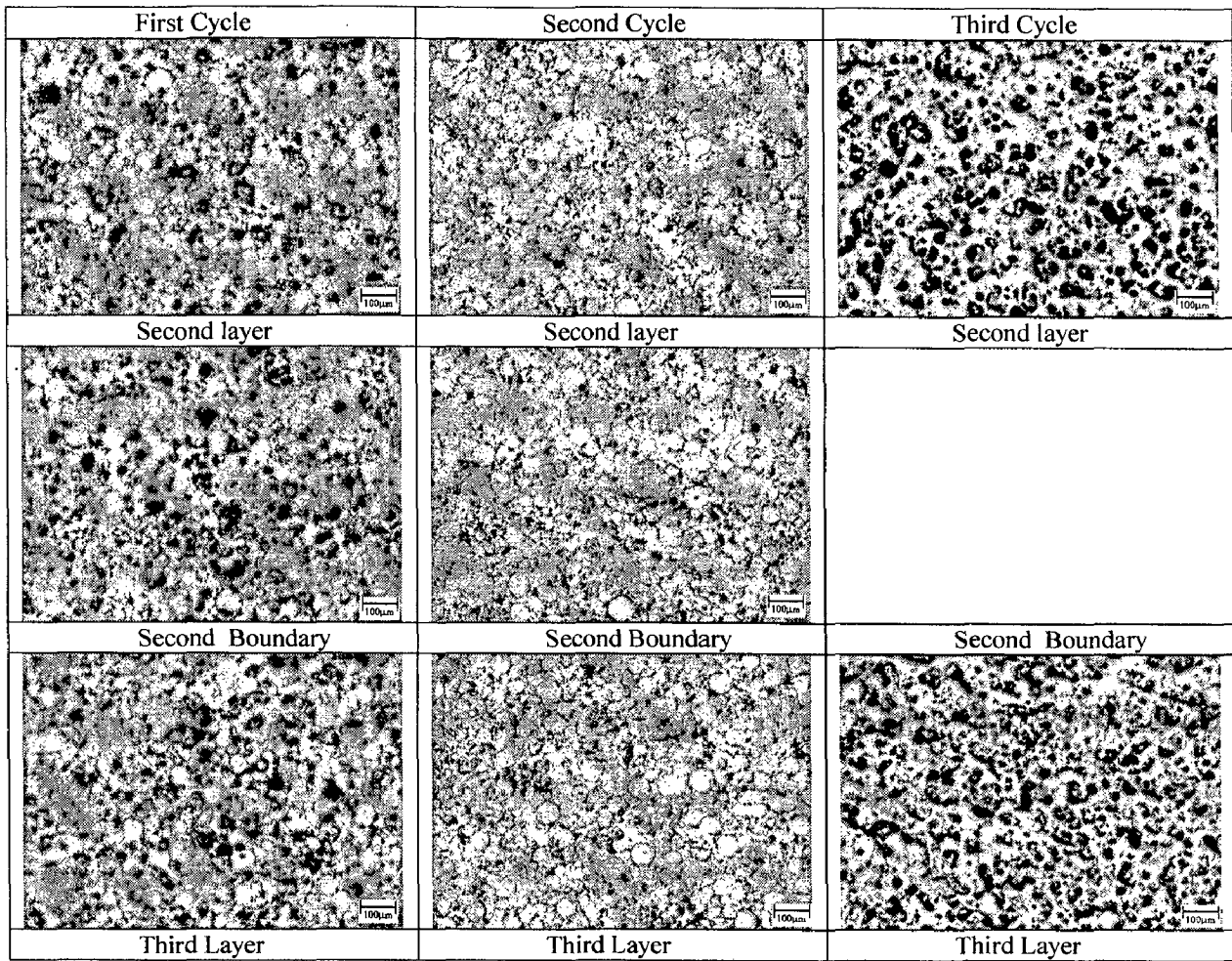


Figure 20

Third Boundary of C1:

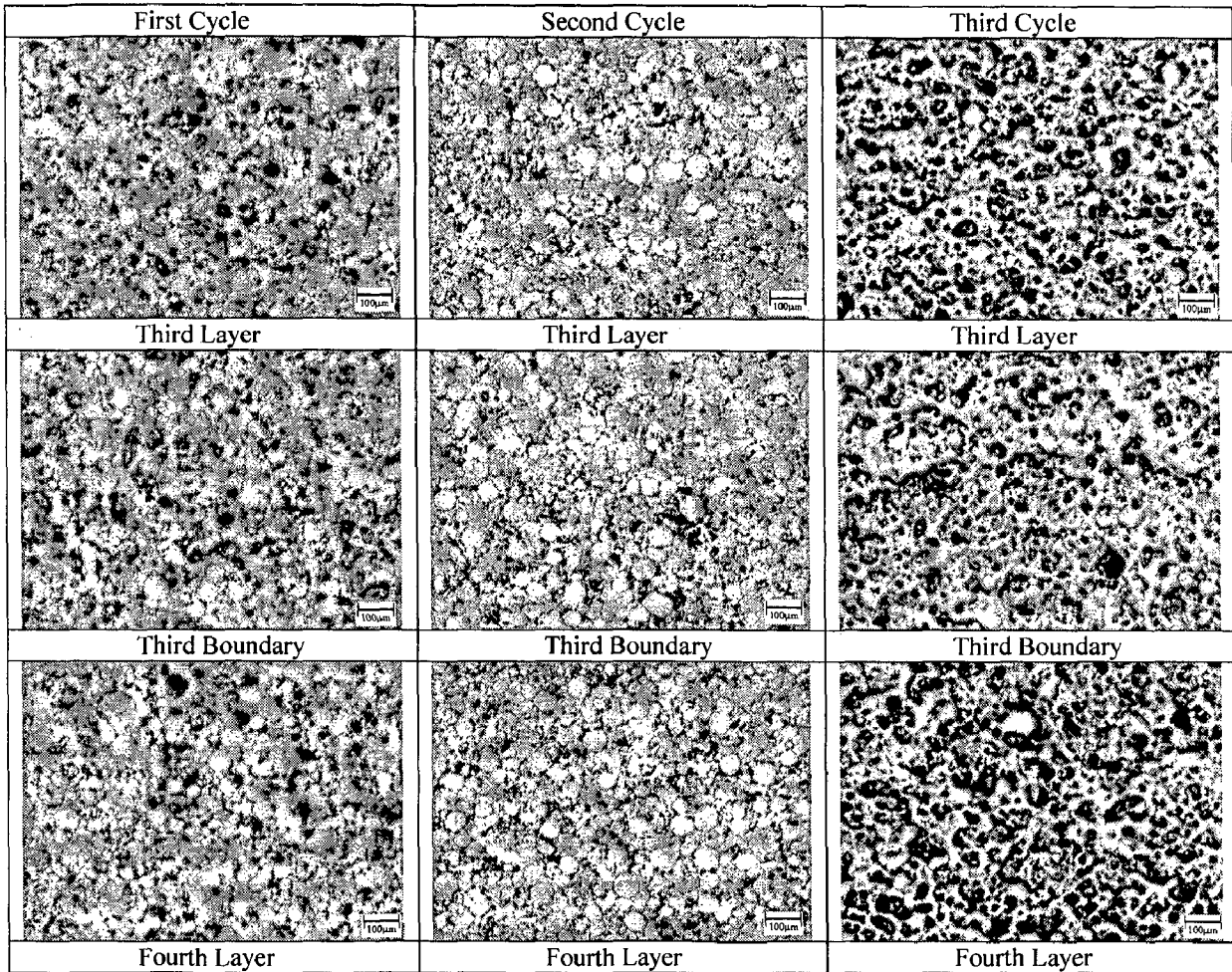


Figure 21

First Boundary of C2:

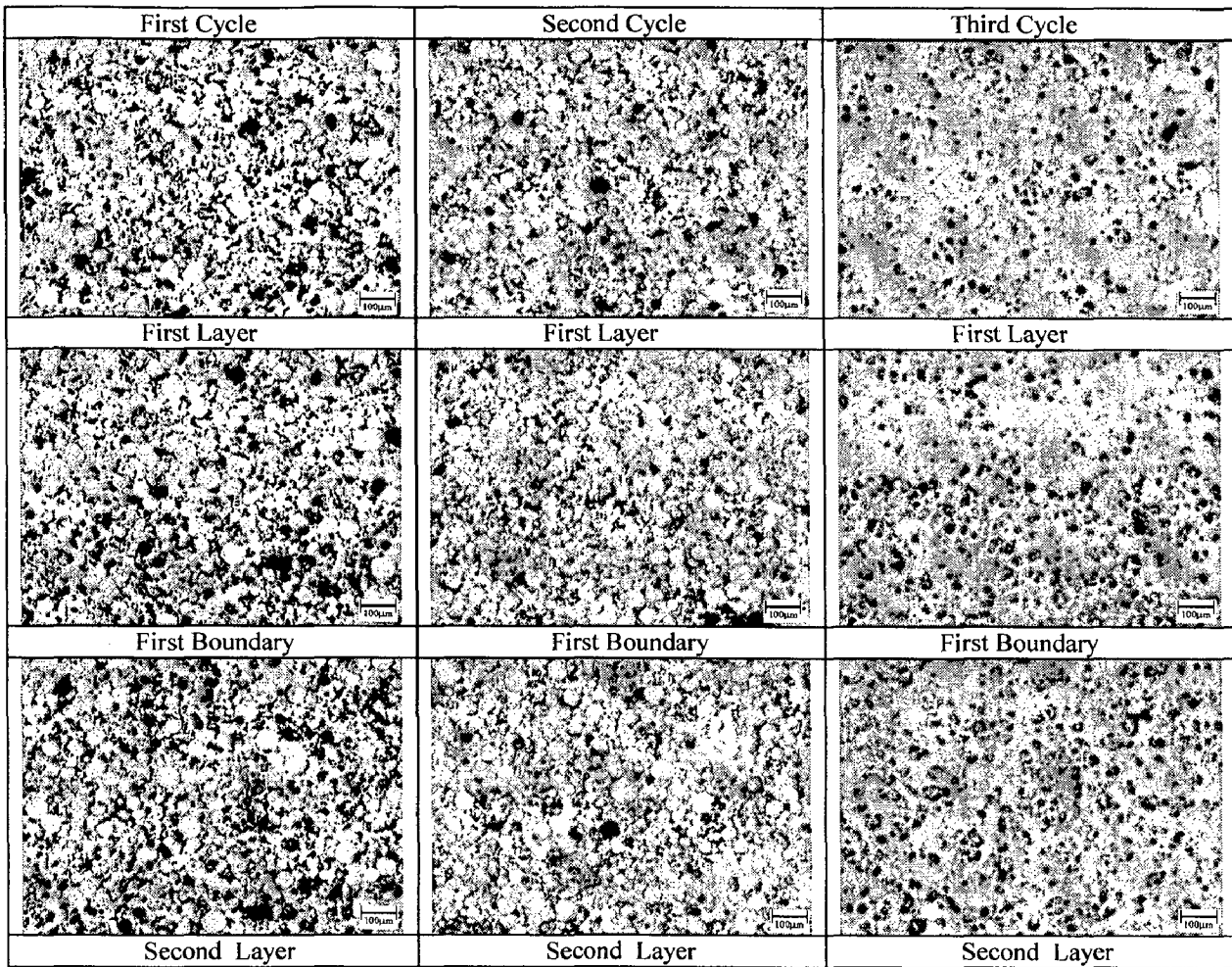


Figure 22

Second Boundary of C2:

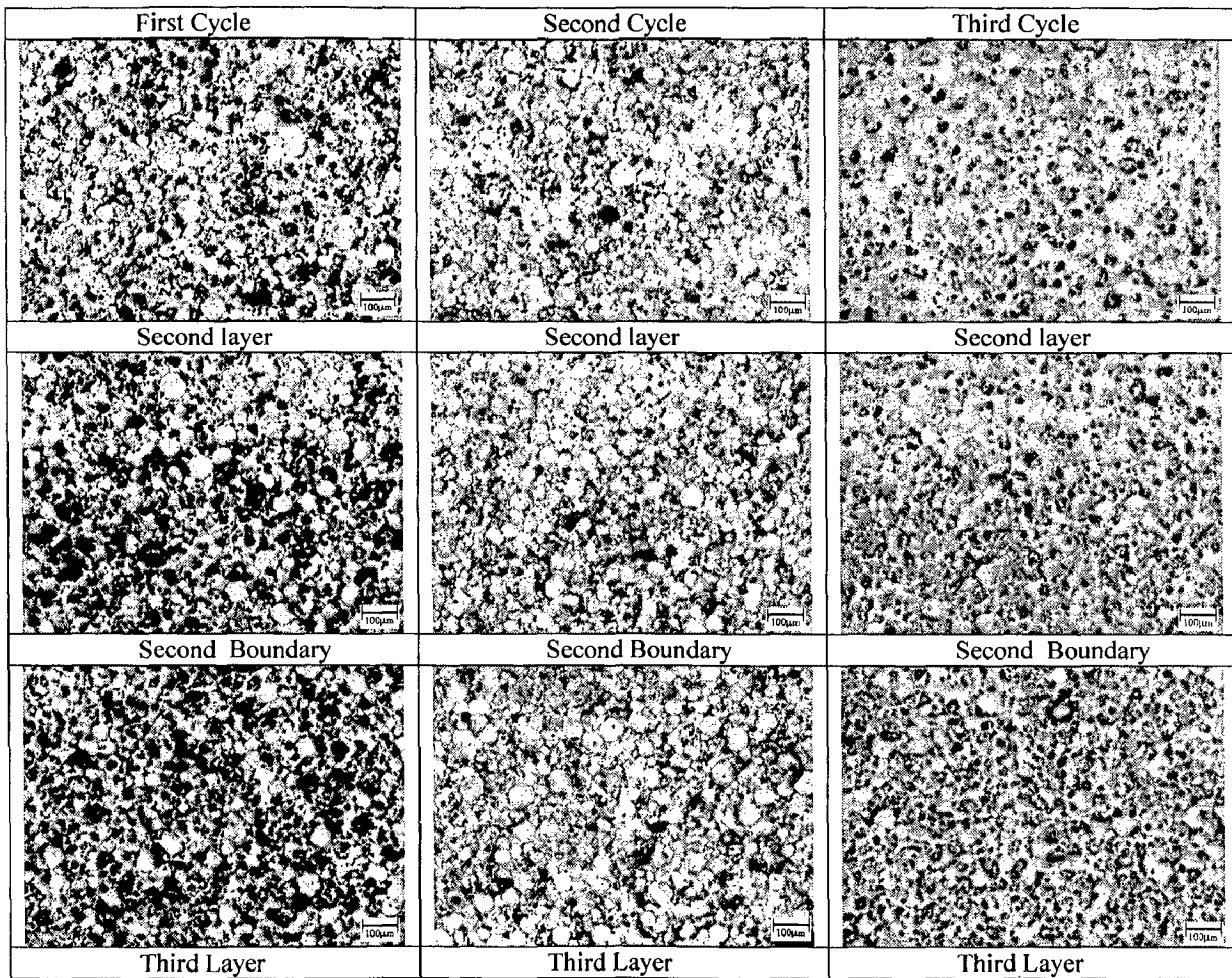


Figure 23

Third Boundary of C2:

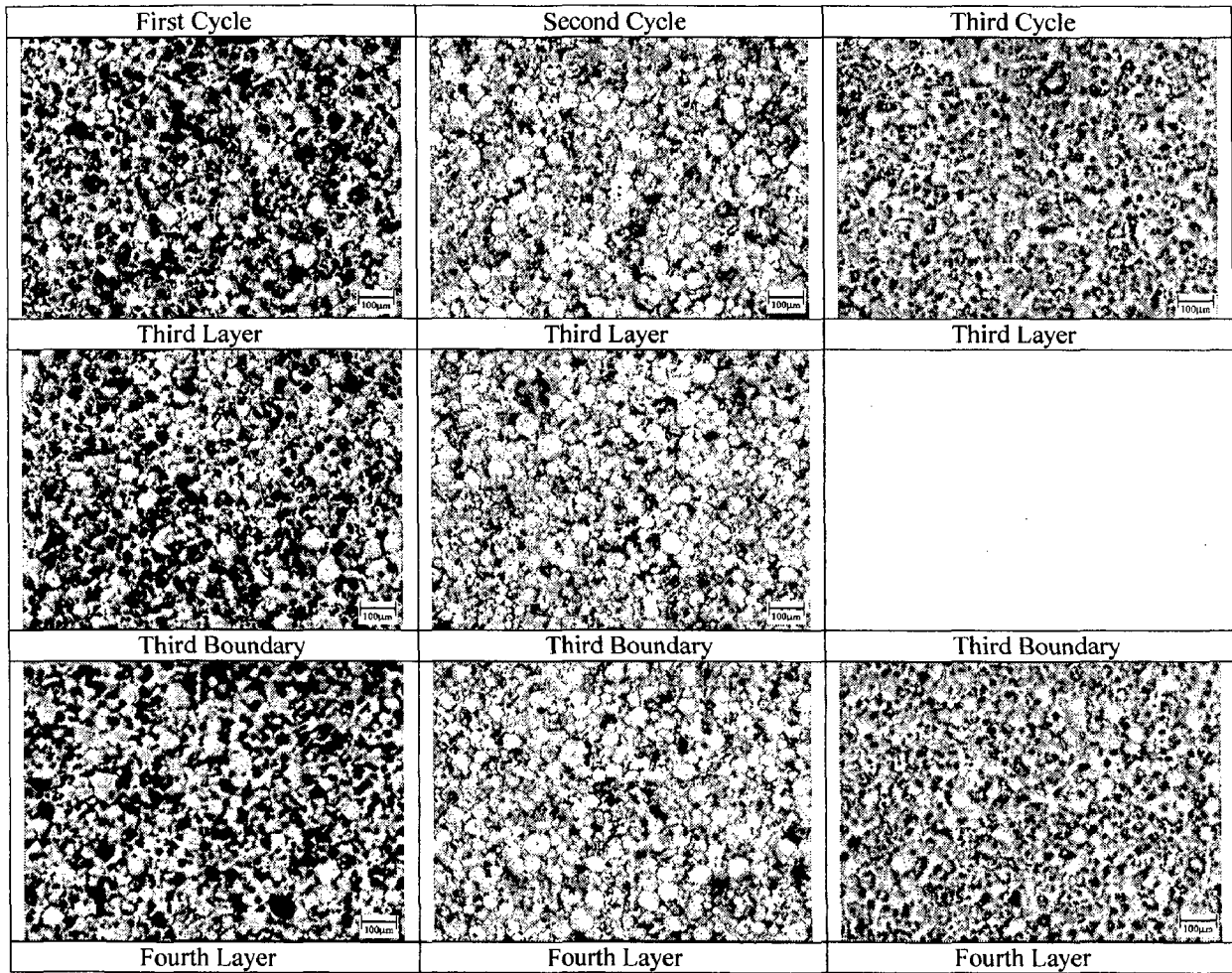


Figure 24

First Boundary of C3:

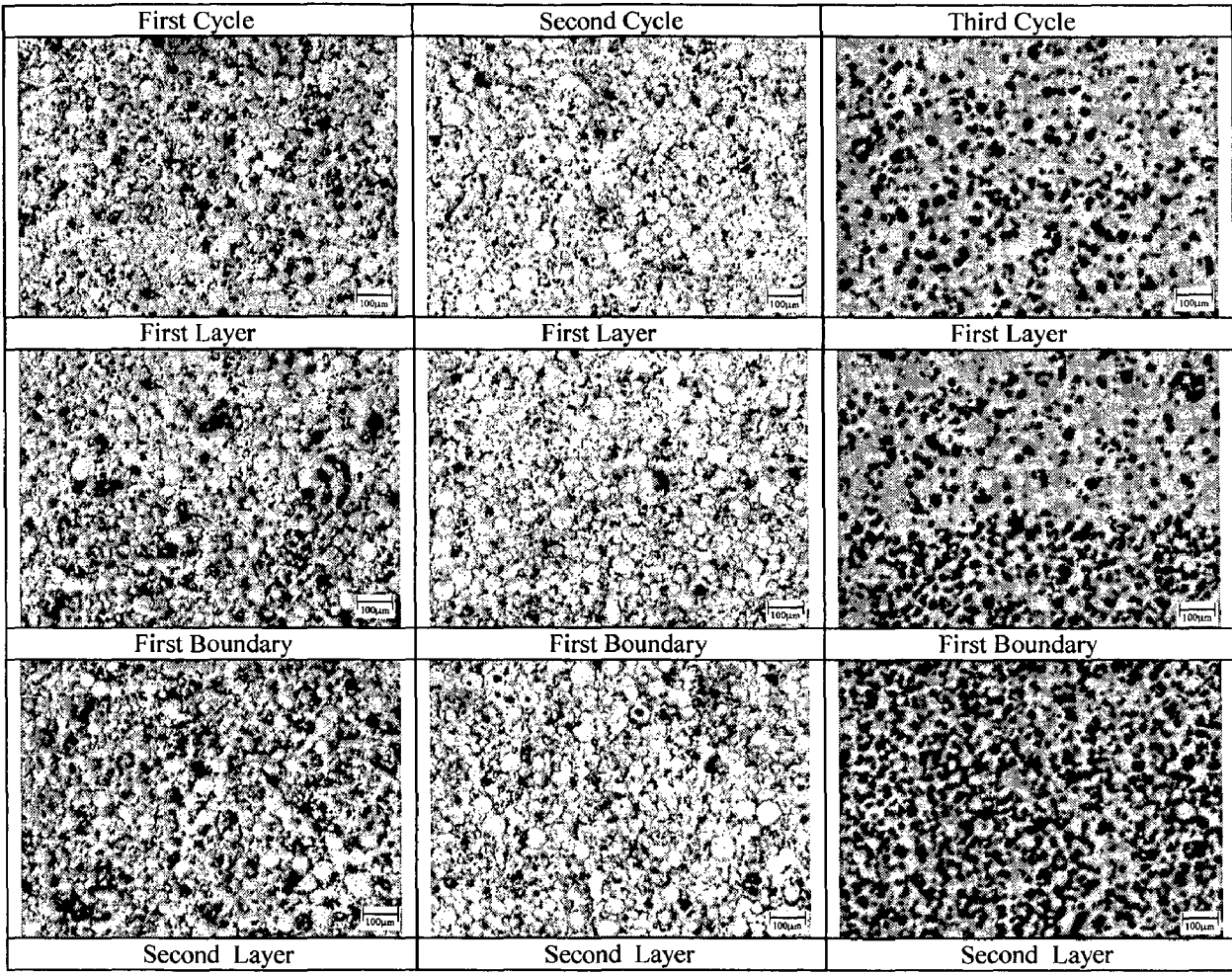


Figure 25

Second Boundary of C3:

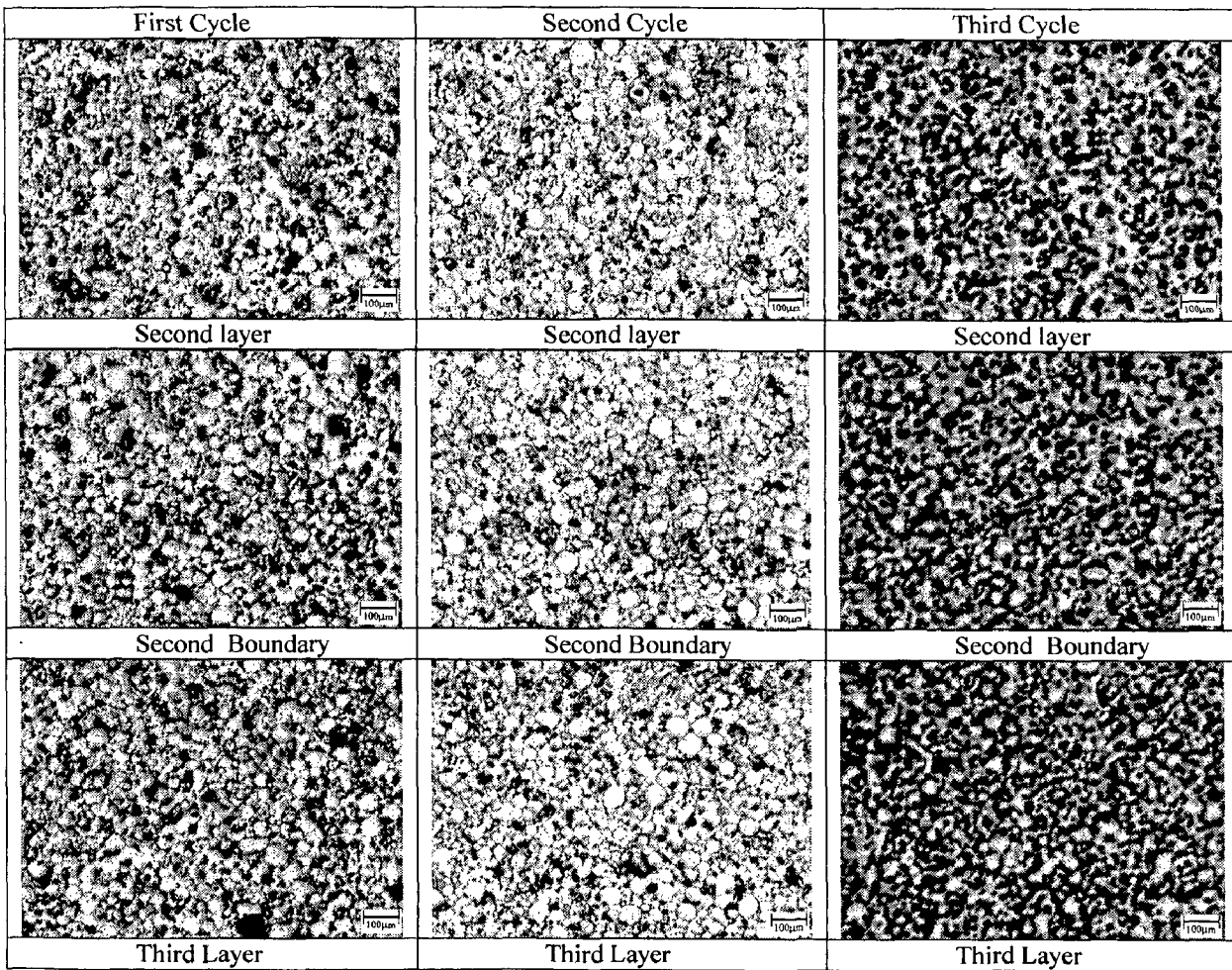


Figure 26

Third Boundary of C3:

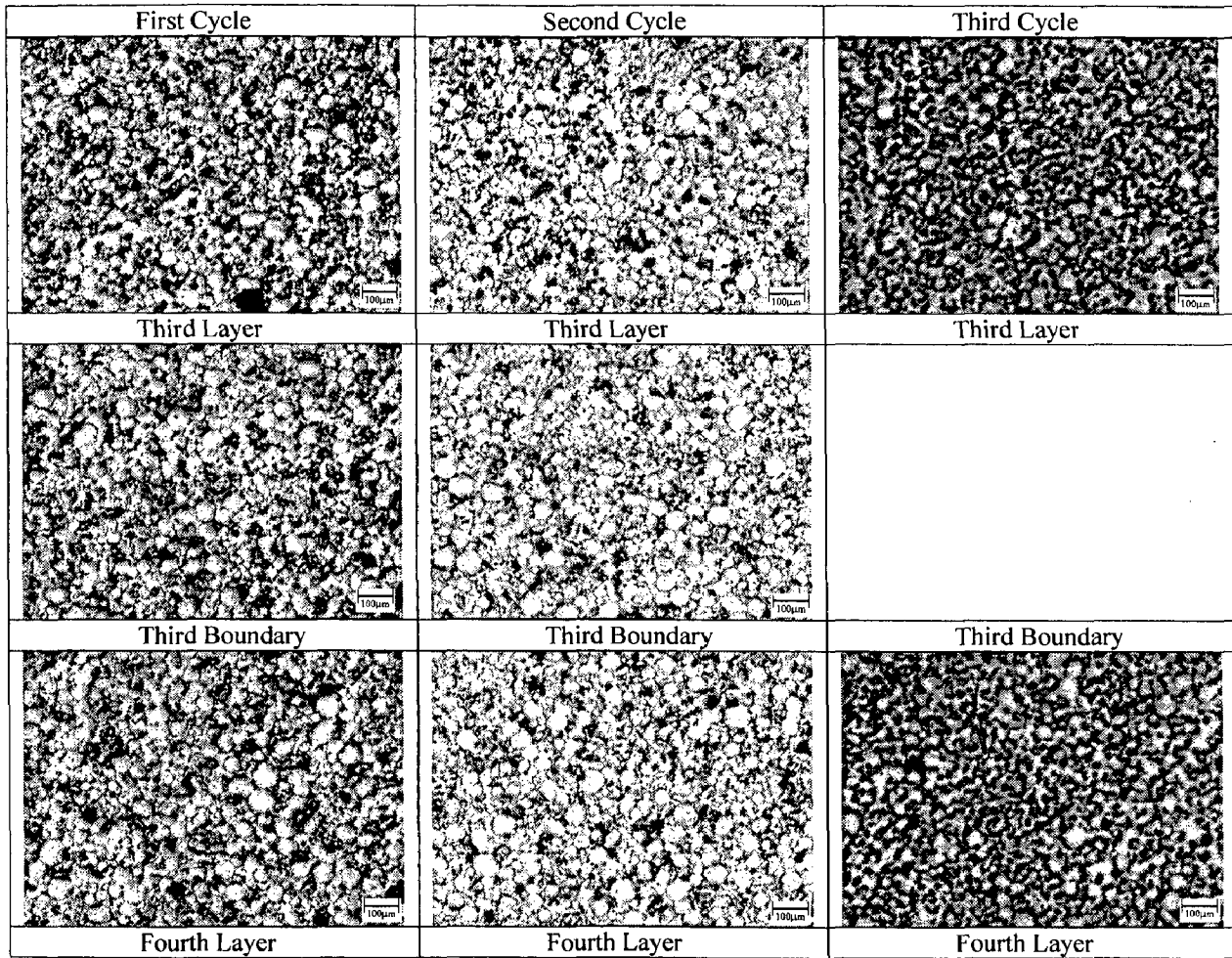


Figure 27

First Boundary of C4:

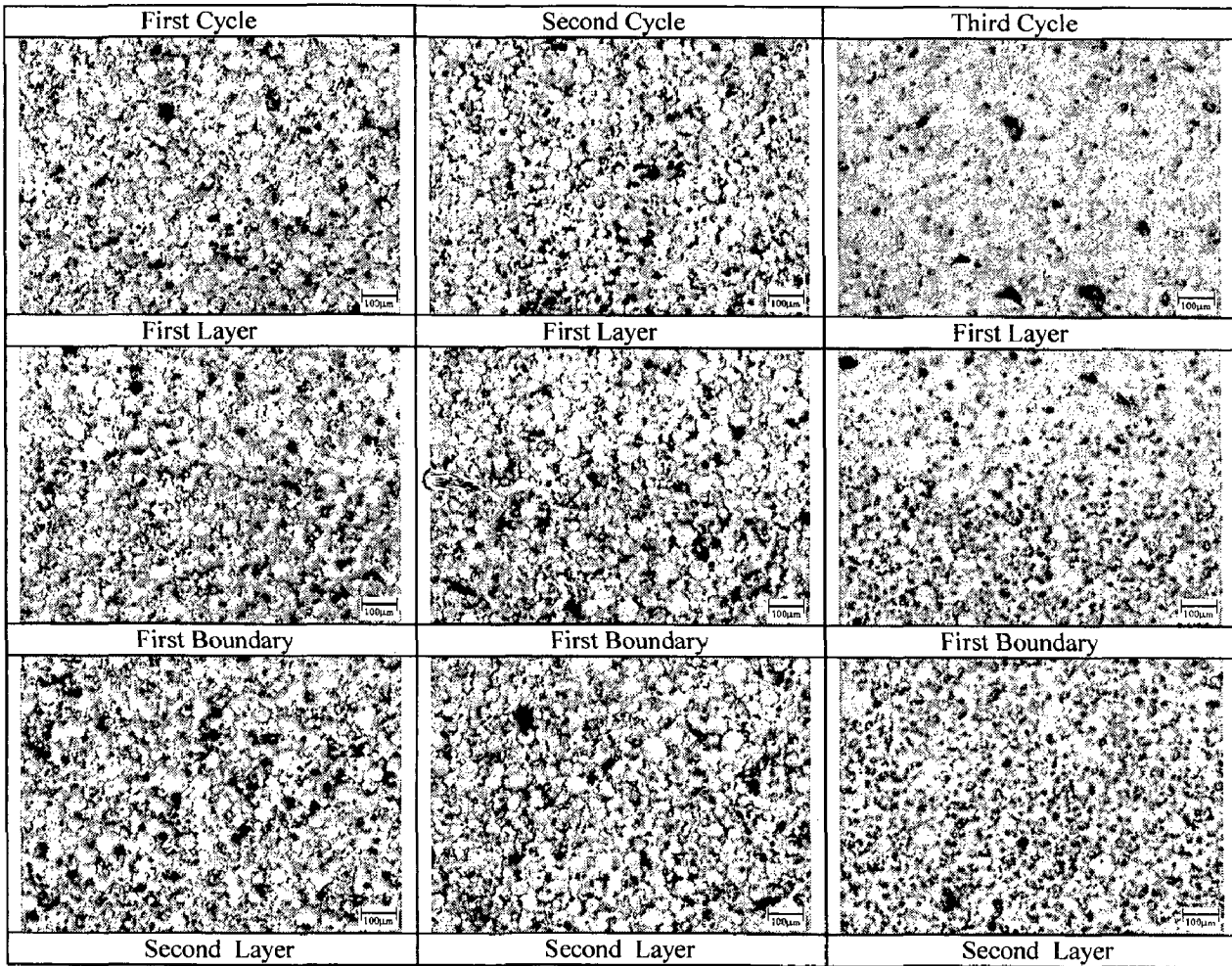


Figure 28

Second Boundary of C4:

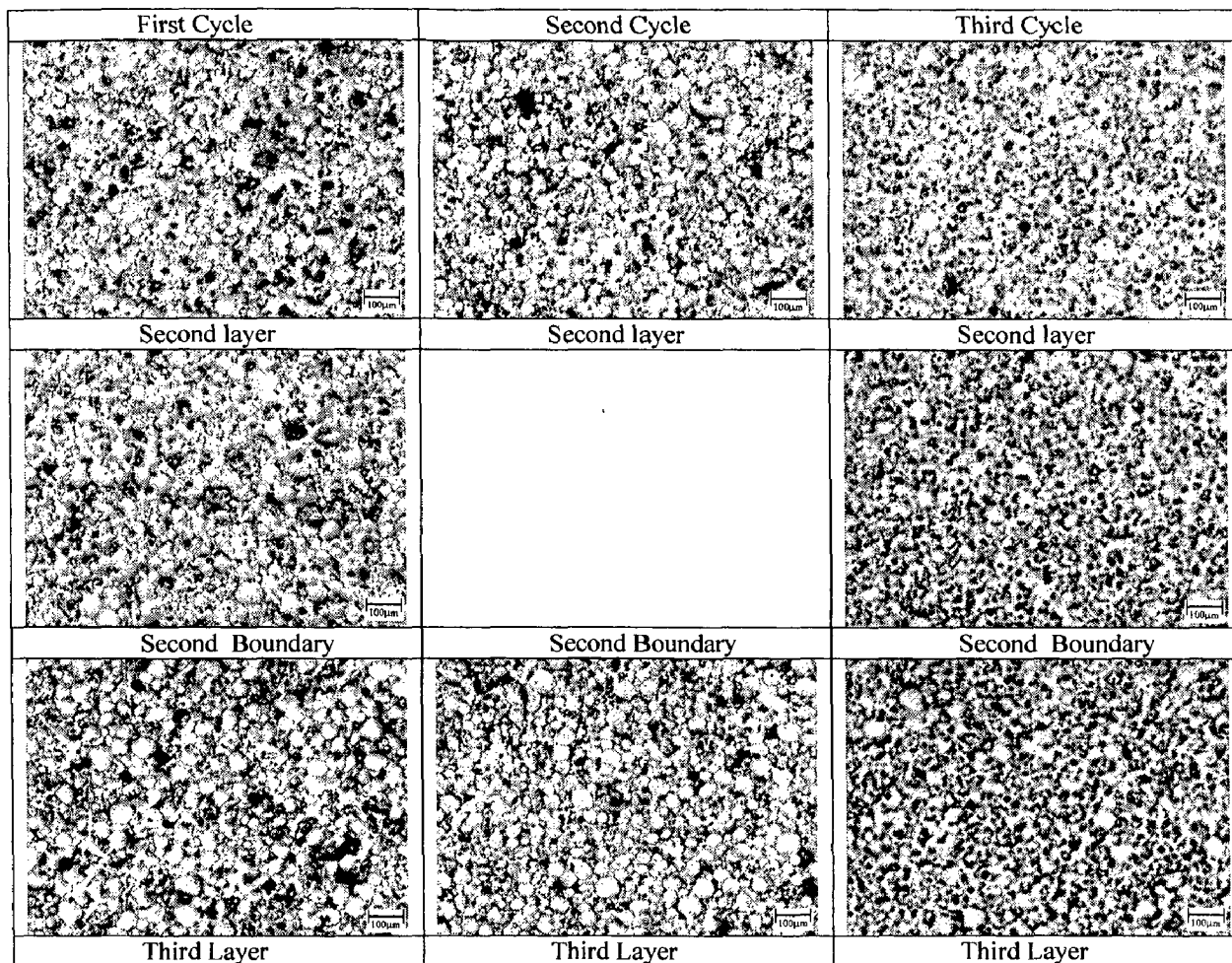


Figure 29

Third Boundary of C4:

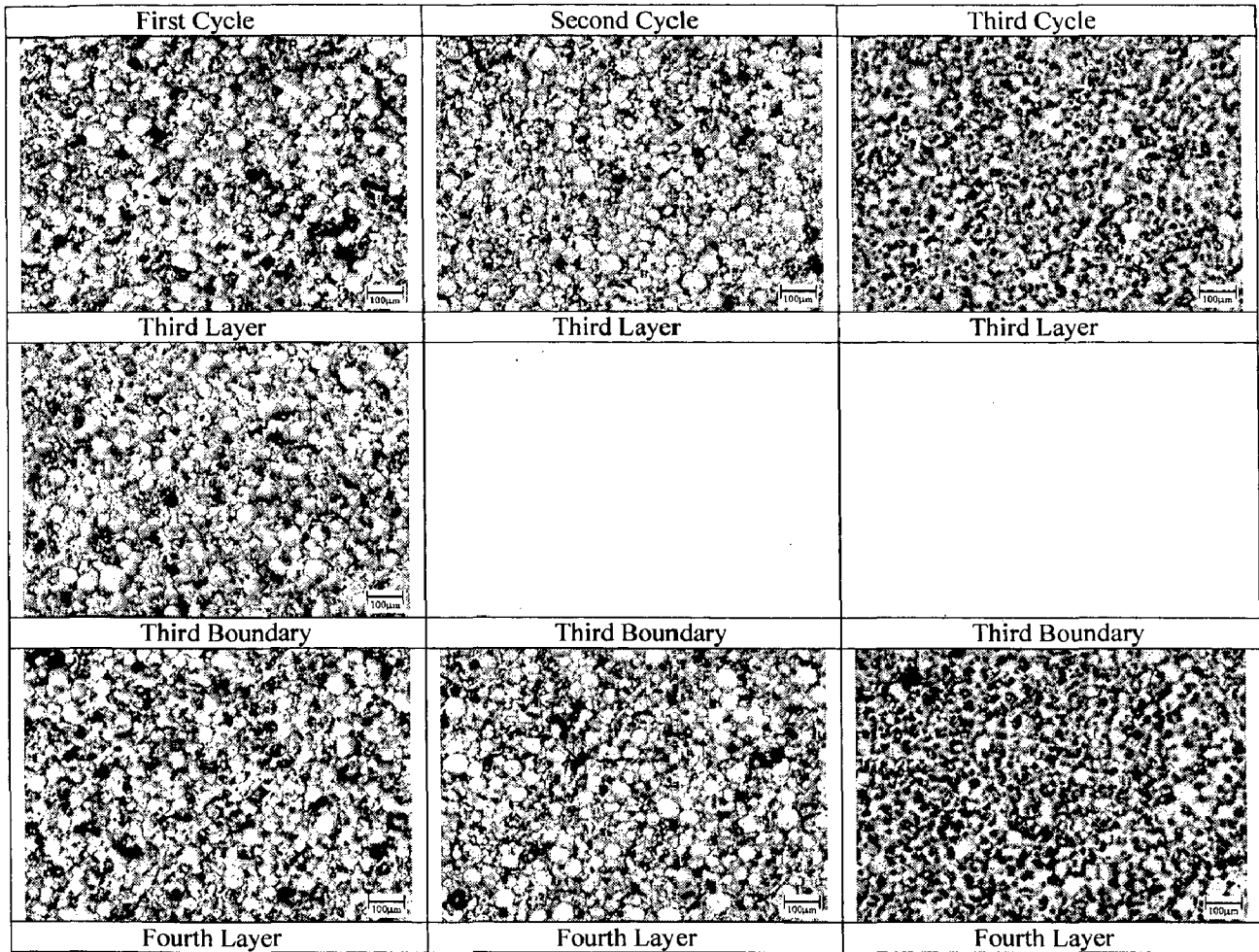


Figure 30

First Boundary of C5:

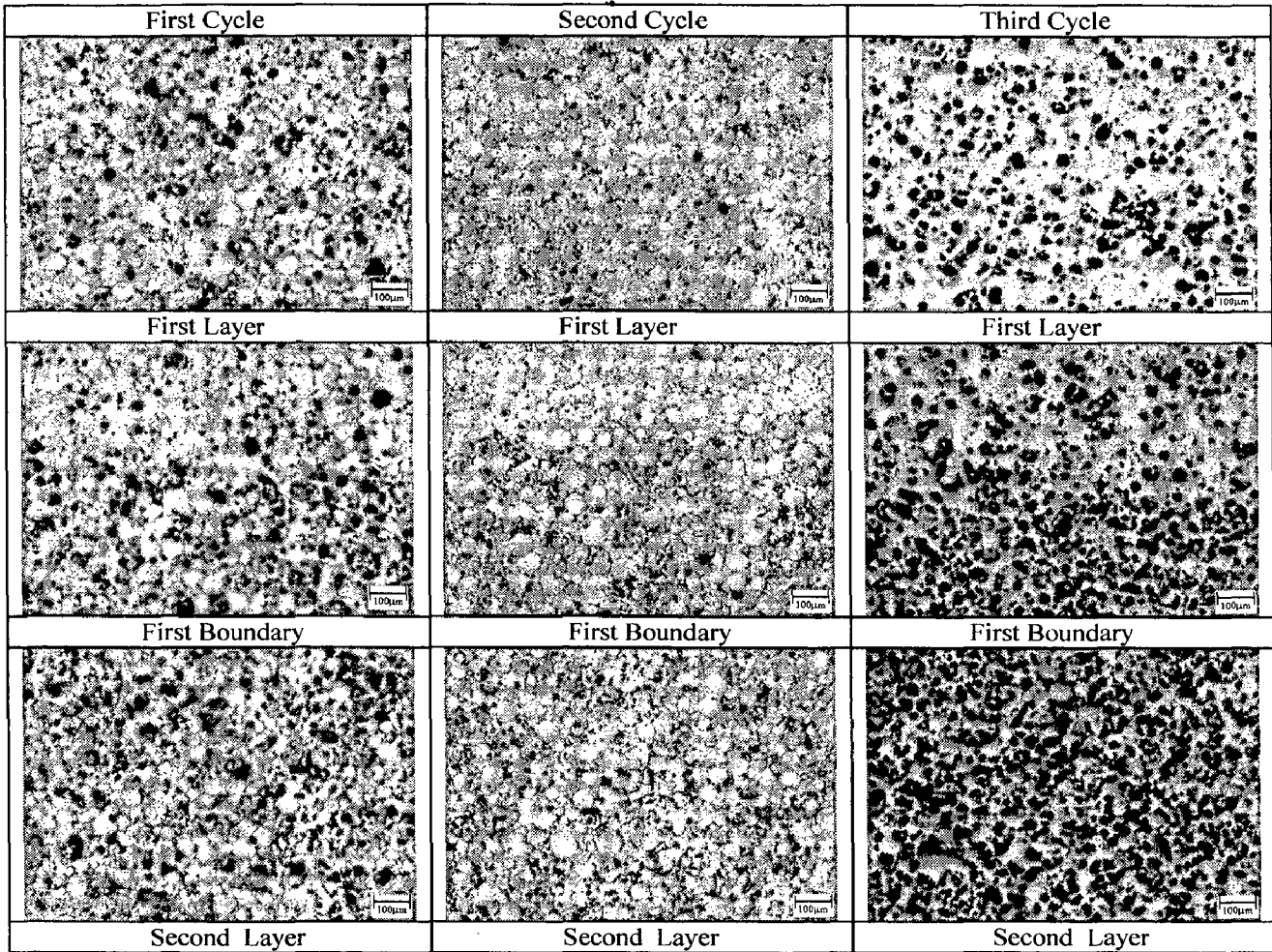


Figure 31

Second Boundary of C5:

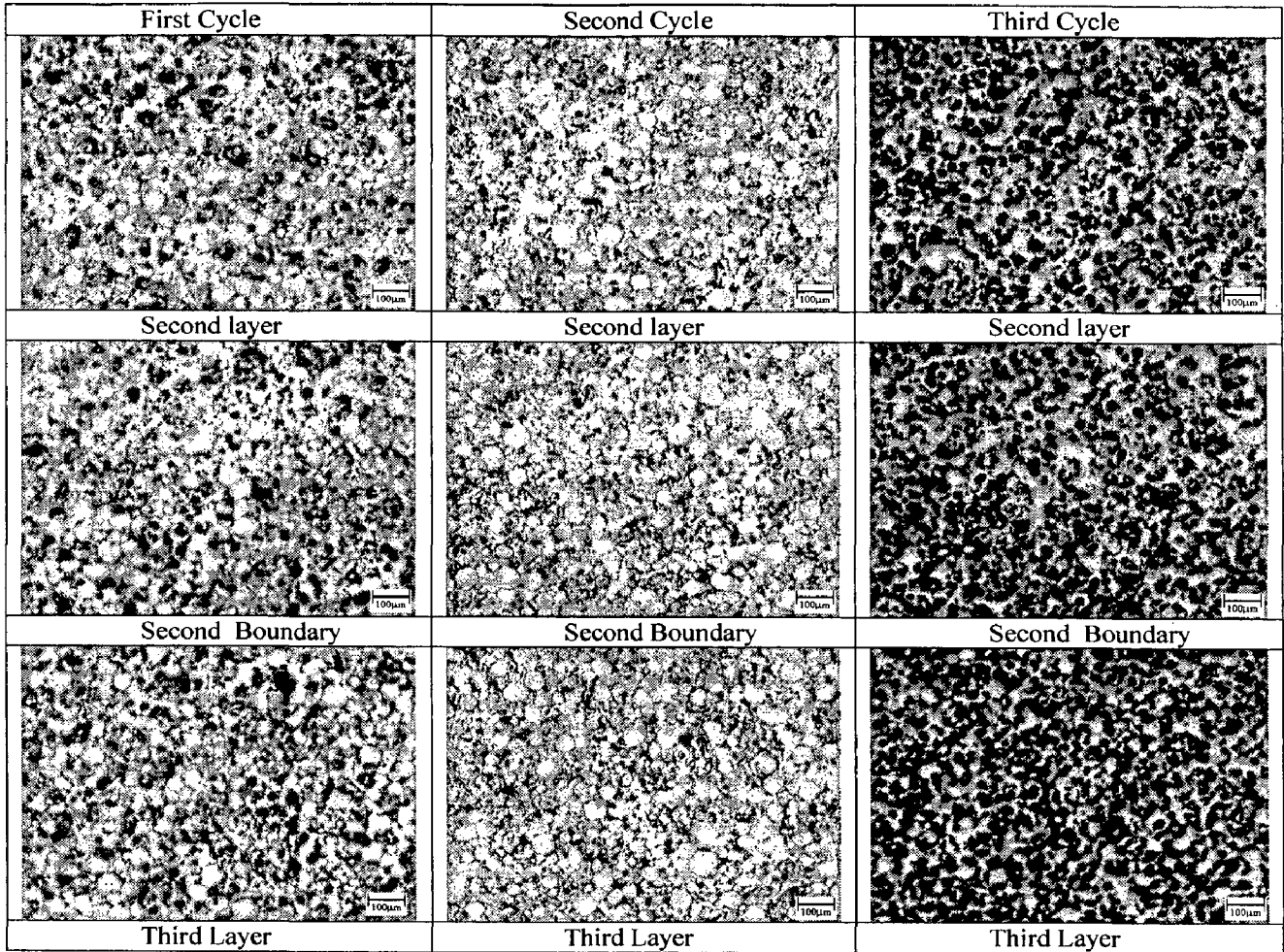


Figure 32

Third Boundary of C5:

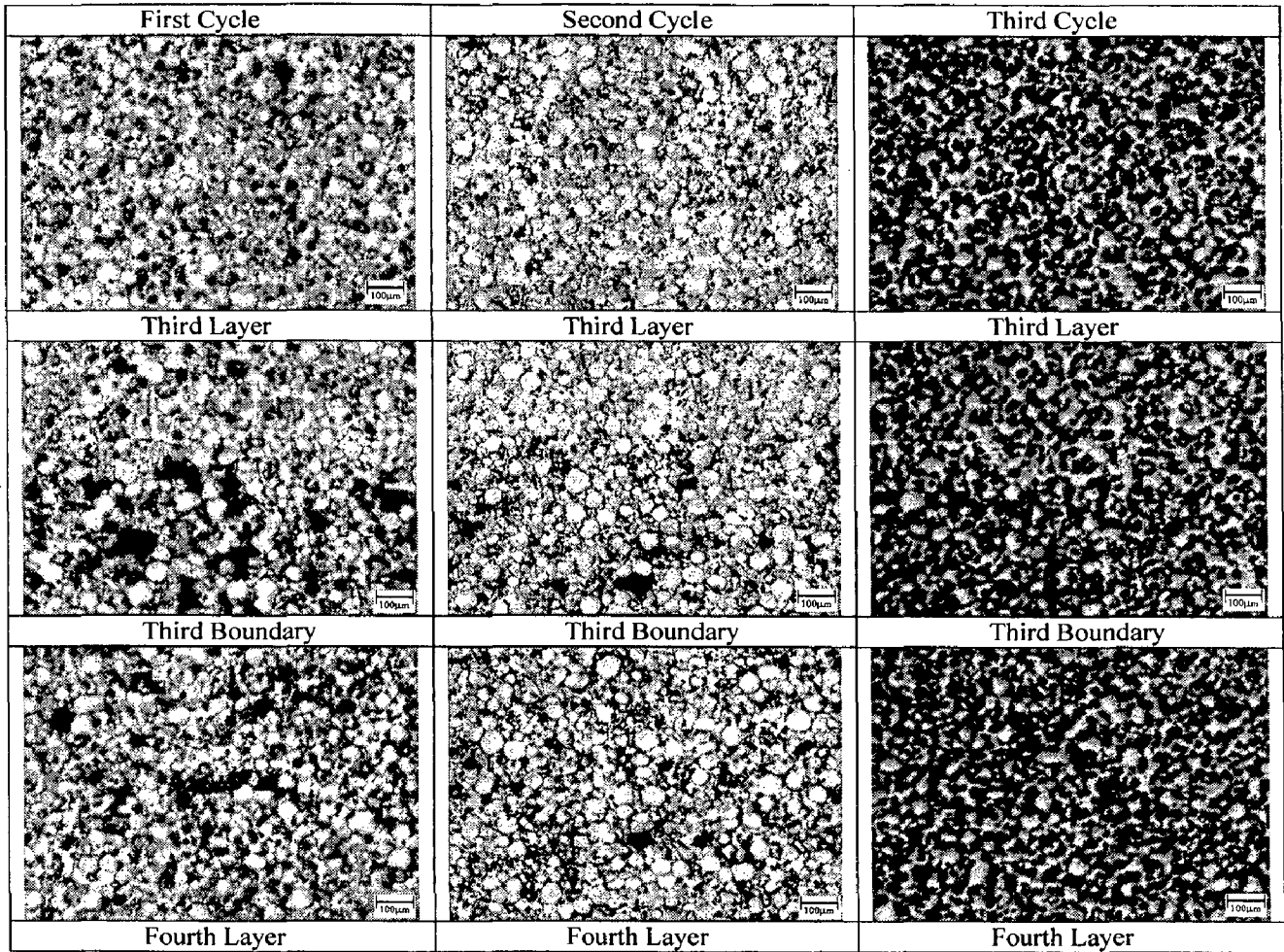


Figure 33

First Boundary of C6:

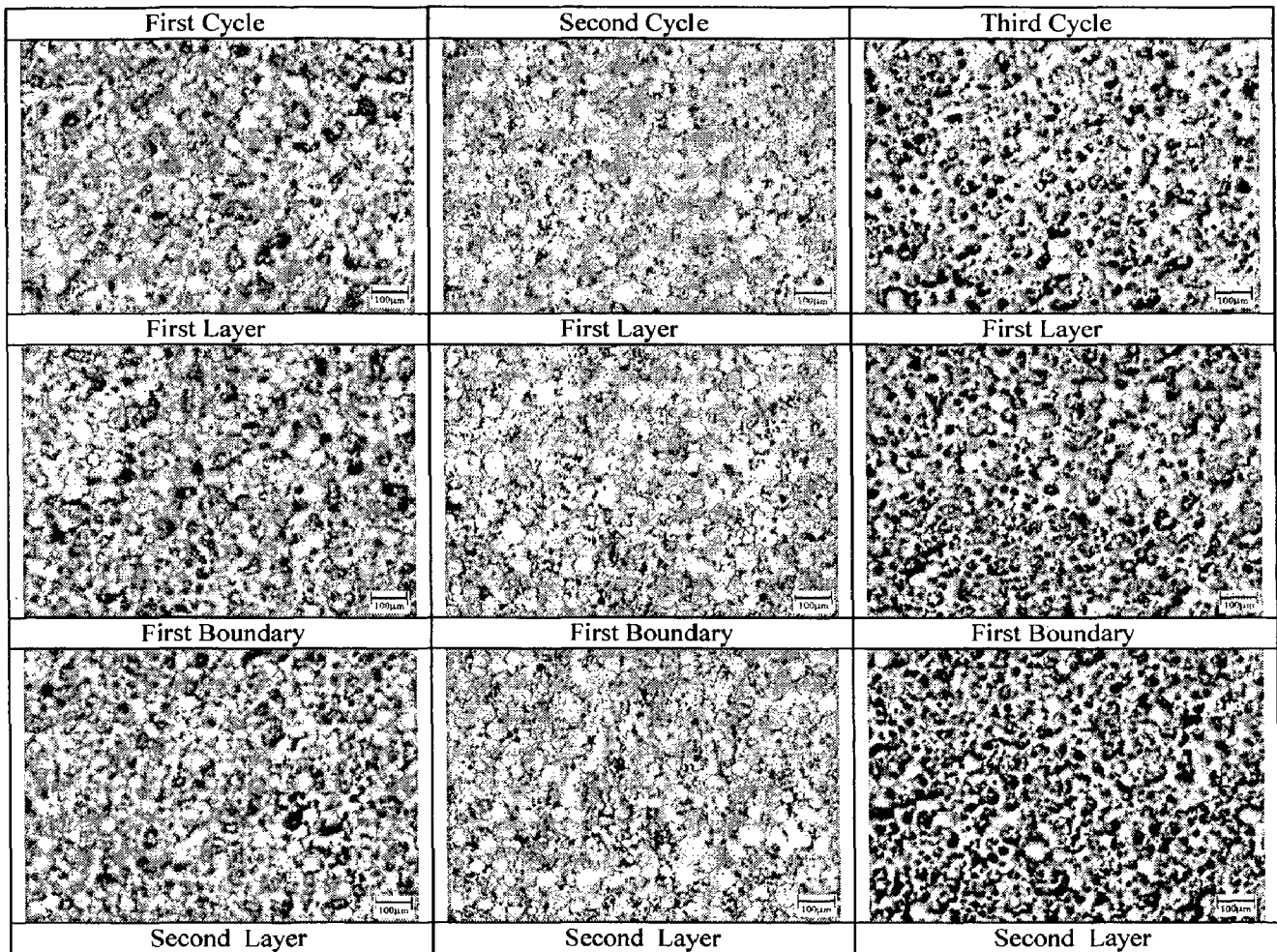


Figure 34

Second Boundary of C6:

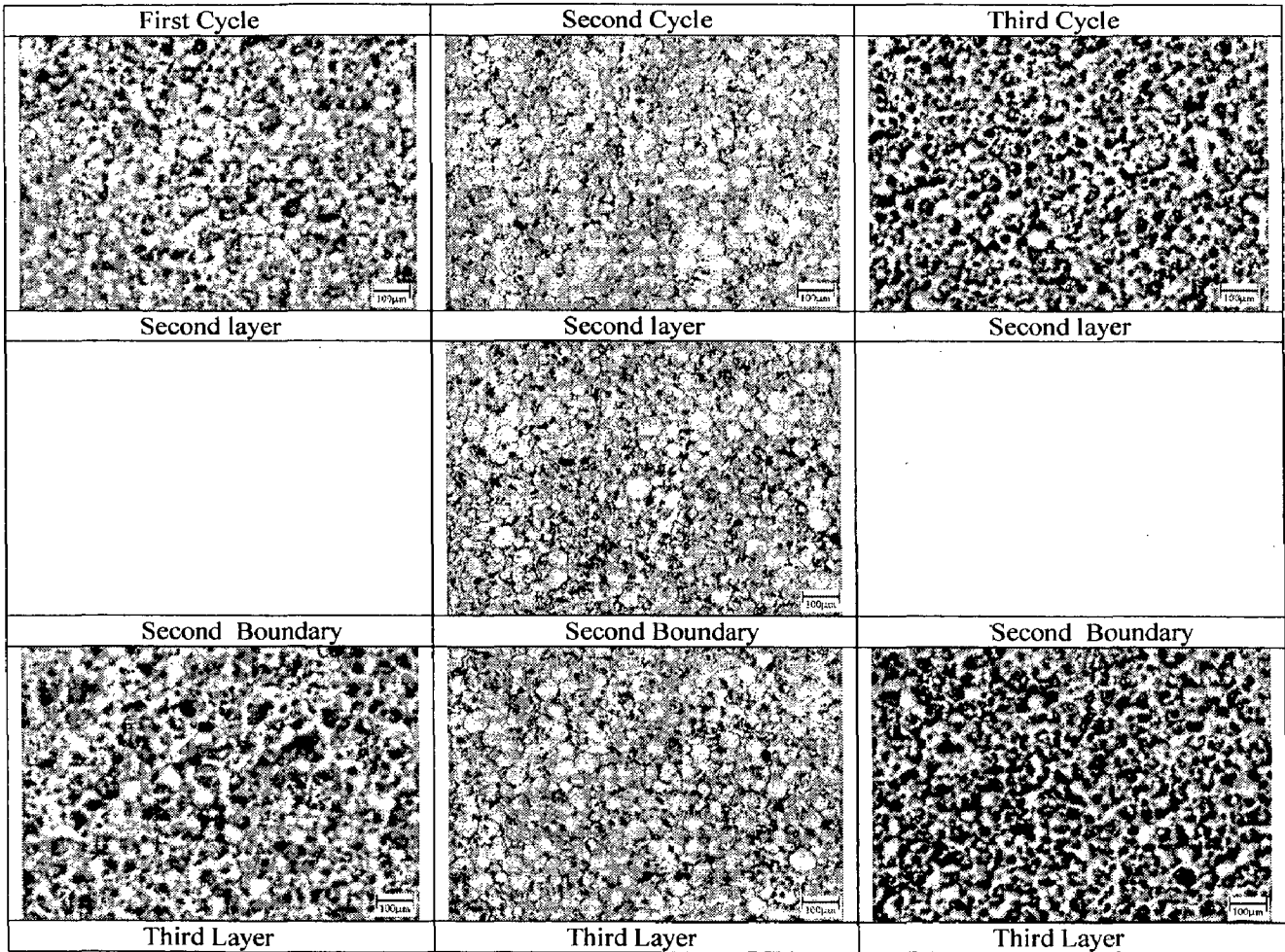


Figure 35

Third Boundary of C6:

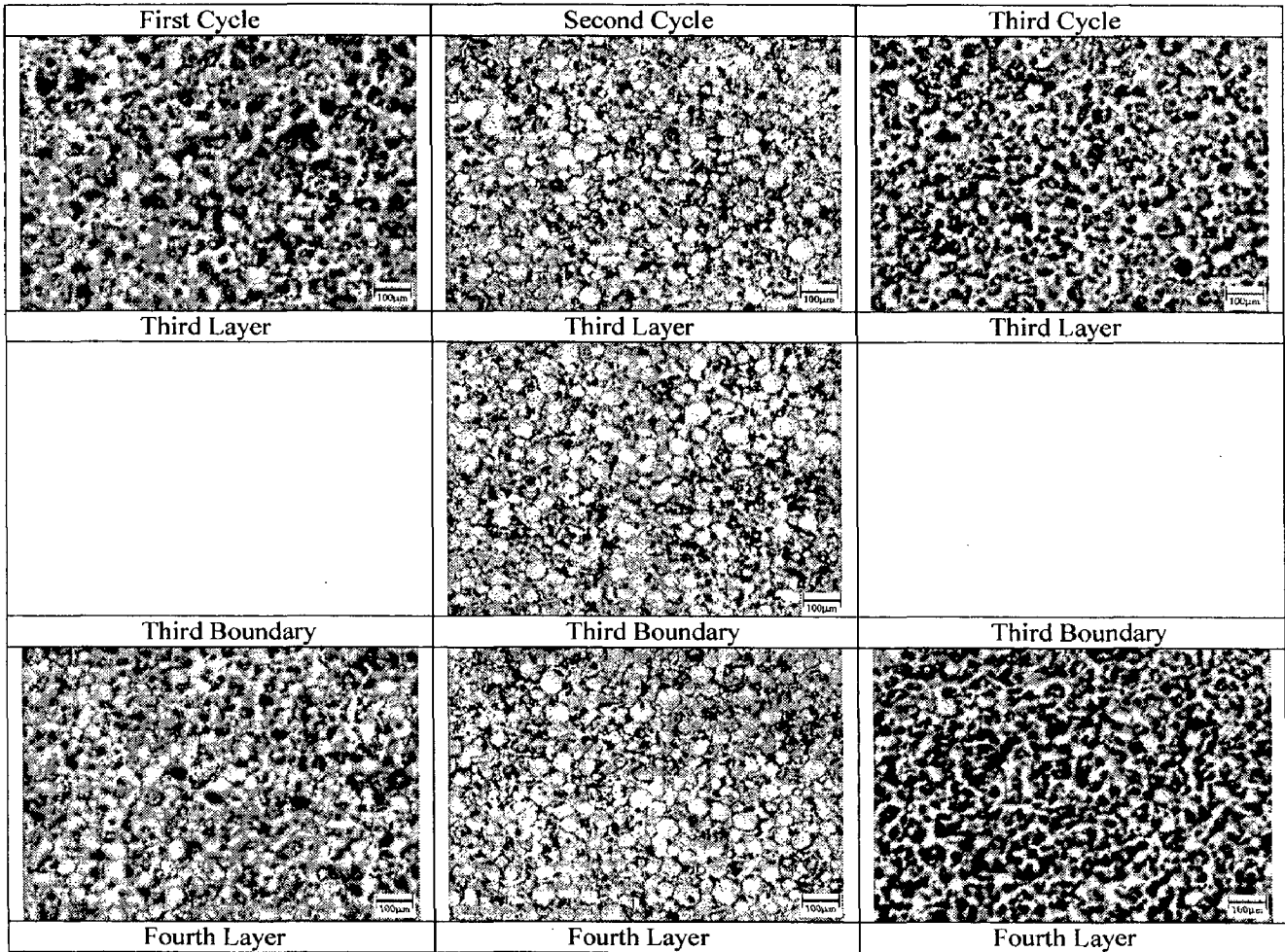


Figure 36

Microstructures after Rolling

**1000°C Specimens
Microstructures of C1**

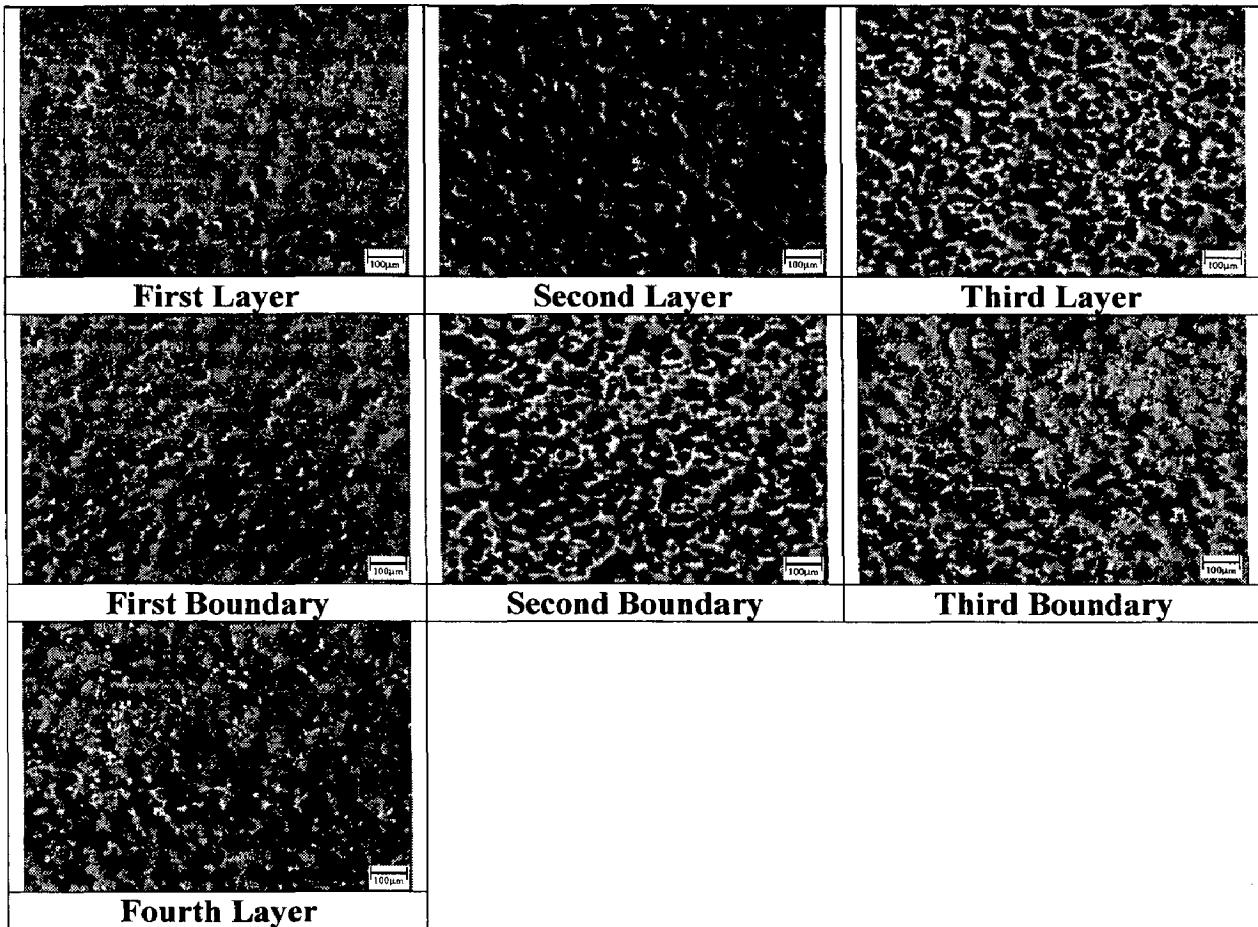


Figure 37

Microstructures of C2

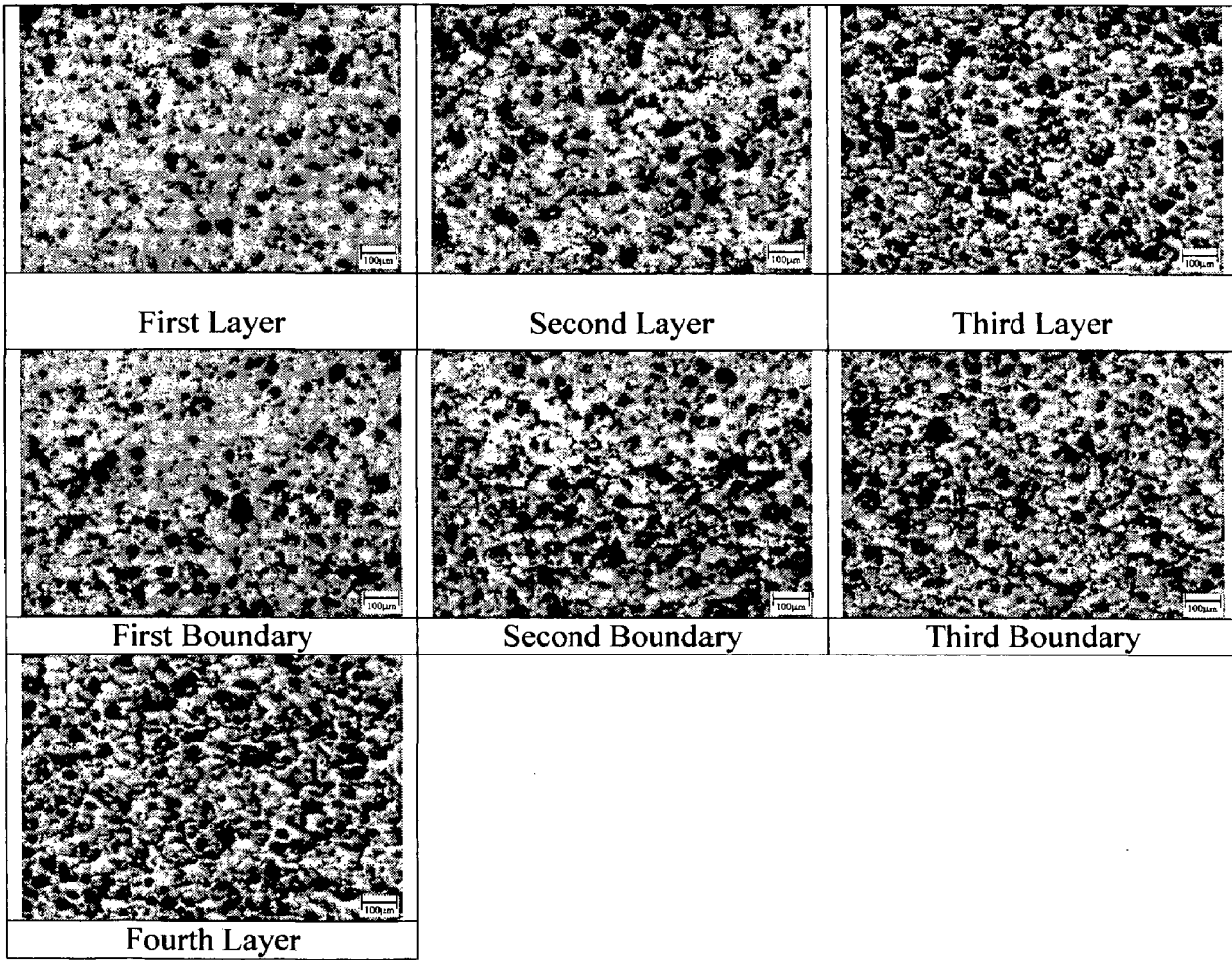


Figure 38

Microstructures of C3

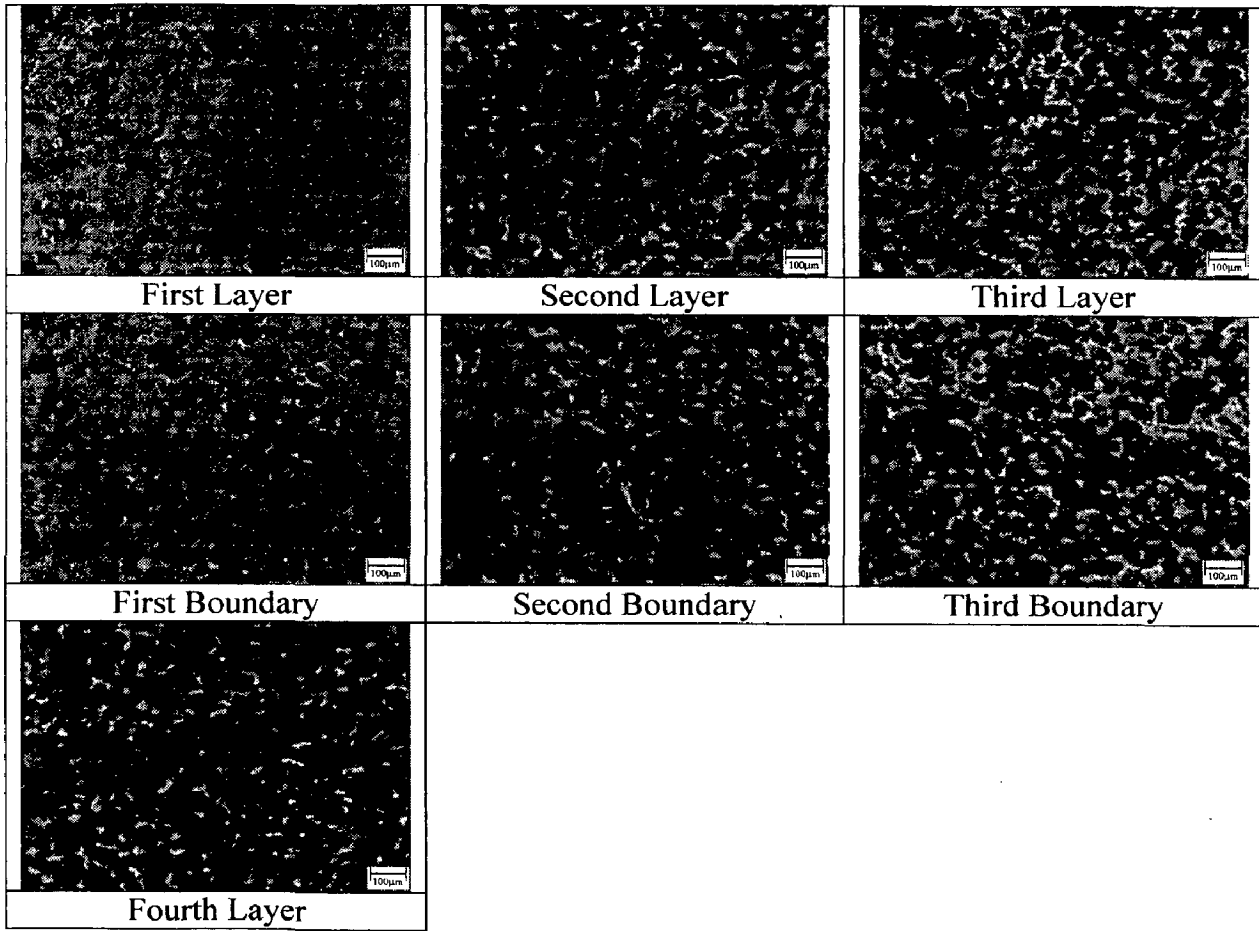


Figure 39

Microstructures of C4

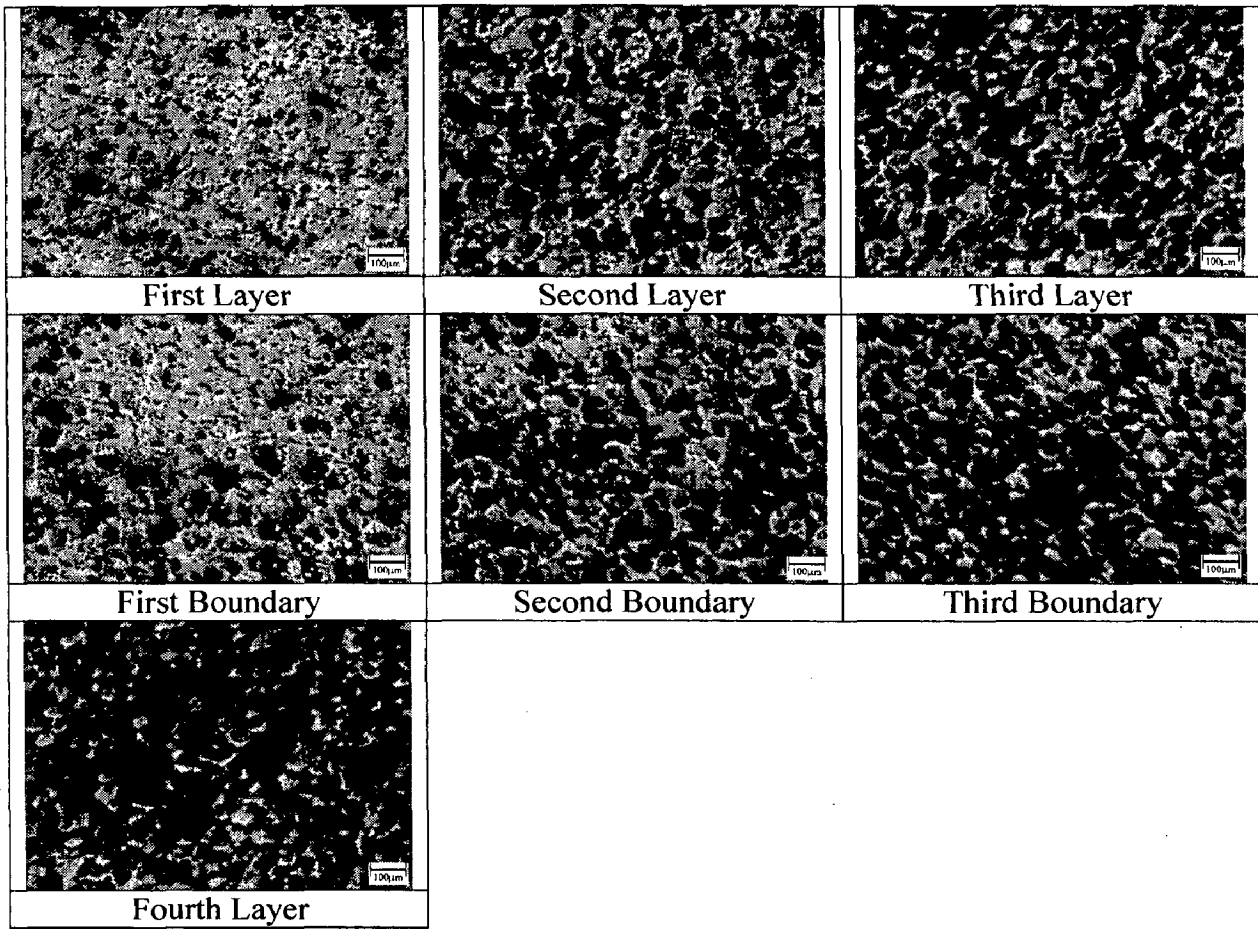


Figure 40

Microstructures of C5

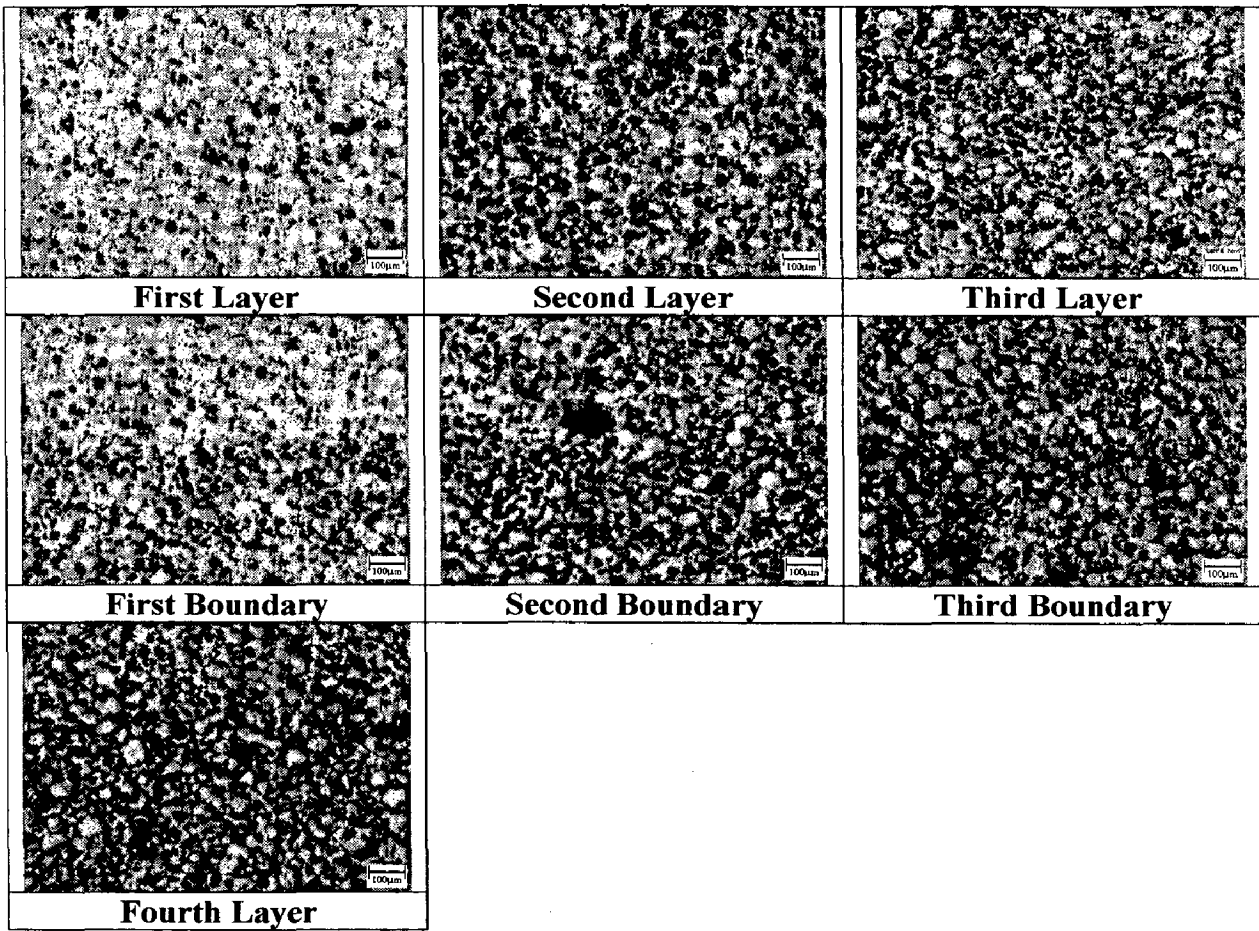


Figure 41

Microstructures of C6

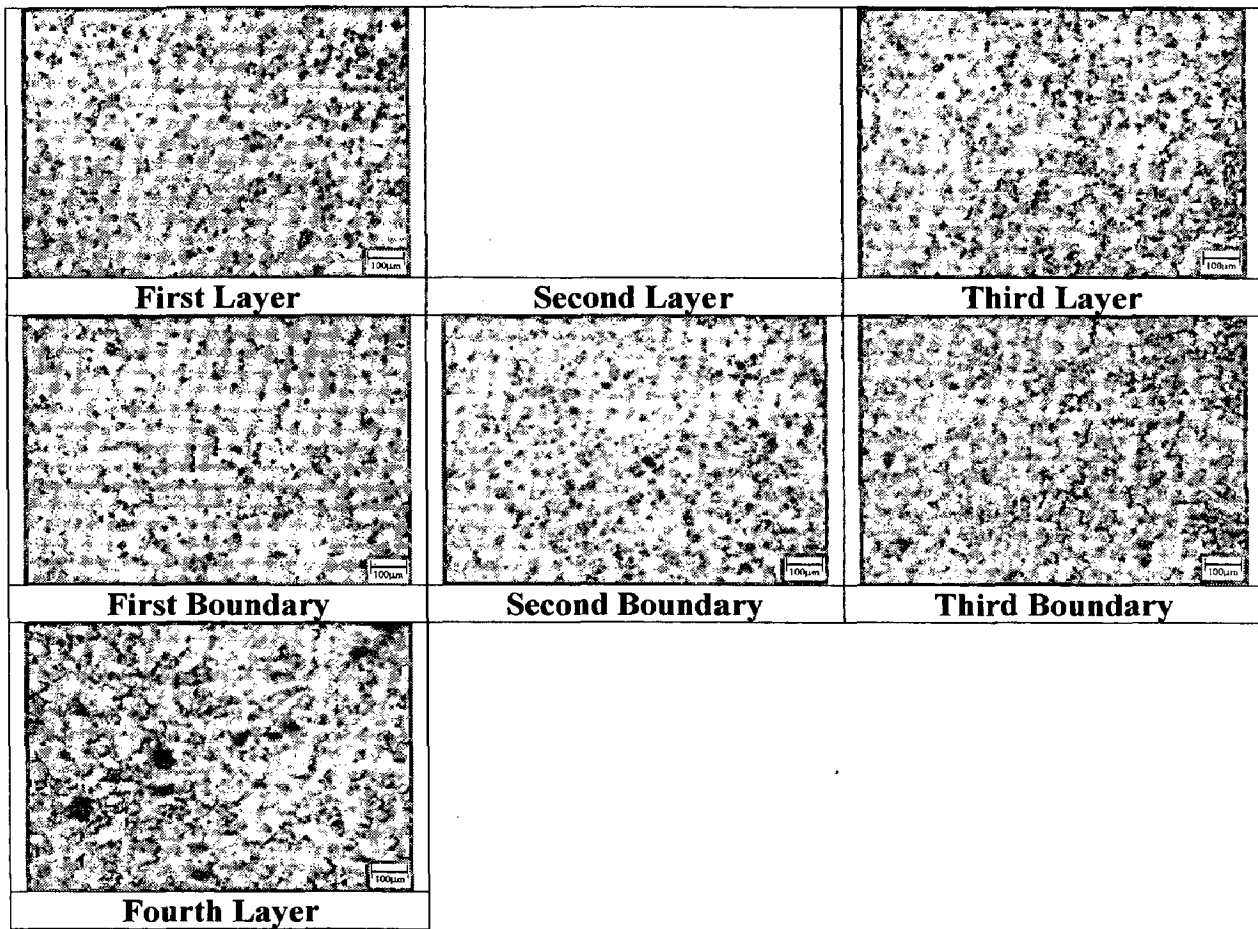


Figure 42

Microstructures of 800°C Specimens

Microstructures of C1

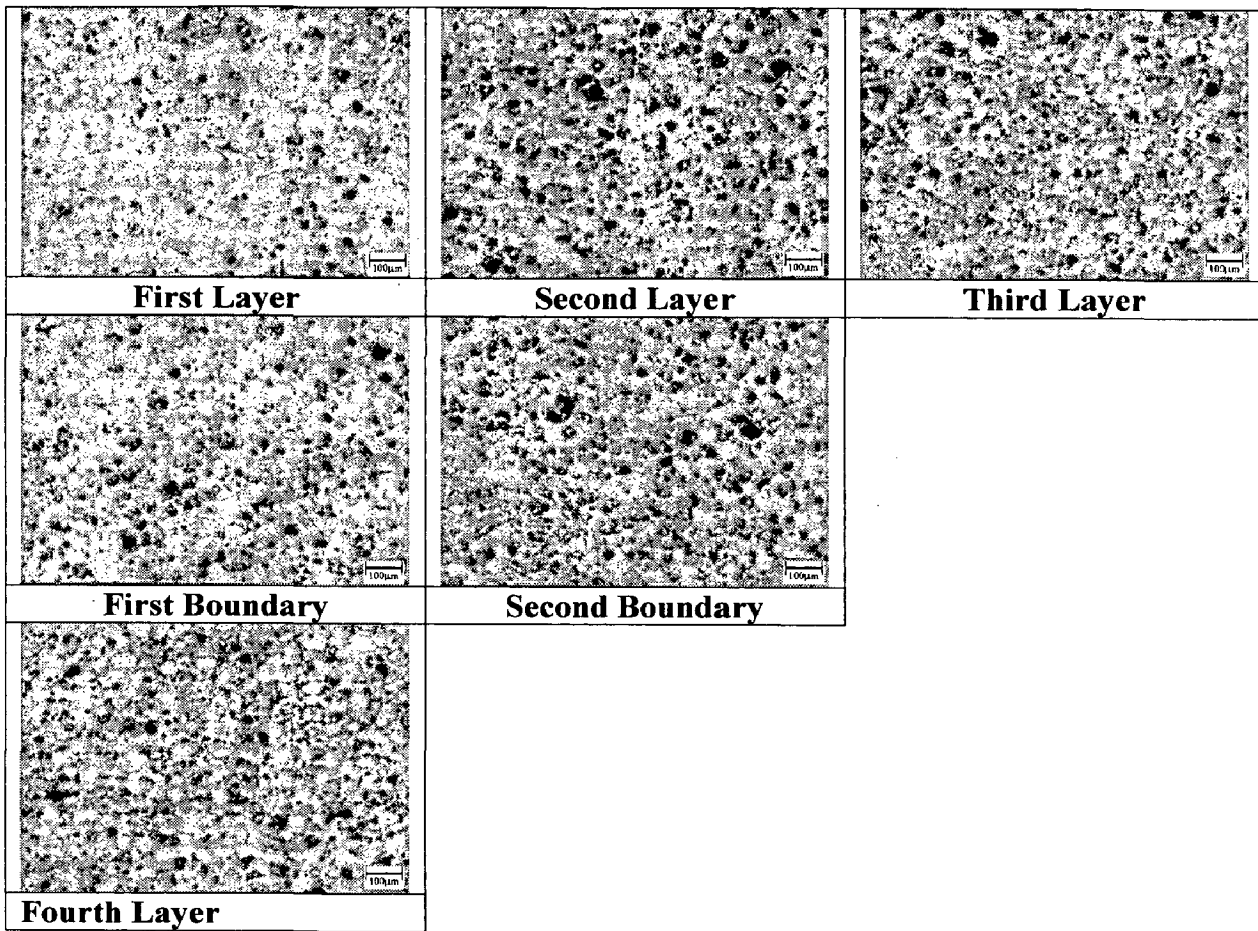


Figure 43

Microstructures of C2

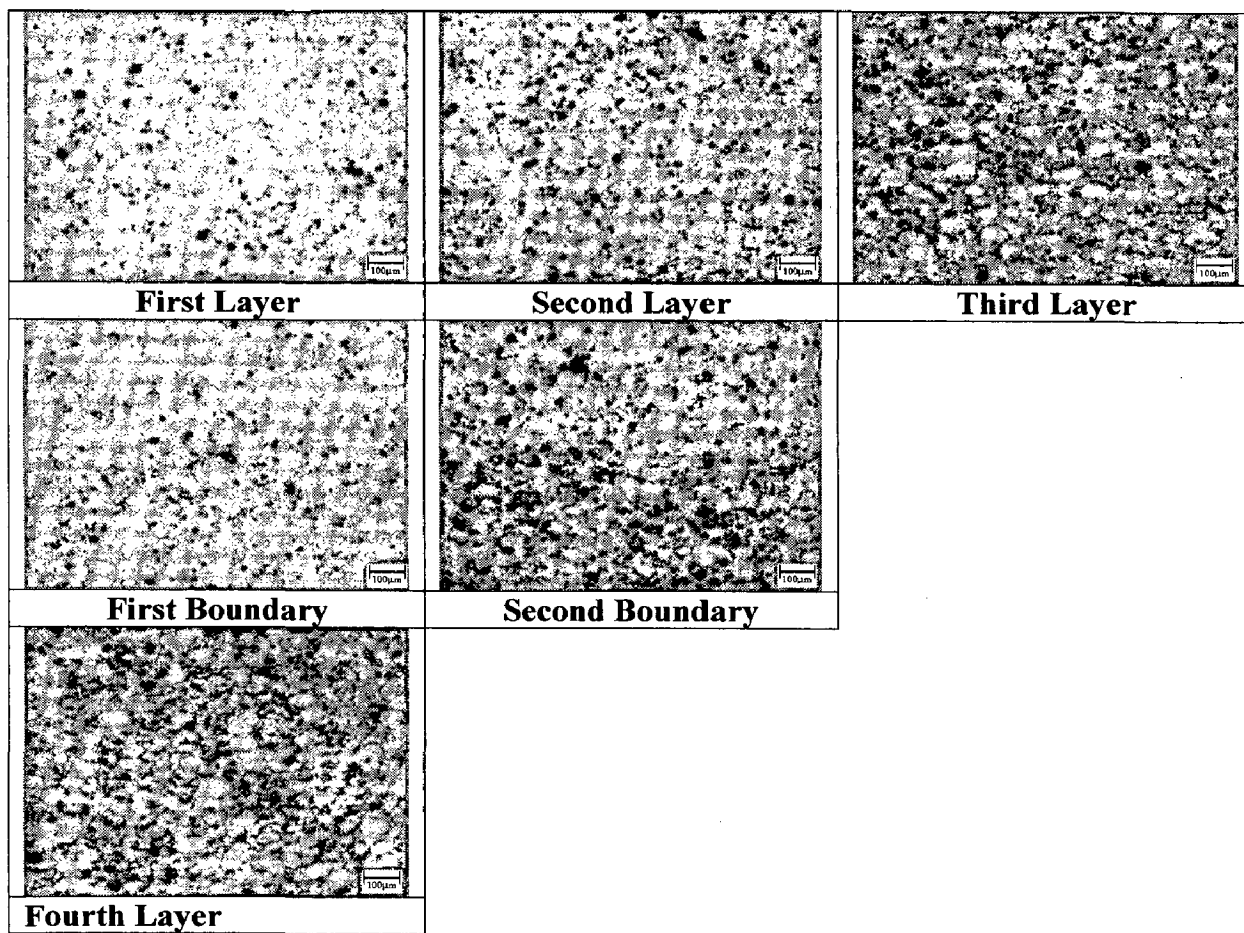


Figure 44

Microstructures of C4

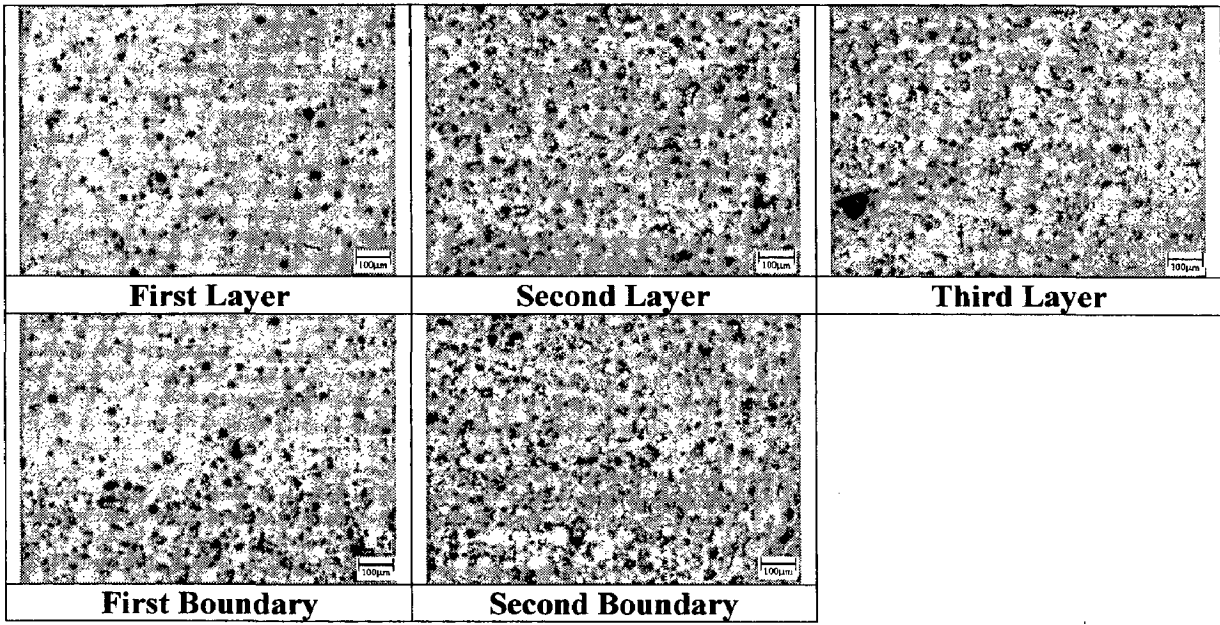


Figure 46

Microstructures of C2

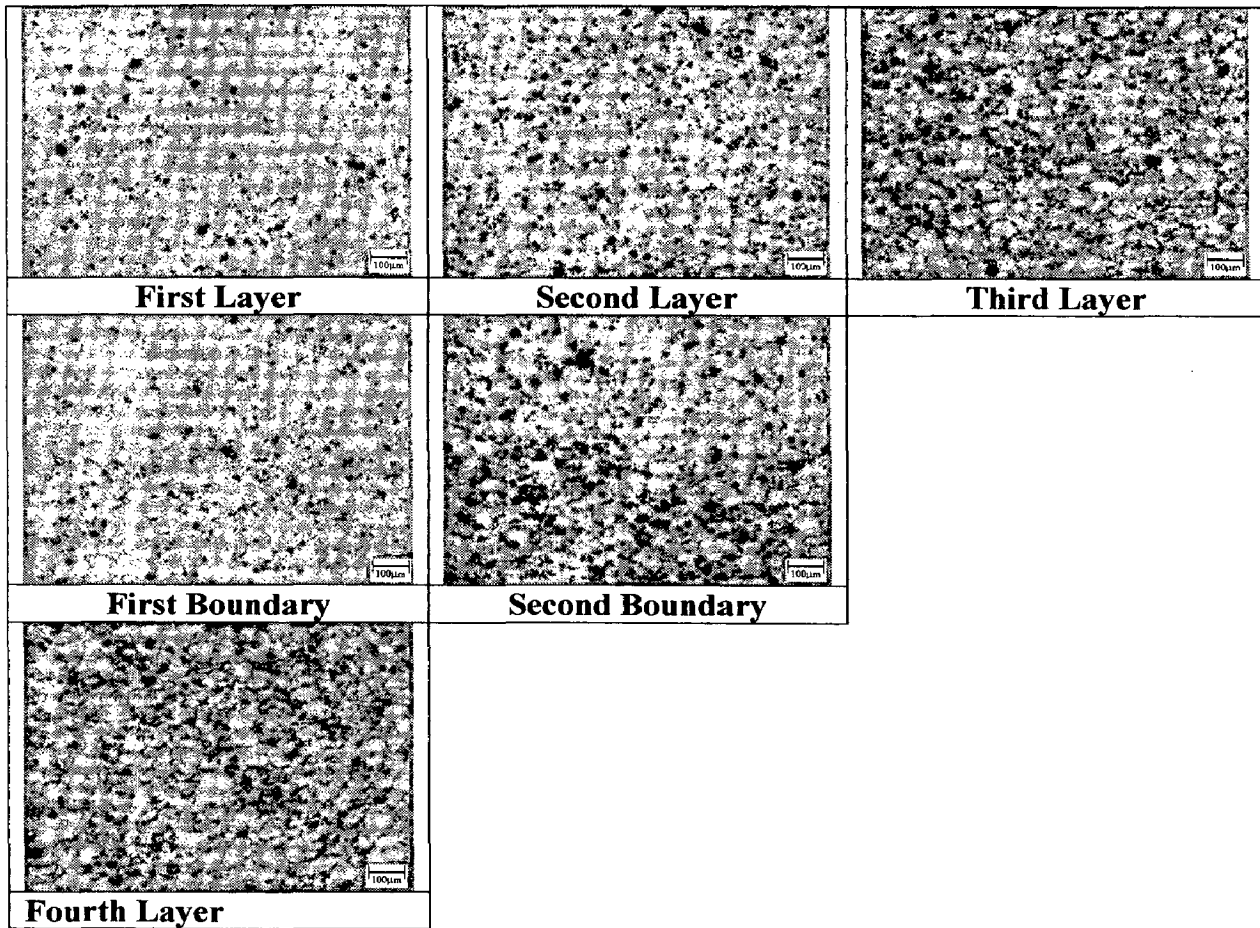


Figure 44

Microstructures of C3

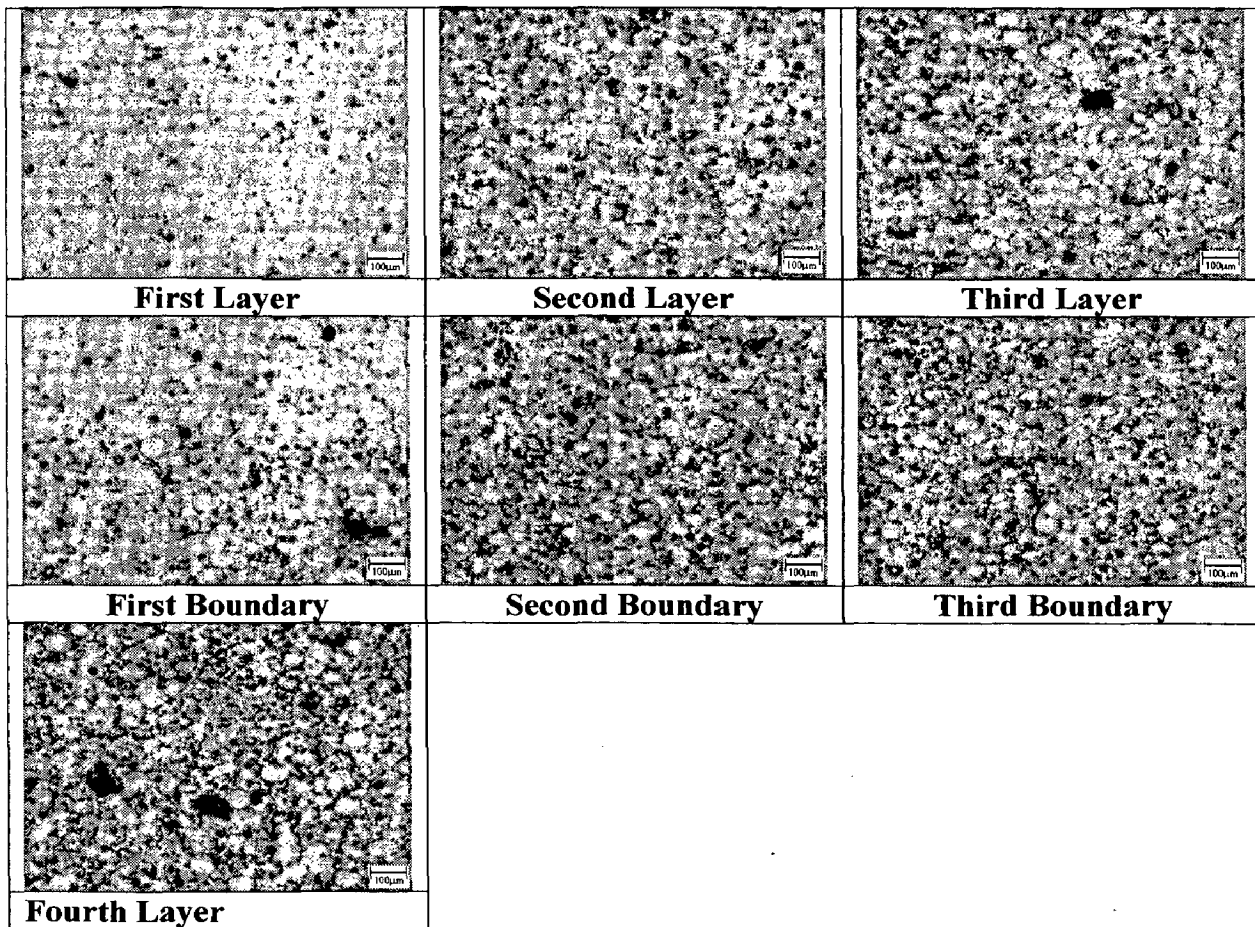


Figure 45

Microstructures of C4

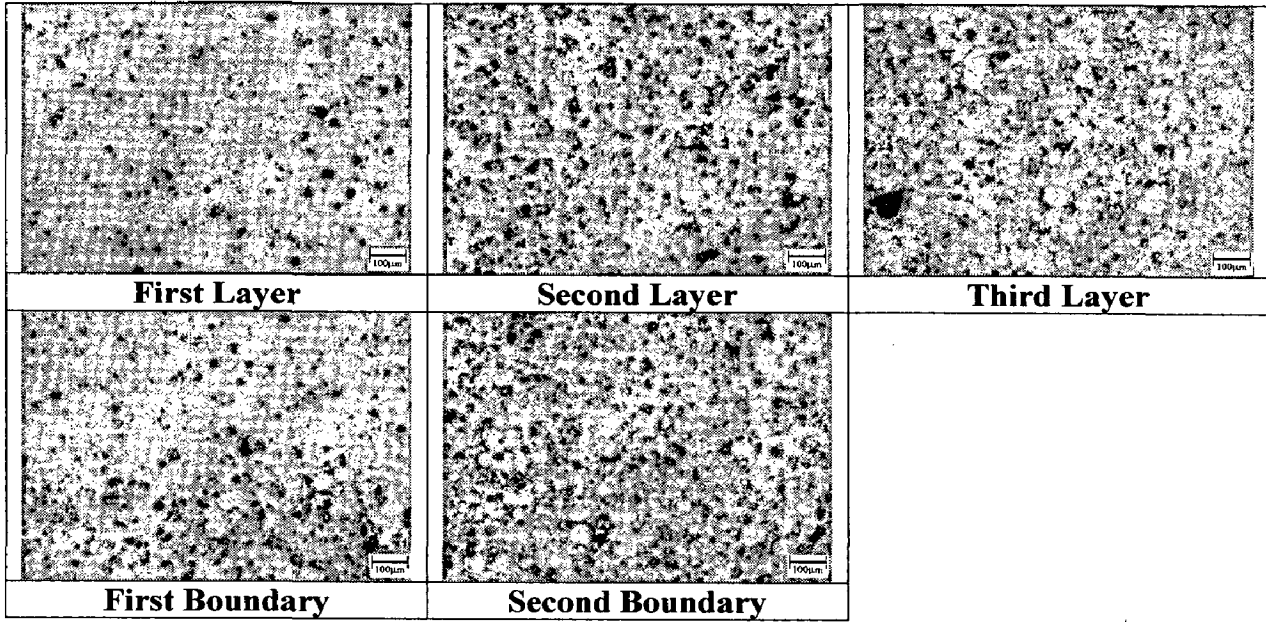


Figure 46

Microstructures of Explosive Compact

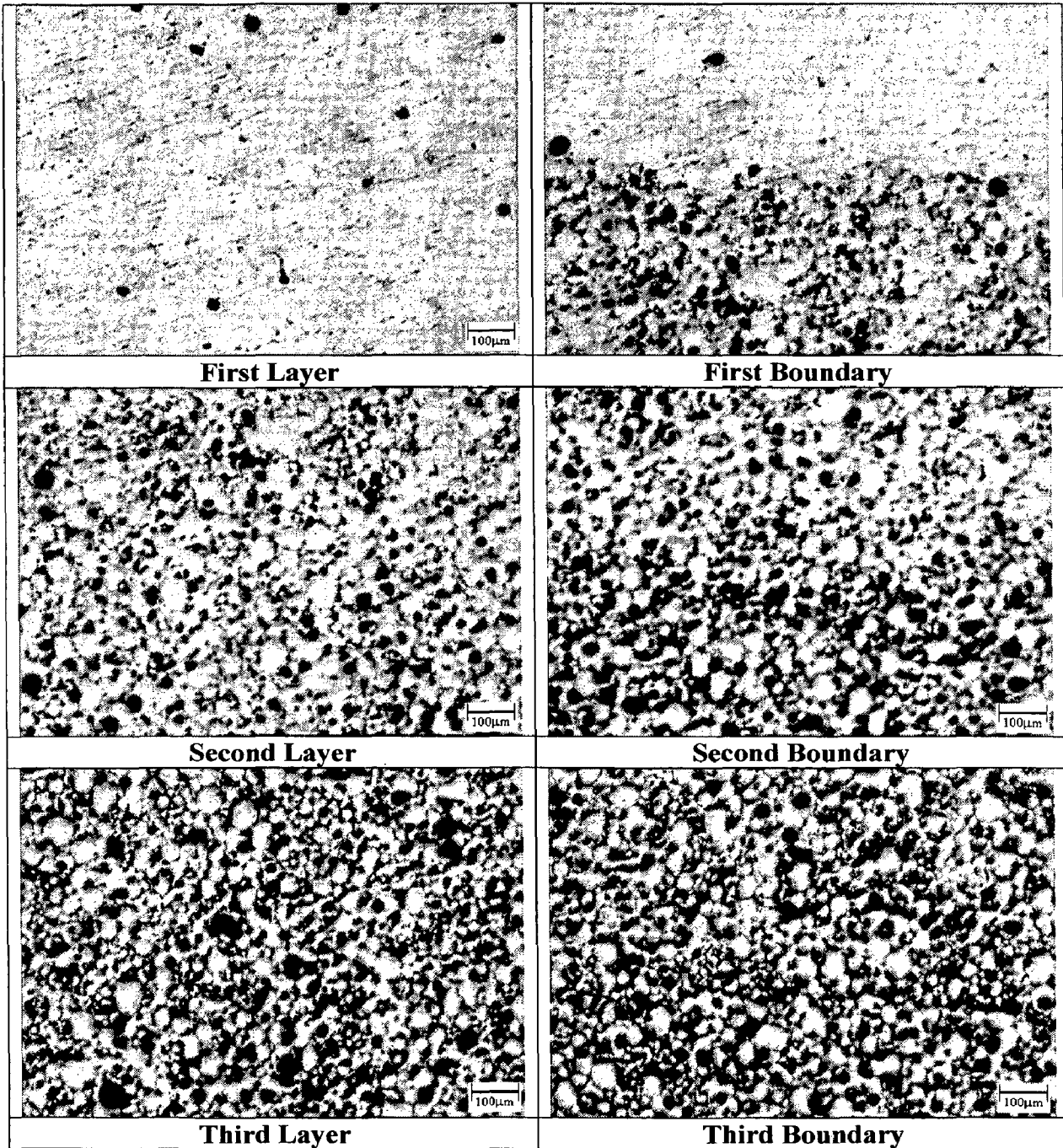


Figure 47

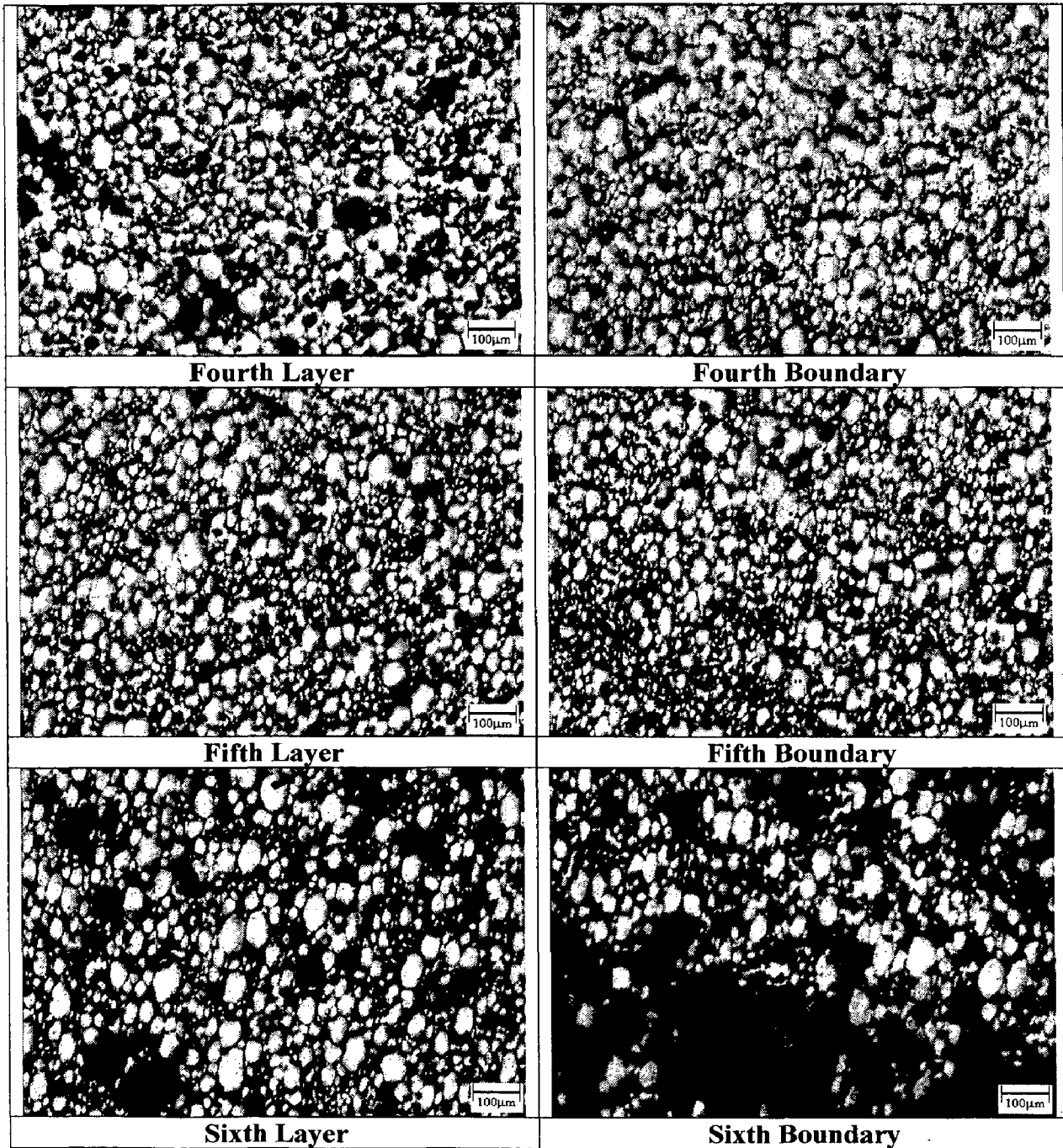
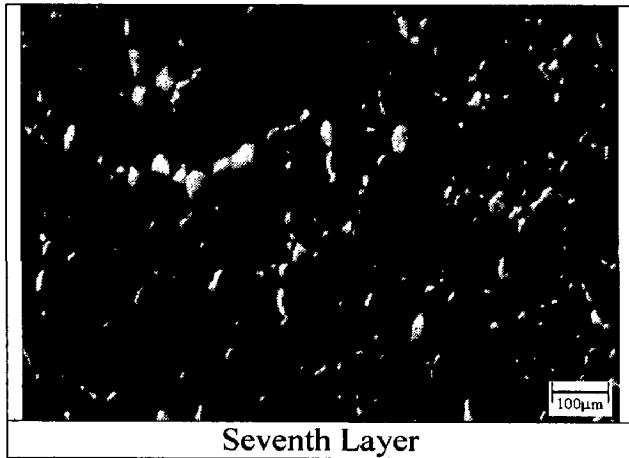


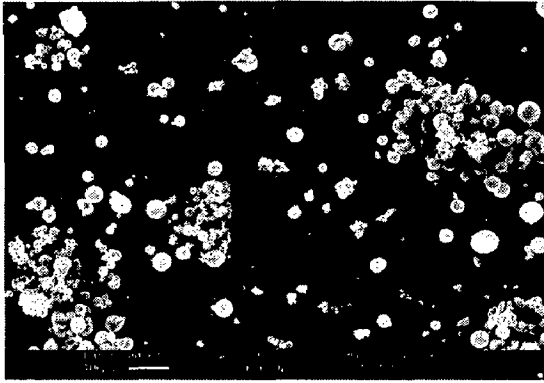
Figure 48



Seventh Layer

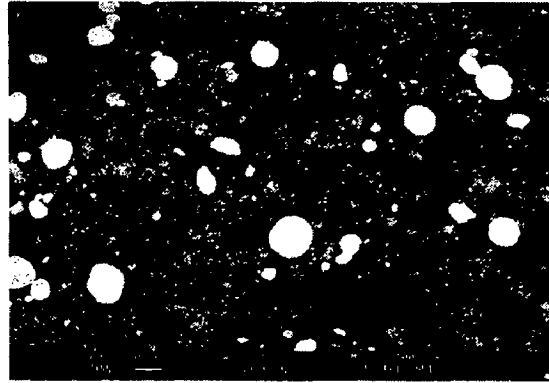
Figure 49

Powder Sample



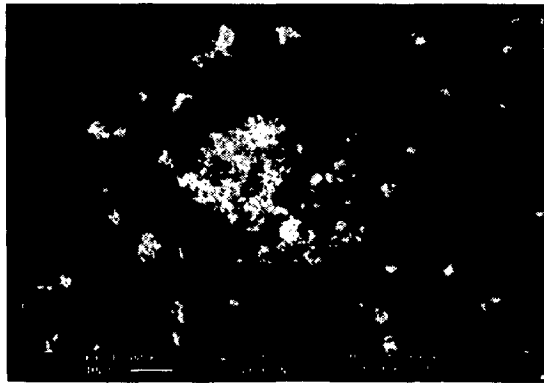
(a)

Copper Powder



(b)

Copper Powder



(c)

Alumina Powder

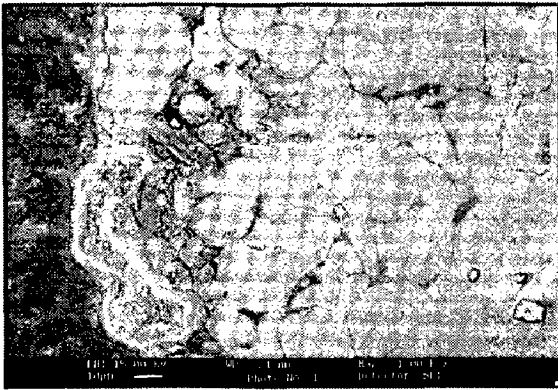


(d)

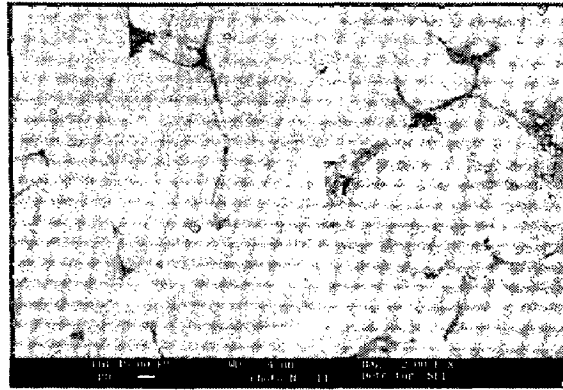
Alumina Powder

Figure 50

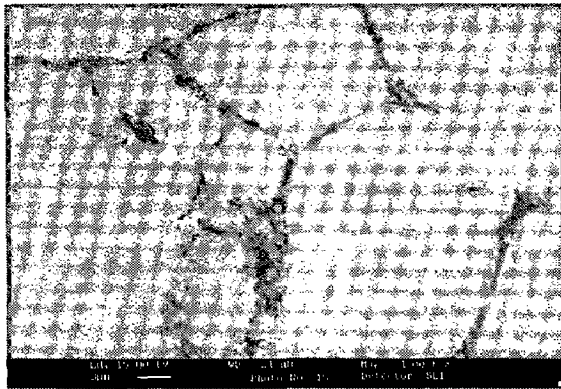
Sintered Specimens



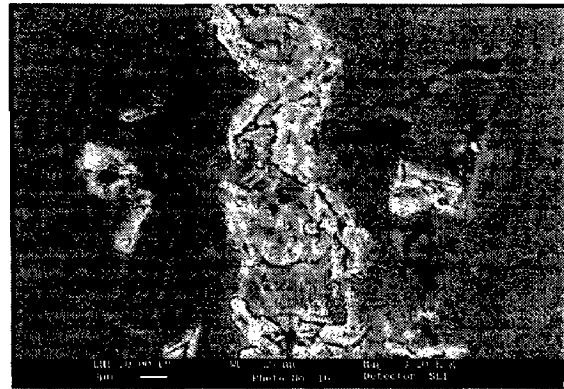
(a)



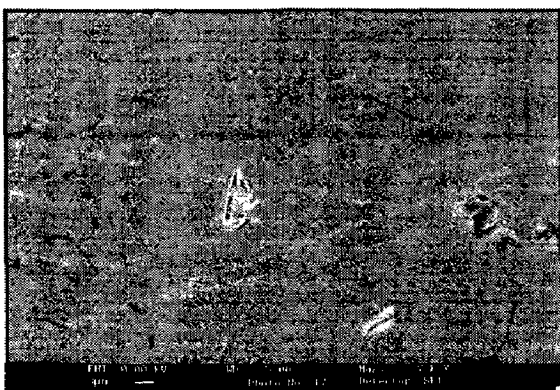
(b)



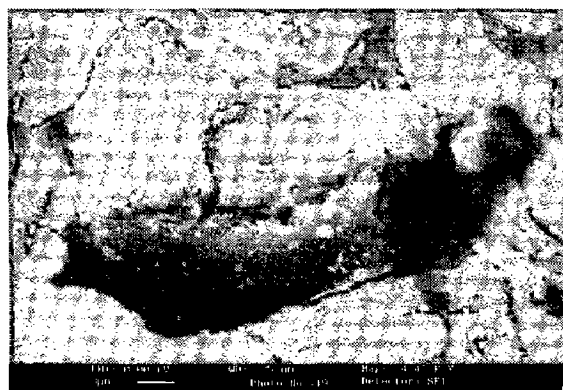
(c)



(d)

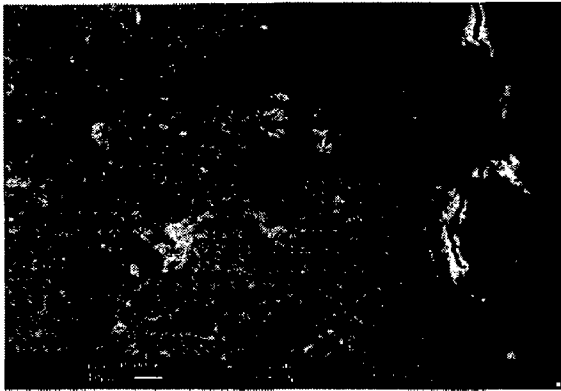


(e)

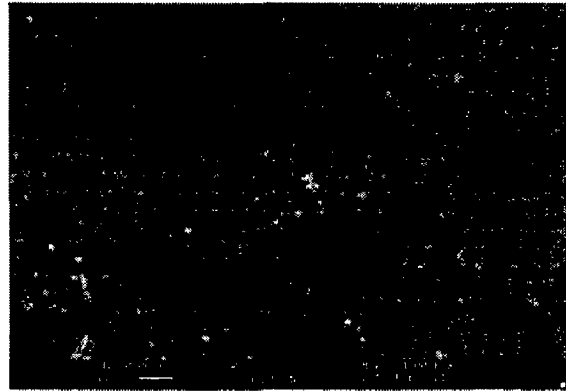


(f)

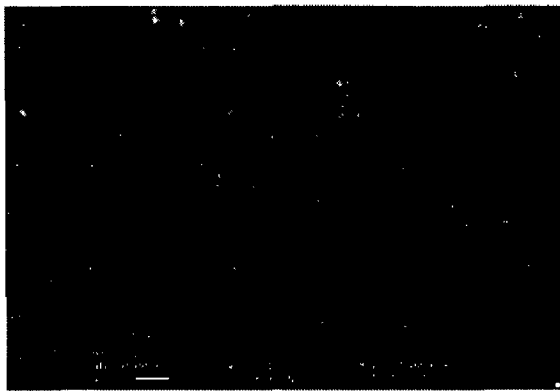
Figure 51



(a)



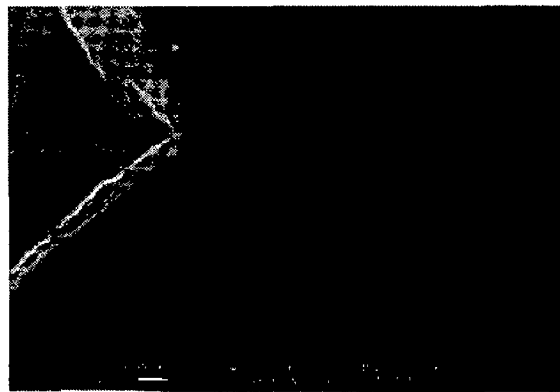
(b)



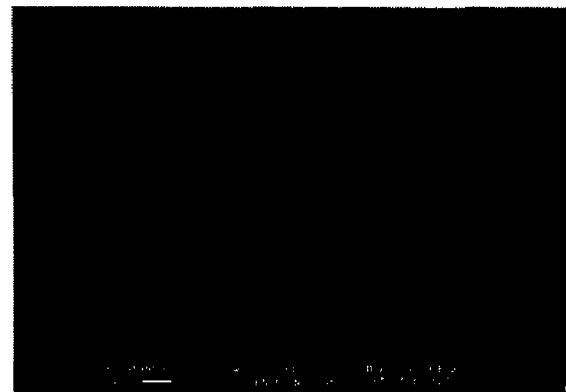
(c)



(d)

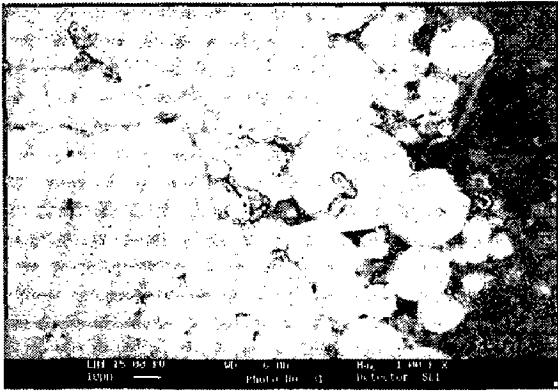


(e)

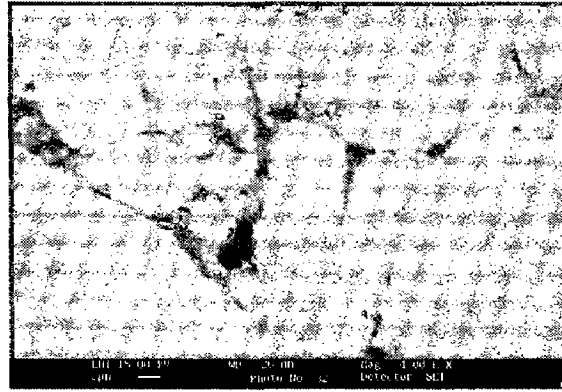


(f)

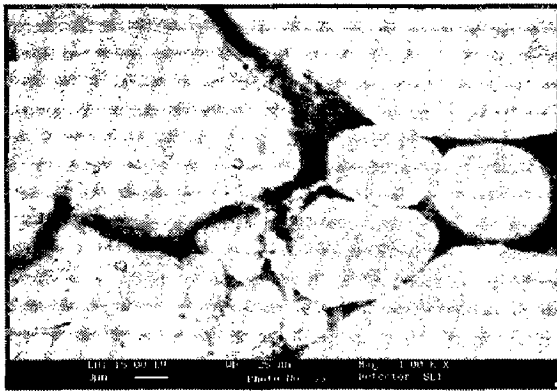
Figure 52



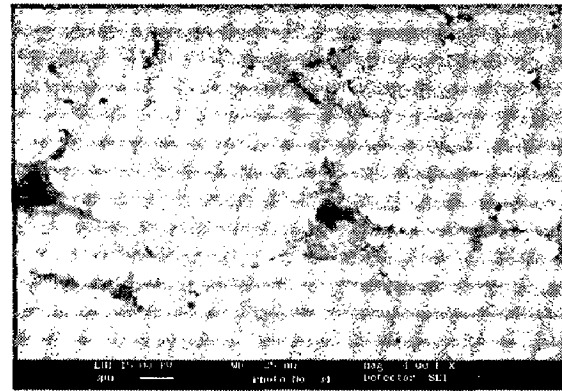
(a)



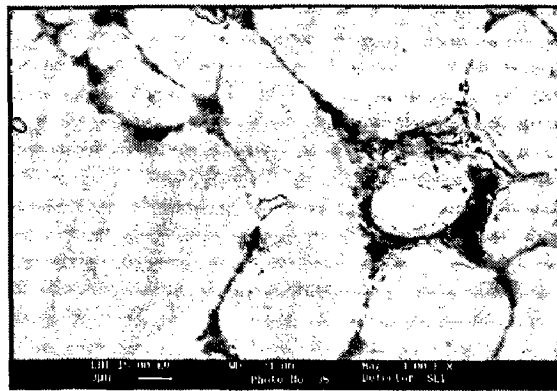
(b)



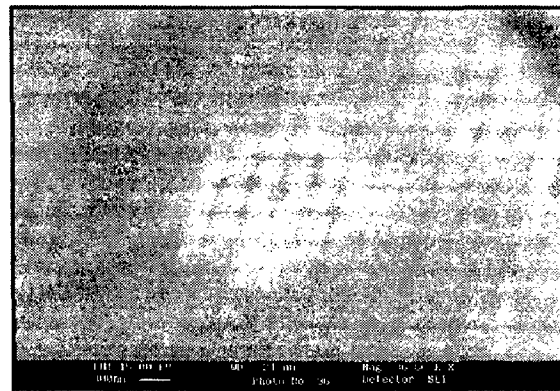
(c)



(d)



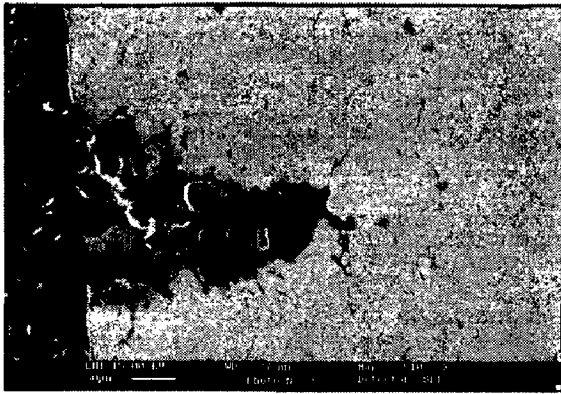
(e)



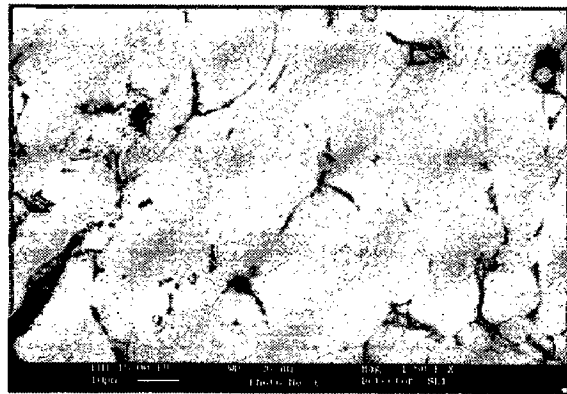
(f)

Figure 53

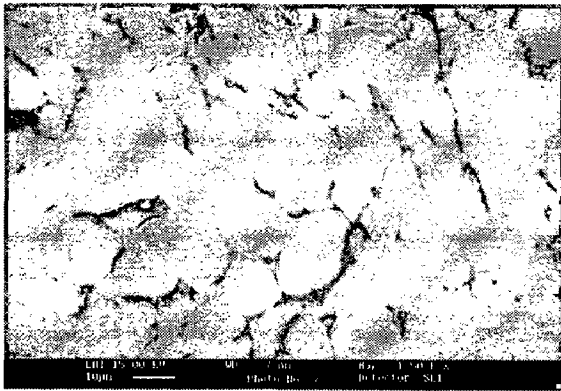
Specimens after Rolling



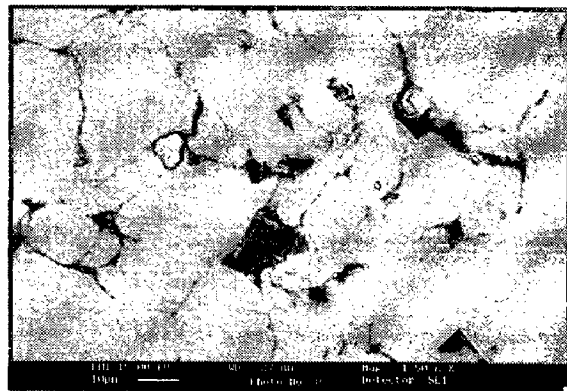
(a)



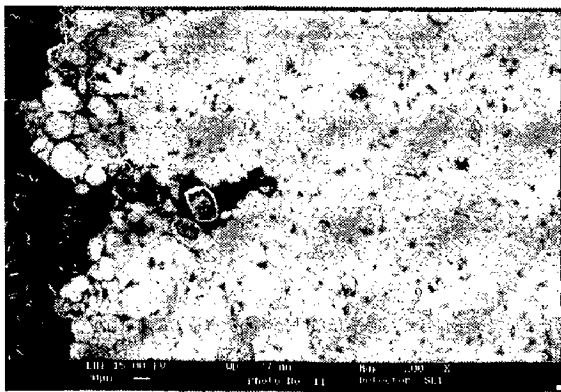
(b)



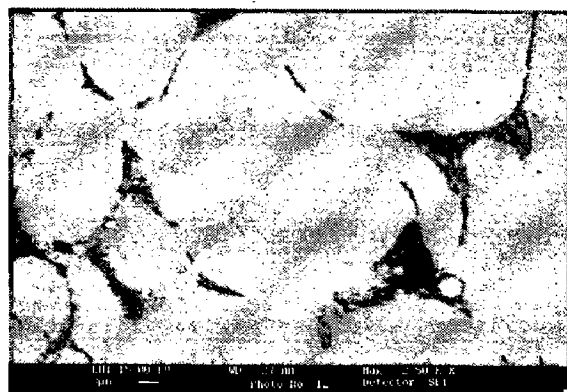
(c)



(d)

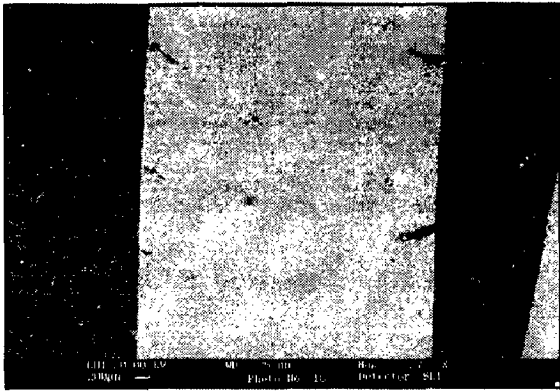


(e)

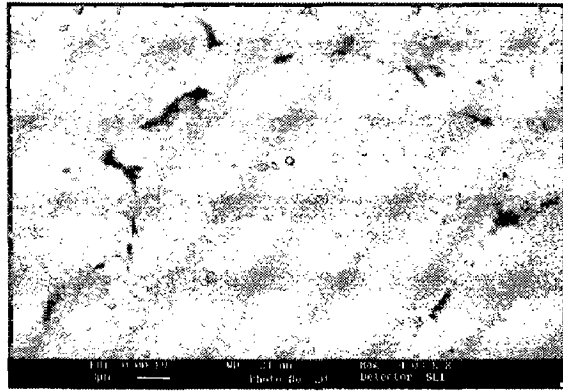


(f)

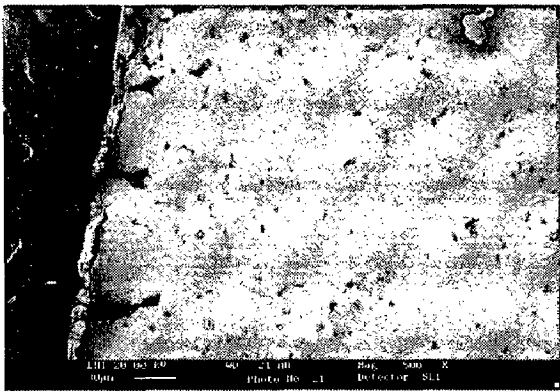
Figure 54



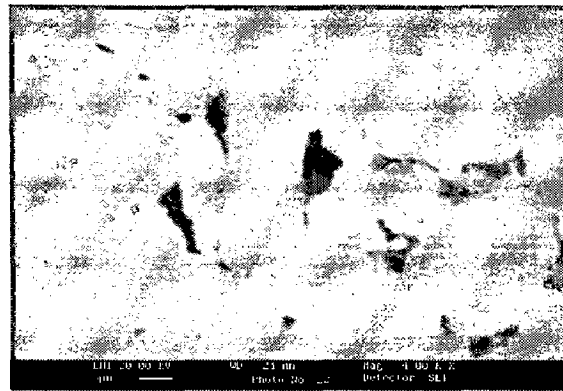
(a)



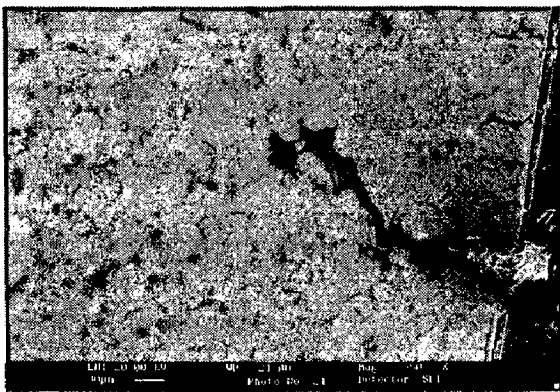
(b)



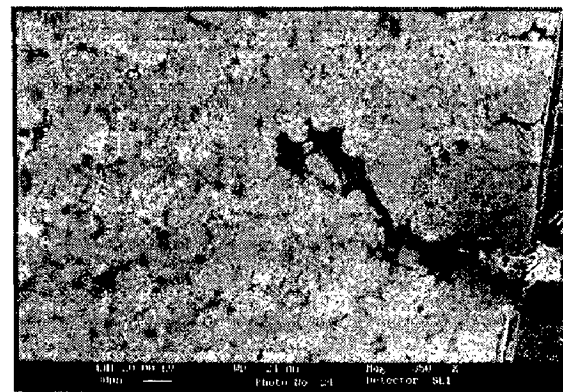
(c)



(d)



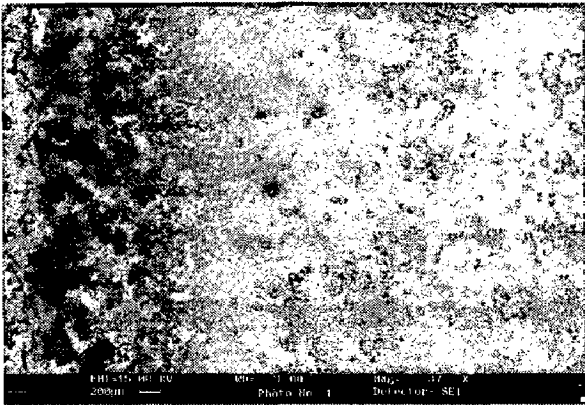
(e)



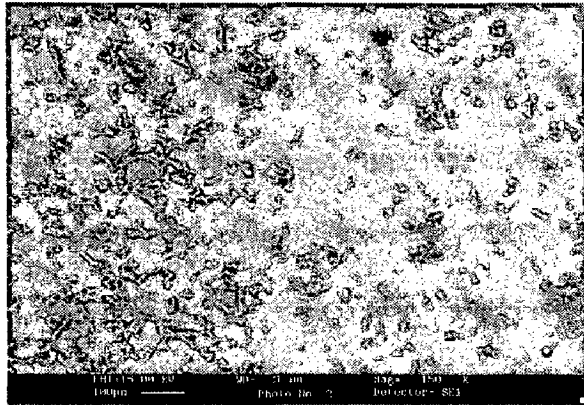
(f)

Figure 55

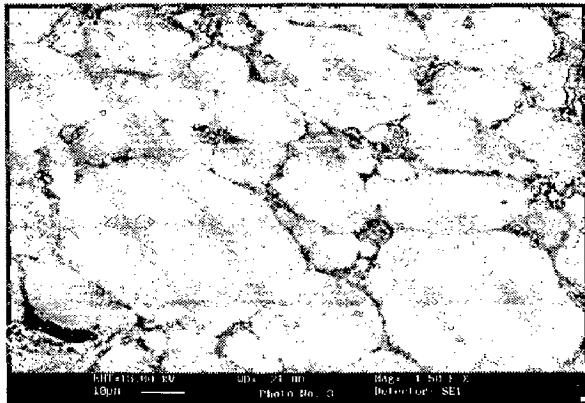
Explosive Forming Specimens



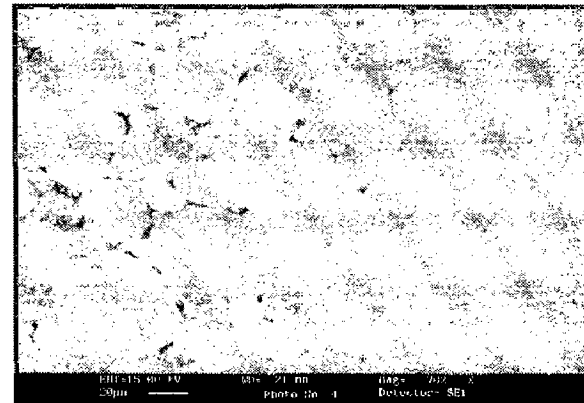
(a)



(b)



(c)



(d)

Figure 56

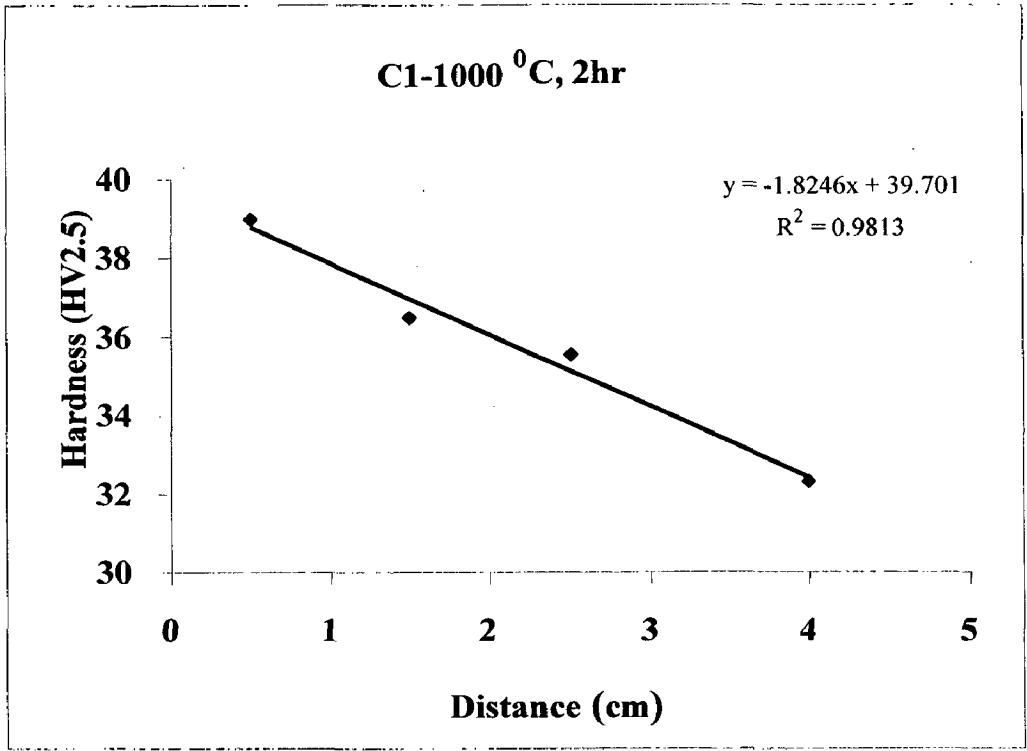


Figure 57

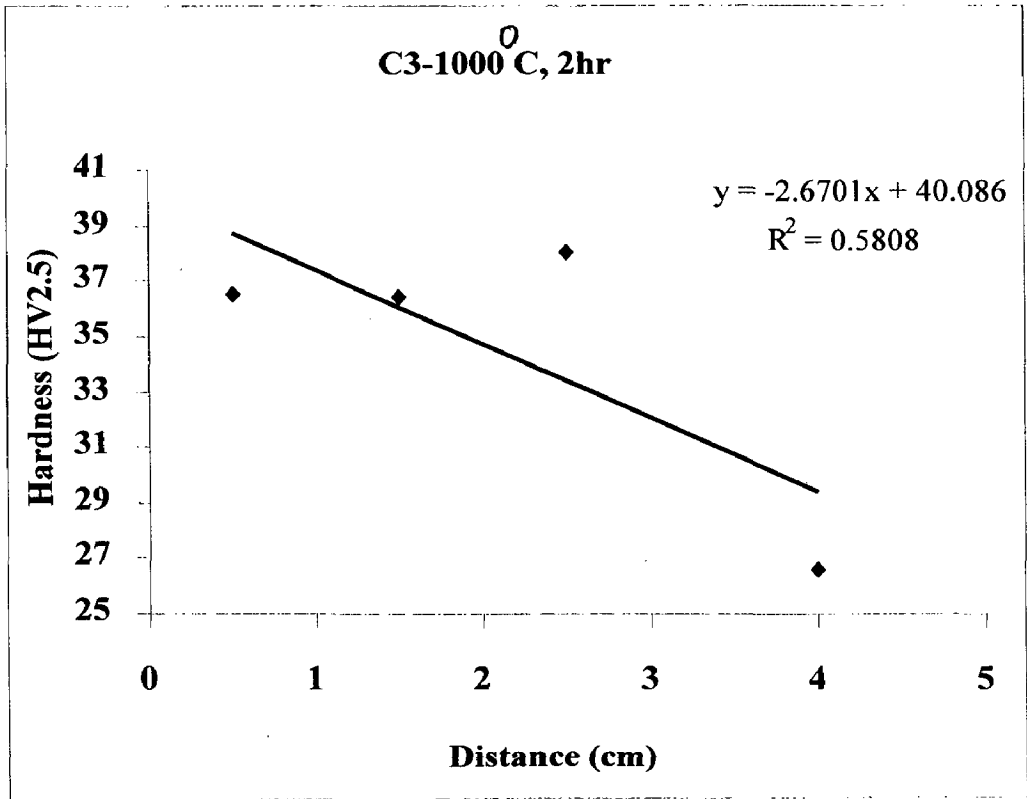
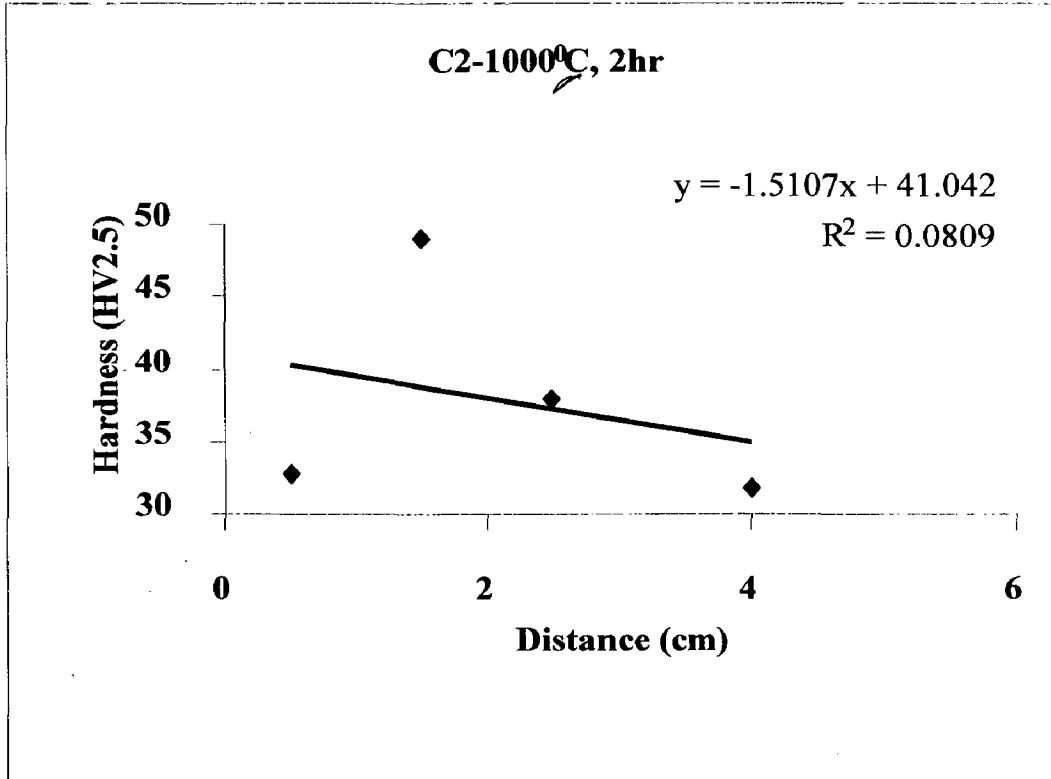


Figure 58



*?
What is
difference?*

Figure 59

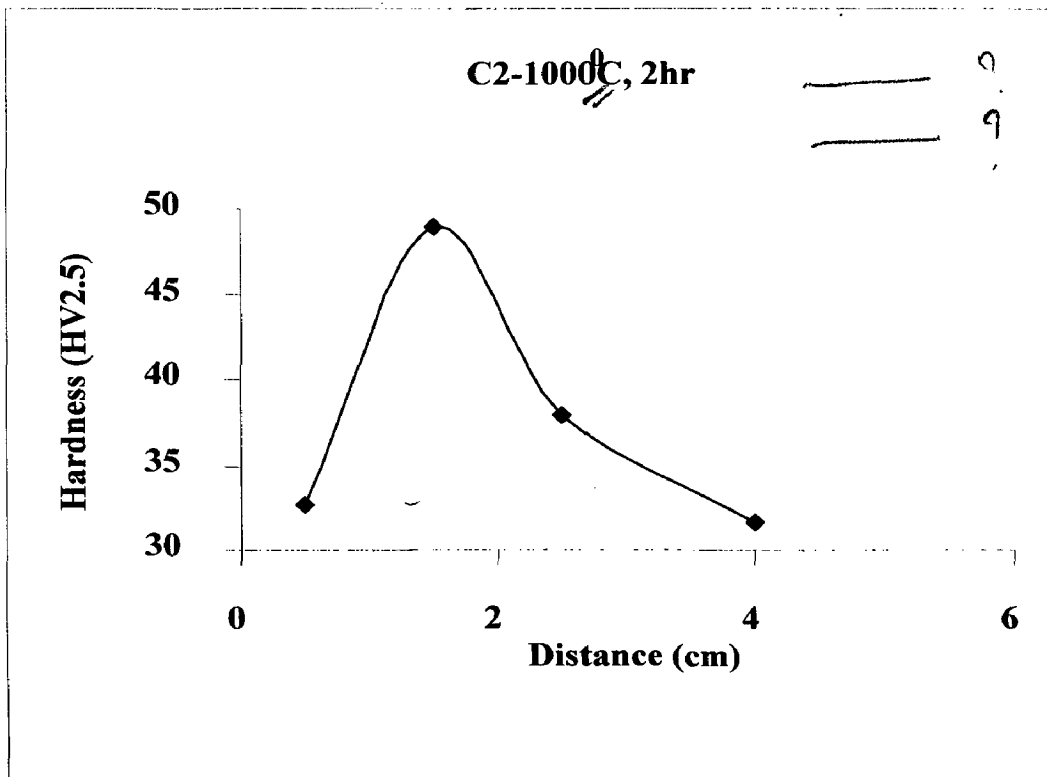


Figure 60

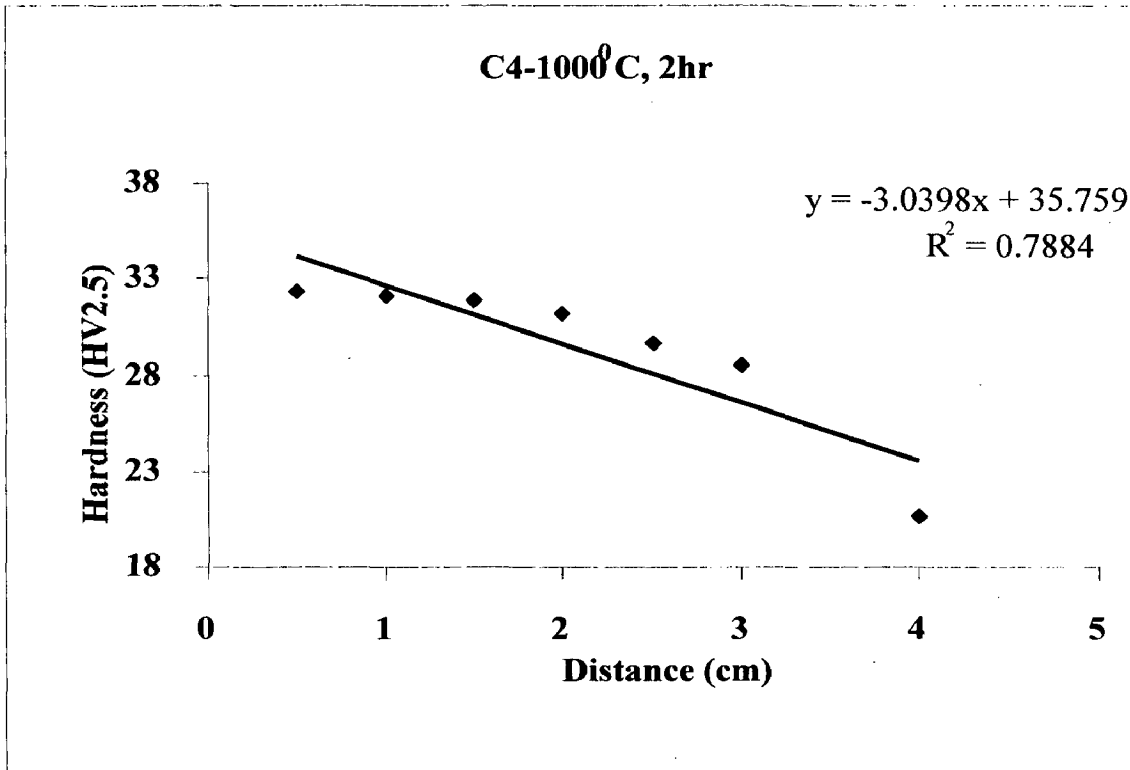


Figure 61

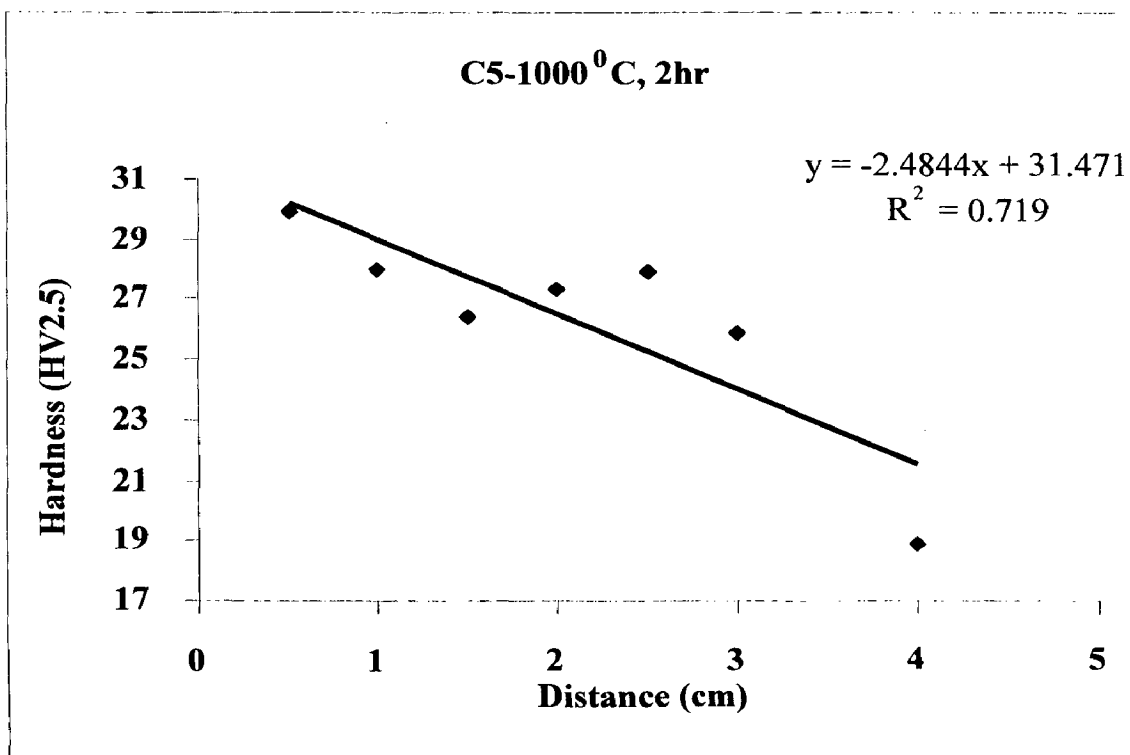


Figure 62

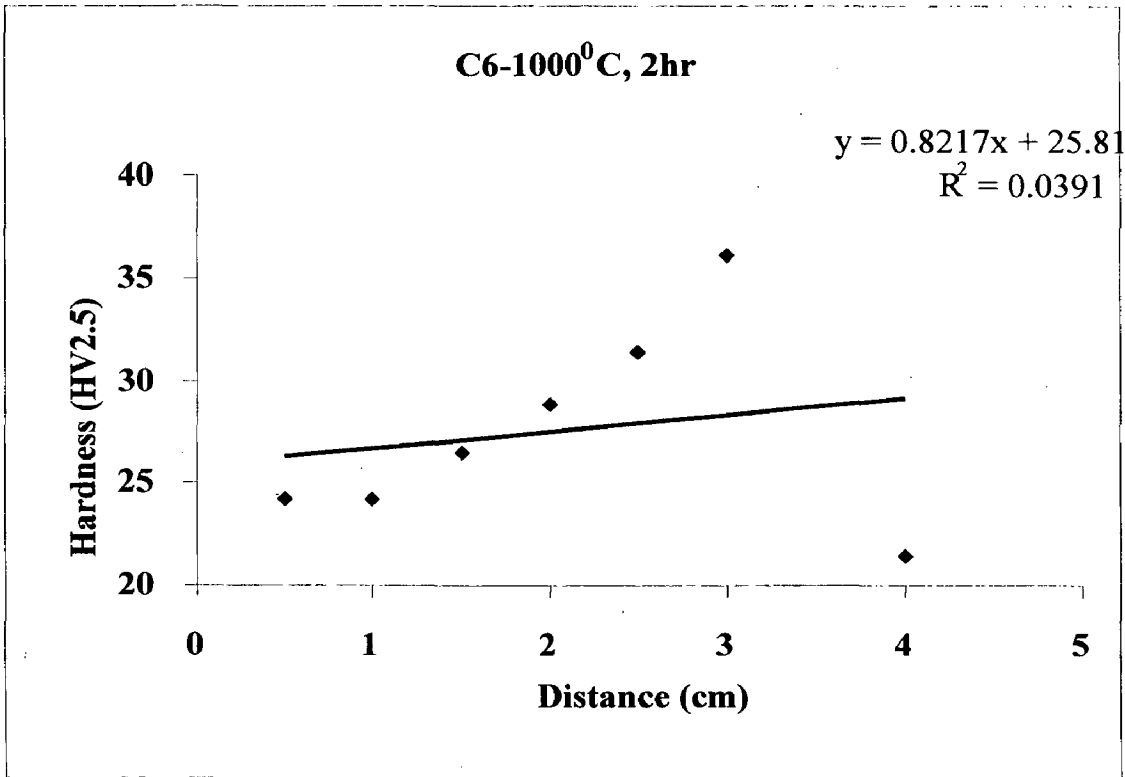


Figure 63

within diff

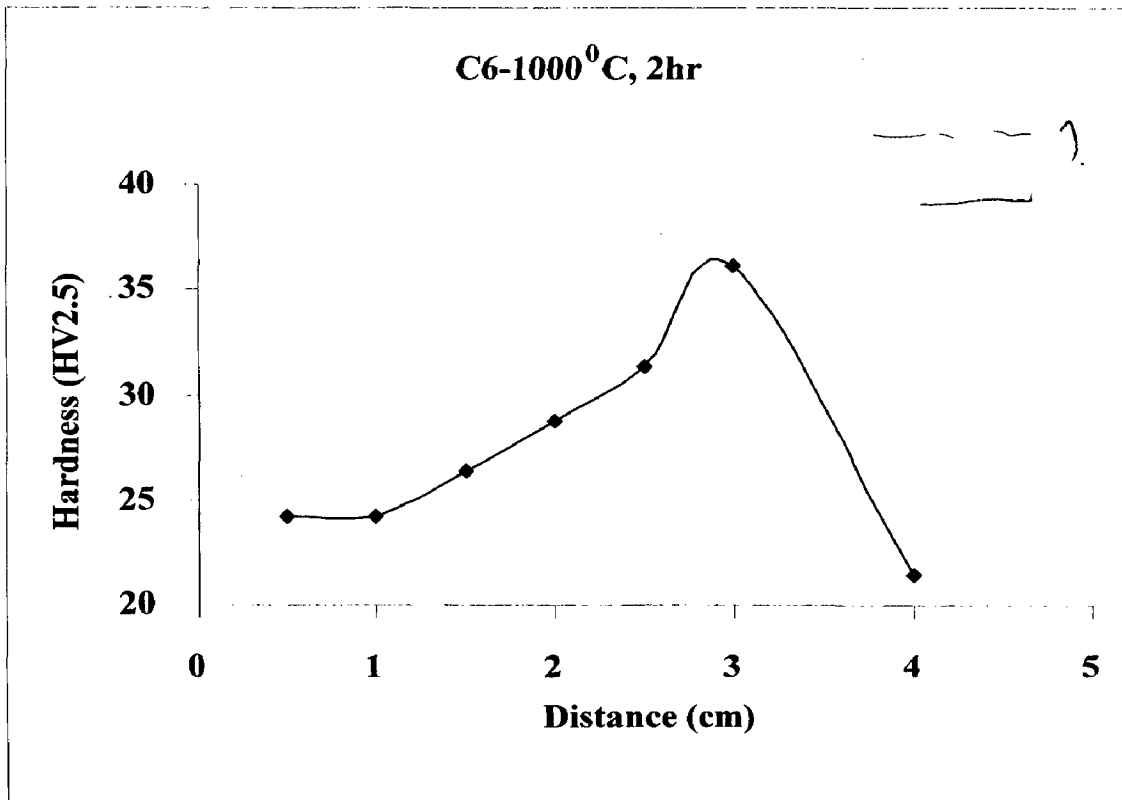


Figure 64

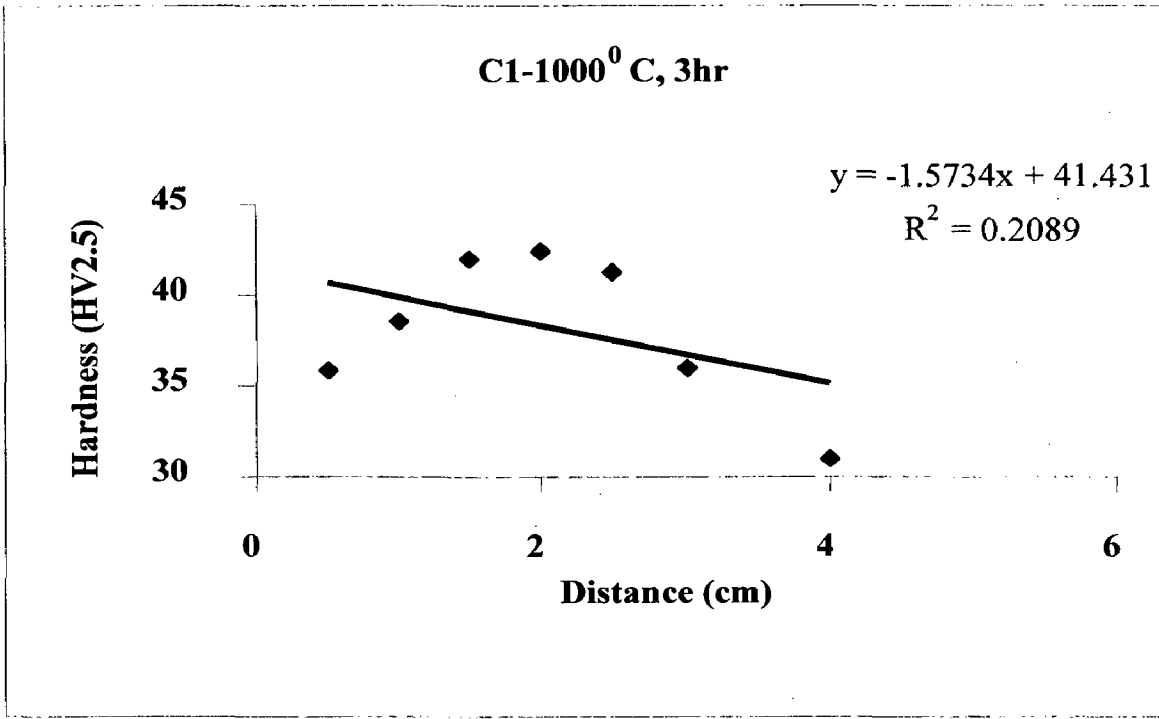


Figure 65

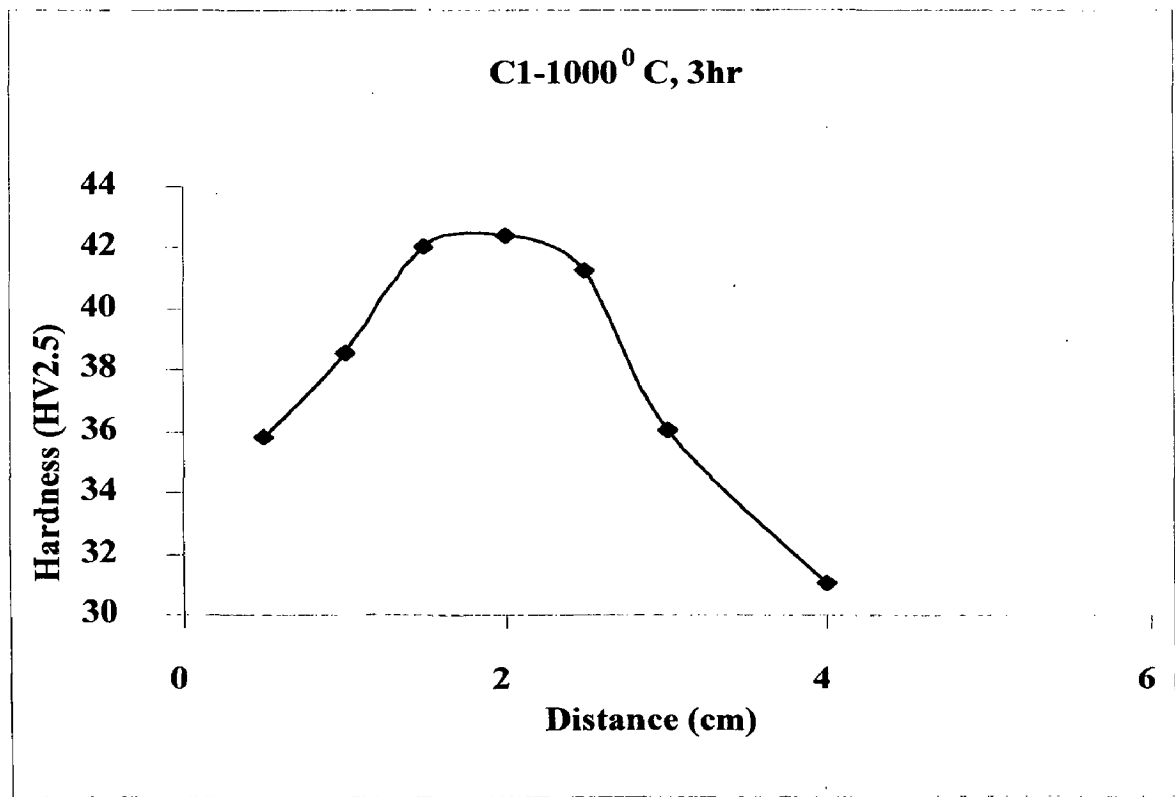


Figure 66

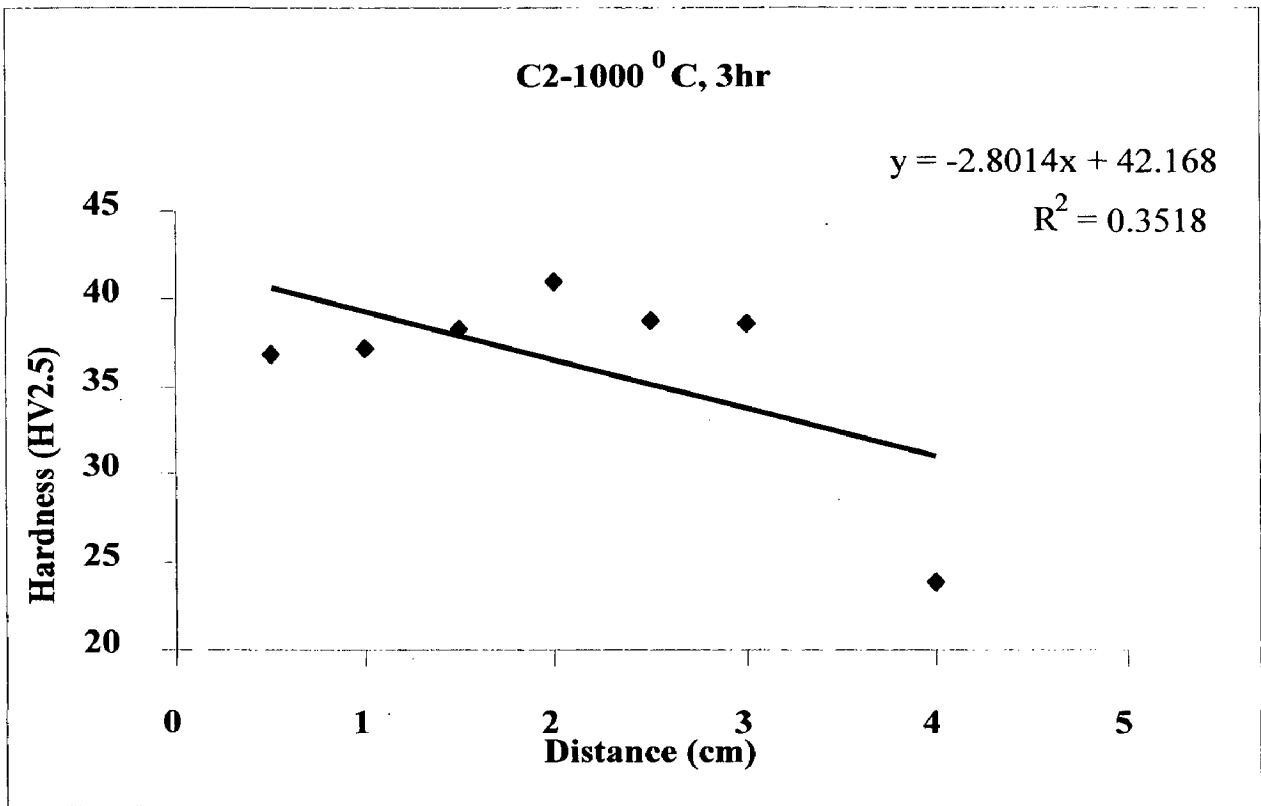


Figure 67

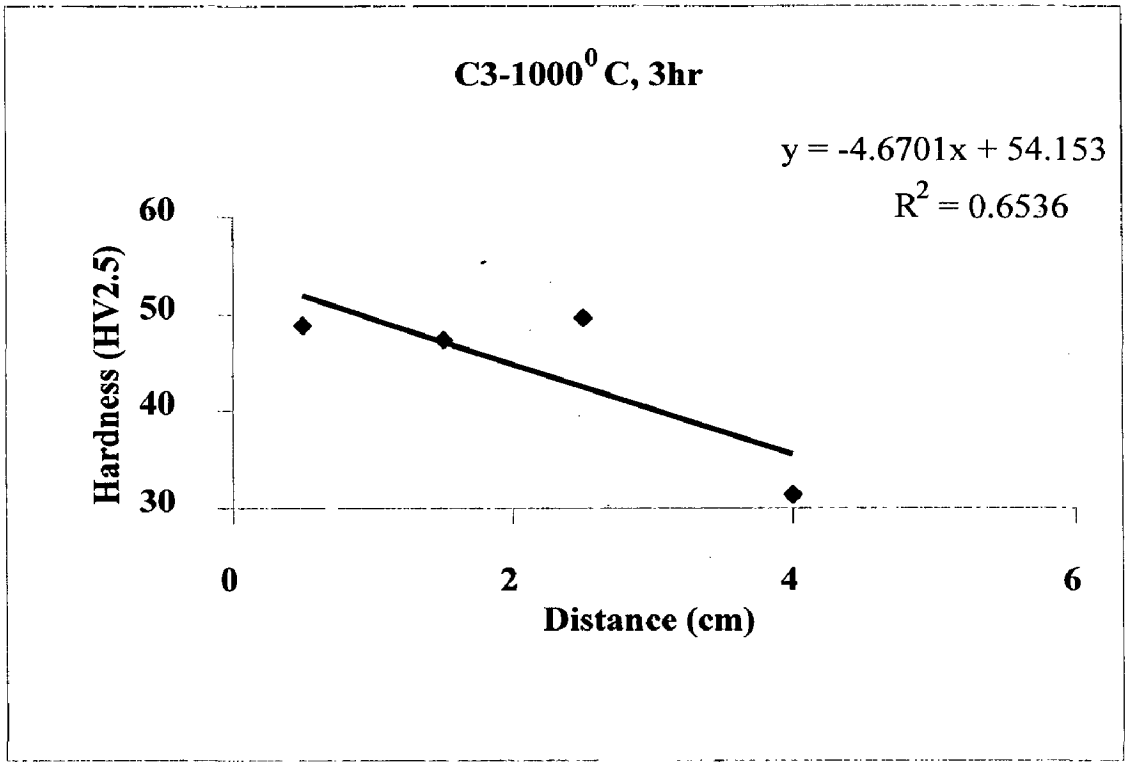


Figure 68

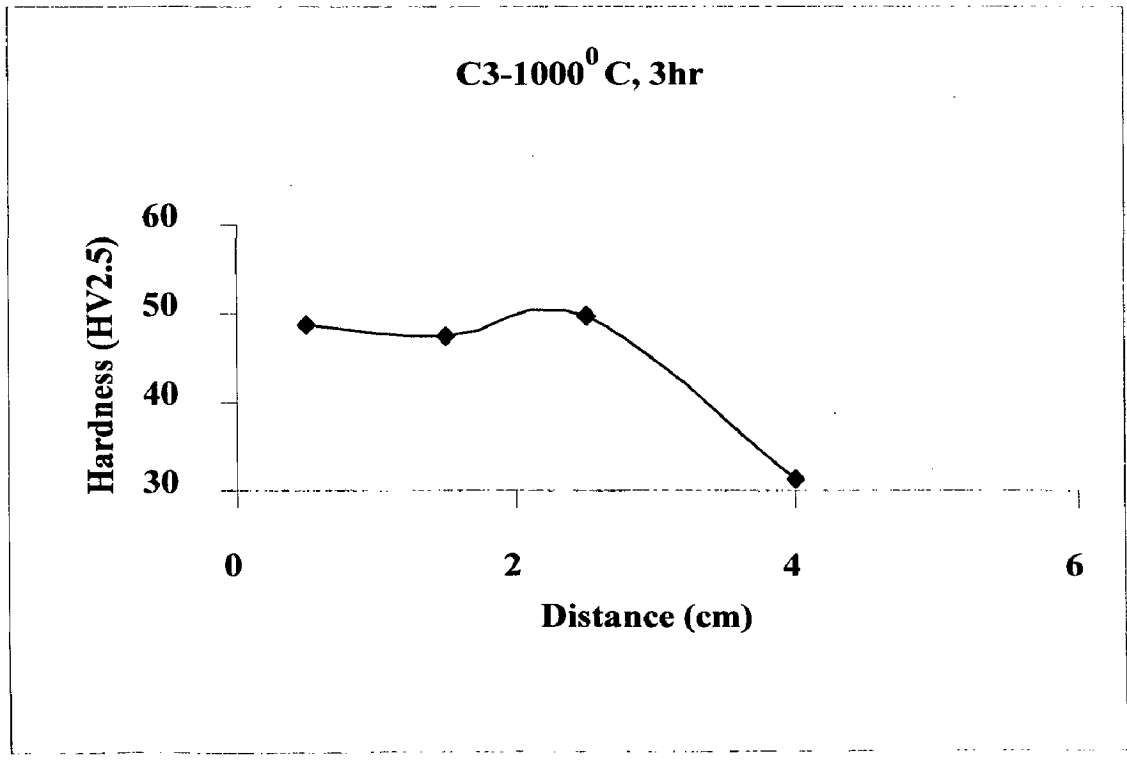


Figure 69

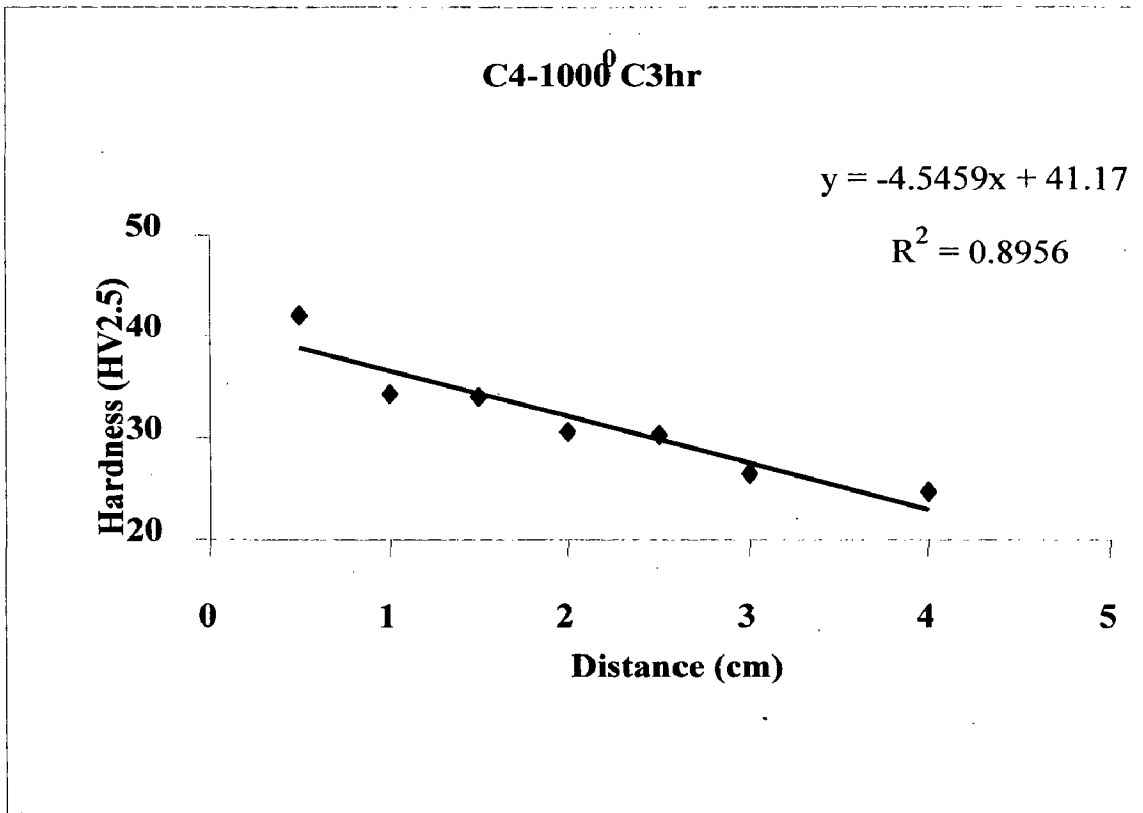


Figure 70

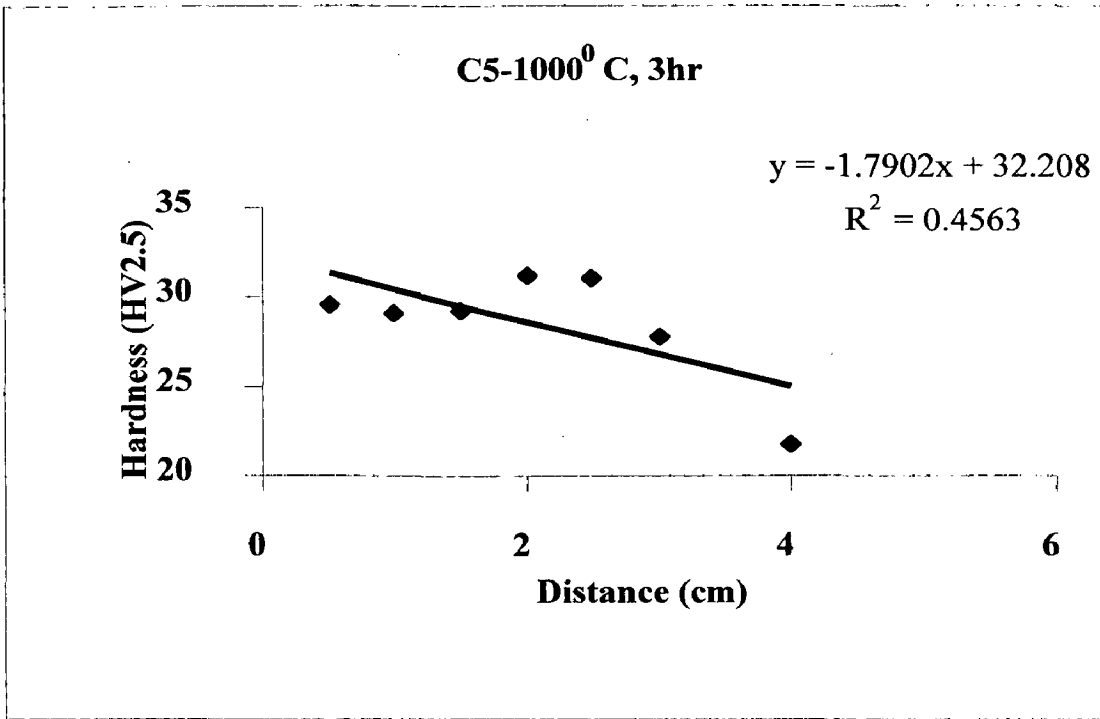


Figure 71

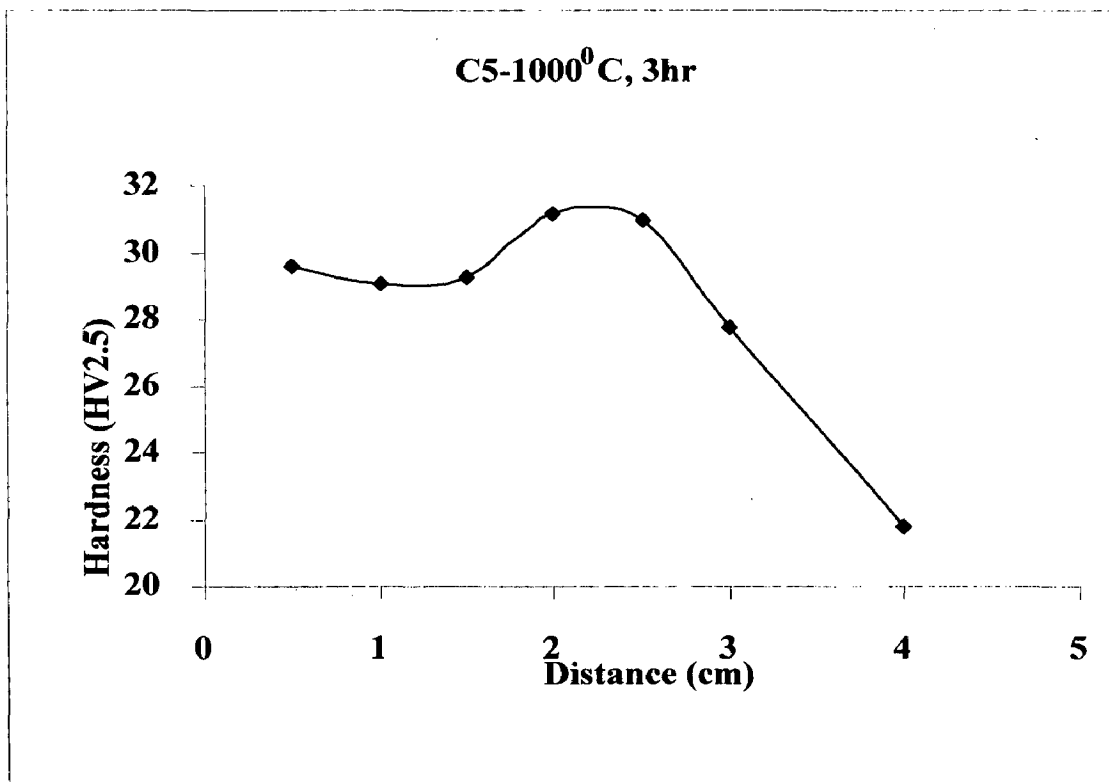


Figure 72

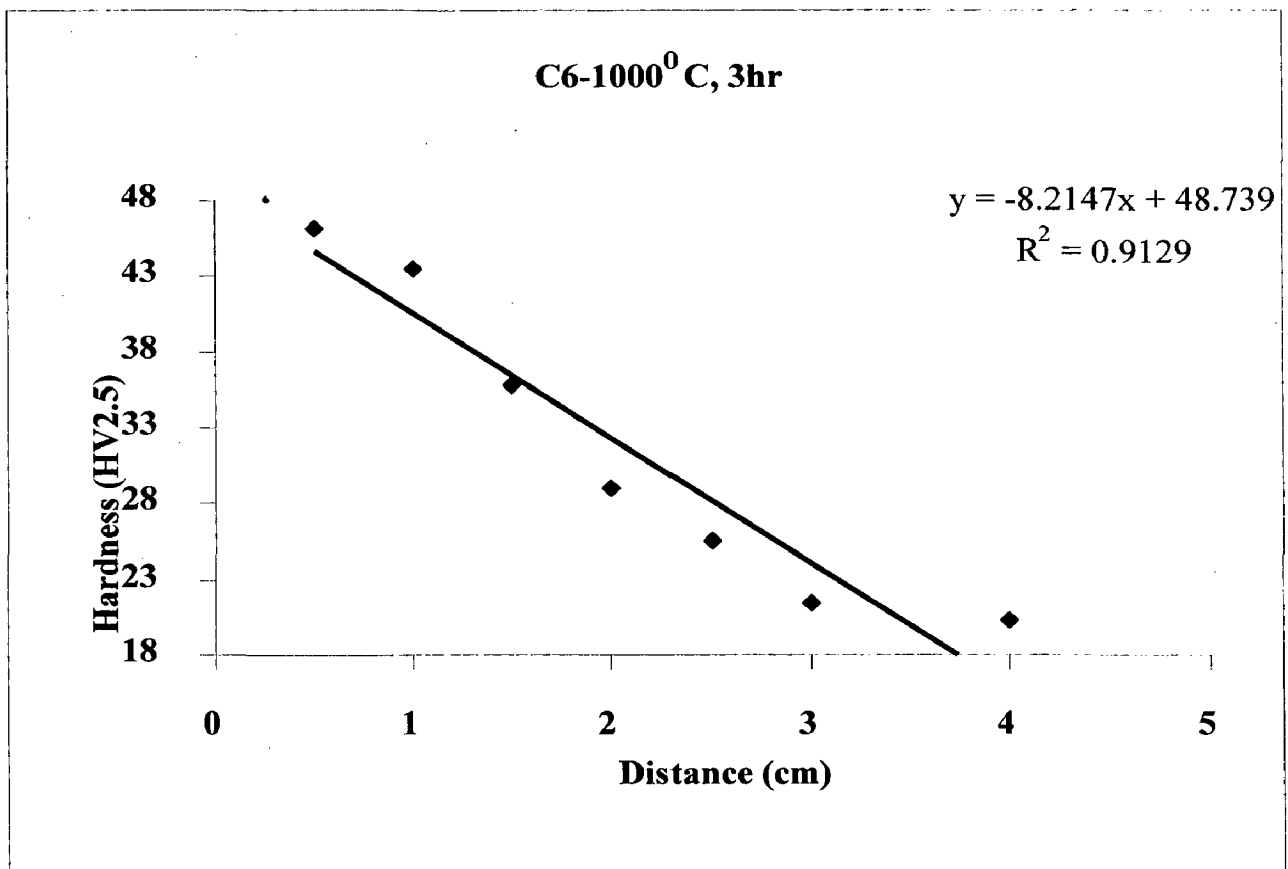


Figure 73

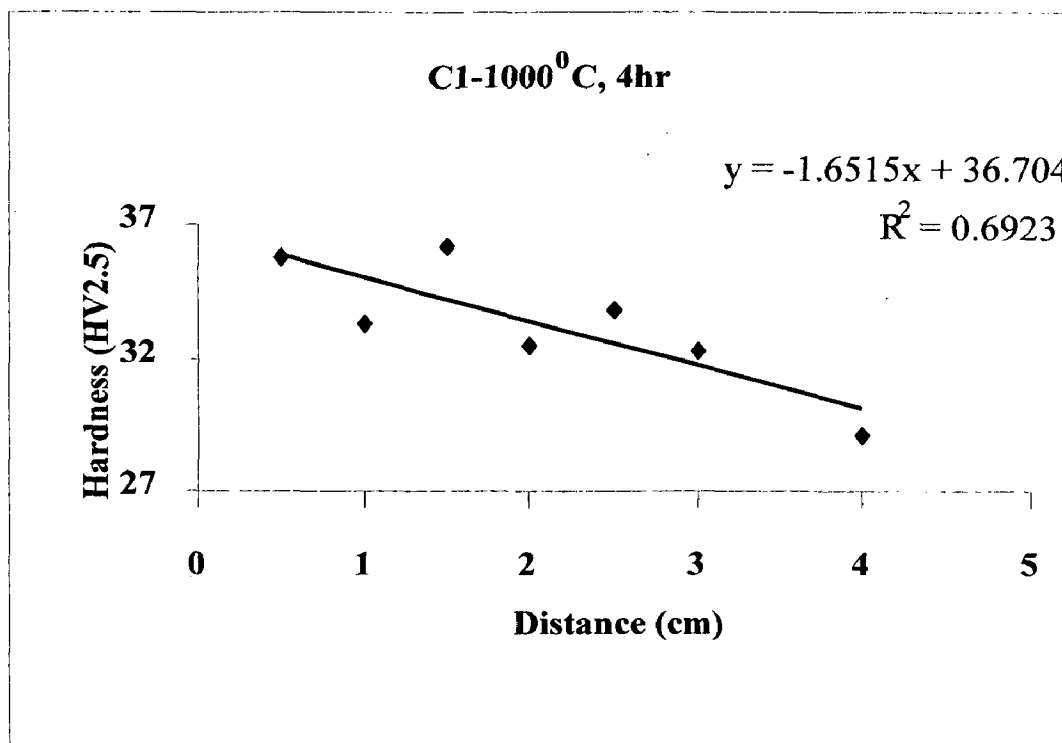


Figure 74

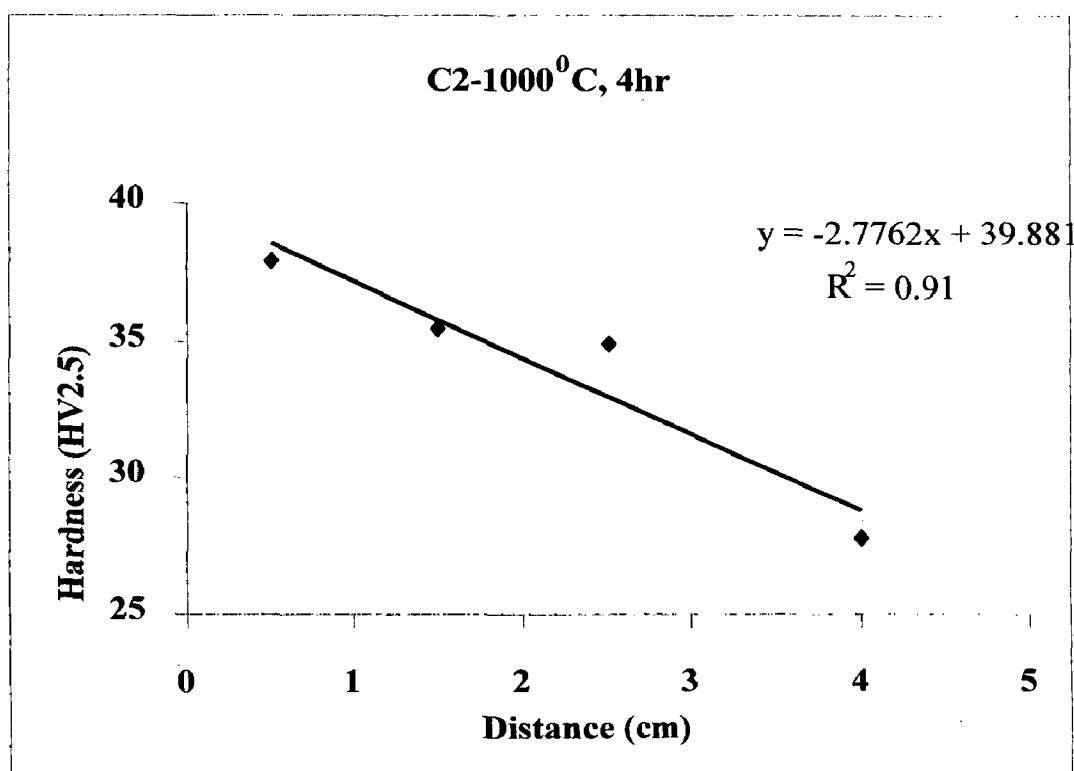


Figure 75

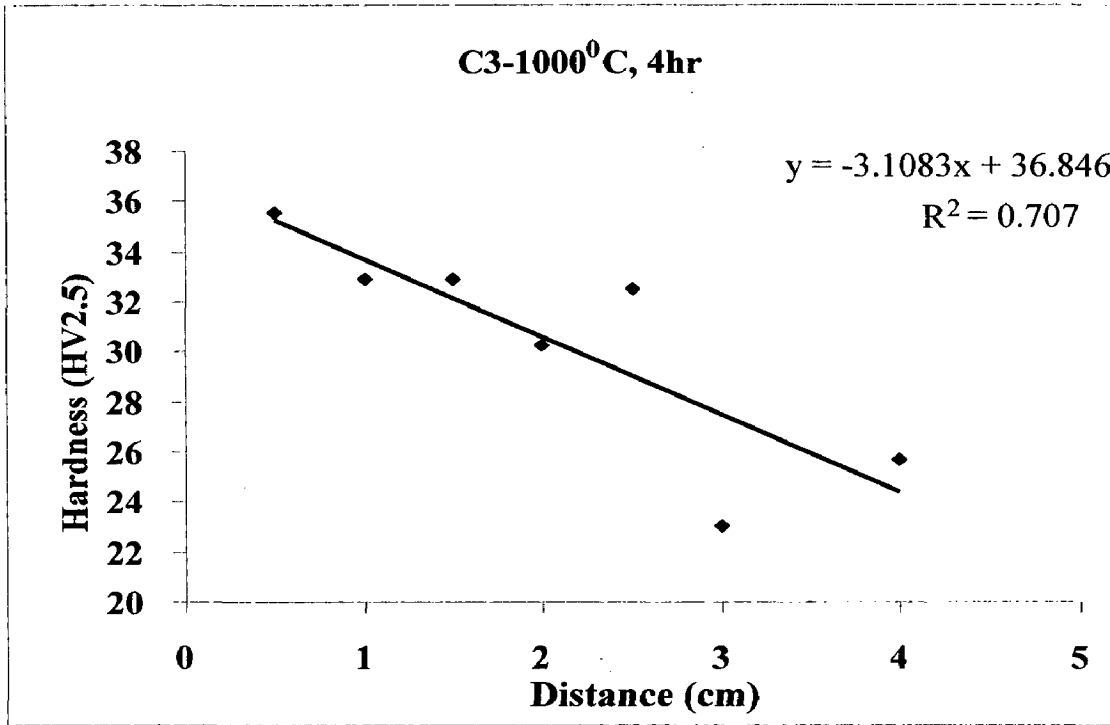


Figure 76

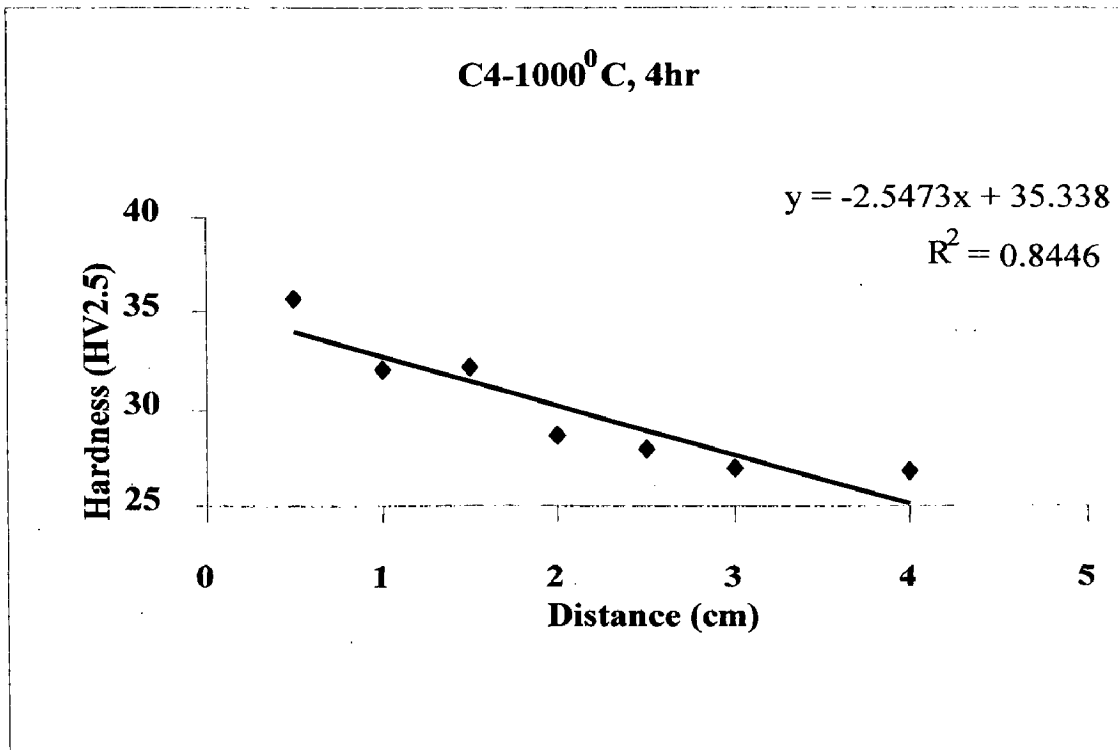


Figure 77

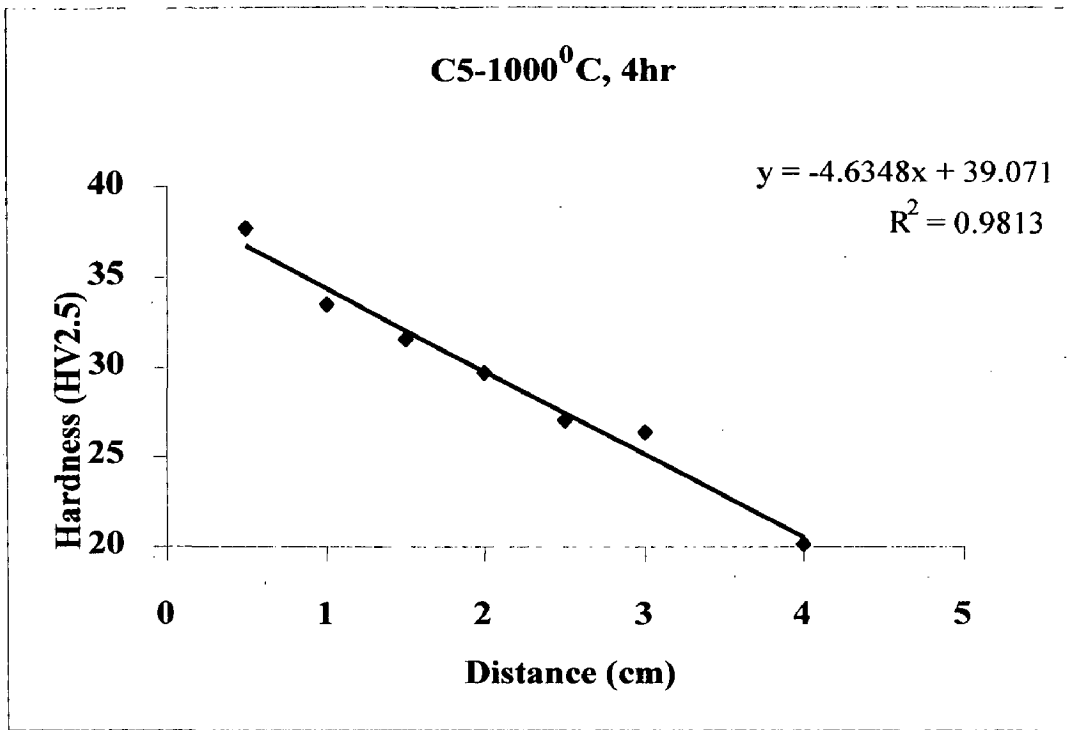


Figure 78

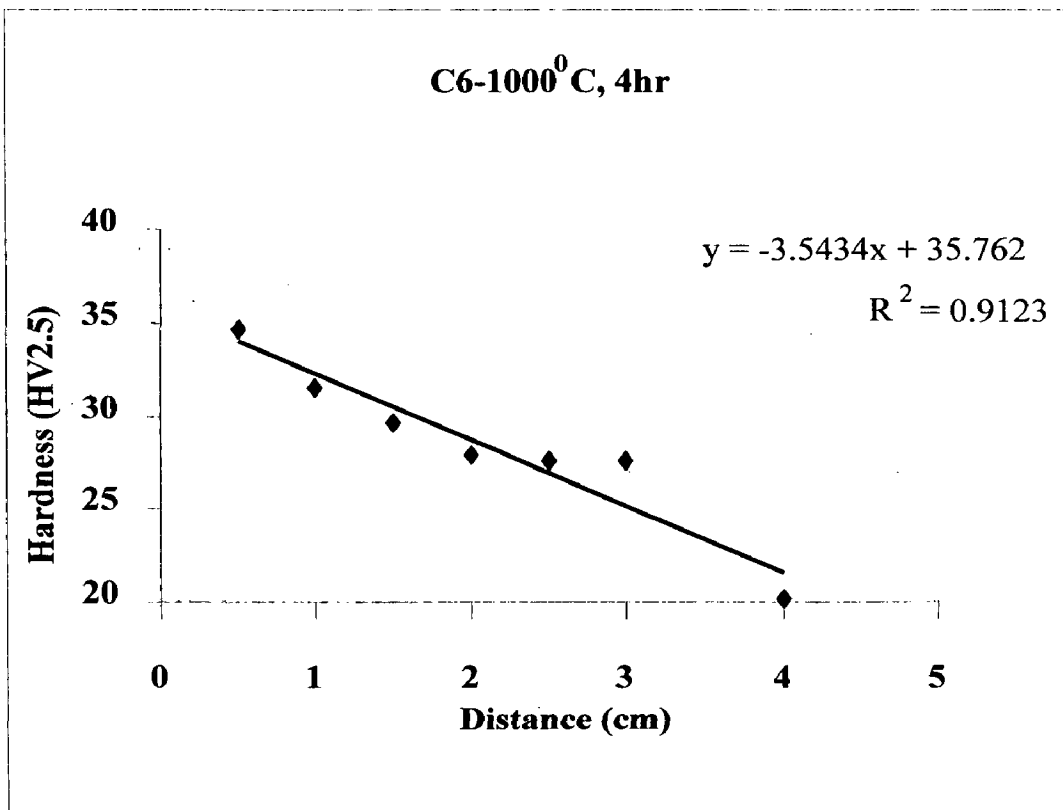


Figure 79

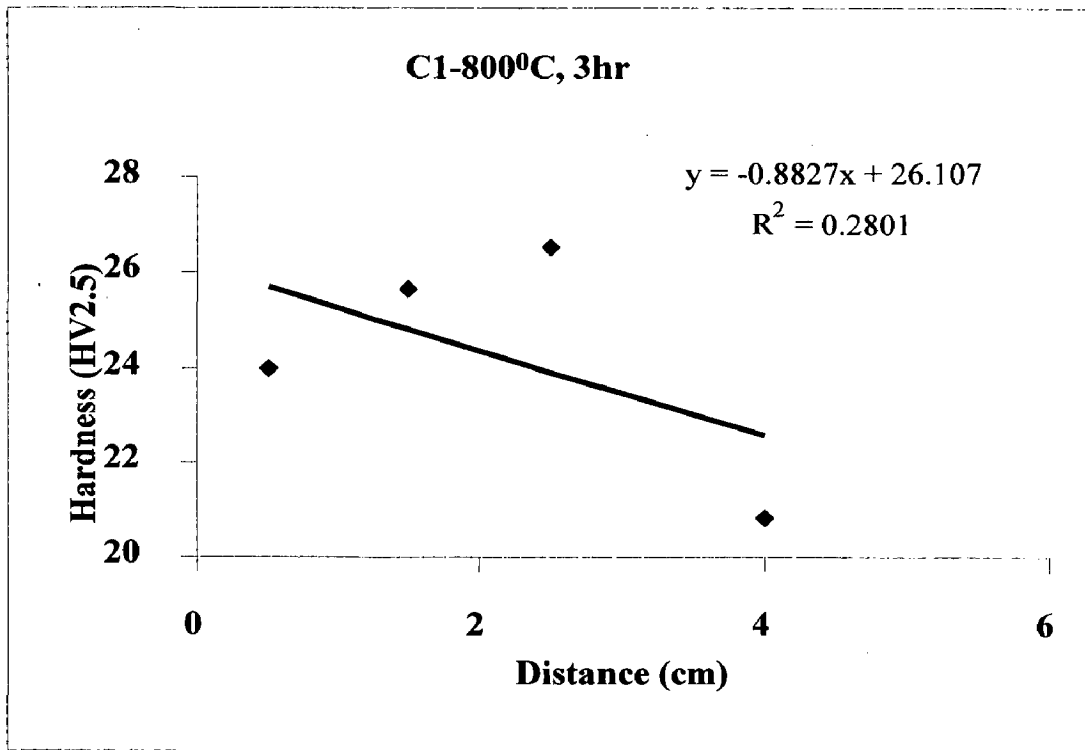


Figure 80

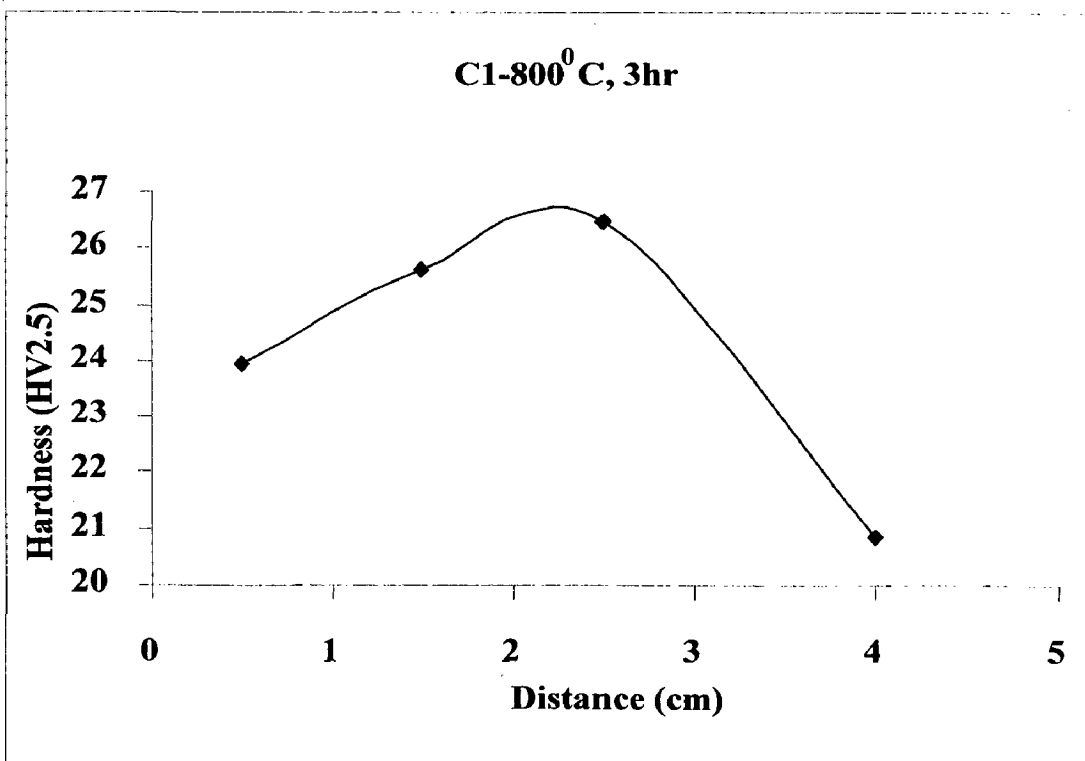


Figure 81

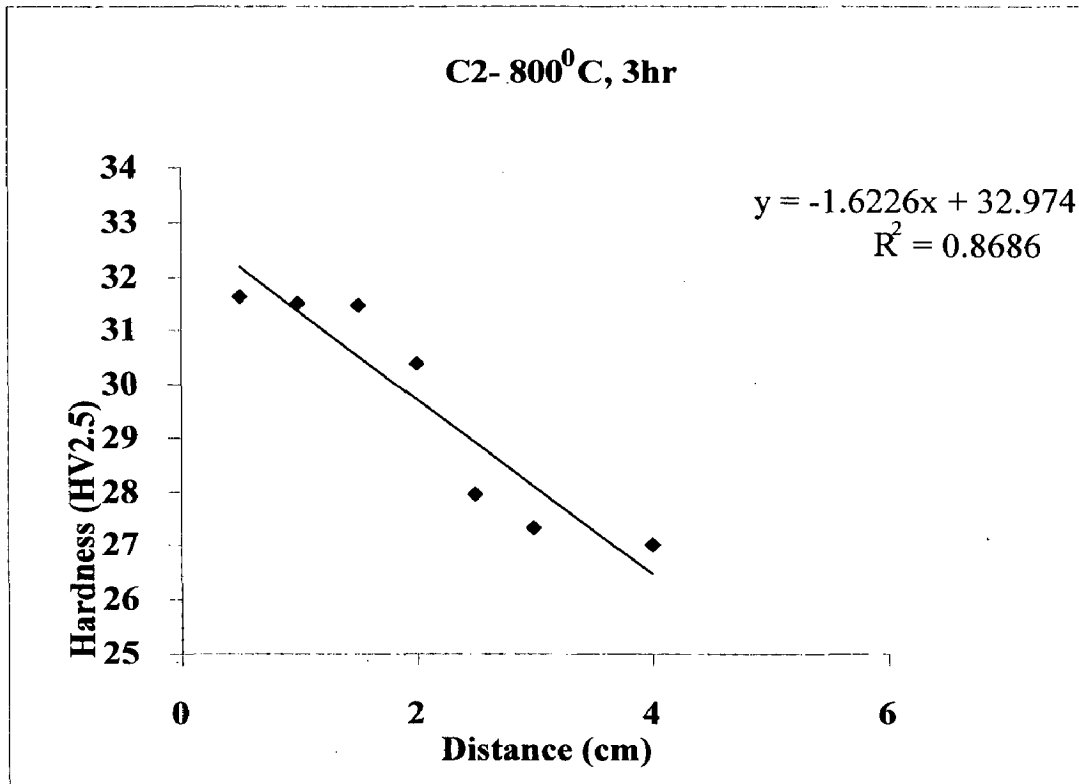


Figure 82

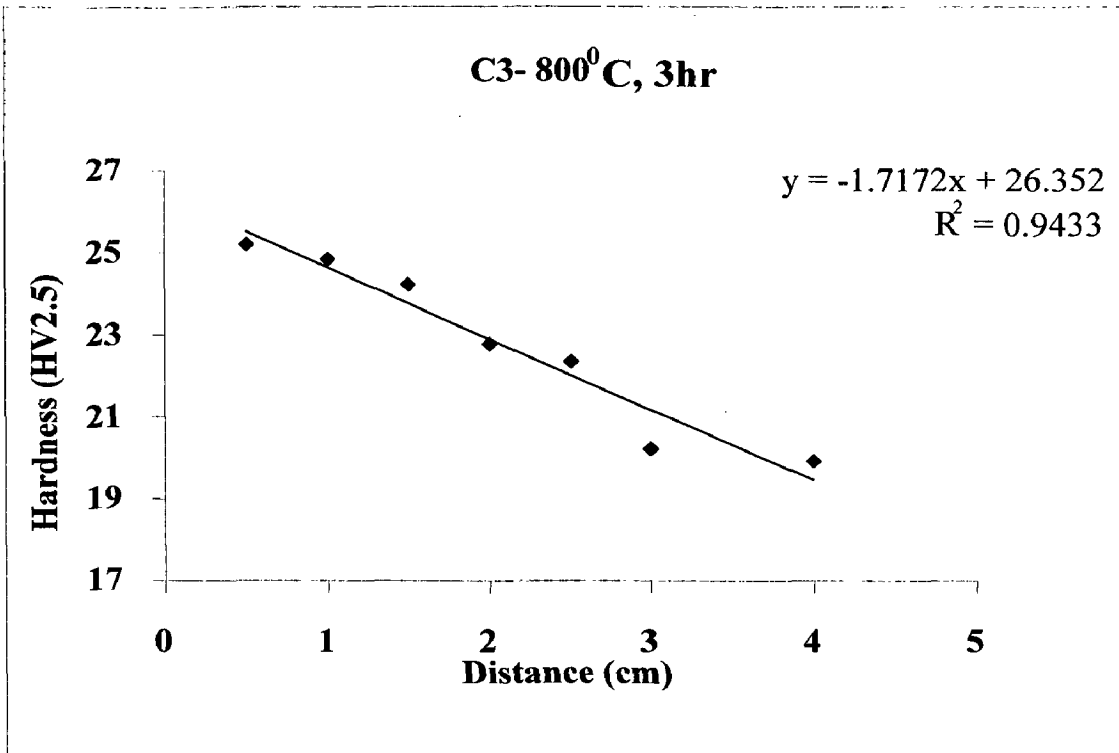


Figure 83

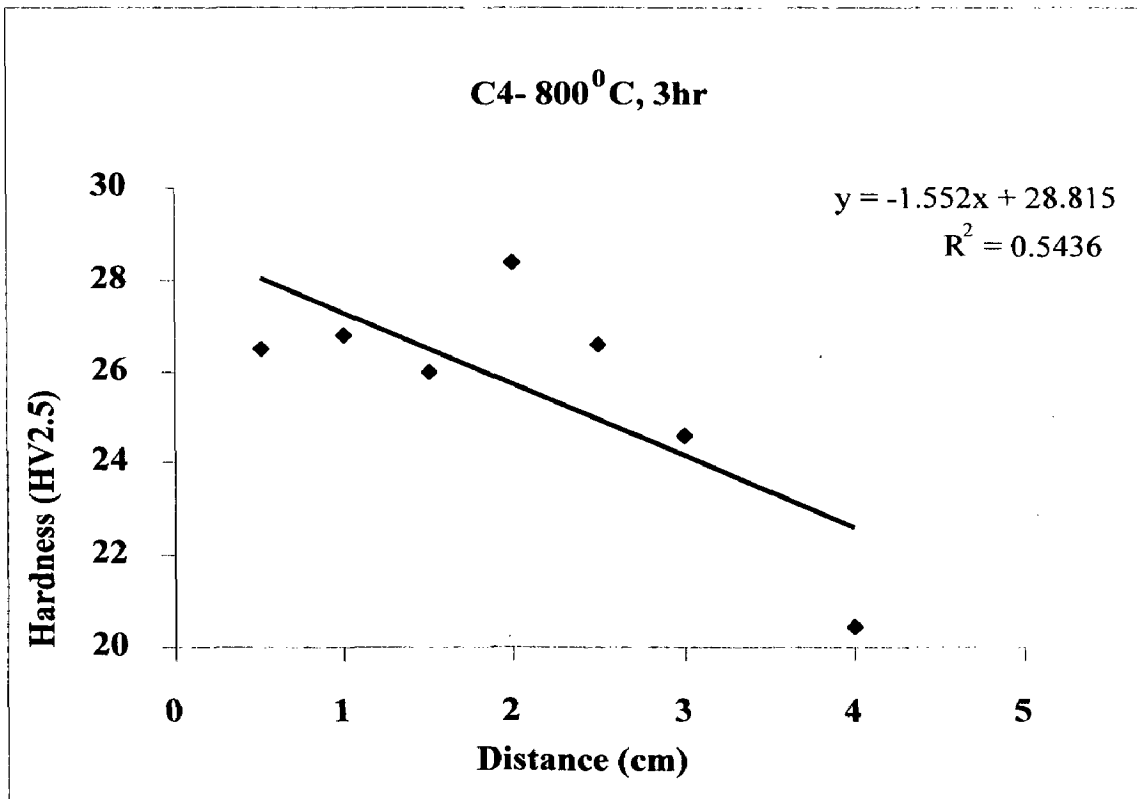


Figure 84

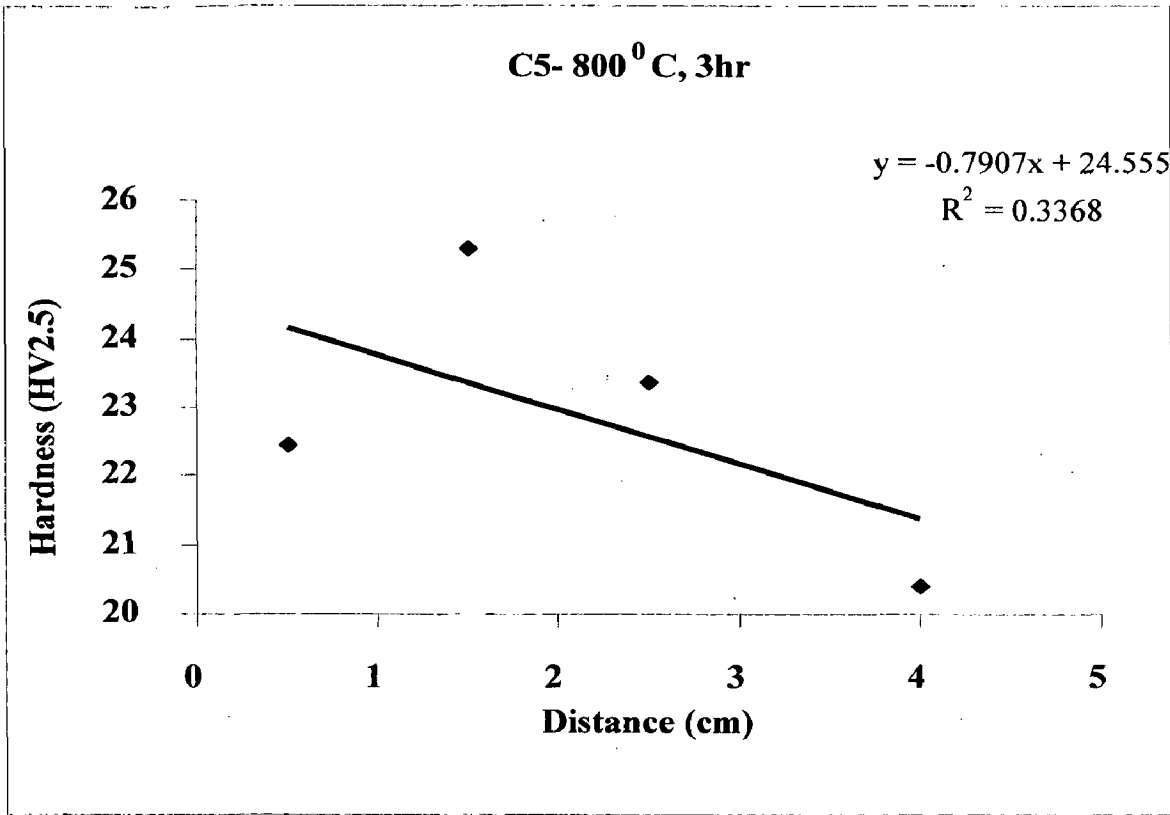


Figure 85

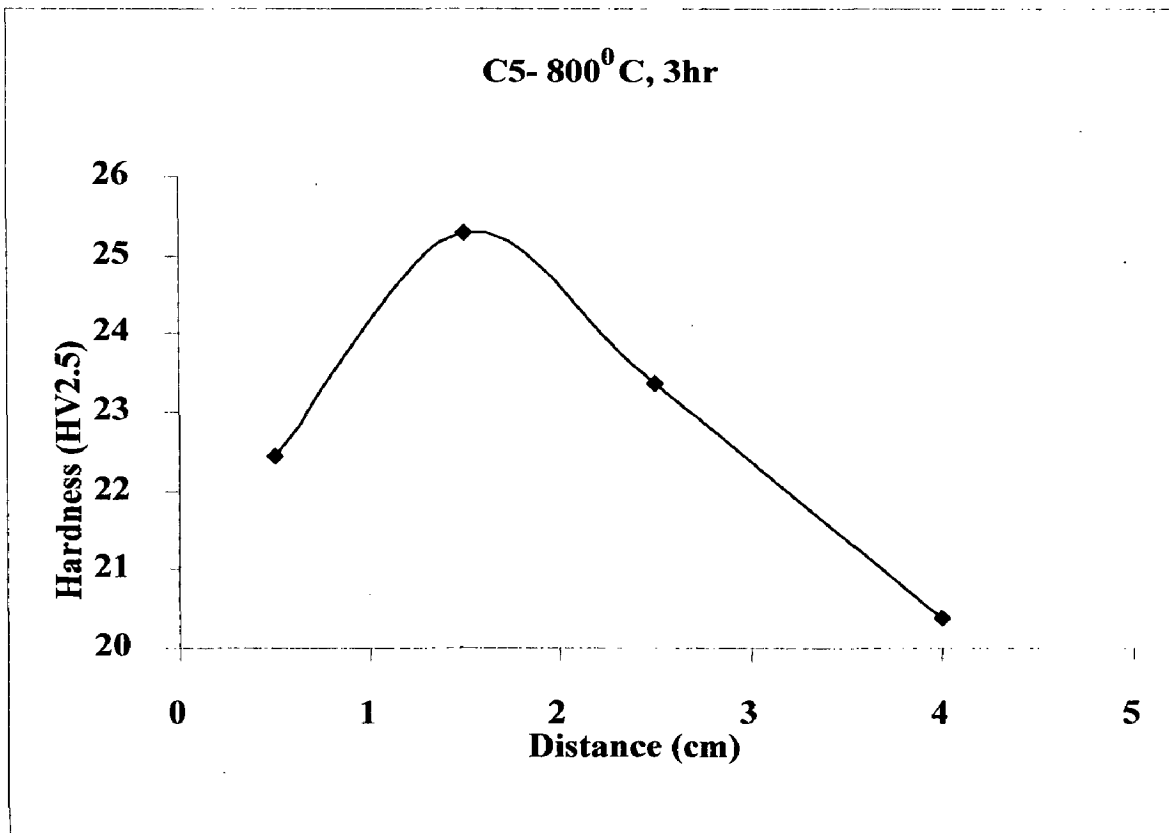


Figure 86

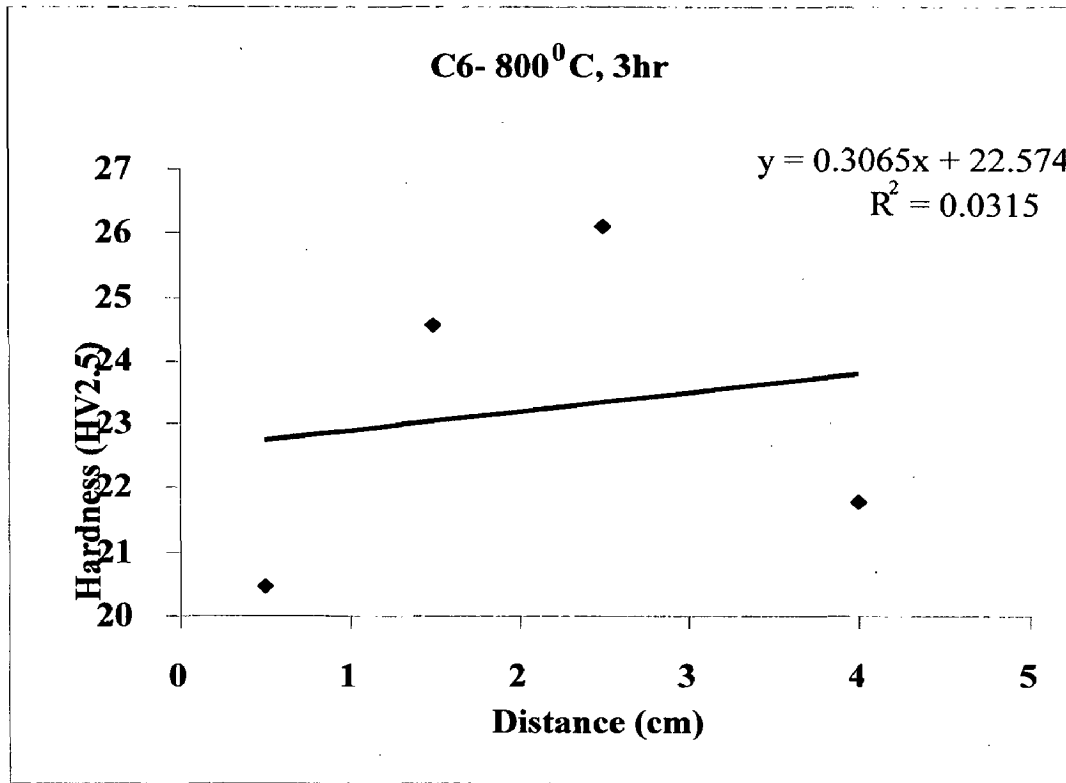


Figure 87

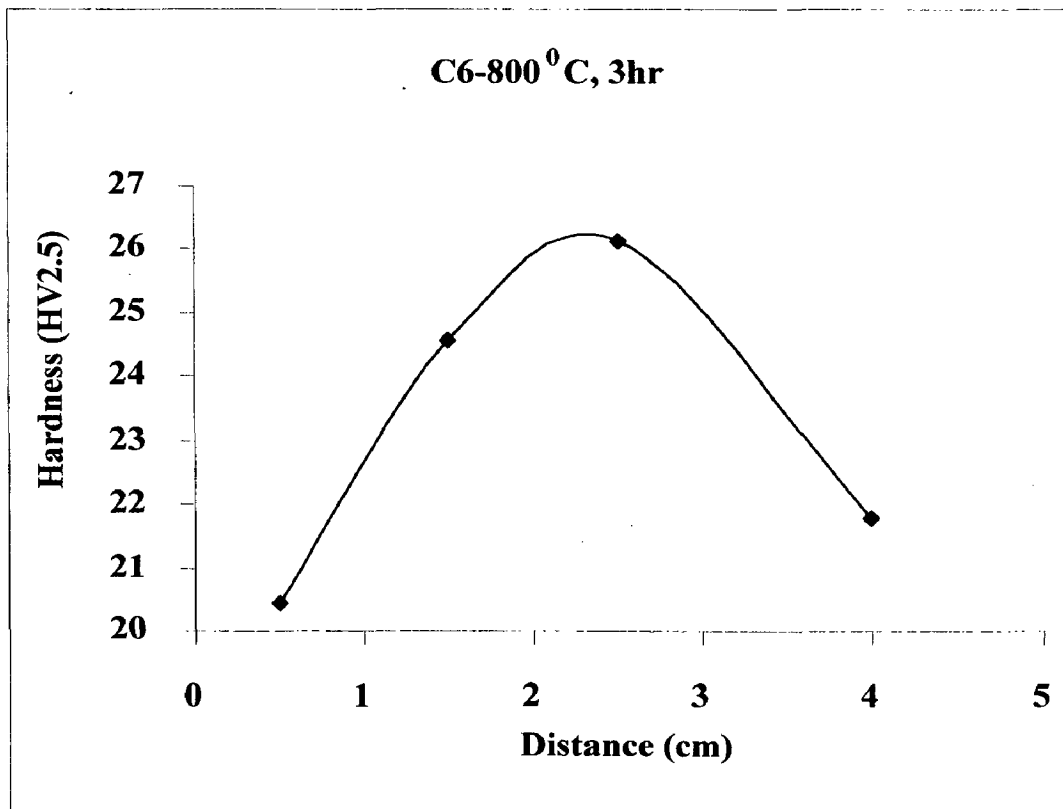


Figure 88

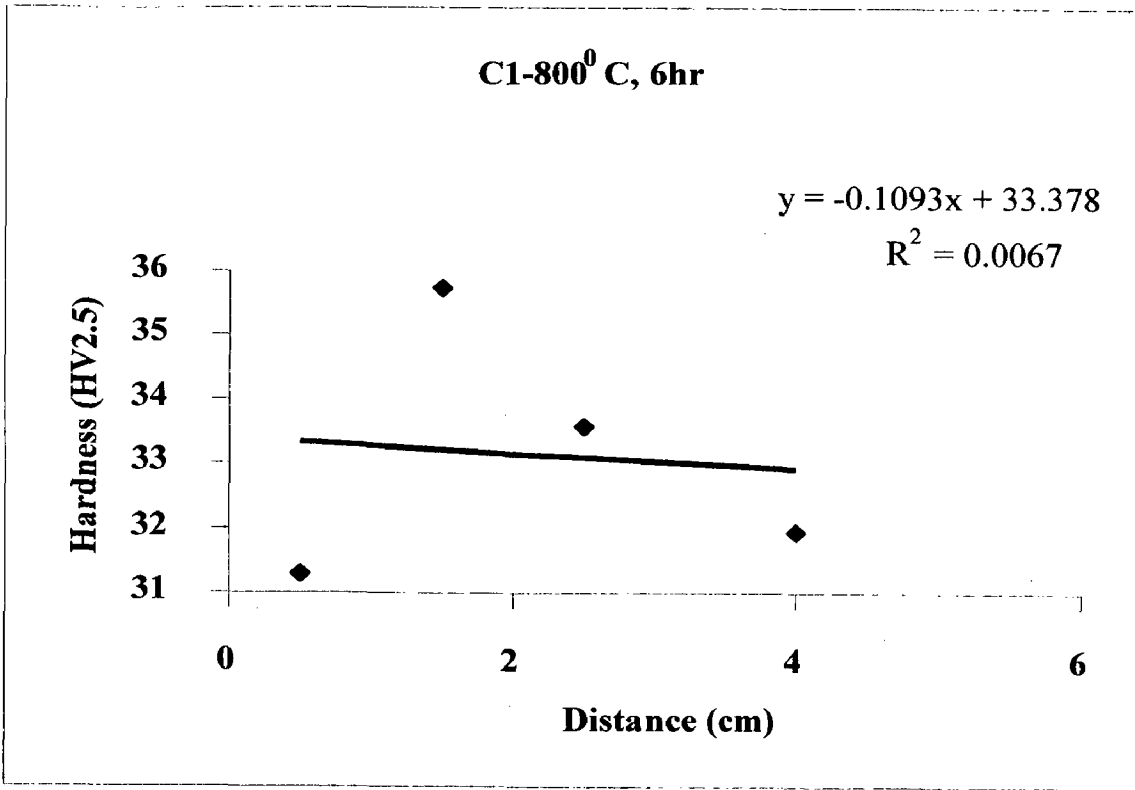


Figure 89

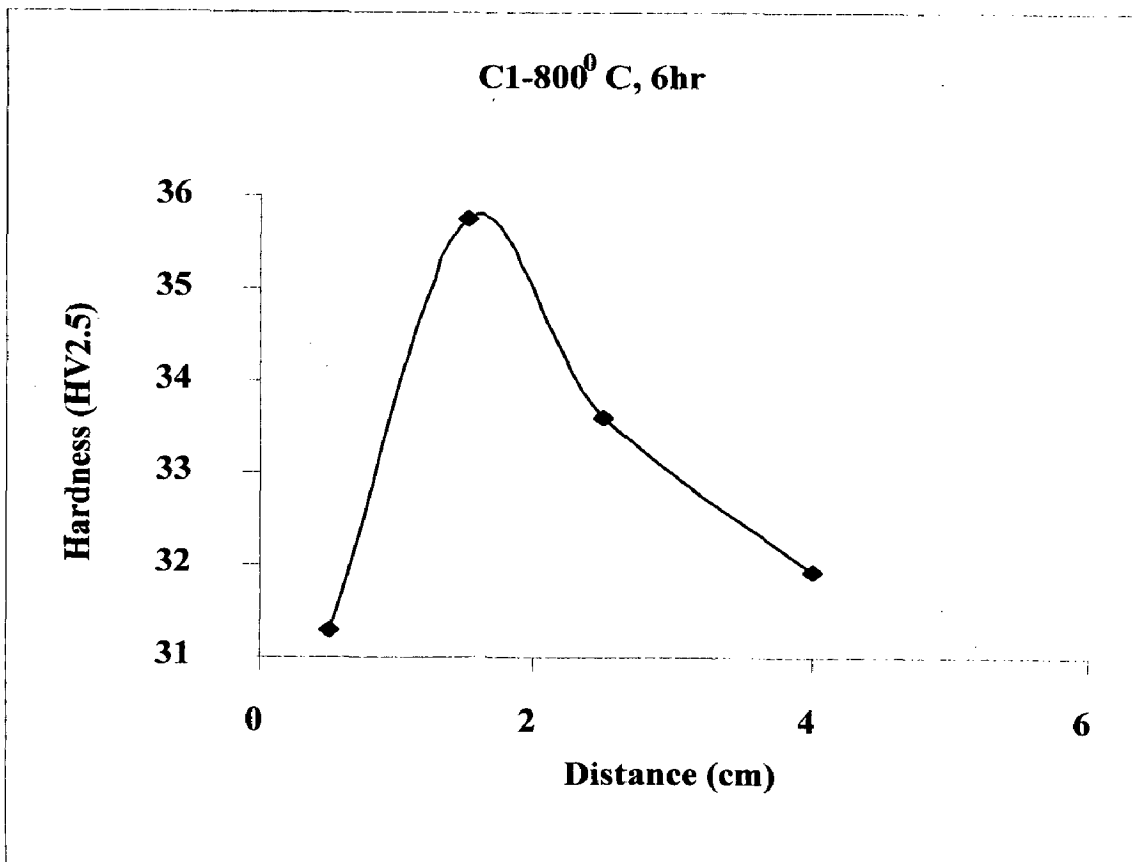


Figure 90

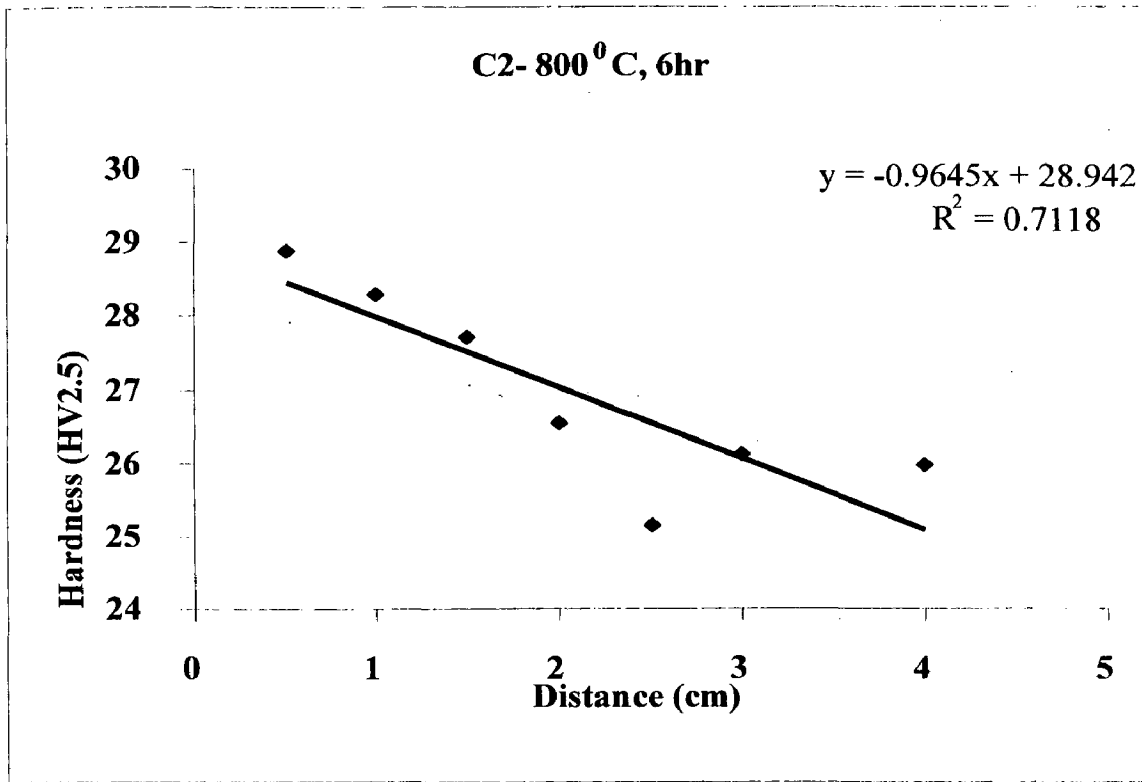


Figure 91

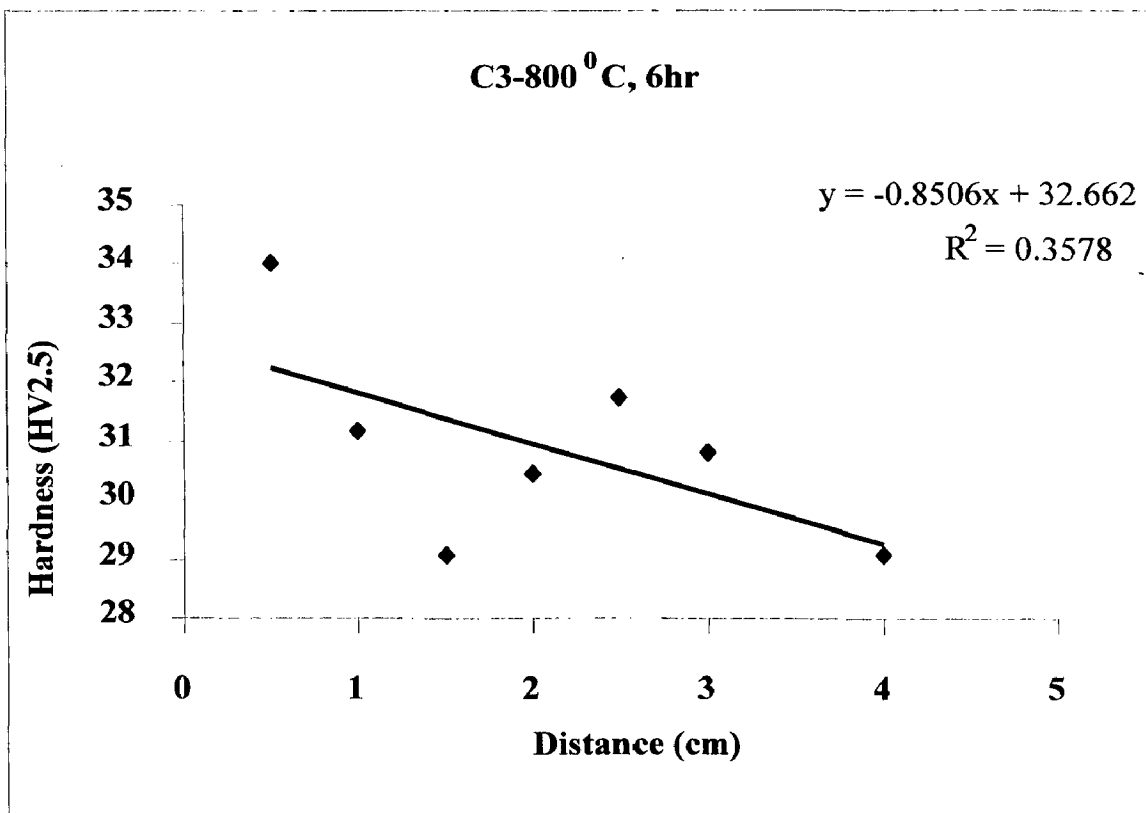


Figure 92

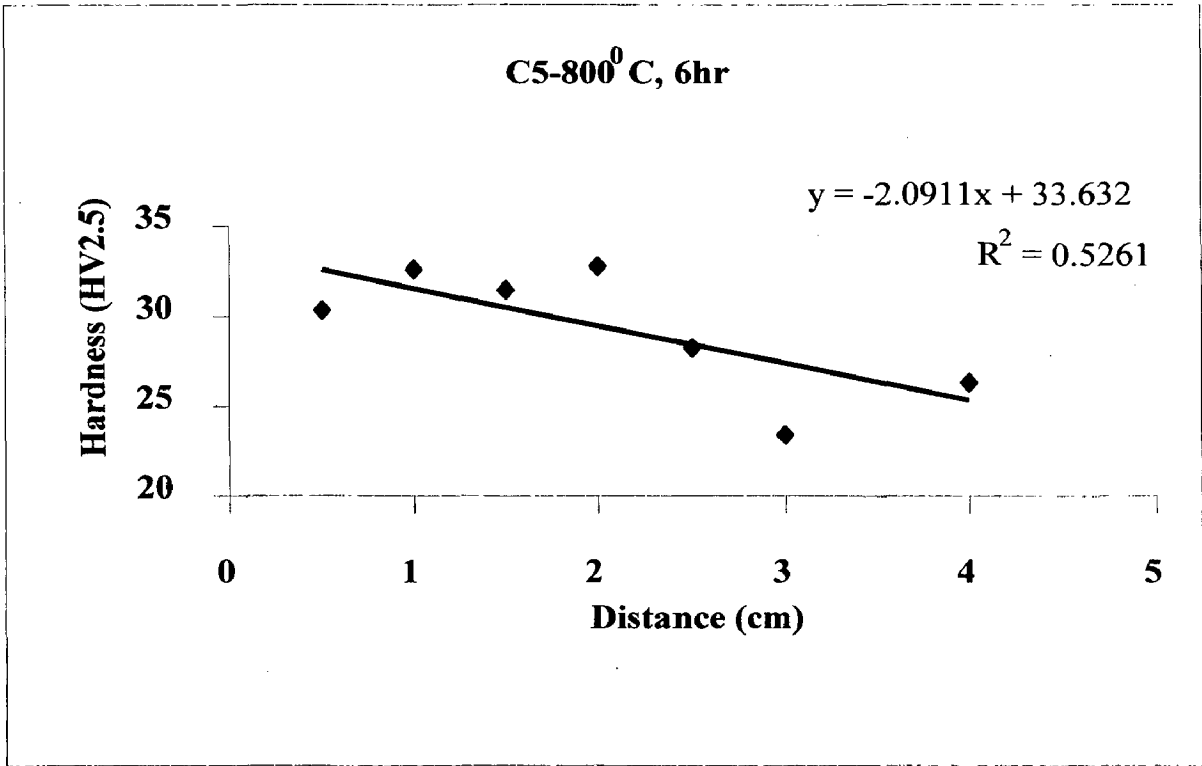


Figure 94

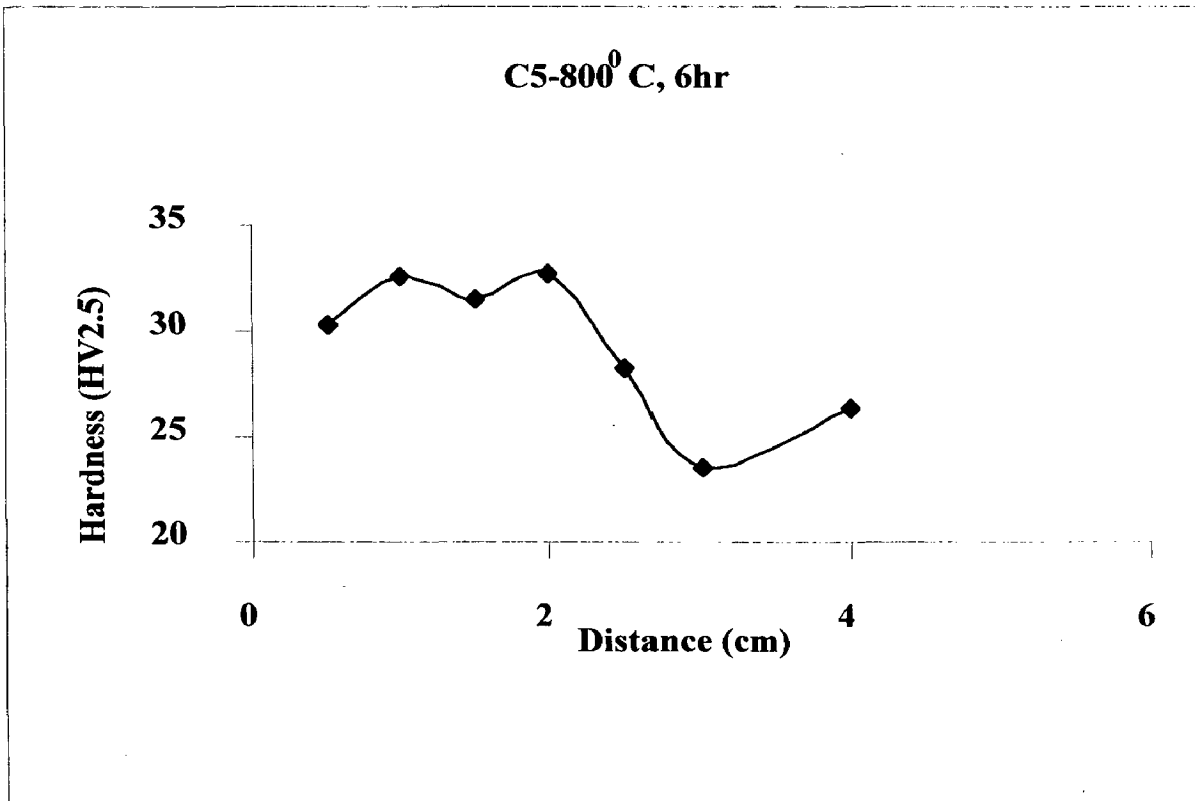


Figure 95

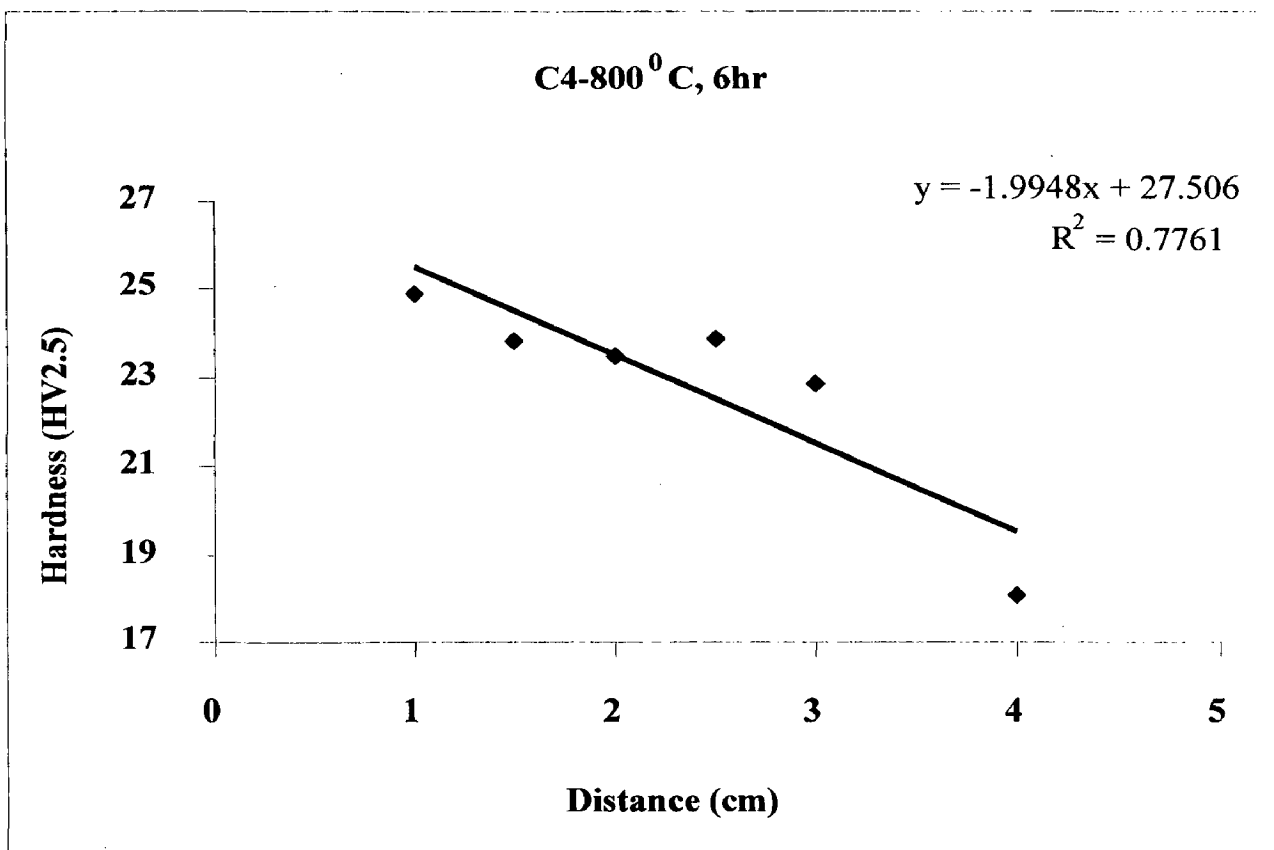


Figure 93

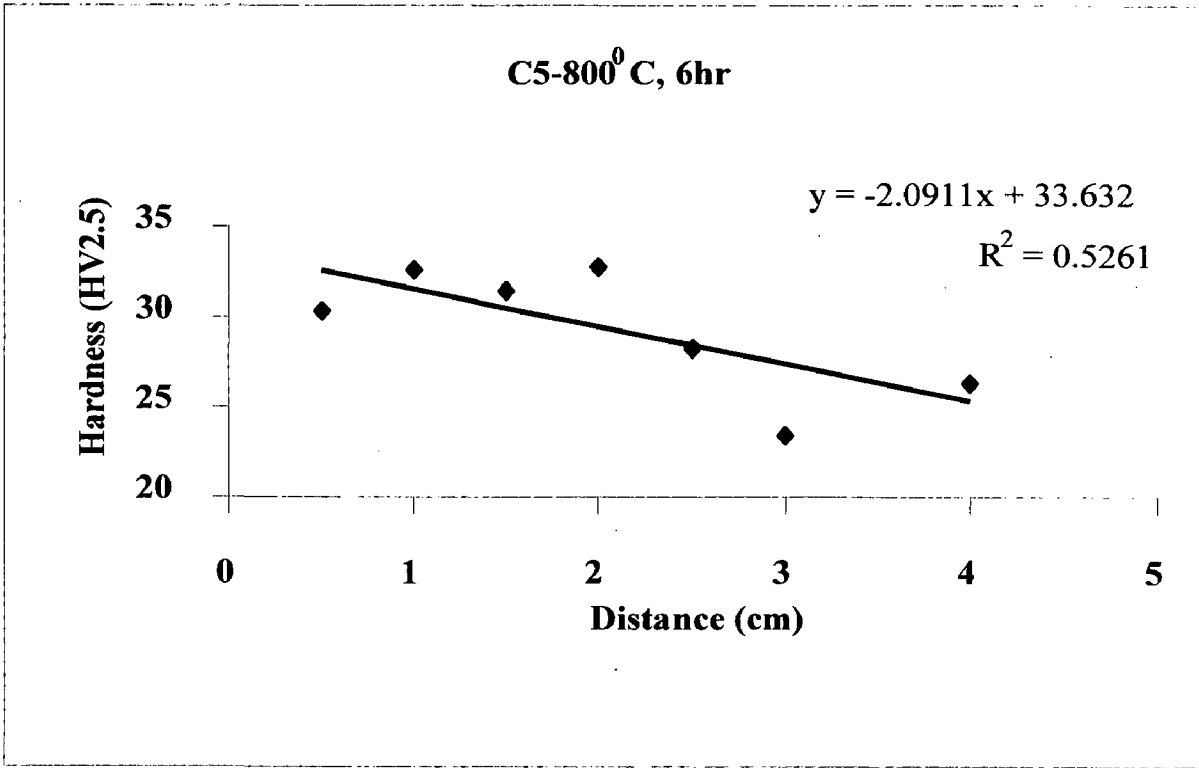


Figure 94

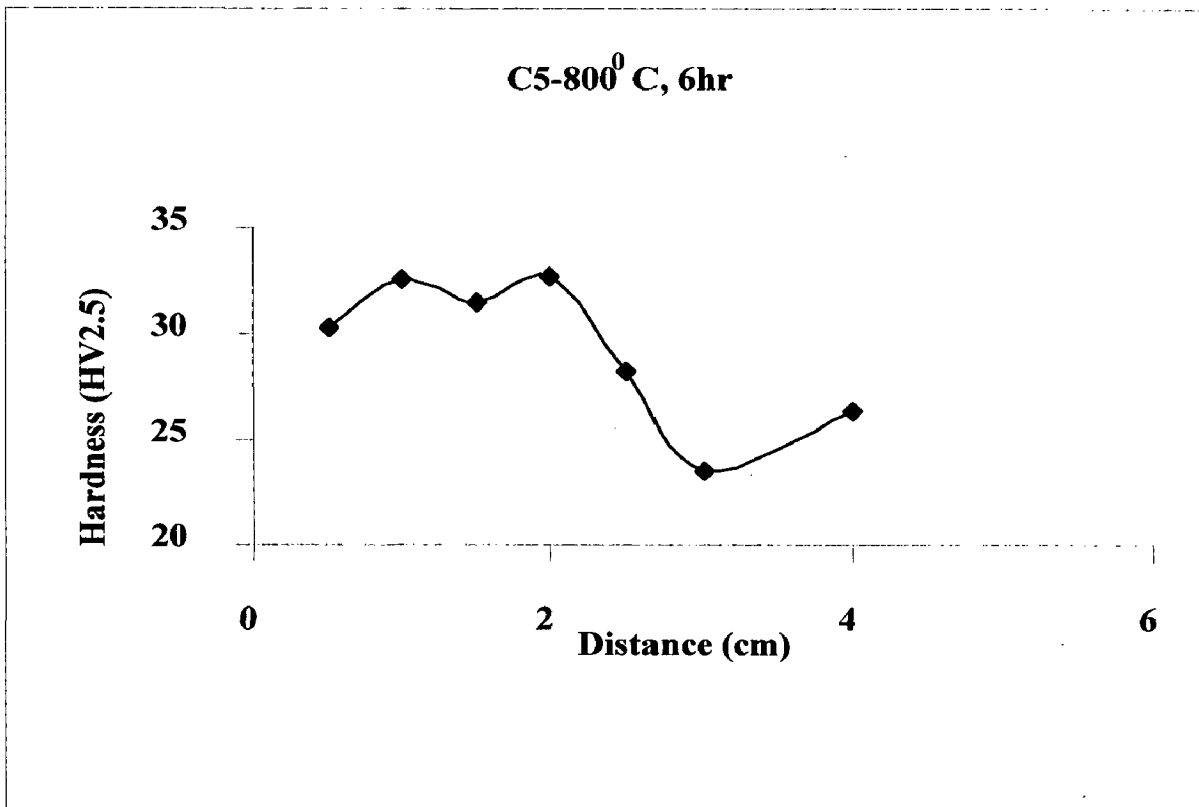


Figure 95

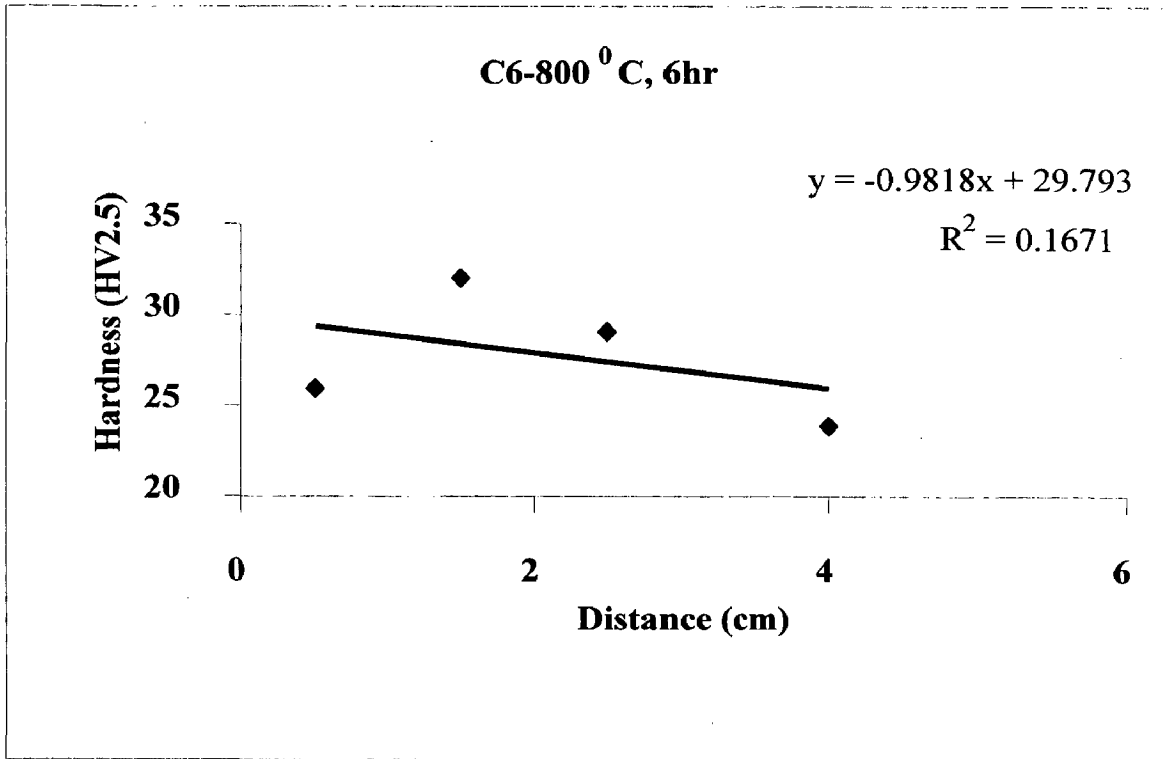


Figure 96

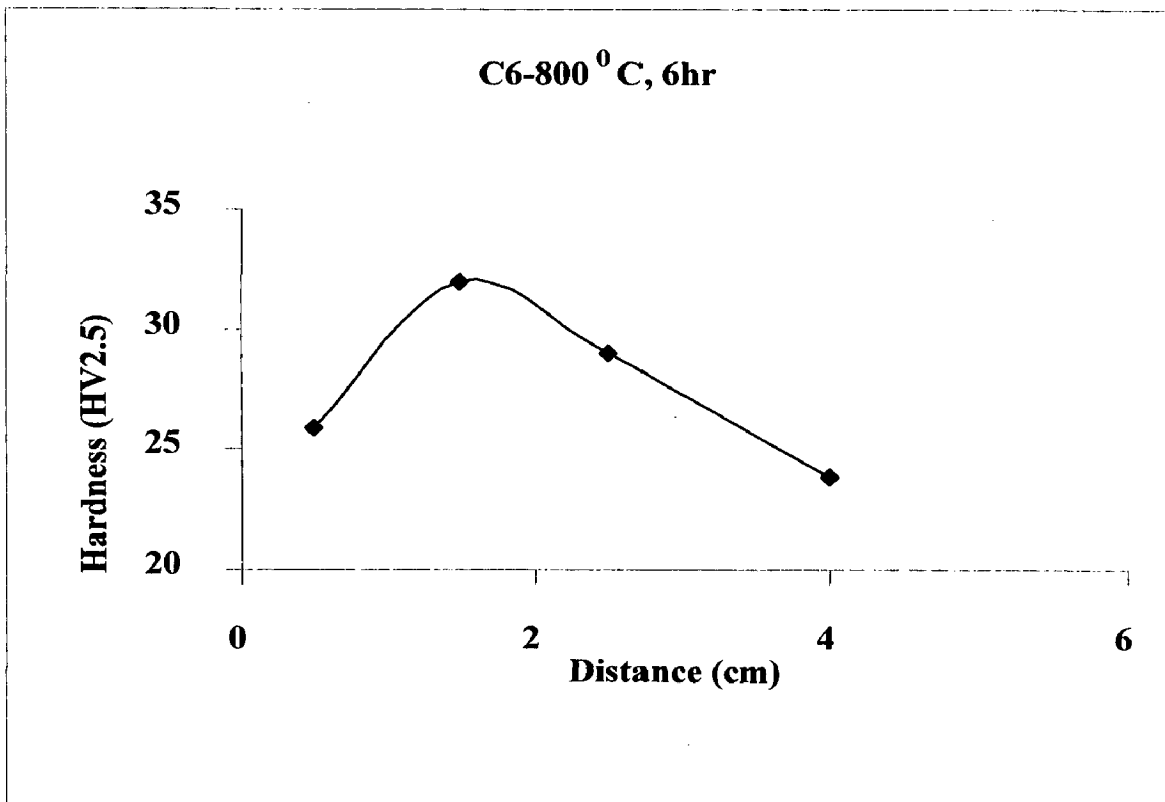


Figure 97

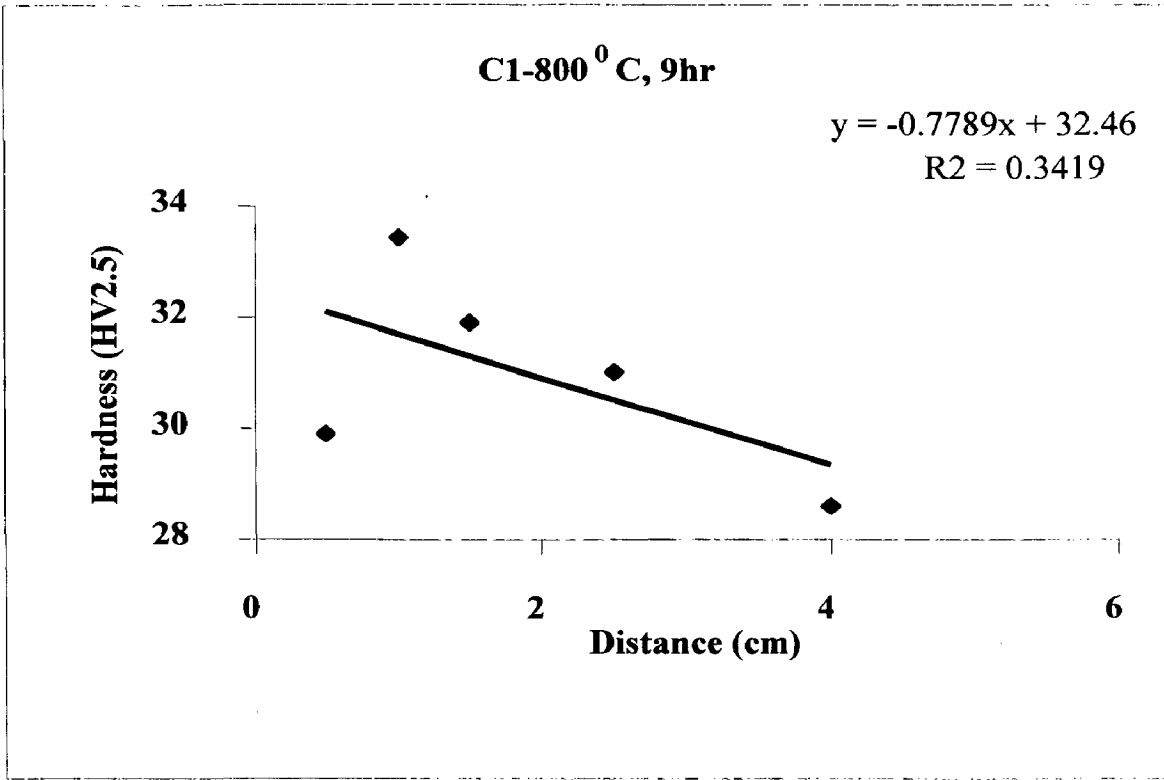


Figure 98

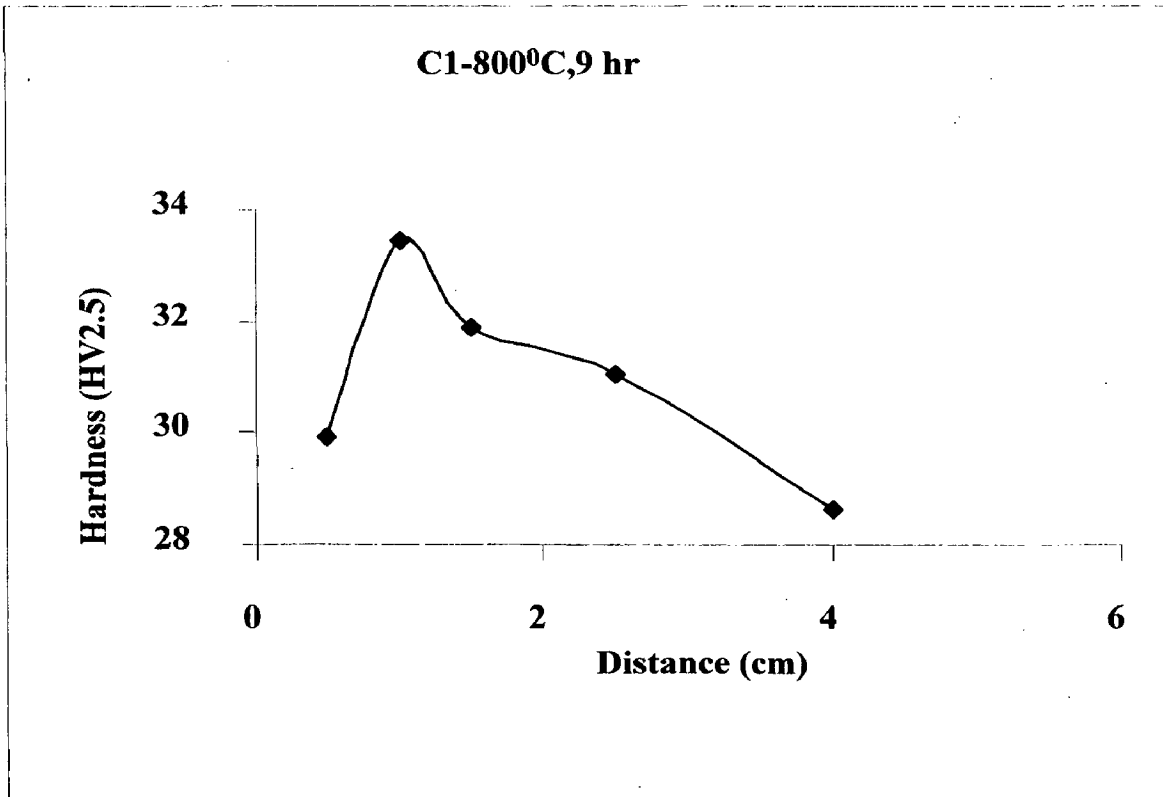


Figure 99

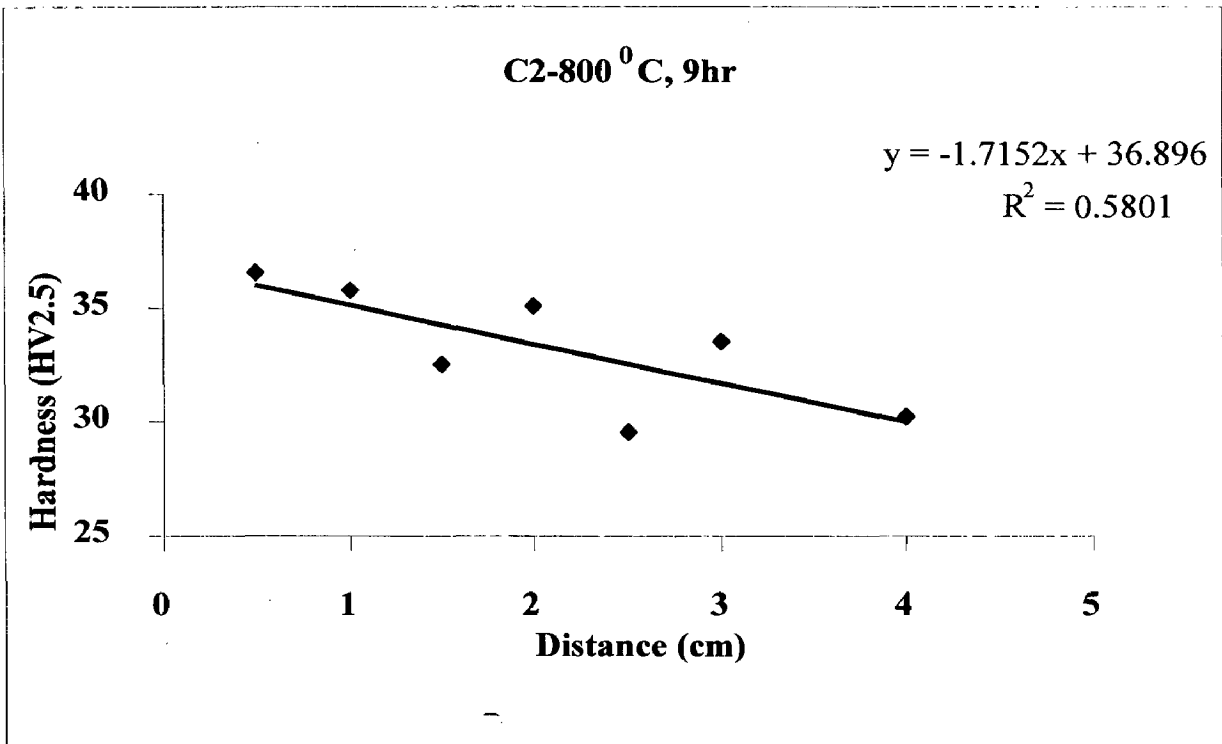


Figure 100

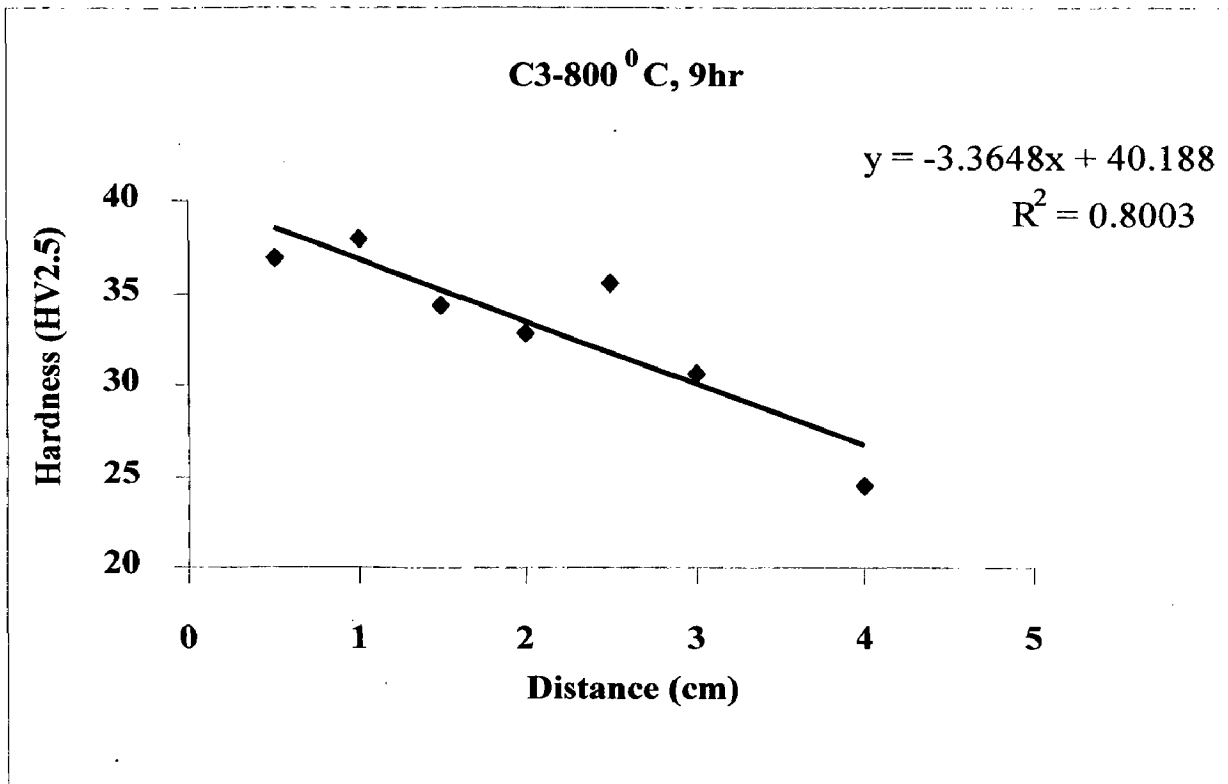


Figure 101

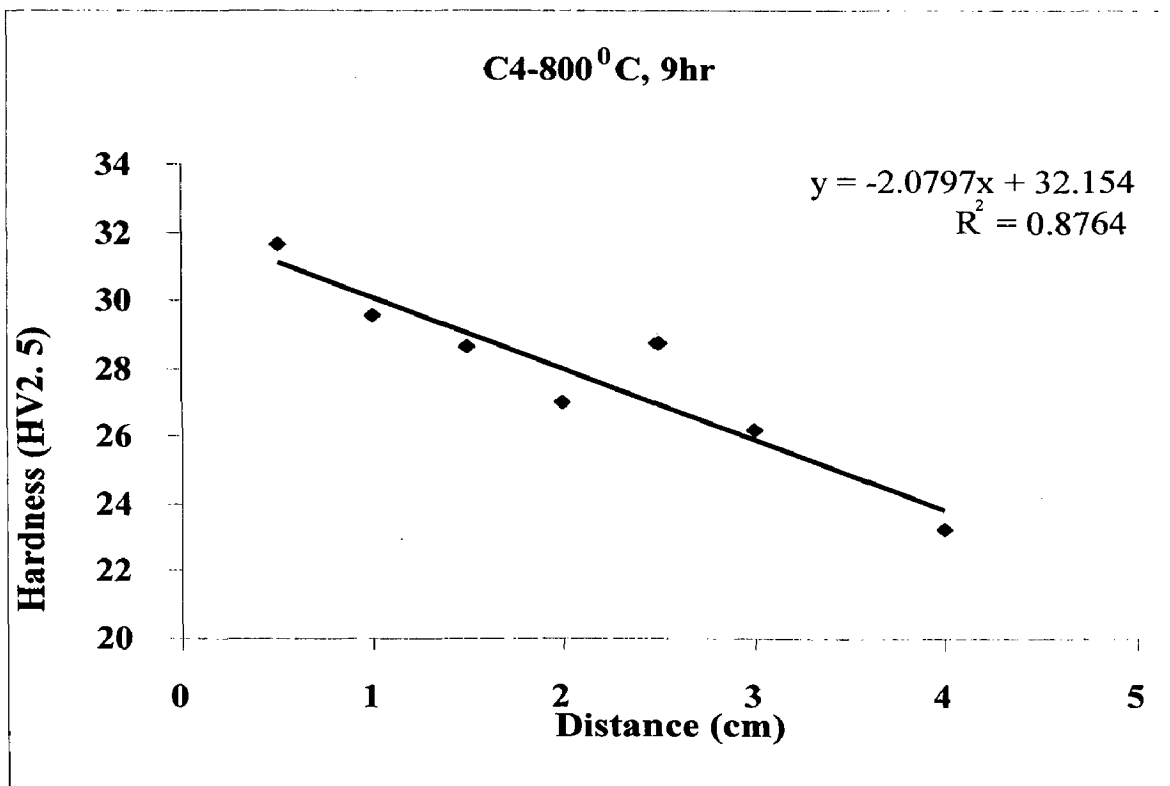


Figure 102

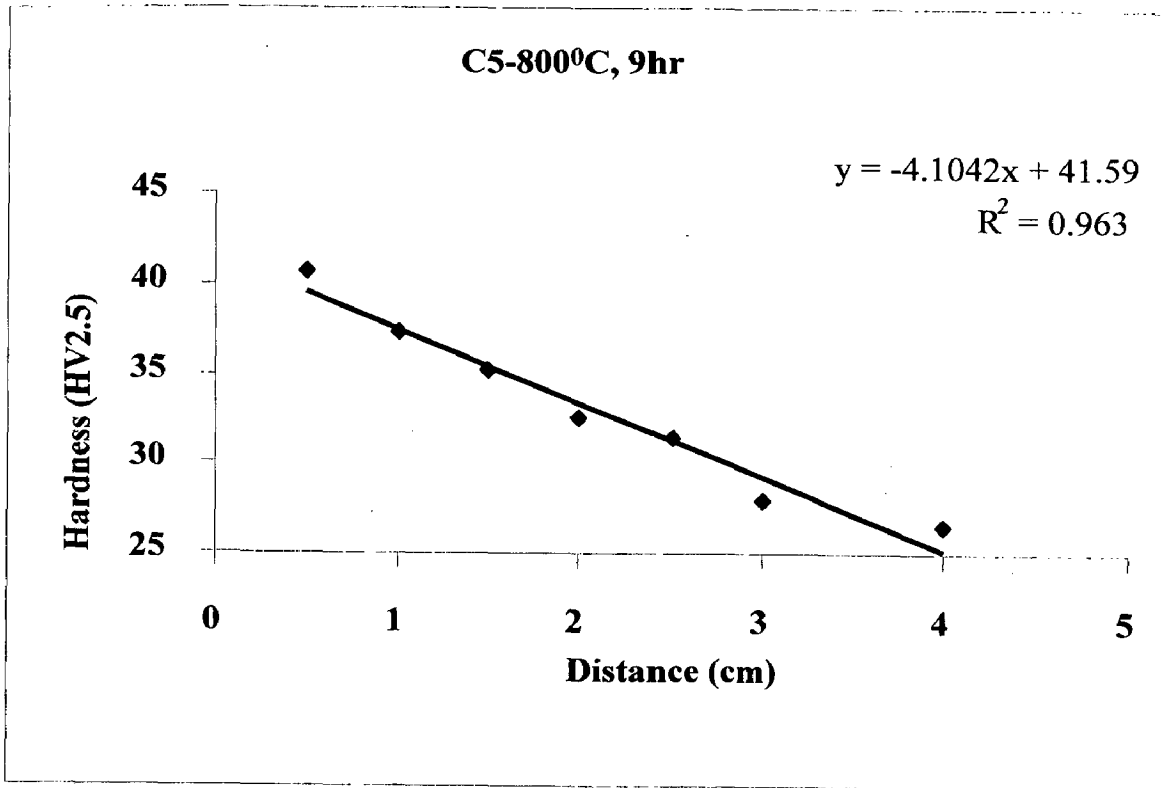


Figure 103

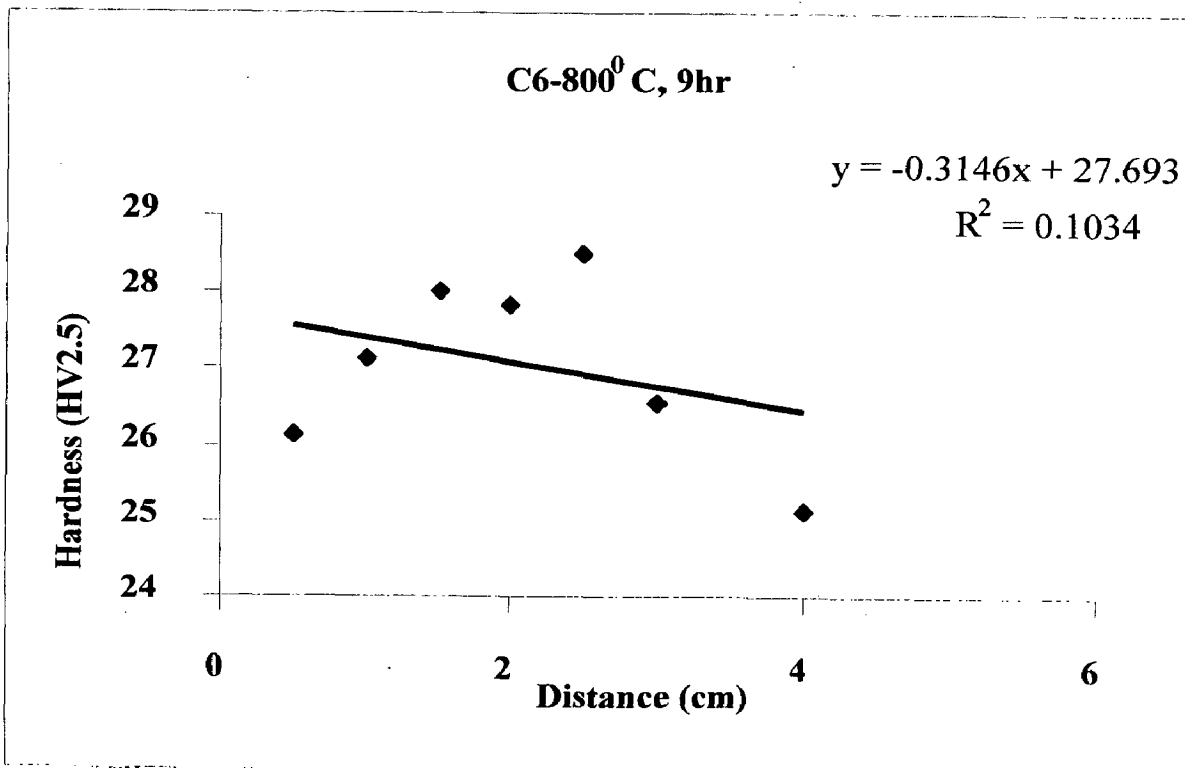


Figure 104

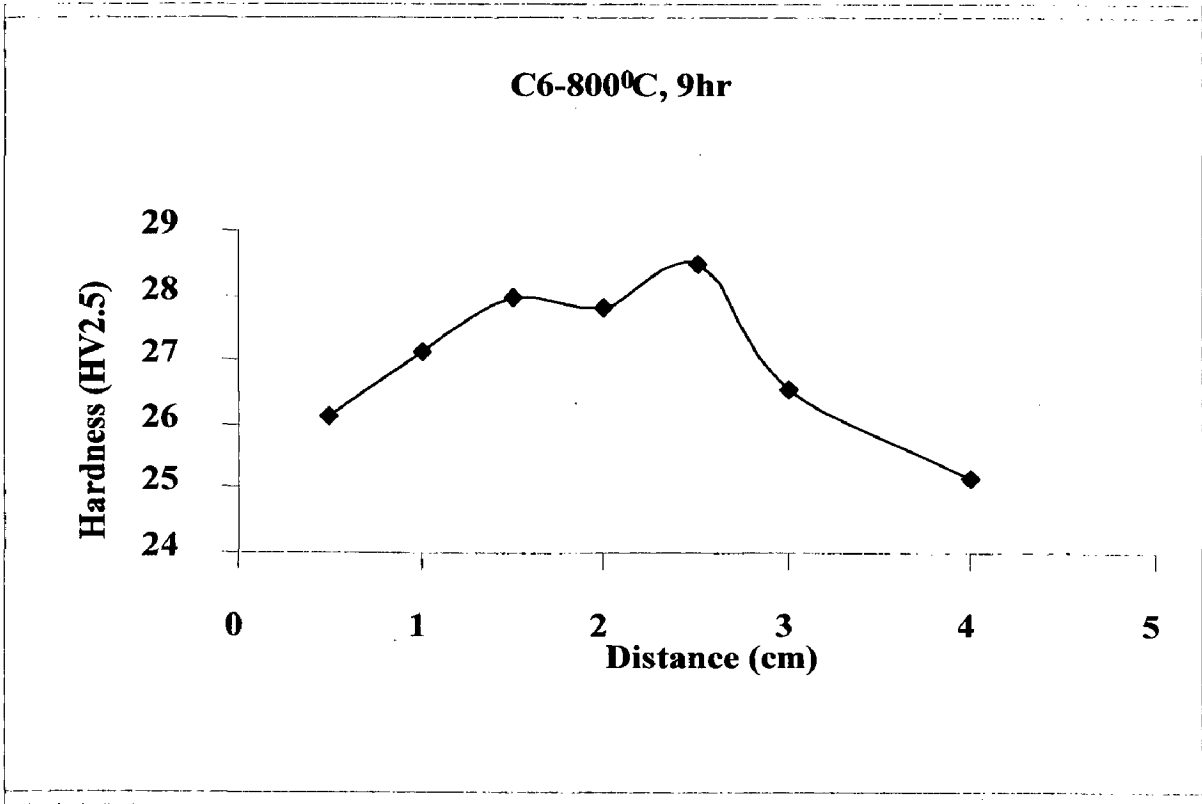


Figure 105

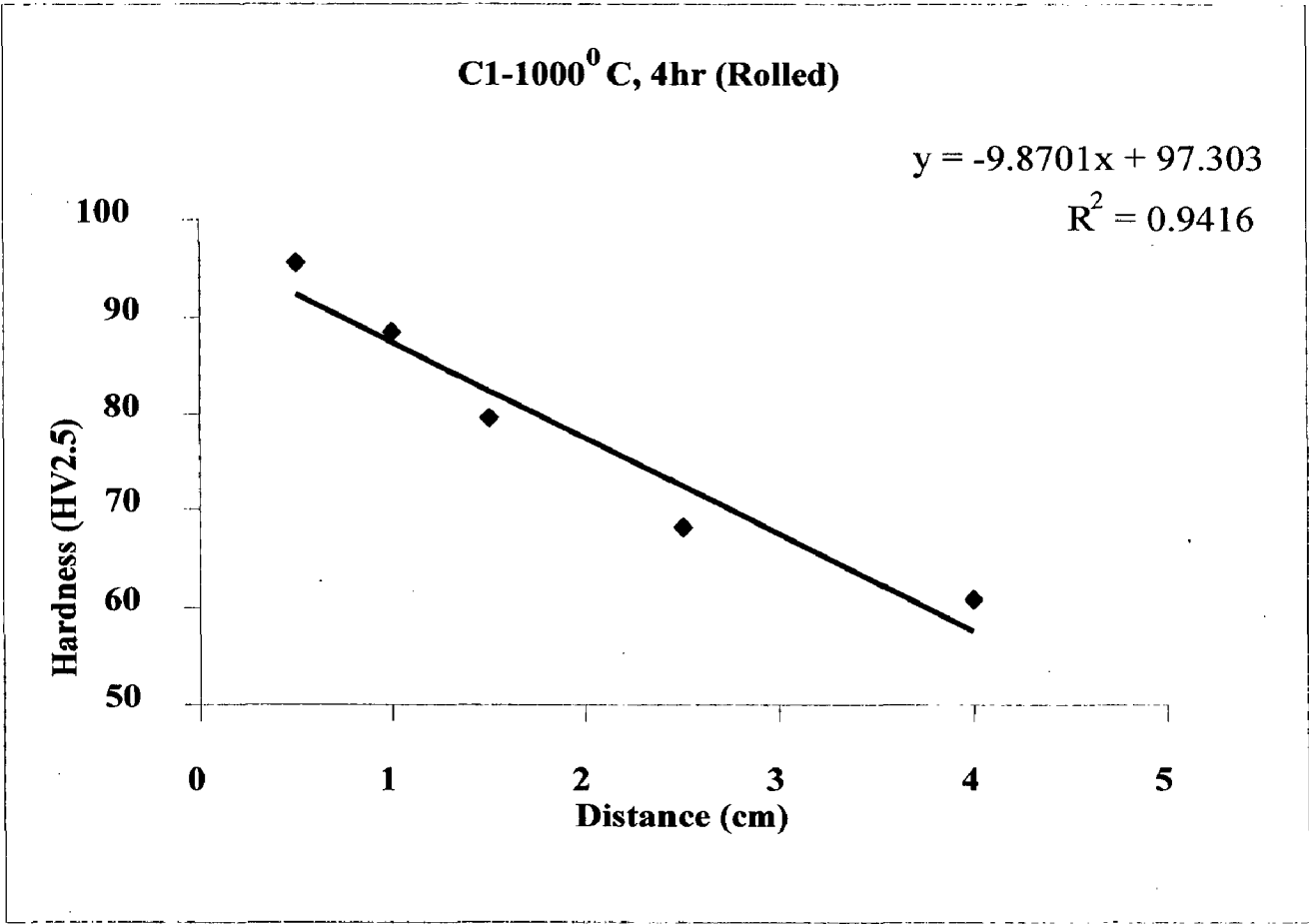


Figure 106

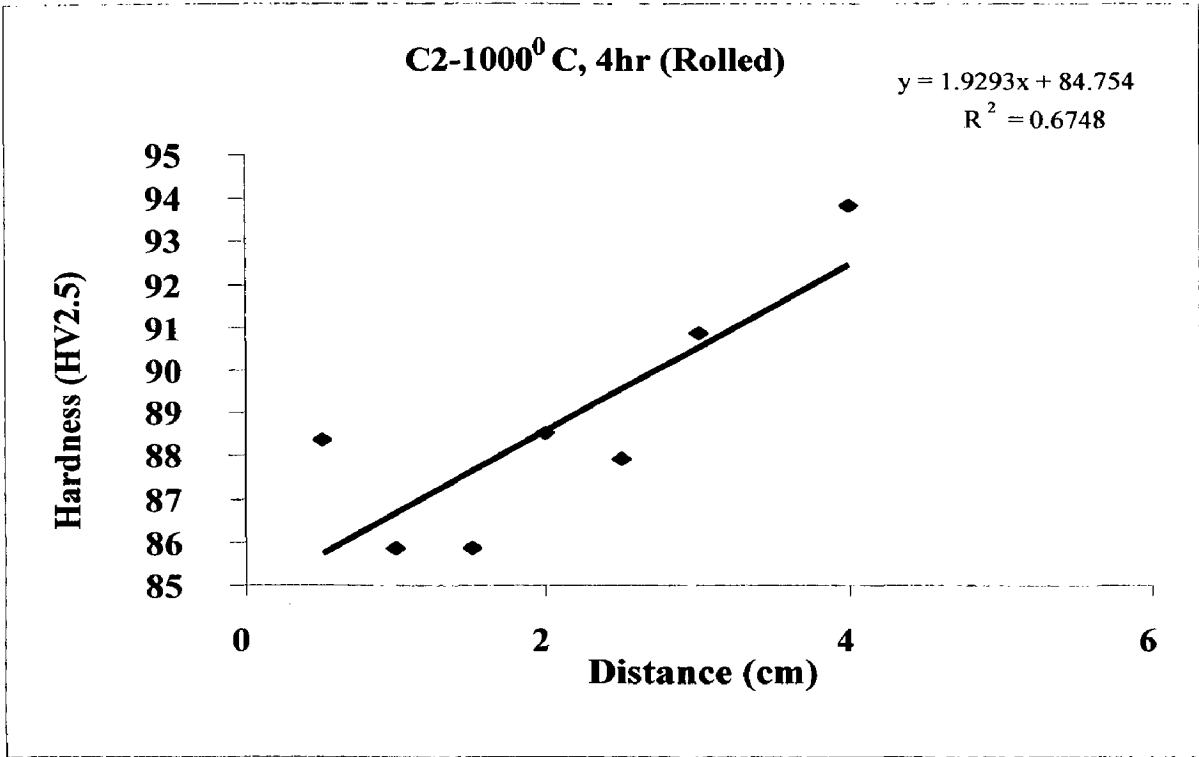


Figure 107

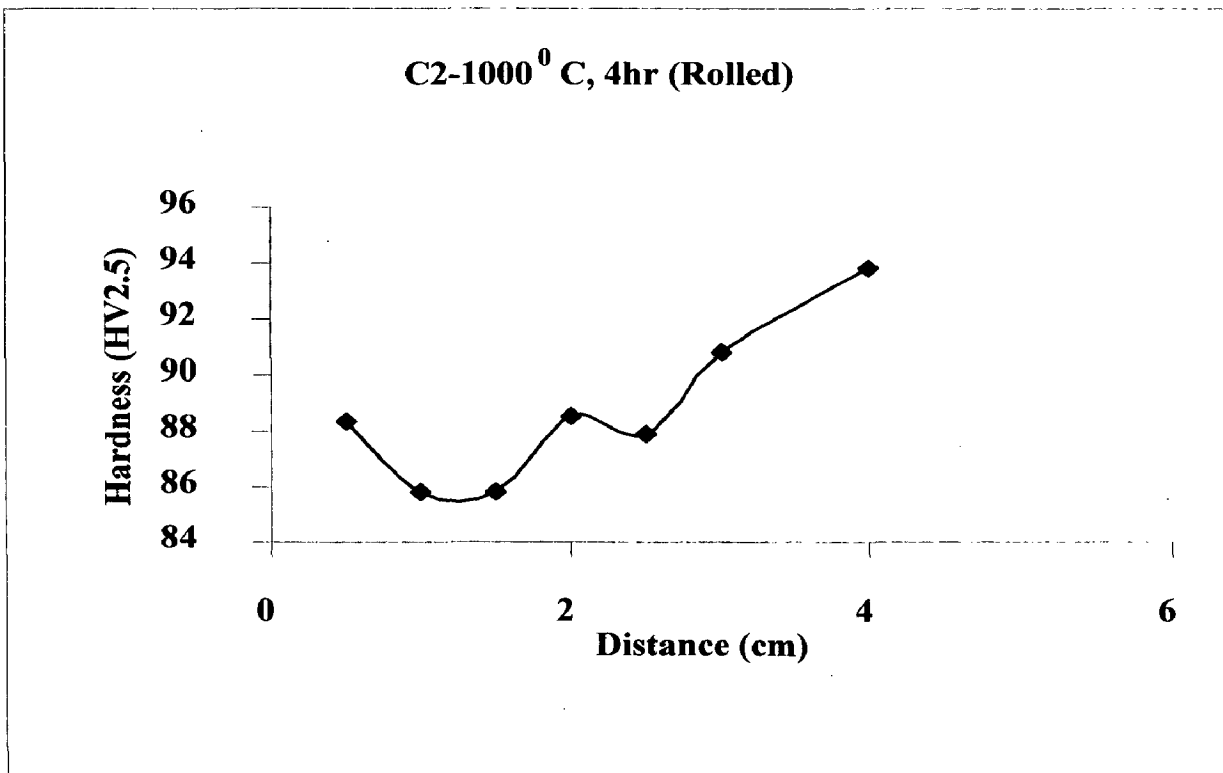


Figure 108

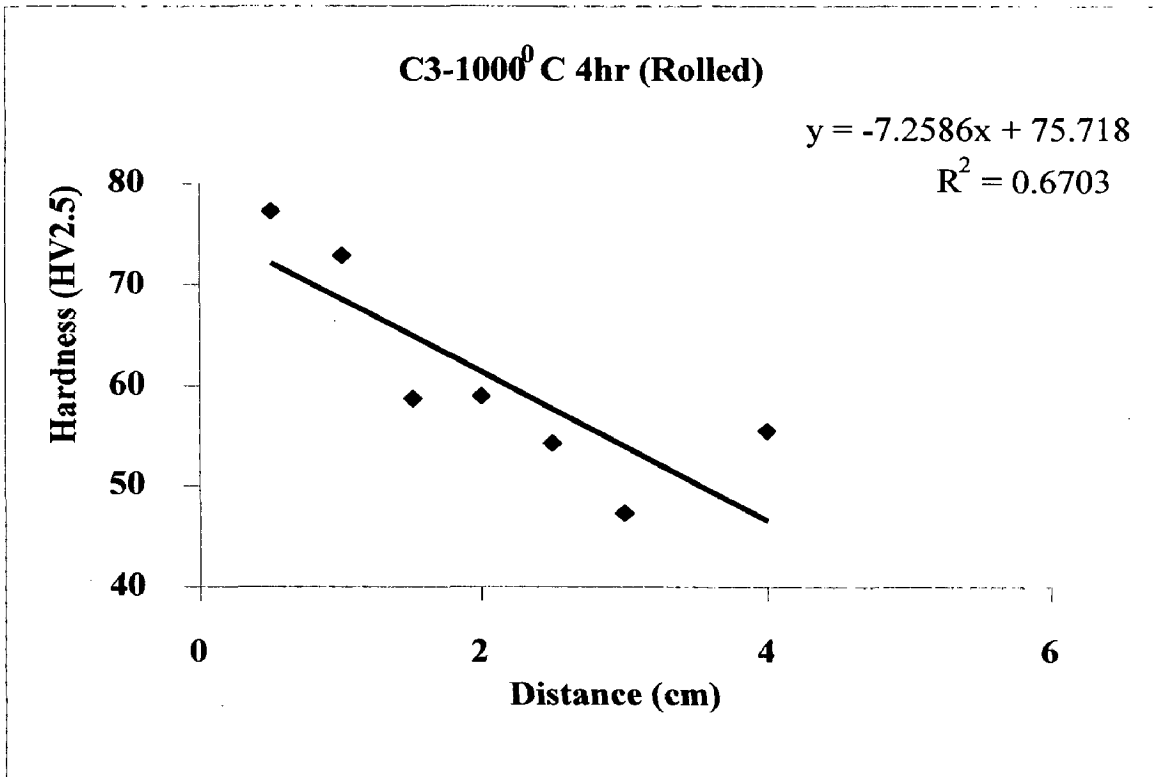


Figure 109

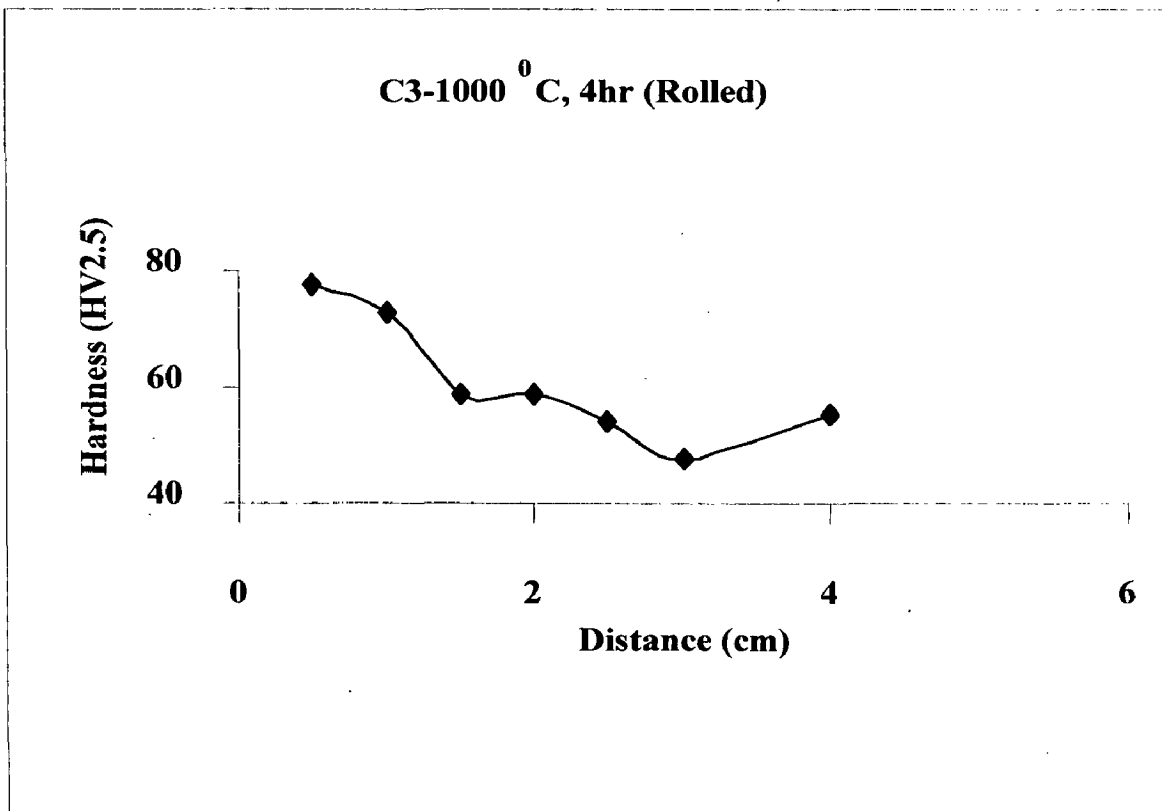


Figure 110

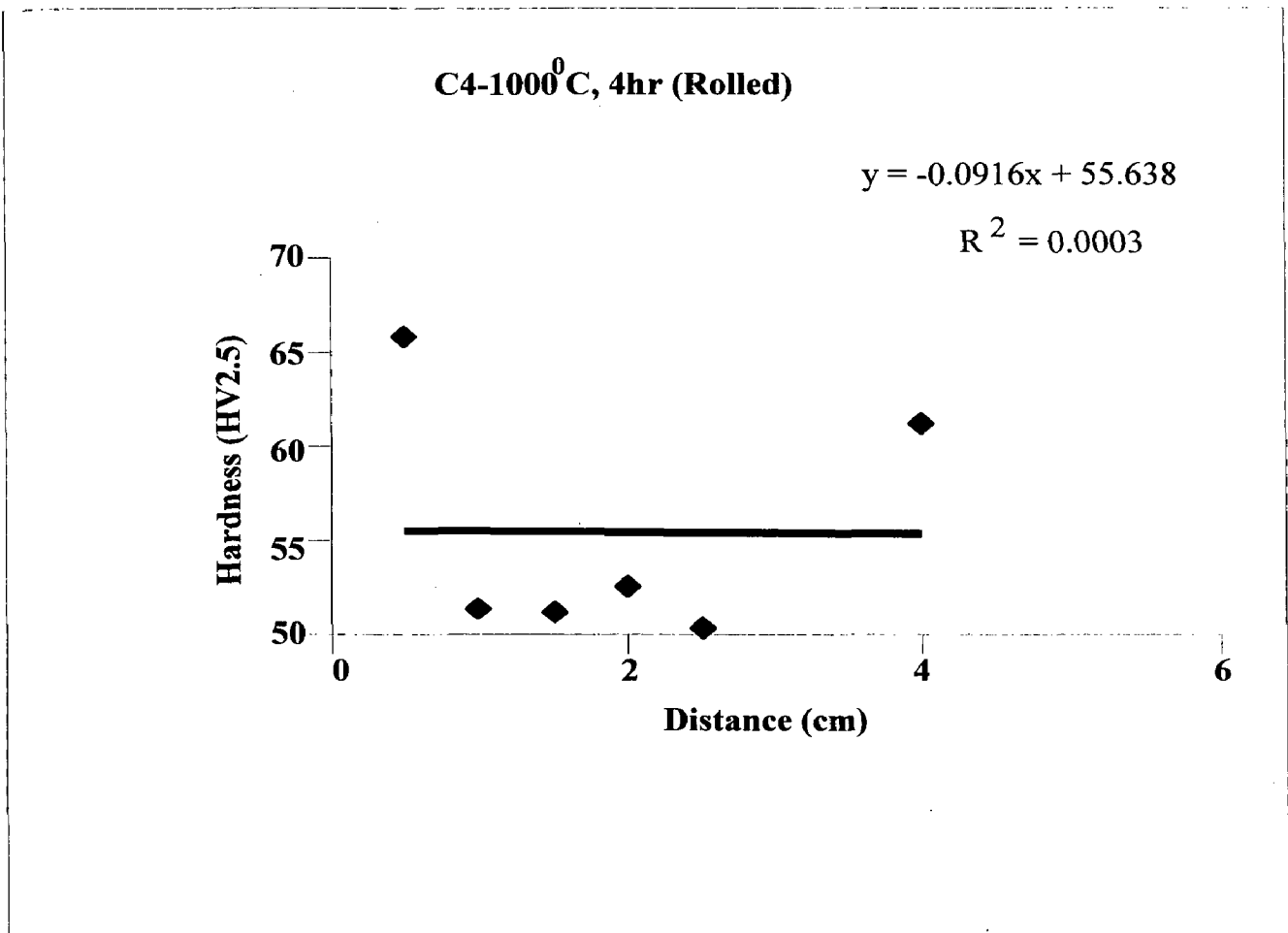


Figure 111

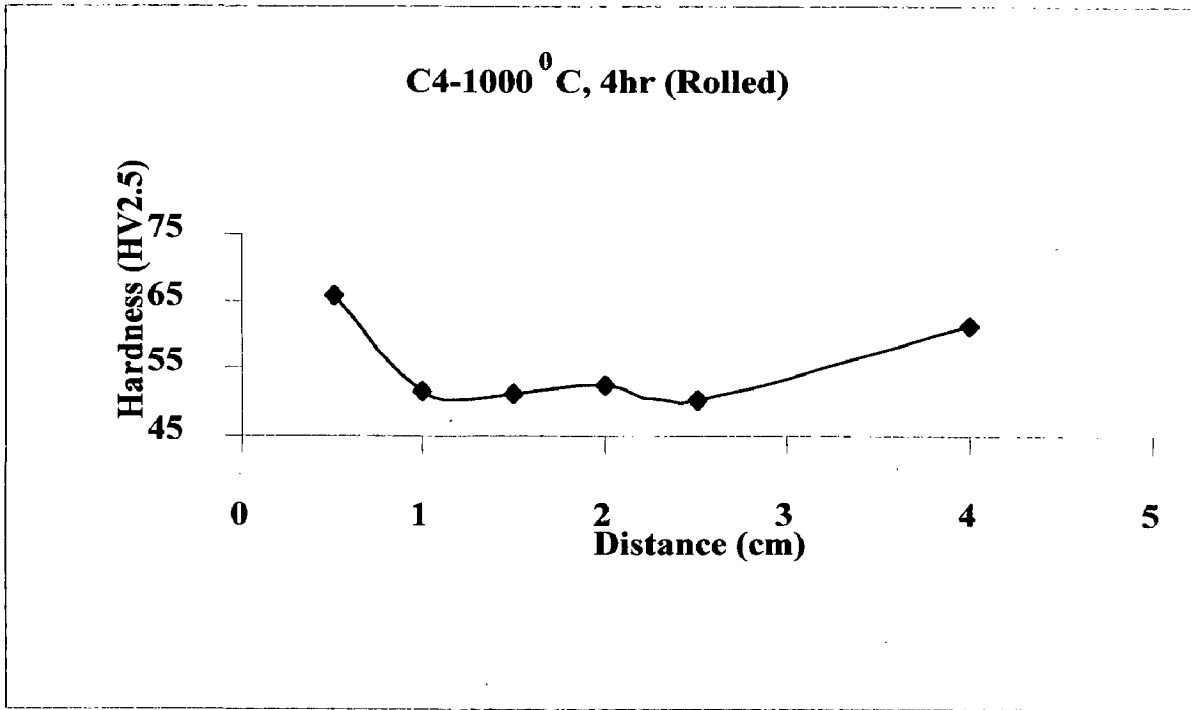


Figure 112

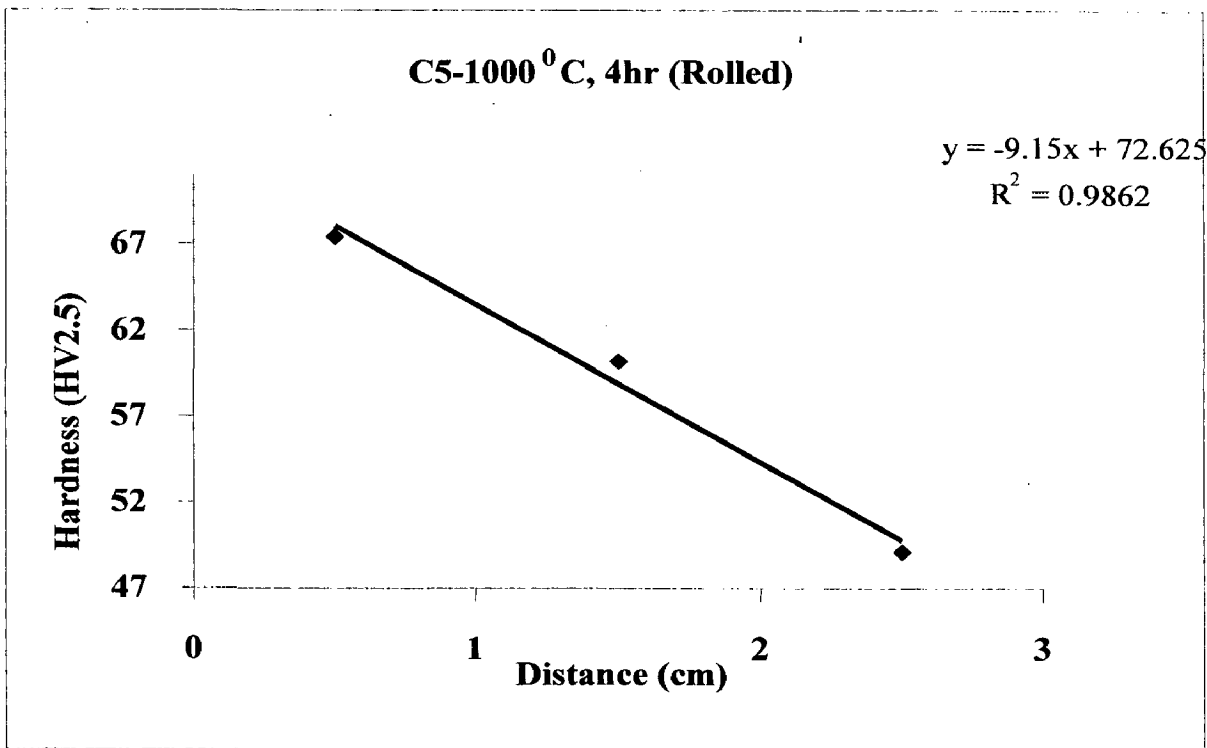


Figure 113

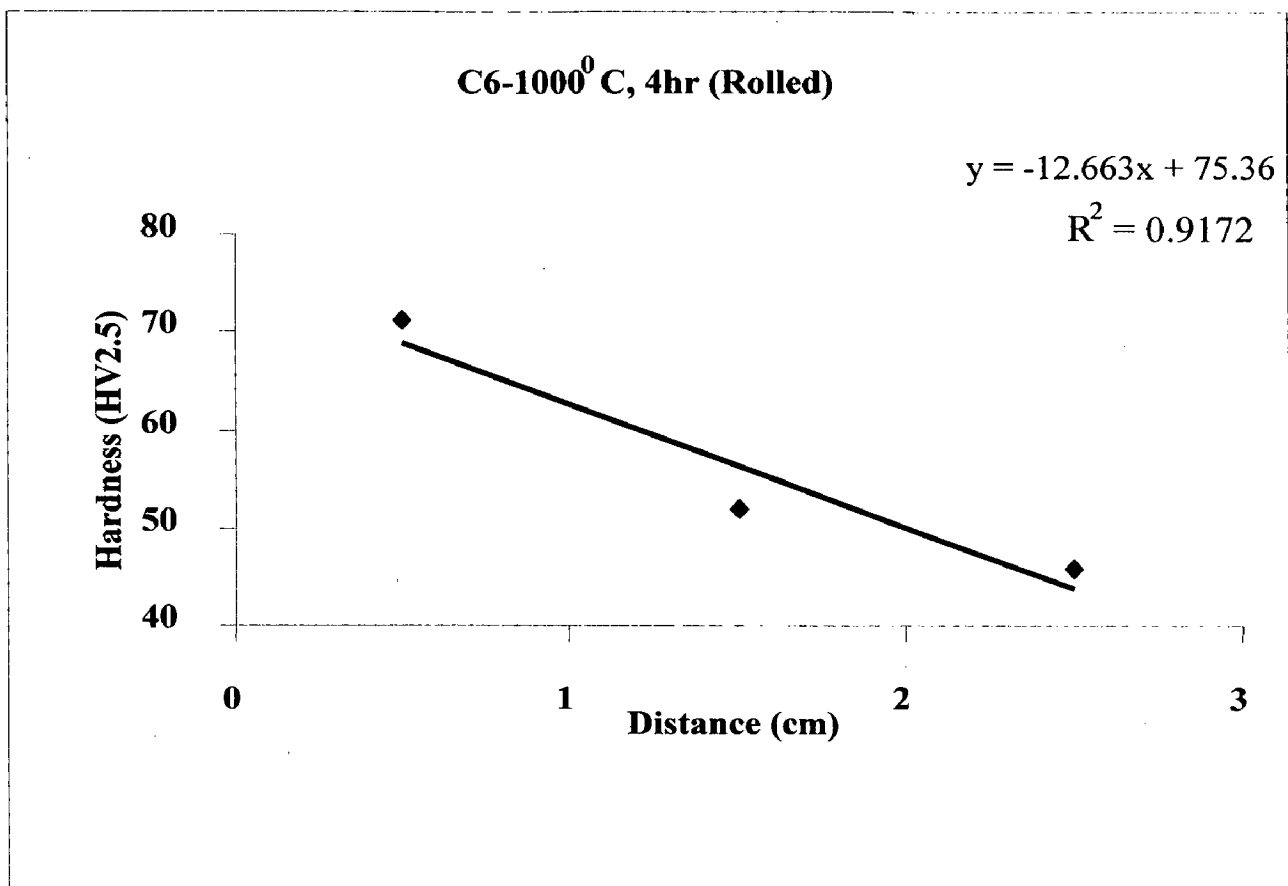


Figure 114

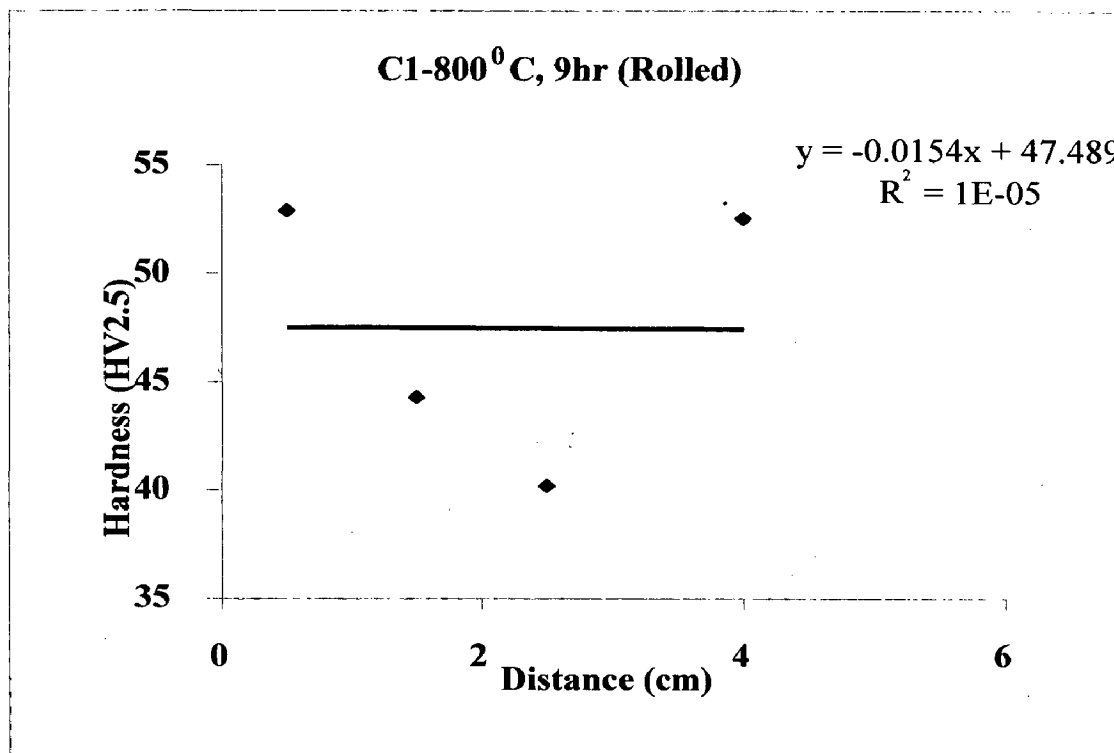


Figure 115

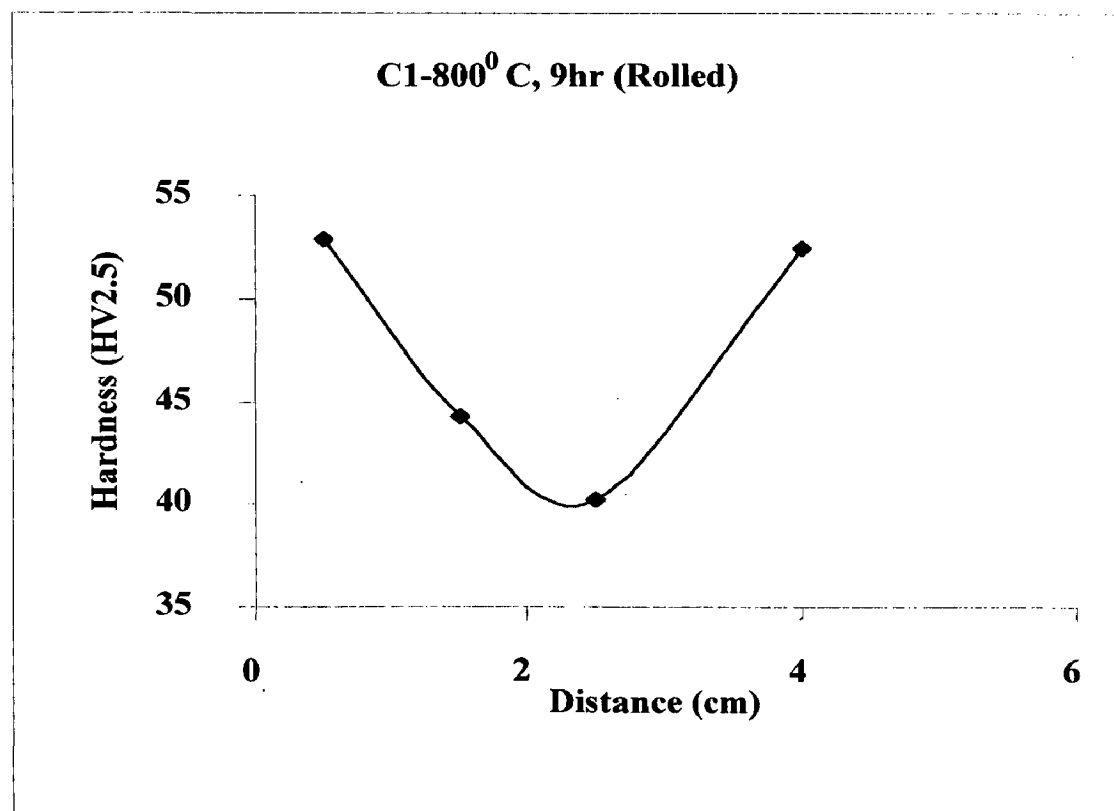


Figure 116

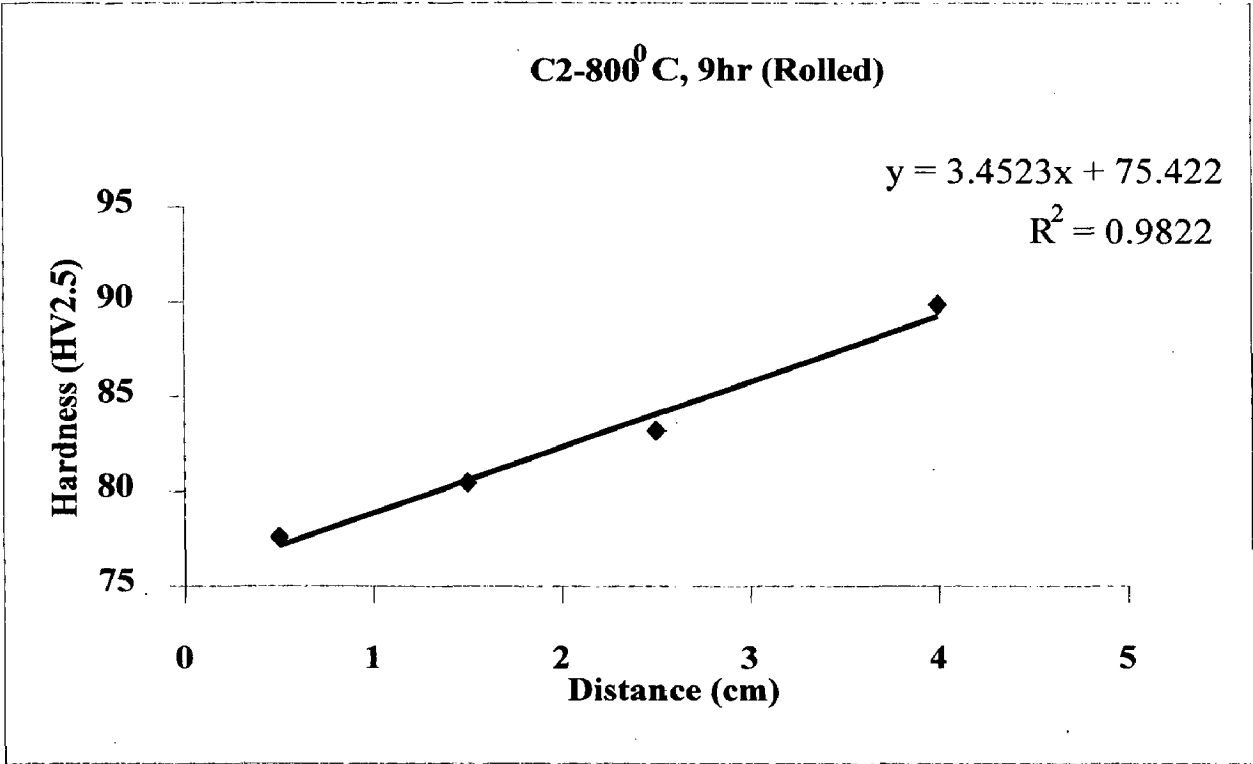


Figure 117

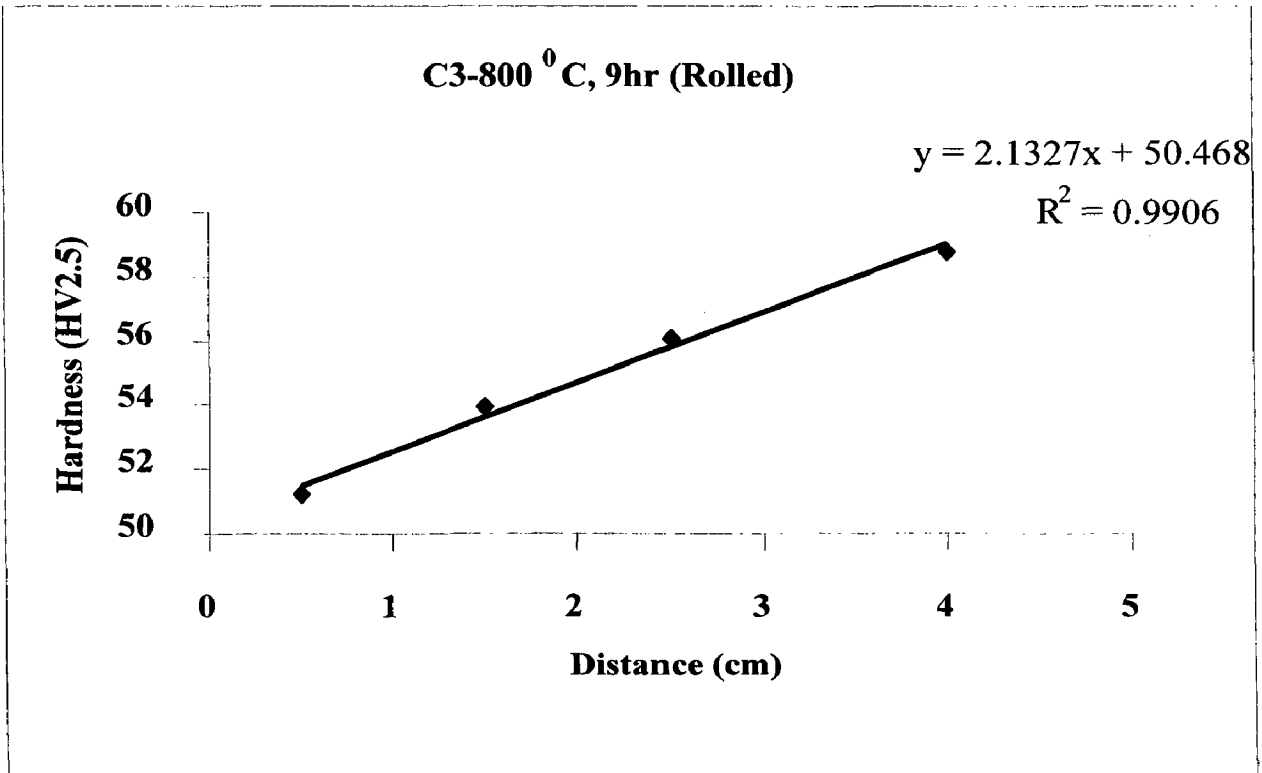


Figure 118

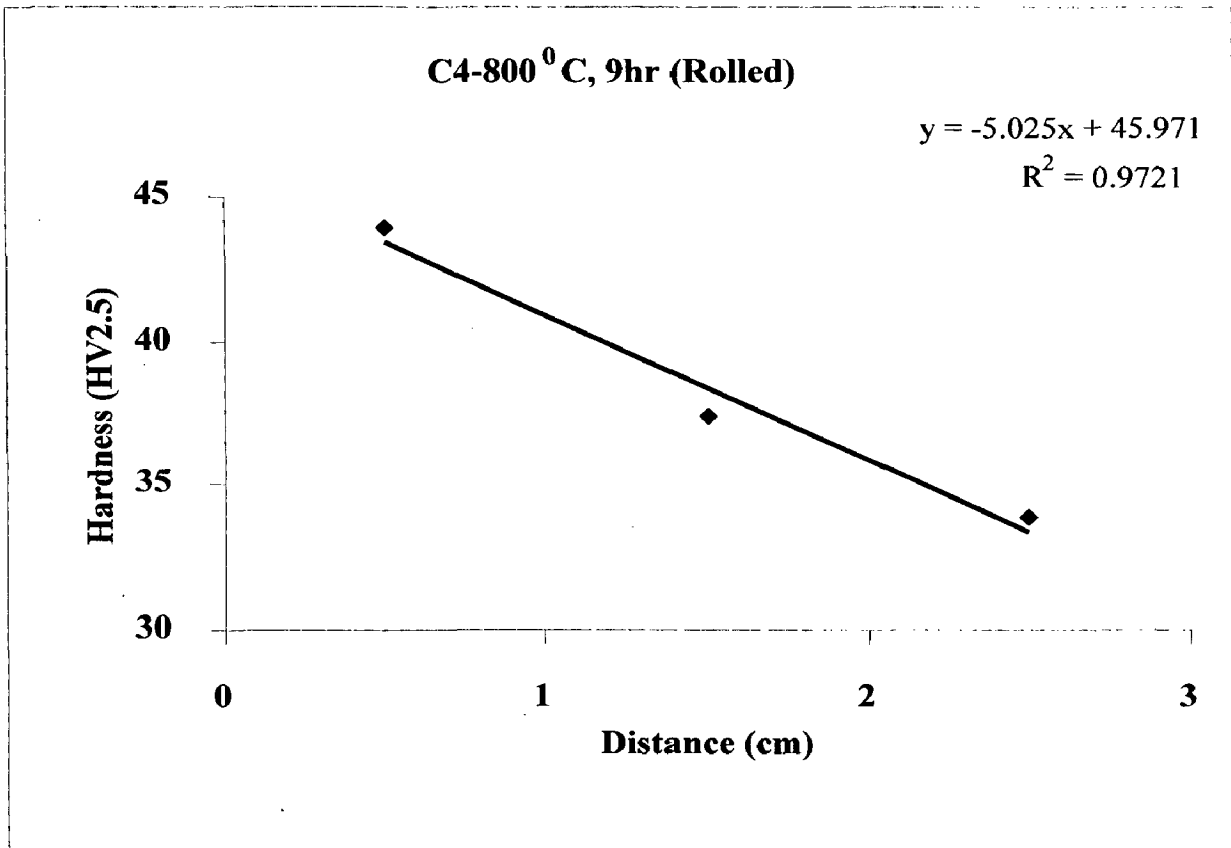


Figure 119

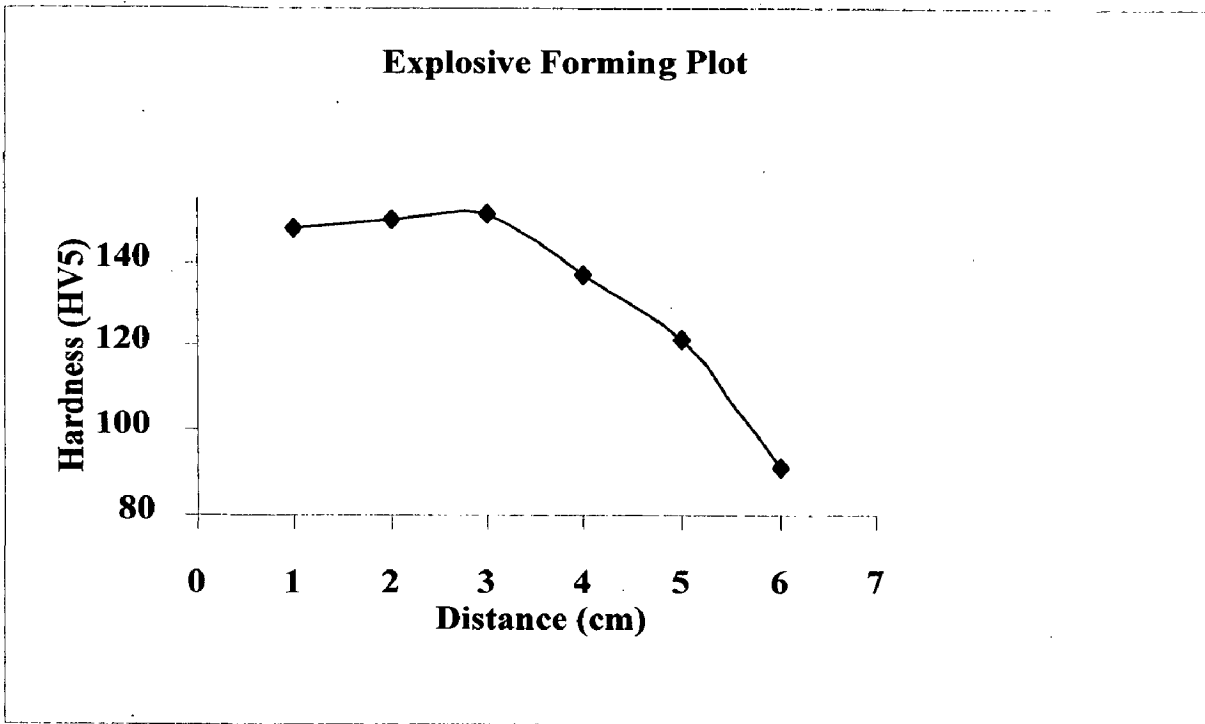


Figure 120

APPENDIX A

Property	Value
Atomic number	29
Atomic weight (mass)	63.54
Atomic radius	1.275×10^{-10} m
Valencies	1 and 2
Ionic radius: Cu ⁺²	0.72×10^{-10} m
Cu ⁺¹	0.96×10^{-10} m

Table 1: Atomic properties of copper [Ref: " Copper and its alloys" E.G.West, John Wily & Sons, p-21]

Property	Value
Color - reflected light	Salmon red
- transmitted light	Green
crystallographic structure	Face centered cubic
lattice constant, <i>a</i>	0.3608 nm
slip plane- primary	1,1,1
twinning plane	1,1,1
Density	8.96 g/cm ³
Volume change on solidification	4.0%
Melting point	1083 deg C
Boiling point	2590 deg C
Electrical conductivity	100-103 % IACS
Electrical resistivity	1.667 μ ohm cm
Cu- K _α wavelength	1.54056 angstroms

Table 2: Physical properties of pure copper (at 20 deg C) [Ref: " Copper and its alloys" E.G.West, John Wily & Sons, p-21]

	Soft	Hard worked
Modulus of elasticity (N/mm ²)	11721	124104
Modulus of rigidity (N/mm ²)	44815	51710
Poisson's ratio	0.35	0.35

Table 3: Elastic properties of copper [Ref: " Copper and its alloys" E.G.West, John Wily & Sons, p-21]

Form	Temper	Size range	0.1% proof stress (N/mm ²)	Tensile strength (N/mm ²)	Elongation %
Plate	Annealed	--	46	215	50-60
Sheet & strip	Hot rolled	6.25 thick	12.5-14.0	215-247	40-50
	Cold rolled	0.15-2.5	230	280	25-35
Rolled rod	Annealed		46	215	50-55
	Cold rolled	6.25-25 dia	200	132	20-30
Wire	Annealed	1.25 dia	--	215	35
	Cold drawn	2.55 dia	--	400	--
Tube	Annealed		62	215	50
	Cold drawn	12.5-100 o	185	280	30
Extrude sections	Extruded &				
	Cold worked	3.2-12.5	170	240	40
Forgings	Hot worked	75	93	230	40

Table 4: Typical tensile properties of wrought copper [Ref: " Copper and its alloys" E.G.West, John Wiley & Sons, p-30]

Copper family	UNS numbers	Characteristics		
Coppers	C10 000-C15 999	wrought and cast copper with minimum content of 99.3% Cu high-copper alloys for wrought products, less than 99.3% but more than 96% Cu, which do not fall into any other alloy groups; for cast alloys in excess of 94% Cu, to which silver may be added for special properties		
	C80 000-C81 299			
	C16 000-C19 999			
	C81 300-C82 999			
Brasses	C20 500-C28 599	Cu-Zn alloys } with or without other designated alloying elements, such as iron, aluminum, nickel, and silicon		
	C31 200-C38 599			
	C40 400-C49 999			
	C83 300-C85 899			
	C86 100-C86 399			
	C86 400-C86 899			
	C87 300-C87 999			
Bronzes	C50 100-C52 499	Cu-Sn-P wrought alloys (phosphorus bronzes) Cu-Sn-Pb-P alloys (lead phosphorus bronzes) Cu-Al alloys (aluminum bronzes) Cu-Si alloys (silicon bronzes) Cu-Sn cast alloys (tin bronzes) Cu-Sn-Pb alloys (lead tin bronzes) Cu-Sn-Ni alloys (nickel-tin bronzes) Cu-Al alloys (aluminum bronzes)		
	C33 200-C54 899			
	C60 600-C64 499			
	C64 700-C66 199			
	C90 200-C91 799			
	C92 200-C94 399			
	C94 700-C94 999			
	C95 200-C95 900			
	Copper-nickels		C70 100-C71 999	Cu-Ni alloys with or without other elements
			C96 200-C96 999	
Nickel-silvers	C73 000-C79 999	Cu-Ni-Zn alloys, contain no silver		
	C97 300-C97 999			
Lead coppers	C98 200-C98 999	Cu-Pb cast alloys, without tin or zinc		
Special copper alloys	C99 300-C99 999	chemical compositions do not fall into any of the above categories		

Table 5: ASTM system of categorizing copper and its alloys [Ref: Materials Science and Technology, Cahn, Haasen, Kramer, vol. 8, p- 292]

Alloy Type	condition	Electrical Conductivity (%IACS)	0.2% proof stress(N/mm ²)	Tensile Strength (N/mm ²)	Elongation (%)	Hardness (VDH)
Cu-Cr	W	35	45-50	230	50-40	65-70
	WP	75-85	250-360	370-400	26-22	120-125
	W(H)P	----	320-420	430-510	20-10	130-160
Cu-Zr	W	-----	60	230	45	60
	W(H)P	85-90	400-420	490-500	10	150
Cu-Cr-Zr	W(H)P	80	320-420	450-510	15	130-160

W= Solution treated; WP= precipitation hardened; W (H) P= Solution treated, cold worked and precipitation hardened.

Table 6: Average mechanical and electrical properties of low alloyed coppers [Ref: "Copper and its alloys" E.G.West, John Wily & Sons, p-139]

Alloy	Temperature (°C)	Stress(N/mm ²) to produce 0.1% plastic strain, 1000 h.
Cu- 1% Cr	280	165
	320	108
	350	86

Table7: Typical creep data for Cu-Cr alloys. [Ref: " Copper and its alloys" E.G.West, John Wiley & Sons, p-146]

Alloy	Degree of cold work (%) before solution treatment	Electrical conductivity (m Ω ⁻¹ mm ⁻²)	Hardness. HV ₅
Cu-0.44Cr	17	20.49	43.38
	30	20.61	44.37
	50	20.84	44.80
	70	20.86	46.20
Cu-0.94Cr	11	18.61	47.7
	30	18.53	49.1
	50	18.57	50.75
	70	18.69	42.79

Table 8: Properties of samples after solution treatment [Ref: Influence of aging temperature and time on hardness and electrical conductivity of Cu-Cr alloys, J.Rys, Z.Rdzawski, Metals Technology, Jan 1980, p- 32-35.

Diameter (mm)	Amount of Coldwork %	Tensile strength (a) [MPa]	Hardness HRB	Electrical conductivity % IACS
Rod				
24	0	325	60	90
22	13	245	65	
19	39	415	70	
16	56	450	70	
6	93	325	60	
Wire				
2	98.5	565	--	90
1	99.5	650	--	
0.5	99.9	725	--	

(a) Properties will vary, depending on extrusion ratio and temperature.

Table 9: Typical mechanical and electrical properties of Cu- 0.2Al₂O₃ [Ref: ASM HANDBOOK, Vol. 2, ISBN: 0-87170-378-5, p-282]

Size (mm)	Amount of cold work%	Tensile strength [MPa] (a)	Hardness HRB	Electrical Conductivity %IACS
Flat products (thick)				
0.76	91	570	--	89
0.51	95	585	--	
0.25	97	605	--	
Rod (Ø)				
24	0	470	74	89
18	42	510	78	
10	82	550	80	

(a) Properties will vary, depending on extrusion ratio and temperature.

Table 10: Typical mechanical and electrical properties of Cu- 0.4Al₂O₃ [Ref: ASM HANDBOOK, Vol. 2, ISBN: 0-87170-378-5, p-283]

Properties	Condition	units	960P	975P	995P	96S	ZTA
Mechanical Properties							
Al ₂ O ₃ minimum		%	96.0	97.6	99.7	99.6	80
Bulk Density	20 ⁰ C	g/cm ³			3.96	3.77	4.1
Tensile Strength	20 ⁰ C	MPa	205	205	220	nd	-
Flexural Strength	20 ⁰ C	MPa	375	375	410	295	450
Elastic Modulus	20 ⁰ C	GPa	300	355	375	nd	340
Hardness	20 ⁰ C	Kg/mm ²	10	12	14	nd	16
Fracture Toughness	20 ⁰ C	MPa.m ^{1/2}	4-5	4-5	4-5	nd	7
Porosity	20 ⁰ C	%	0	0	0	0	0
Thermal Properties							
Max. Working Temperature		⁰ C	1600	1650	1700	na	1500
Coef. Thermal Expansion	25-300 ⁰ C	10 ⁻⁶ / ⁰ C	7.1	7.2	7.8	6.7	
	25-1000 ⁰ C	10 ⁻⁶ / ⁰ C	7.4	7.7	8.1	7.4	8.1
Thermal Conductivity	20 ⁰ C	W/m ⁰ K	24	26	28	2806	23
Electrical Properties							
Dielectric Strength	2.5mm tk	ac-kv/mm	9.2	9.02	10	30	-
Dielectric Constant	1MHz	-	9.0	9.4	9.7	9.8	-
Volume Resistivity	20 ⁰ C	Ohm-cm	>10 ¹⁴	>10 ¹⁴	>10 ¹⁴	>10 ¹⁴	-
	300 ⁰ C	Ohm-cm	10 ⁹	10 ⁹	10 ¹⁰	10 ¹²	-
	1000 ⁰ C	Ohm-cm	10 ⁶	10 ⁶	10 ⁶	10 ⁶	-
Loss Factor	1MHz	-	0.028	0.012	0.009	0.0015	-
Dissipation Factor	1MHz	-	0.0003	0.0002	0.0001	-	-

Table 11: Typical mechanical, thermal and electrical properties of Al₂O₃

APPENDIX B

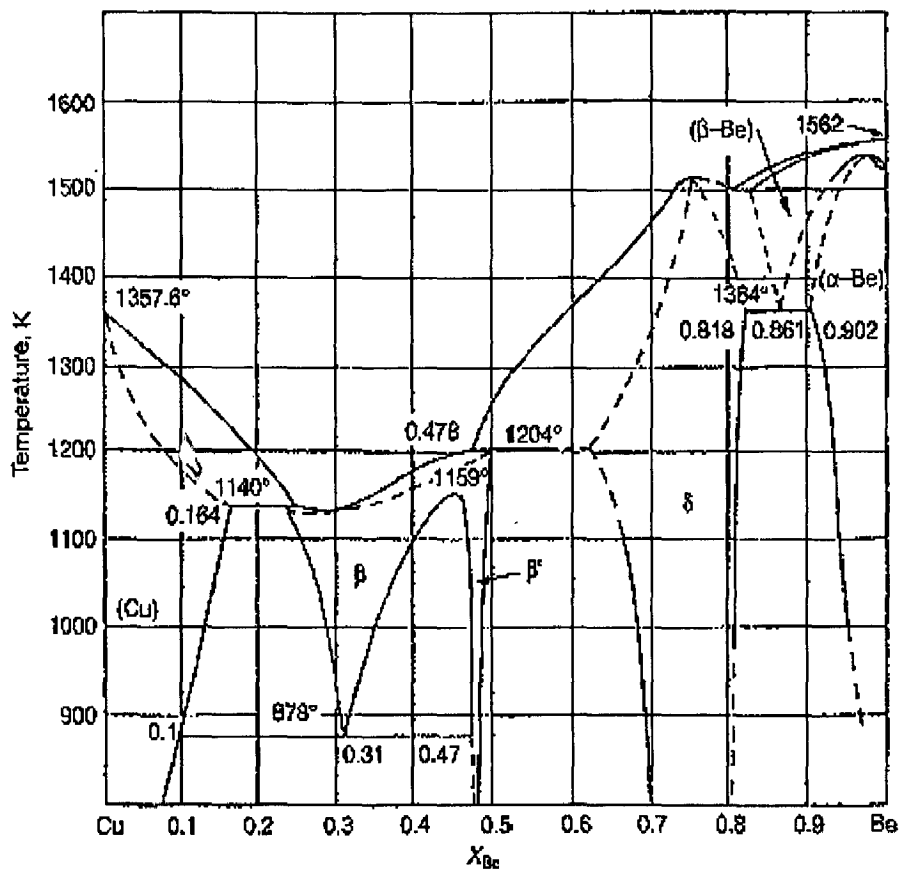


Figure 1: Cu-Be equilibrium diagram [Ref: COPPER, Its Trade, Manufacture, Use, and Environmental Status, Konrad J.A. Kundig, ASM International, 1999, p-60]

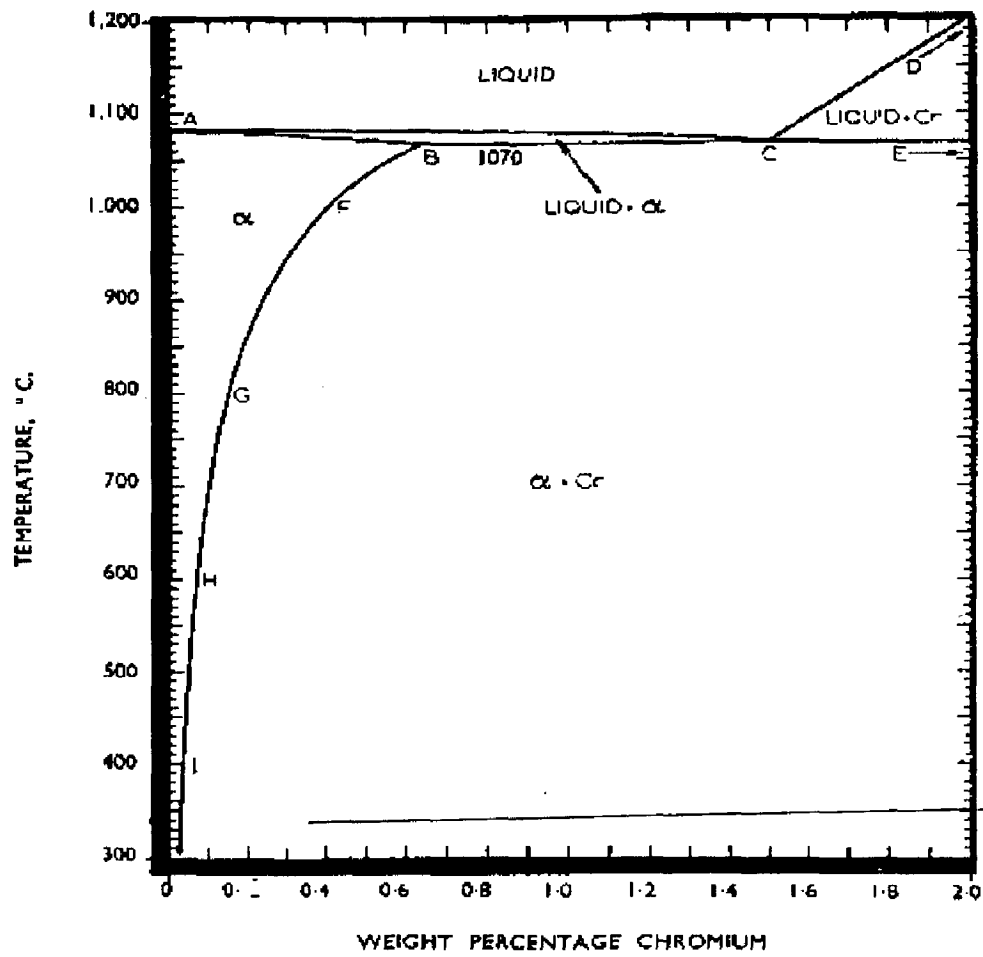


Figure 2: Cu-Cr equilibrium diagram [Ref: "Copper and its alloys" E.G. West, John Wiley & Sons, p-126]

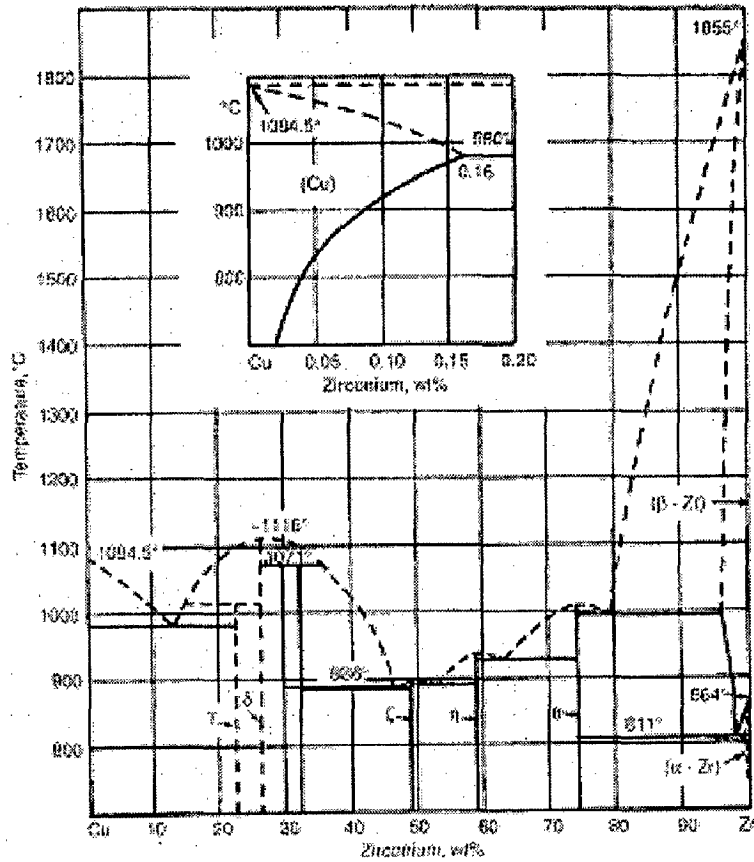


Figure 3: Cu-Zr equilibrium diagram [Ref: COPPER, Its Trade, Manufacture, Use, and Environmental Status, Konrad J.A. Kundig, ASM International, ISBN:0-87170-656-3, 1999, p-62]

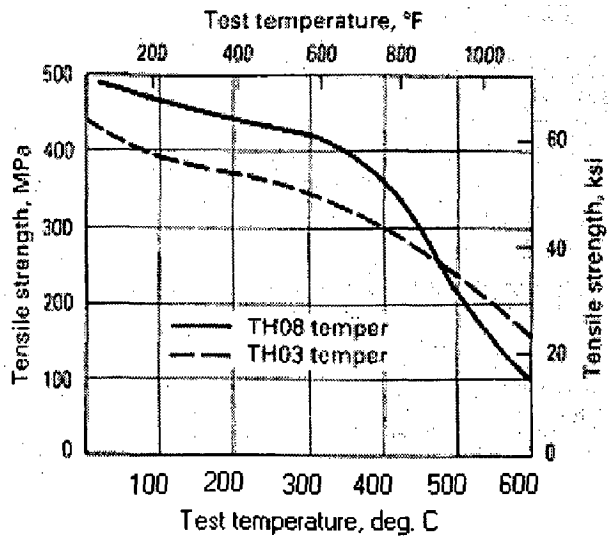


Figure 4: Short-term elevated-temperature tensile properties of C15000 (99.85Cu-0.1Zr). [Ref: ASM HANDBOOK, Vol. 2, ISBN: 0-87170-378-5, p-279]

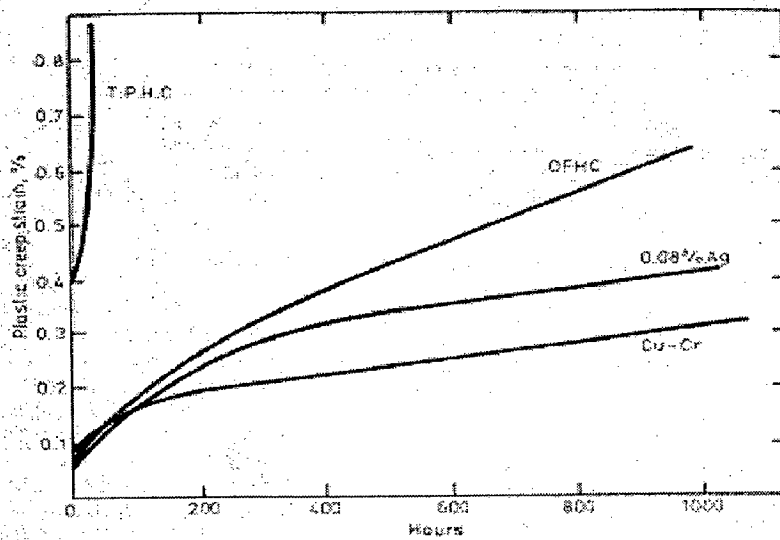


Figure 5: comparison of creep resistance at 225°C of copper-chromium alloy (cold worked 33%) at 231N/mm², with three high conductivity coppers (cold worked 25%), namely; Tough Pitch at 41.3 N/mm²; Oxygen Free at 96.5 N/mm²; Silver Copper at 137.8 N/mm². [Ref: " Copper and its alloys" E.G.West, John Wily & Sons, p-148]

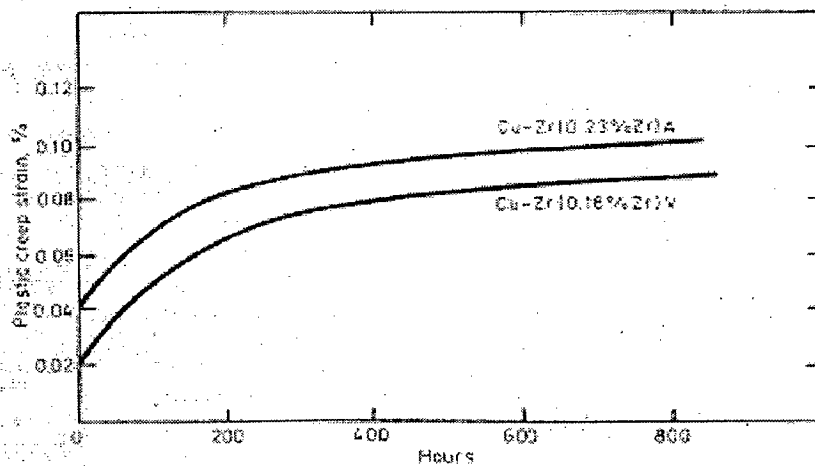


Figure 6: Creep resistance of copper- zirconium alloys at 230°C and 308 N/mm²: A = Air melted and cast; V= Vacuum melted and cast. [Ref: " Copper and its alloys" E.G.West, John Wily & Sons, p-148]

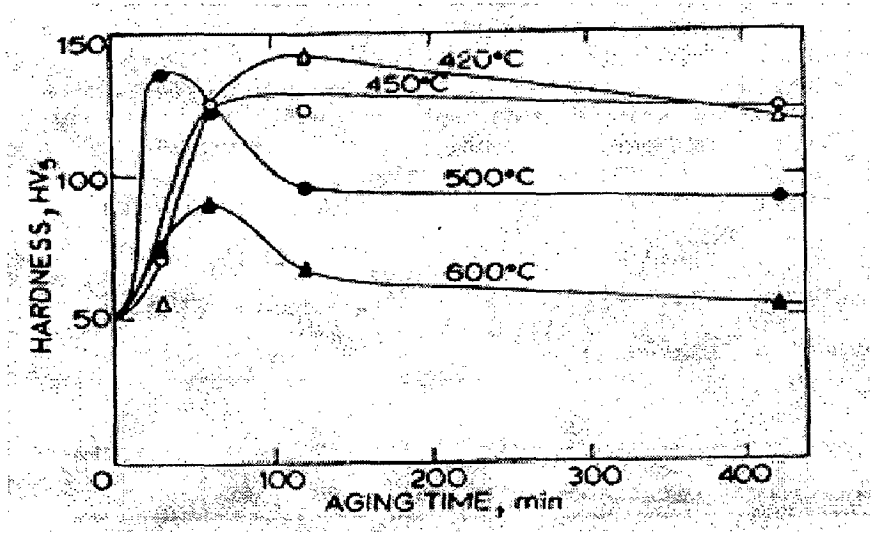


Figure 7: Variation of hardness after aging(Cu-Cr) [Ref: Influence of aging temperature and time on hardness and electrical conductivity of Cu-Cr alloys, J.Rys, Z.Rdzawski, Metals Technology, Jan 1980, p- 33].